



The 5th International INQUA Meeting on
**Paleoseismology,
Active Tectonics and
Archeoseismology**

21~ 27 September 2014
BUSAN, KOREA



Proceeding of the 5th International INQUA Meeting on
Paleoseismology, Active Tectonics and Archeoseismology

21-27 September 2014

Editors

Christoph Grutzner

Jin-Hyuck Choi

Paul Edwards

Young-Seog Kim





Published by

The Geological Society of Korea (GSK)

7 Teheran-ro, Gangnam, Seoul, Republic of Korea

<http://www.gskorea.or.kr/>

Korean Institute of Geoscience and Mineral Resources (KIGAM)

124 Gwahang-ro, Yuseong, Daejeon, Republic of Korea

<http://www.kigam.re.kr>

Edited by

Christoph Grutzner

Department of Earth Sciences, University of Cambridge

United Kingdom

&

Jin-Hyuck Choi, Paul Edwards, Young-Seog Kim

Department of Earth & Environmental Sciences, Pukyong National University

Republic of Korea

ISBN: 9791195344109 93450

1st edition, 100 pcs.

Printed in Busan, Korea.



Vol. 5: Proceeding of the 5th International INQUA Meeting on Paleoseismology, Active Tectonics and Archeoseismology (C. Grutzner, J.-H. Choi, P. Edwards & Y.-S. Kim, eds.). ISBN 9791195344109 93450. Printed in Korea, 2014. 5th International INQUA Meeting on Paleoseismology, Active Tectonics and Archeoseismology, Busan (Korea).

Vol. 4: Seismic Hazard, Critical Facilities and Slow Active Faults (C. Grutzner, A. Rudersdorf, R. Perez-Lopez & K. Reicherter, eds.). ISBN 978-3-00-0427-96-1. Printed in Germany, 2013. 4th International INQUA Meeting on Paleoseismology, Active Tectonics and Archeoseismology, Aachen (Germany).

Vol. 3: Earthquake Geology and Archeoseismology: Society and Seismic Hazard (R. Perez-Lopez, P.G. Silva, M.A. Rodriguez Pascua, V.H. Garduno Monroy, G. Suarez & K. Reicherter, eds.) Printed in Mexico, 2012. 3rd INQUA-IGCP 567 International Workshop on Earthquake Geology, Paleoseismology and Archeoseismology, Morelia (Mexico).

Vol. 2: Earthquake Geology and Archeoseismology: Society and Seismic Hazard (C. Grutzner, R. Perez-Lopez, T. Fernandez-Steeger, I. Papanikolaou, K. Reicherter, P.G. Silva & A. Vott, eds.) ISBN: 978-960-466-093-3. Printed in Greece, 2011. 2nd INQUA-IGCP 567 International Workshop, Corinth (Greece).

Vol. 1: Archaeoseismology and Paleoseismology in the Alpine-Himalayan Collisional Zone (R. Perez-Lopez, C. Grutzner, J. Lario, K. Reicherter & P.G. Silva, eds.) ISBN: 978-84-7484-217-3. Printed in Spain, 2009. 1st INQUA-IGCP 567 International Workshop, Baelo Claudia, Cadiz (Spain).

This event was organized by **The Geological Society of Korea**



This event was hosted by **Korean Institute of Geoscience and Mineral Resources KIGAM**

This event was supported by:

- INQUA Focus Group on Paleoseismology and Active Tectonics
- INQUA Project 1229 "EEE METRICS"
- Korean Federation of Science and Technology Societies
- Korea Tourism Organization
- Busan Tourism Organization
- Pukyong National University
- Nuclear Energy Group of the Geological Society of Korea
- Structural Geology & Energy Geology Group of the Geological Society of Korea
- BK21 PLUS, Institute of Earth Atmosphere Astronomy, Yonsei University
- BK21 PULS, School of Coastal Earth Environment, Busan National University
- Institute of Environmental Geosciences, Pukyong National University



Radiocarbon Dating Without Regrets



BETA

Beta Analytic
Radiocarbon Dating
www.radiocarbon.com

- Reliable turnaround time
- High-quality, ISO 17025 accredited results
- Prompt responses within 24 hours

Results in as little as 2-3 days

Australia Brazil China India Japan Korea UK USA

Preface [I]

Since the successful launch of our regular meetings on Paleoseismology, Active Tectonics and Archeoseismology in Baelo Claudia (Spain, 2009), and the following two meetings in Corinth (Greece, 2011) and Morelia (Mexico, 2012), in collaboration with the former IGCP Project on Earthquake Archaeology, Last year took place the last workshop of the series in Aachen (Germany, 2013) with the only support of INQUA renamed as 4th PATA Days, which stands for "Paleoseismology, Active Tectonics and Archeoseismology". This, year the 5th meeting of the series will be held in Busan (South Korea) again under the umbrella of the INQUA-TERPRO Commission.

These meetings are supported by The INQUA Focus Group on Paleoseismology and Active Tectonics, producing basic proceedings with a large number of 4-5 pages abstracts illustrating the progress in earthquake geology, paleoseismology and archeoseismology. Also in these meetings we have seen fruitful and intense discussions, we kicked off dozens of joint projects and we started international collaborations and initiatives to extend the knowledge on past earthquakes. A large number of peer reviewed articles has been published in Special Vols. as an outcome of these conferences. During the Aachen 2013 meeting (4th PATA Days) about 150 people attended the meeting and more of 100 contributions were presented and collected in the proceedings.

The INQUA Focus Group on Paleoseismology and Active Tectonics (<http://tierra.rediris.es/aequa/paleoinqua.html>) decided to elaborate an annual calendar to support this joint initiative. It is planned to proceed with the meetings, so we have chosen Busan, South Korea, to be the host this year. The last meeting in the INQUA inter-congress period will be in spring 2015 in Fucino (Italy). We switched to half a year earlier than normal because of the INQUA meeting in 2015 in Nagoya (Japan), where we need to present the results in the TERPRO frame of our INQUA Project 1299 - EEE METRICS PARAMETRIZATION OF EARTHQUAKE ENVIRONMENTAL EFFECTS (2011-2015): Relationships between source parameters and ESI-2007 Intensity for Modern, Historic, Ancient and Paleo Earthquakes

(more: <http://www.terpro.org.ar/paleoseismology.htm>). Early, during this year (February, 2014) a business meeting was held in Madrid (Spain), in order to prepare new strategies for the forthcoming INQUA inter-congress period (2015 – 2019).

After the business meeting held in Madrid, the members of the INQUA Focus Group attending the sessions identified two main topics to be developed in the near future: a) Minimum Magnitude Surface Rupture, and PFDHA; and b) Earthquake Mapping. The topics will be developed during this year in order to provide project proposals for the group activities after the next INQUA Nagoya Congress (August, 2015), but to be ready to propose specific projects at the end of this year 2014 (December). For sure, new discussions and ideas will emerge during the upcoming 5th PATA Days in Busan. The workshop will be again coordinated through the website <http://www.paleoseismicity.org>, where earthquake information and blog posts are openly shared.



Pablo G. Silva

Preface [II]

The 5th International INQUA Meeting on Paleoseismology, Active Tectonics and Archeoseismology (5th PATA Days) will be held in Busan, Korea during 21–27 September 2014. First of all, we are very pleased and greatly honorable to organize the important meeting in a dynamic city, Busan. A number of outstanding paleo-earthquake related researchers from all over the world would attend this meeting for intensive discussion on current issues in this field. This is the first PATA Days meeting in Asia and we aimed to expand the number of members from Asian countries and furthermore to make a strong Asian network for the future meetings. We hope that this meeting provides an opportunity to link the Asian countries and other European and American countries to exchange their experiences and knowledge on this subject.

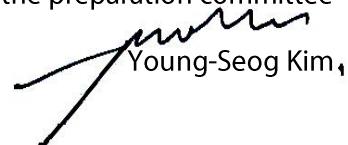
This meeting will include a 2-day workshop with keynote lectures, talks and posters on the seven sessions: Earthquake Geology, Paleoseismology, Archeoseismology, Secondary Effects of Earthquakes, Remote Sensing & Geomorphology, Seismic Hazard Assessment for Critical Facilities, and Korean Active Tectonics. Over 40 scientific papers from 17 countries and regions will be presented, and these excellent presentations will provide very active discussions for the recent and future issues related with paleo-earthquake.

In addition, a 3-day field trip is planned for much practical discussion for several important topics in Korean neo-tectonics: Development and ages of Quaternary marine terraces, Critical issues in NPP site selection, Characteristics of Korean active faults, and Archeoseismology in the old capital city, Gyeongju. It must be an outstanding scientific meeting on the issues for international exchange of the current state in earthquake geology research and for the Korean active tectonics. I hope it is a fruitful and memorial meeting as we have done during the previous four successful meetings (Spain, 2009; Greece, 2011; Mexico, 2012; Germany, 2013). Please enjoy the Korean geology, culture and food during the most dynamic and friendly meeting in Busan!

The meeting is organized by the Geological Society of Korea (GSK) based on the support of the Korean Federation of Science and Technology Societies (KOFST) and hosted by the Korean Institute of Geoscience and Mineral Resources (KIGAM). We also highly appreciate the INQUA Focus Group on Paleoseismology and Active Tectonics as well as INQUA Project 1229 "EEE METRICS" for their support for young scientists and students. Finally, we expect another successful meeting in Fucino, Italy 2015 and gratefully acknowledge for the support of:

- *Korean Federation of Science and Technology Societies*
- *Korea Tourism Organization*
- *Busan Tourism Organization*
- *Pukyong National University*
- *Nuclear Energy Group of the Geological Society of Korea*
- *Structural Geology & Energy Geology Group of the Geological Society of Korea*
- *BK21 PLUS, Institute of Earth Atmosphere Astronomy, Yonsei University*
- *BK21 PULS, School of Coastal Earth Environment, Busan National University*
- *Institute of Environmental GeoSciences, Pukyong National University*

On behalf of the preparation committee



Young-Seog Kim,

We gratefully acknowledge for the help and work of:

International Committee

Organizing Committee:

A. Michetti (ITA), P.G. Silva (ESP),
K. Reicherter (GER), L. Guerrieri (ITA),
K. Okumura (JPN), A. Soehaimi (IND),
D. Cheong (KOR), W.-S. Kee (KOR),
C. Grutzner (GER), Y.-S. Kim (KOR)

Scientific Committee:

J. McCalpin (USA), S. Marco (ISR),
T. Rockwell (USA), P.G. Silva (ESP),
K. Reicherter (GER), M. Sintubin (BEL),
Y.-S. Kim (KOR)

Keynote Speakers:

J. McCalpin (USA), J. Suppe (TWN),
S. Marco (ISR), J.R. Arrowsmith (USA),
R. Tatevossian (RUS), H.-K. Lee (KOR)

Invited Speakers:

T. Rockwell (USA), W. Lettis (USA),
P.G. Silva (ESP), K. Reicherter (GER),
M. Sintubin (BEL), D. Inoue (JPN),
T. Azuma (JPN), S. Solaymany Azad (IRAN),
M.-S. Jun (KOR)

General Secretary:

J.-H. Choi (KOR)

Local Committee

Organizing Committee-Chair:

Daekyo Cheong

Honorary Preparatory Committee-Chairs:

Jai Bok Kyung, Hee-Kwon Lee

Preparatory Committee-Chairs:

Weon-Seo Kee, Young-Seog Kim

General Advisory Group:

Jeong-Hwan Kim, Kiehwa Lee, Tae Woo Chang

Scientific Advisory Group:

Hyeon Cho Shin, Uee Chan Chwae, Jae Ha Hwang,
Jin-Han Ree, Sung-Ja Choi

Members:

Pom-Yong Choi, Weon-Hack Choi, Sang Sun Lee,
Si-Tae Yun, Moon Son, Hyunwoo Lee,
Jeong-Heon Choi, Raehee Han, Kwangmin Jin,
Sae-Woon Choi, Jin-Hyuck Choi

Field-trip Committee-Members:

Weon-Seo Kee, Sung-Ja Choi, Pom-Yong Choi,
Weon-Hack Choi, Jeong-Heon Choi, Young-Seog Kim,
Kwangmin Jin, Jin-Hyuck Choi

Program

21 September (SUN)

Arrival in Busan and Icebreaker Party

Arrival in Busan

20:00 Icebreaker Party at the New Malden

22 September (MON)

Pre-meeting field trip

Eastern coastal area: Quaternary terraces & NPP sites

09:00 Excursion to Eastern coastal area: Departure at VISTAS, PKNU

10:40 Field work at site.1 - Quaternary marine terrace (Yonghan-ri site)

12:00 Field work at site.2 - Suryum Fault

13:00 Lunch

14:00 Field work at site.3 - Unusual columnar joints

14:30 Field work at site.4 - Monitoring System for Epcheon Fault

15:30 Field work at site.5 - Nuclear waste disposal site

19:00 End of excursion and arrival in PKNU

1st day of Main Conference

09:00 Registration

10:00 Opening Ceremony

10:20 Session [1] Earthquake Geology

Time	Chaired by : Luca Guerrieri and Vince Cronin	
10:20-10:50 Keynote	John Suppe	Active folding of landscapes and sedimentary basins
10:50-11:05 Keynote	Vincent Cronin	Seismo-Lineament Analysis Method(SLAM), Using Earthquake Focal Mechanisms to Help Recognize Seismogenic Faults
Coffee break		
11:25-11:45 Invited	Klaus Reicherter	Progress in active bedrock normal fault investigations throughout the Mediterranean
11:45-12:00 Talk	Alessandro Maria Michetti	Late Quaternary evolution and potential for faulting along the Monferrato Arc, N Italy
12:00-12:15 Talk	Luca Guerrieri	Fault Displacement Hazard in urban areas in Italy: a first assessment
12:15-12:30 Talk	Yukari Miyasita	Correlation between fault activity and fault gouge color: toward the development of a new method for evaluating fault activity

12:30 Lunch

13:40 Session [2] Remote Sensing & Geomorphology

Time	Chaired by : Christoph Gruetzner and Paul Edwards	
13:40-14:10 Keynote	Ramon J. Arrowsmith	High resolution topography and active faulting
14:10-14:30 Invited	Daiei Inoue	Lineament analysis using ASTER satellite images around the coastal area of Korean Peninsula
14:30-14:45 Talk	Weon-hack Choi	Neotectonic evolution of the Ulsan fault system at the southeastern part of Korean peninsula
14:45-15:00 Talk	Raqueul Felix	Mapping of the Inabanga Fault in Bohol, Philippines using High Resolution LIDAR Imagery and Field Mapping Verification

15:00 Poster Session & Coffee break

16:05 Session [3] Archeoseismology

Time	Chaired by : Koji Okumura and Kwangmin Jin	
16:05-16:35 Keynote	Shmulik Marco	What can we learn about paleo-earthquakes from the anisotropy of magnetic susceptibility?
16:35-16:50 Talk	Miklos Kazmer	Damages to the 9th century Prambanan temple caused by the 2006 Yogyakarta earthquake (Java, Indonesia)

16:50 Lecture

Archaeoseismology. Where do we stand a century after Sir Arthur Evans? (*by Sintubin Manuel*)

18:00 Welcoming Dinner: Haeundae, Busan (move to by bus)

2nd day of Main Conference

09:00 Session [4] Paleoseismology

Time	Chaired by : Shahryar Solaymani Azad and Takashi Azuma	
09:00-09:30 Keynote	James McCalpin	Surface faulting without earthquakes; sackung and salt tectonics
09:30-09:50 Invited	Thomas Rockwell	Great earthquakes in the western Transverse Ranges of southern California on the Pitas Point-Ventura thrust system
09:50-10:10 Invited	Takashi Azuma	Reconstruction of a lateral offset paleo-channel on the Kego fault, western Japan
10:10-10:25 Talk	Koji Okumura	Important Issues Solved and Unsolved on the Paleoseismology of the North Anatolian Fault
10:25-10:45 Invited	Shahryar Solamany Azad	Persia as a Paradise for Paleoseismological Studies, Example: Paleoseismologic and Geodynamic Issues, NW Iran
10:45-11:00 Talk	Sowreh Rezaei	Geometric and kinematic characteristics of the Mosha-North Tehran Fault system, Northern Iran

11:00 Coffee break

11:20 Session [5] Korean Active Tectonics

Time	Chaired by : Heekwon Lee and Jeong-Heon Choi	
11:20-11:50 Keynote	Heekwon Lee	Review of paleoseismological studies in South Korea
11:50-12:10 Invited	Myung-Soon Jun	Earthquake characteristics in and around the Korean Peninsula and their tectonic implication
12:10-12:25 Talk	Jeong-Heon Choi	Optical dating of marine terrace sediments along the eastern coast of Korea, relevant to local crustal stability and Quaternary tectonics: Experiences and Expectations
12:25-12:40 Talk	Sung-Ja Choi	Distribution of Marine terraces and their tectonic implication, Southeastern Korea

12:40 Lunch

14:00 Session [6] Seismic Hazard Assessment for Critical Facilities &
 Session [7] Secondary Effects of Earthquakes

Time	Chaired by : Alessandro Michetti and Hyunwoo Lee	
14:00-14:30 Keynote	Ruben Tatevossian	Earthquake databases in hazard assessment of critical facilities
14:30-14:50 Invited	William Lettis	Emerging Concepts In Probabilistic Seismic Hazard Analysis and the Use of the SSHAC Process for Assessing Uncertainty
14:50-15:05 Talk	Tomas Fernandez-Steeger	Evaluation of seismic stability of coherent landslides: Analytical approach versus FEM
15:05-15:20 Talk	Kenji Satake	Long-term Forecast of Large Earthquakes: Lessons from the 2011 Tohoku Earthquake
15:20-15:35 Talk	Yael Braun	Paleo- tsunami event reconstruction using sediment cores along the upper shelf of the eastern Mediterranean basin- Caesarea and Jisr Al-Zarka, Israel

15:35 Poster Session & Coffee break

16:30 Lecture

Paleoseismology as a tool to view long-term earthquake production on plate boundary faults (*by Thomas Rockwell*)

17:10 2015 Meeting in Fucino, Italy

17:20 Awards ceremony

18:00 Main reception: Gijang area, Busan (move by bus)

25 September (THU)

Post-meeting field trip (I)

Active faults along the Yangsan-Ulsan Fault system

- 09:00 Excursion to active fault sites: Departure at the VISTAS, PKNU
- 10:00 Field work at site.1 - Southern part of the Yangsan Fault: Gacheon site
- 11:30 Field work at site.2 - Middle part of the Ulsan Fault: Ipsil and Malbang sites
- 12:30 Lunch
- 14:00 Field work at site.3 - Middle part of the Ulsan Fault: Jinhyun site
- 16:00 Field work at site.4 - Northern part of Yangsan Fault: trench site (or Wangsan Fault)
- 18:00 End of excursion and arrival in the KT&G Training Center

26 September (FRI)

Post-meeting field trip (II)

Archeoseismology in Gyeongju

- 09:00 Excursion to archeological sites: Departure at the KT&G Training Center
- 10:30 Field work at site.1 - Fallen Yeolam Buddha statue
- 11:40 Lunch
- 12:30 Field work at site.2 - Ancient observatory: Cheomseongdae
- 13:00 Field work at site.3 - Ancient tomb: Cheonmachong
- 14:00 Field work at site.4 - Seokguram
- 15:30 Field work at site.5 - Bulguksa Temple
- 18:00 End of excursion and arrival in KT&G Training Center

27 September (SAT)

Departure

- 10:00 Bus transfer to Busan International Airport

Poster Sessions

No.	Author	Title
1	Soehaimi, Asadani*, J.H Setiawan, Marjiyono	Seismotectonics and active faults of Bali Island
2	Jin, Kwangmin*, Young-Seog Kim	Interpretation for the propagation characteristics associated with the 1999 Chi-Chi earthquake faulting event
3	Whitney, Beau*, James Hengesh, Dan Clark	The Western Australia shear zone
4	Schürmann, Evelyn, Christoph Grützner*, Jochen Hürtgen, Klaus Reicherter	Slow active faults in an intracontinental setting – limits of standard morphometric analyses in tectonic geomorphology
5	Cita, Akbar*, Soemantri Poedjoprajitno	Geomorphologic Indicator of Tectonic Activities in Bakauheni, Lampung, Indonesia
6	Yudhicara*, Dicky Muslim, A. Sudradjat, D.H. Natawidjaja, R. Siahaan	Identifying an active Sumatra Fault Segment In Liwa Region using a Morphotectonic Approach
7	Kim, Hyun-Tae*, Young-Seog Kim, J. Ramón Arrowsmith, Kwang-Jae We	A case study of the application of LiDAR technique
8	Choi, Jin-Hyuck*, Young-Seog Kim	Damaged speleothems and their implications for Paleo-earthquake: A case study from Seongryu Cave in Uljin, Korea
9	Jin, Kwangmin*, Young-Seog Kim, Hee Cheol Kang, Hyeon Cho Shin	Preliminary study on developing characteristics of the Quaternary Gusan Fault
10	Hwang, JongSun*, Sung-II Cho, Weon-Hack Choi, Jae-woong Ryu	Operation and Management of Eupcheon Fault Monitoring System in South Korea
11	Kim, Ju-Yong*	Last Glacial Neotectonic Records in Prehistory Archeological Sites of Inland, Korea
12	Biju John*, C.P Rajendran, Yogendra Singh	Surface deformation characteristics at two locations in Peninsular India and its implications on seismic hazard
13	Folguera, Andrés*, Guido Gianni, Lucía Sagripanti, Emilio Rojas Vera, Bruno Colavitto, Darío Orts, Victor A. Ramos	Active tectonics in southern South America: a general review about its development and mechanisms
14	Hengesh, James*, Beau Whitney	Quaternary Reactivation of Australia's Western Passive Margin: Inception of a New Plate Boundary?

**Oral
Presentation
Abstracts
(Presentation
Order)**

Tuesday 23 September

Session One: Earthquake Geology



Active folding of landscapes and sedimentary basins

John Suppe (1)

(1) Department of Geosciences, National Taiwan University, Taipei 106 Taiwan. Email: suppe@princeton.edu

Abstract: Large kilometer-scale folds that actively deform the landscape or sedimentary basins are typically closely linked to major faults at depth. Much of this fold growth is coseismic in major earthquakes, for example the Tungshi anticline in Taiwan grew ~12m in the 1999 Chi-Chi earthquake ($M_w=7.6$). In contrast, some folds grow continuously such as the Tainan anticline in Taiwan, which is uplifting at ~1cm/y above a creeping backthrust. These "fault-related folds" provide important geomorphic, stratigraphic and geodetic records of their growth from which we can constrain both the long-term and short-term slip on their associated faults. Quantitative relationships have been demonstrated between fault-displacement histories and the progressive stratigraphic changes in fold size and shape for several important folding mechanisms. We illustrate some of these phenomena and methodologies by introducing several well-characterized case studies from the active western Taiwan fold-and-thrust belt, the southern Tianshan in western China, and California.

Key words: Coseismic folding, fold scarps, fault-related folding, blind thrust faults, fault-slip rates

INTRODUCTION

This paper presents a brief introduction and partial overview of active fold growth that deforms the surface of the Earth. It is a subject that provides a direct interface between structural geology, earthquake geology, surface processes and tectonic geodesy. For structural geology this interaction with the surface provides fundamental constraints on fold kinematics and insight into how structures grow by the summation of incremental deformation, in many cases in large earthquakes but also by continuous creep. For tectonic geomorphology it provides insight into the mechanisms by which the land surface is forced, providing a boundary condition for surface processes such as bedrock incision (e.g. Cook et al., 2014). For earthquake hazards, the progressive changes in fold shape and size within a sequence of dated geomorphic surfaces or horizons of growth strata provides a decipherable record from which a long-term fault slip history can be extracted (e.g. Suppe et al., 1991; Shaw & Suppe, 1994, 1996). Holocene paleoseismic records of major blind-thrust earthquakes have been obtained by excavation of fold scarps in the Los Angeles basin (Leon et al., 2007, 2009). Study of ancient inactive fold scarps in outcrop has given a basic understanding of their kinematic and stratigraphic complexities, which is needed for active tectonic applications (Suppe et al., 1997).

FOLD SCARPS & FOLDING MECHANISMS

Several fundamental end-member folding mechanisms are well documented based on analysis of seismic imaging, especially for compressive deformation. These include fault-bend folding, shear fault-bend folding, fault-propagation folding and detachment folding (e.g. Suppe, 1983; Suppe et al., 2004; Gonzalez-Mieres & Suppe, 2006, 2011). Many structures combine these

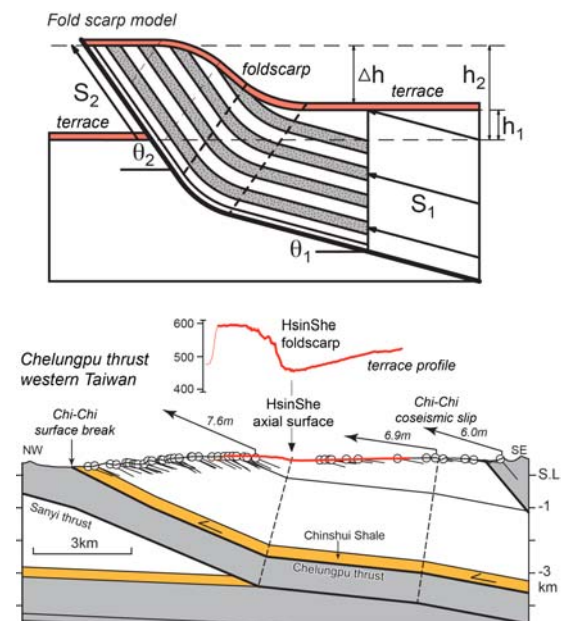


Fig. 1: Fold scarp produced by slip of a bedding-parallel thrust sheet through a fault bend. The magnitude of slip through the bend since the formation of a geomorphic surface can be deciphered from quantities that describe the fold geometry. The fault slip recorded by the terrace profile is 525m in the last 30Ka; the Chi-Chi coseismic slip was ~7m (Lai, et al., 2006; Chen et al., 2007; Yue et al., 2005, 2011; Le Béon et al., 2014).

mechanisms, as is best known from interpretation of petroleum seismic images (Shaw et al., 2005).

In classic fault-bend folding, kink bands progressively widen as fault slip increases, which can produce fold scarps at the surface. For example the HsinShe cumulative fold scarp in Fig. 1 grew by about 7m fault slip in the 1999 Chi-Chi earthquake and by about 525m



slip in the last 30Ka, based on a sequence of dated terraces (Le Béon et al., 2014).

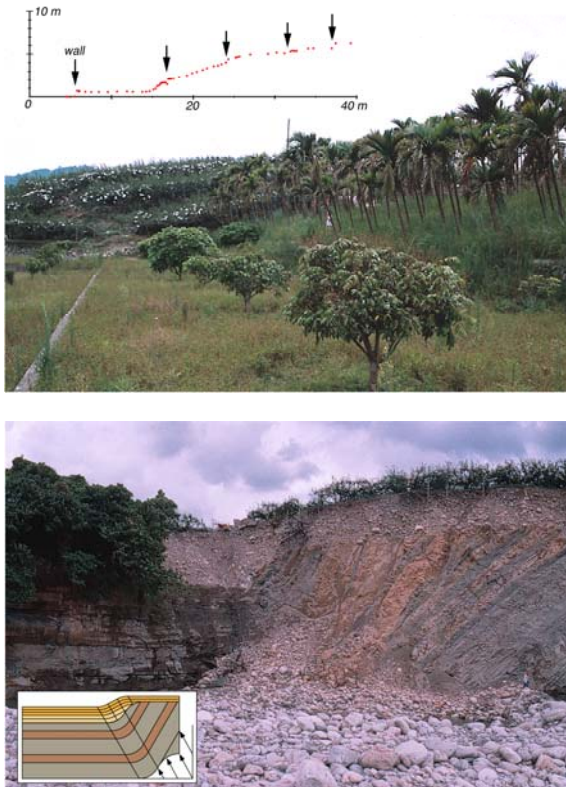


Fig. 2: Coseismic fold scarp of the 1999 Chi-Chi earthquake, showing tilted betel nut trees at Hsiaolipu. The fold scarp is wider in the distance on an older surface covered by pear trees beyond a terrace riser. The nearby river cut across the same fold scarp shows an internal structure characteristic kink-band migration (cf. inset and Suppe et al., 1997; Hubert-Ferrari et al., 2007), recording substantial folding prior to strath formation, followed by two folding events with the overlying gravel recording an old buried fold scarp, prior to the Chi-Chi fold scarp.

Fold scarps are now rather widely recognized but in the past were often misinterpreted as fault scarps or terrace risers, especially when they were narrow. Fig. 2 shows a coseismic fold scarp of the Chi-Chi earthquake with trees tilted, reflecting the fact that beds progressively tilt as they pass through fold hinges of finite width. A nearby cross section of this fold scarp is exposed in the river cut and shows characteristic unconformity geometries and thickness changes that imply kink-band migration with an earlier buried fold scarp. The origin of these bed and unconformity geometries is discussed in Suppe et al. (1997).

The relationship between fault slip and fold-scarp geometry is different from that of fault scarps (Suppe, et al., 1997; Hubert-Ferrari, et al., 2007; Le Béon et al., 2014). The scarp width is the width of the underlying fold hinge plus the horizontal component of displacement through the hinge, whereas the scarp height is the vertical component of the folding vector that describes the

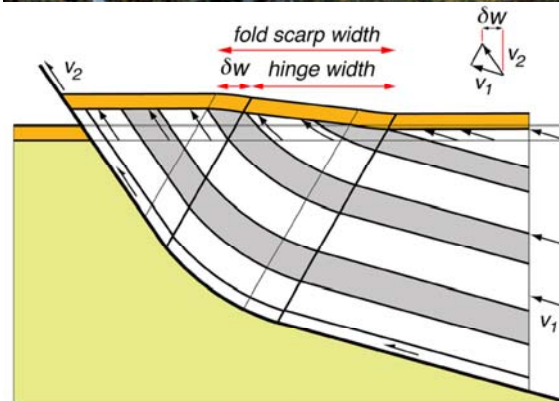
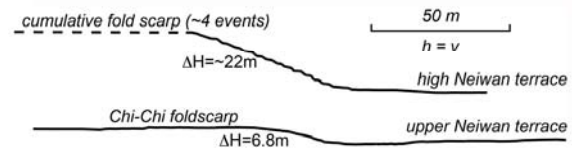


Fig. 3: Coseismic fold scarp of the 1999 Chi-Chi earthquake near Neiwán, which continues into a higher terrace beyond a terrace riser. The fold-scarp in the foreground is ~27m wide, which is substantially wider than the ~7m horizontal displacement in the earthquake. This is because fold-scarp width is the hinge-zone width plus the horizontal displacement through the hinge zone in the earthquake, as discussed in Suppe et al., (1994), Hubert-Ferrari et al., (2007), and Le Beon et al., (2014). In this example it takes about four Chi-Chi earthquakes to traverse the hinge, which is the case for the high terrace beyond. The scarp height ~4.8m is the vertical component of the folding vector, which is the change in particle displacement across the fold.

change in particle displacement across the hinge zone (Fig 3). Many fold hinges are much wider than the slip in a single earthquake and therefore require many earthquakes to traverse their width. The inclination of a point on a folded surface rotates progressively as it traverses the hinge until it reaches a maximum as it exits, for example the cumulative fold scarp on the upper Neiwán terrace is more steeply inclined than on the lower, reflecting more earthquakes (Fig. 3). To fully determine the displacement of a fault at depth requires some knowledge of the underlying structure (e.g. Fig. 1) and in some cases the full 3D motion can be determined (Le Béon et al., 2014).



Cumulative fold scarps forming by kink-band migration can grow to enormous sizes in areas of low erosion such as the 660m high foldscarp on the south limb of Quilitak anticline, southern Tianshan (Fig. 4). In addition to kink-band migration, fold scarps also can grow by a limb-rotation mechanism that is intrinsic to shear fault-bend folding and some detachment folding (Suppe et al., 2004). Coseismic limb rotation was observed on the west limb of the Tungshih anticline in the 1999 Chi-Chi earthquake and cumulative limb rotation is recorded by progressively tilted sequence of terraces on the east limb of the Pakuashan anticline in central Taiwan (Yue et al., 2011).

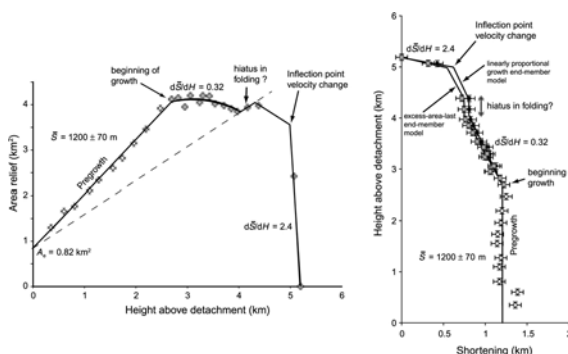
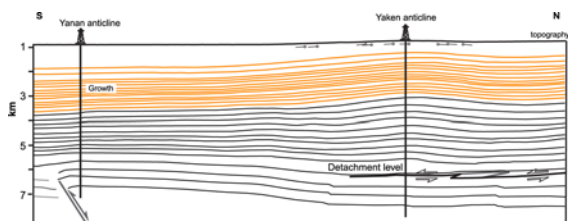
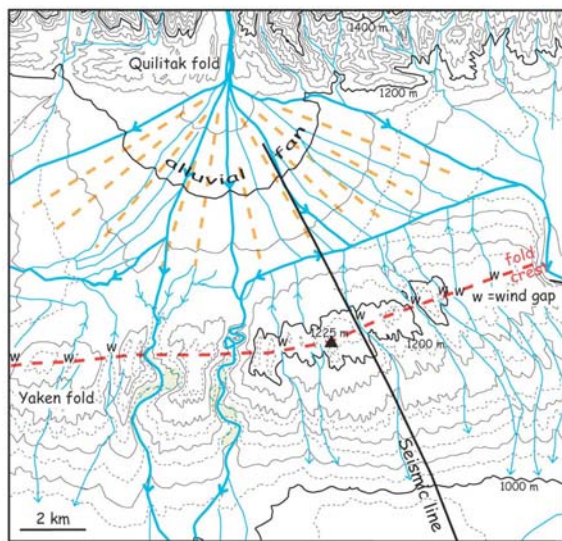


Fig. 5: Low-relief Yakeng anticline deforming alluvial fans south of Quilitak anticline, southern Tianshan China. The complete shortening and detachment slip-rate history is extracted from magnetostratigraphy combined with measurements at every seismic horizon of area of structural relief as a function of height using concepts and techniques developed by Hubert-Ferrari et al. (2005, 2007), Gonzalez-Mieres & Suppe (2006, 2011) and Suppe (2011).

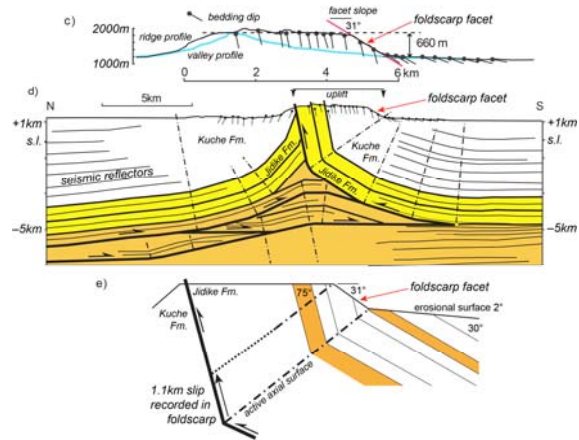
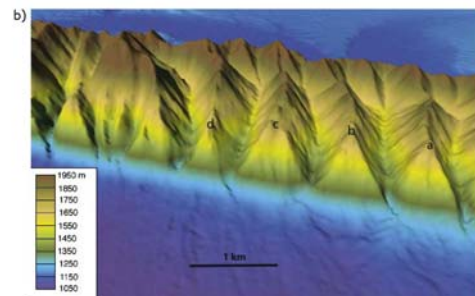


Fig. 4: Giant fold scarps south flank of Quilitak anticline, southern Tianshan in western China, showing 660m high fold scarp that is progressively incised to form triangular facets and wine-glass canyons. The active synclinal axial surface runs along the base of the slope. The surface of the facet has been shown by Hubert-Ferrari et al. (2007) to be the folded equivalent of the flat land surface in the foreground and has a dip of 31° that is predicted by fault-bend folding theory, indicating 1.1km of fault slip since formation of the folded geomorphic surface.

AREA OF RELIEF & SHORTENING HISTORY

The growth of folds produces changes in elevation of pre-existing surfaces, therefore fold growth can be described as an area of structural relief relative to the initial elevation in cross section. We can use these areas of structural relief to accurately determine the shortening consumed in a structure, if relief is measured on many stratigraphic horizons, because horizontal



shortening is the vertical gradient in area of relief (Epard & Groshong, 1993; Gonzalez-Mieres & Suppe, 2006). Classically area of relief was discussed in the context of detachment folding and depth to detachment, but modern concepts and techniques (Hubert-Ferrari, et al., 2005; Gonzalez-Mieres & Suppe, 2006, 2011; Suppe, 2011) can be applied to a wide variety of folding mechanisms with few assumptions, given reasonably well-imaged structures, for example in depth-converted seismic images (e.g. Yue et al., 2011; Li et al., 2012).

Shortening histories of folds can be determined from area-of-relief measurements on growth strata, but shortening is no longer given by the vertical gradient in area of relief. This is because area of relief in growth strata is not just the structural relief, but also includes a stratigraphic thinning or thickening of each growth layer that must be corrected for in determining the shortening history (Gonzalez-Mieres & Suppe, 2011).

An example of a shortening history determined from area of relief is the Yankeng anticline (fig. 5), which is the frontal fold of the south Tianshan thrust belt, just south of the Quilitak anticline (Fig.4) and part of the same thrust sheet (Hubert-Ferrari et al., 2007; Wang et al., 2011). The Yankeng anticline grew very slowly starting ~5.5Ma shortening at ~0.16mm/y with no surface expression, continually buried by growth strata (Hubert-Ferrari et al., 2007; Gonzalez-Mieres & Suppe, 2011). However, about half of the 1.2km total shortening was consumed in the last ~200Ka following with an order of magnitude acceleration in shortening rate to ~1.2-1.6mm/y and an emergence with a folding of the pre-existing alluvial fans and the production of numerous wind gaps. This acceleration is also seen in the previously low-relief Quilitak anticline (Fig. 4), producing widespread wind gaps and extreme topographic relief (Hubert-Ferrari et al., 2007).

Acknowledgements: I am grateful to acknowledge the gracious support of ROC National Science Council grant NSC102-2116-M-002-002, the National Taiwan University and previously Princeton University. I have had the pleasure of working with many co-authors in this research over the years, some of whom are listed in the references below.

References

- Chen, Y.G., Lai, K.Y., Lee, Y.H., Suppe, J., Chen, W.S., Lin, Y.N. N., Wang, Y., Hung, J.H., & Kuo, Y.T, (2007). Coseismic fold scarps and their kinematic behavior in the 1999 Chi-Chi earthquake Taiwan. *Journal of Geophysical Research*, 122, 15pp.
- Cook, K.L., Turowski, J.M, & Hovius, N., 2014, Gorge eradication by downstream sweep erosion. *Nature Geoscience* doi:10.1038/NGE02224.
- Epard, J.L., & Groshong, J.R.H., (1993). Excess area and depth to detachment. *American Association of Petroleum Geologists Bulletin*. 77, 1291-1302.
- Gonzalez-Mieres, R. & Suppe, J., (2006). Relief and shortening in detachment folds. *Journal of Structural Geology* 28, 1785-1807.
- Gonzalez-Mieres, R. & Suppe, J., (2011). Shortening histories of active detachment folds. In: *Thrust Fault-Related Folding* (McClay, K.R., Shaw, J.H. & Suppe, J. eds). American Association of Petroleum Geologists Memoir 94, 39-67.
- Hubert-Ferrari, A., Suppe, J., Wang, X., & Jia, C., (2005). The Yankeng detachment fold, China. In: *Seismic Interpretation of Contractional Fault-Related Folds* (Shaw, J.H., Connors, C.D. & Suppe, J., eds). American Association of Petroleum Geologists, 110-113.
- Hubert-Ferrari, A., Suppe, J., Gonzalez-Mieres, R., & Wang, X., (2007). Mechanisms of active folding of the landscape (southern Tianshan, China). *Journal of Geophysical Research* 112, 39pp.
- Le Béon, M., Suppe, J., Jaiswal, M.K., Chen, Y.G., and Ustaszewski, (2014). Deciphering cumulative fault slip vectors from fold scarps: relationships between long-term and coseismic deformation in western Taiwan. *Journal of Geophysical Research*, DOI: 10.1002/2013JB010794.
- Leon, L.L., Christofferson, S.A., Dolan, J.F., Shaw, J.H., & Pratt, T.L., (2007). Earthquake-by-Earthquake fold growth above the Puente Hills blind thrust fault, Los Angeles, California: Implications for fold kinematics and seismic hazards. *Journal of Geophysical Research* 112, 18pp.
- Leon, L.L., Dolan, J.F., Shaw, J.H., & Pratt, T.L., (2009). Evidence for large Holocene earthquakes on the Compton thrust fault, Los Angeles. *Journal of Geophysical Research* 114, 18pp
- Lai, K.Y., Chen, Y.G., Hung, J.H., Suppe, J., Yue, L.F., & Chen, Y.W., (2006). Surface deformation related to kink-folding above an active fault: Evidence from geomorphic features and coseismic slips. *Quaternary International*. 147, 44-54.
- Li, S., Wang, X., & Suppe, J. (2012). Compressional salt tectonics and synkinematic strata of the western Kuqa foreland basin, southern Tian Shan, China. *Basin Research*. 23, 23pp.
- Shaw, J.H., & Suppe, J., (1994). Active faulting and growth folding in the eastern Santa Barbara Channel, California. *Geological Society of America Bulletin*. 106, 607-626.
- Shaw, J.H., & Suppe, J., (1996). Earthquake hazards of active blind-thrust faults under the central Los Angeles basin, California. *Journal of Geophysical Research*. 101, 8623-8642.
- Shaw, J.H., Connors, C.D. & Suppe, J., (2005). *Seismic Interpretation of Contractional Fault-Related Folds*. American Association of Petroleum Geologists, 156pp.
- Suppe, J., (1983). Geometry and kinematics of fault-bend folding. *American Journal of Science*, 283, 684-721.
- Suppe, J., Connors, C.D., & Zhang, Y., (2004). Shear Fault-bend folding. In: *Thrust Tectonics and Hydrocarbon Systems* (McClay, K.R., Ed), American Association of Petroleum Geologists Memoir 82, 303-323.
- Suppe, J., Chou, G.T. & Hook, S.C., (1991). Rates of folding and faulting determined from growth strata. In: *Thrust Tectonics* (McClay, K.R., ed). Chapman & Hall, London, 105-121.
- Suppe, J., F. Sabat, J. A. Muñoz, J. Poblet, E. Roca, and J. Verges, (1997). Bed-by-bed fold growth by kink-band migration: Sant Llorenç de Morunys, eastern Pyrenees. *Journal of Structural Geology* 19, 443-461.
- Suppe, J., (2011). Mass-balance and thrusting in detachment folds. In: *Thrust Fault-Related Folding* (McClay, K.R., Shaw, J.H. & Suppe, J. eds). American Association of Petroleum Geologists Memoir 94, 21-37.
- Wang, X., Suppe, J., Hubert-Ferrari, A., & Jia, C., (2011). Structure of the Cenozoic Quche fold belt, China. In: *Thrust Fault-Related Folding* (McClay, K.R., Shaw, J.H. & Suppe, J. eds). American Association of Petroleum Geologists Memoir 94, 215-243.
- Yue, L.F., Suppe, J. & Hung, J.H., (2005). Structural geology of a classic thrust belt earthquake: the 1999 Chi-Chi earthquake Taiwan ($M_w=7.6$). *Journal of Structural Geology* 27, 2058-2083.
- Yue, L.F., Suppe, J. & Hung, J.H., (2011). Two contrasting kinematic styles of active folding above thrust ramps, western Taiwan. In: *Thrust Fault-Related Folding* (McClay, K.R., Shaw, J.H. & Suppe, J. eds). American Association of Petroleum Geologists Memoir 94, 153-186.



INQUA Focus Group on Paleoseismology and Active Tectonics



paleoseismicity.org

NOTES



Seismo-Lineament Analysis Method (SLAM), Using Earthquake Focal Mechanisms to Help Recognize Seismogenic Faults

Cronin, Vincent S. (1)

(1) Geology Department, Baylor University, Waco, Texas 76798-7354, USA. Email: Vince_Cronin@baylor.edu

Abstract: *The Seismo-Lineament Analysis Method (SLAM) uses an earthquake focal mechanism in a process intended to spatially correlate a shallow-focus earthquake with the ground-surface trace of the fault that generated the earthquake. The nodal planes (NP) derived from the focal mechanism are projected upward to the ground surface, represented by a topographic/hillshade map based on a digital elevation model. The intersection of a NP and the ground is called a seismo-lineament. When uncertainties in hypocenter location and NP orientation are incorporated, the seismo-lineament is a swath on the ground surface. If the NP is the fault-plane solution (i.e., coincides with the causative fault), the fault that generated the earthquake is likely to be found within the seismo-lineament if the fault is emergent and approximately planar from the hypocenter to the ground. Faults that are spatially correlated with earthquakes as small as M 2.9 have been located using SLAM.*

Key words: *earthquake, focal mechanism, active faulting, paleoseismology, fault geomorphology*

INTRODUCTION

The fundamental goal of the paleoseismology community is to identify and usefully characterize seismogenic faults that can generate damaging earthquakes, so that the risks associated with these hazards can be avoided or mitigated. Faults that have ruptured the ground surface and that have generated moderate or larger ($M > 5$) earthquakes are generally good targets for trench studies. Some faults capable of generating significant earthquakes are inaccessible to trenching because they are not emergent (i.e., they are "buried" or "blind"). Some seismogenic faults have not caused co-seismic ground-surface rupture during historic times, and have remained unrecognized. There are many examples of faults that had not been recognized as seismogenic (or that were not mapped at all) before they produced damaging earthquakes. The quality, completeness, and coverage of active-fault mapping is still highly variable worldwide.

Most earthquakes along a typical fault do not rupture the entire fault surface -- large faults do not generate only large earthquakes, and small earthquakes do not occur only along small faults (Cronin et al., 2008). Active faults that can produce major earthquakes also produce myriad smaller earthquakes that spatially correlate with the primary fault surface. We can use small earthquakes to help us identify seismogenic faults that are capable of producing large earthquakes.

The Seismo-Lineament Analysis Method, or SLAM, uses earthquake hypocenter and focal mechanism data, hillshade maps derived from digital elevation models (DEM), geomorphic analysis and geologic field work to help identify the ground-surface trace of faults that produce earthquakes (Cronin et al., 2008). The current version of SLAM can accommodate a triaxial-ellipsoidal

uncertainty region around the hypocenter, and incorporates reported uncertainties in nodal-plane orientation (Cronin & Cronin, 2014). SLAM has been used to spatially correlate faults and well-located earthquakes with reported magnitudes as low as 2.9. SLAM has also been used to discover new faults and to spatially correlate earthquakes with mapped faults that were not thought to be seismogenic, faults that were thought to have Neogene displacement but that were not known to have been seismogenic in historic times, and faults that had been associated with historic earthquakes (Cronin et al., 2008; Millard, 2007; Lindsay, 2012; Reed, 2013). I will use the pronoun "we" throughout this single-author paper because the development and initial applications of SLAM have been collaborative efforts involving several co-workers, acknowledged at the end of this paper.

GENERAL DESCRIPTION OF SLAM

Details about focal mechanism solutions and their derivation are available elsewhere (e.g., Dziewonski et al., 1981; Reasenber & Oppenheimer, 1985; Hardebeck & Shearer, 2002; Stein & Wysession, 2003; Shearer, 2009; Cronin, 2010). Some comments about focal mechanisms are appropriate here in the interest of clarity. The focal mechanism for an earthquake with a double-couple mechanism includes two nodal planes, oriented perpendicular to one another. The fault that generated the earthquake is coincident with one of the nodal planes (called the *fault-plane solution*), while the other plane is a symmetry plane called the *auxiliary plane* that does not (necessarily) have any displacement along it. The slip vector on the fault plane is parallel with the vector normal to the auxiliary plane. The geometry of a focal mechanism solution is often graphically represented using a focal mechanism (or beach ball) diagram.



The *minimal* data required for a SLAM analysis are a hypocenter location (latitude, longitude, depth), the corresponding earthquake focal mechanism (dip azimuth or strike, dip angle, and rake of the hanging-wall slip vector for one of the nodal planes), and a map of the epicentral area. It is better, but not necessary, if the map is a topographic map. The *ideal* input data for a SLAM analysis are the hypocenter location with associated uncertainties, the corresponding focal mechanism with uncertainties, and a DEM of the epicentral area that is of sufficient resolution to capture significant geomorphic features related to fault displacement of the ground surface. Hypocenter locations that result from multiple-event relocation studies of the epicentral region are preferred to single-event locations (e.g., Waldhauser & Ellsworth, 2000; Waldhauser, 2001).

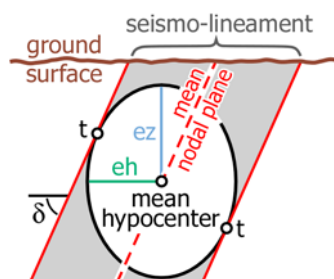


Fig 1. Vertical cross section of a seismo-lineament, shown perpendicular to the strike of the mean nodal plane. δ =dip angle of mean nodal plane, t =tangent point, eh =horizontal uncertainty, ez =vertical uncertainty.

A key element of SLAM is a procedure to project a nodal plane from the hypocenter upward, defining the intersection of the nodal plane and the ground surface (Figure 1). We call this intersection a *seismo-lineament* (Cronin et al., 2008).

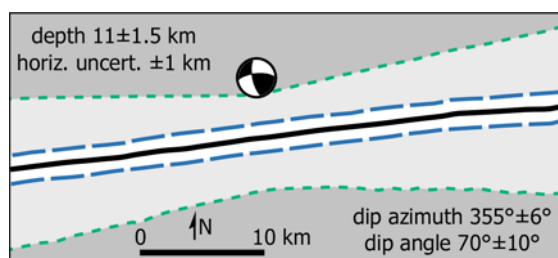


Fig 2. Examples of seismo-lineaments (SL) for an inclined nodal plane projected onto an irregular ground surface. Solid curve is the SL for the mean nodal plane alone, with no uncertainties reported or used. Area between long-dashed curves is the SL for a case when only the hypocenter uncertainty estimates are used. Area between short-dashed curves is the SL when uncertainties for both the hypocenter and nodal plane are used. Focal mechanism diagram plotted at the epicenter.

If the uncertainties in hypocenter location and nodal-plane orientation are not specified, the seismo-lineament will be a line or curve on a ground-surface map (Fig. 2). If the hypocenter location uncertainty is known, two planes that are tangent to the hypocenter uncertainty ellipsoid and that are parallel to the mean

nodal plane are projected to the ground surface, defining the seismo-lineament as a linear swath as seen in map view. If uncertainties are known for both the hypocenter location and nodal plane orientation, the resulting seismo-lineament has the appearance of a bow tie, with the epicenter located near the narrowest part of the swath (i.e., near the "knot" of the bow tie). An open-source code written in *Mathematica* (available via http://bearspace.baylor.edu/Vince_Cronin/www/SLAM/) is used to define the boundaries of a seismo-lineament, using a DEM to represent the ground surface.

The seismo-lineament for a given nodal plane defines the area where the trace of the fault is likely to be found if the causative fault is emergent and approximately planar from the hypocenter to the ground surface, and if the given nodal plane is coincident with the fault.

There are two seismo-lineaments for each earthquake, each corresponding to one of the two nodal planes. We create a hillshade map of the DEM in the area of each seismo-lineament, with low-angle illumination directed parallel to the mean dip direction of the corresponding nodal plane. Fault-related features on the landscape are likely to be oriented perpendicular to this illumination direction. We conduct a geomorphic analysis using the hillshade maps of seismo-lineaments, intending to identify possible fault-related features. We also consult published geologic maps and compile the traces of known faults in our study area. The geomorphic analysis and fault-trace compilation generate hypotheses about the possible causative fault that can be tested during subsequent geologic fieldwork, and help us to differentiate between the fault-plane solution and the auxiliary plane.

An additional aide in differentiating the fault-plane solution from the auxiliary plane involves mapping earthquakes that occurred in the epicentral region perhaps six months before and six months after the main event. Plainly, this would include the aftershock sequence of a large earthquake (Figure 3), but mapping temporally related earthquakes can help us interpret the fault plane solution for smaller events as well.

EXAMPLES

The largest recorded earthquake in the North Tahoe-Truckee area of east-central California is the M_L 6 event of September 12, 1966, at an estimated depth of 10 km (Ryall et al., 1968). This earthquake caused damage throughout the epicentral area, but caused no reported injuries (Kachadoorian et al., 1967). The Dog Valley Fault Zone (DVFZ) was recognized as a result of the 1966 Truckee earthquake, based on geomorphic lineaments that are sub-parallel to the long axis of the aftershock cluster, and also sub-parallel to the strike of the inferred fault-plane solution (Hawkins et al., 1986). Minor, discontinuous ground rupture was mapped in ~7 locations between Prosser Reservoir and Hoke Valley, in a zone that was ~3 km wide (Figure 3). Ground cracking occurred mostly in the area where aftershocks were



concentrated (Kachadoorian et al., 1967; Greensfelder, 1968). Hawkins et al. (1986) described the DVFZ as "concealed" after digging two exploratory trenches across geomorphic lineaments without exposing any faults.

We used the hypocenter location of Ryall et al. (1968) and the focal mechanism of Tsai and Aki (1970) in the SLAM analysis of the 1966 Truckee earthquake (Figure 3). Neither published source provided formal uncertainties for their data. We used horizontal and vertical uncertainties of 2 km to define the seismo-lineament, based on an informal assessment noted by Ryall et al. (1968). Greensfelder (1968) and Ryall et al. (1968) determined the locations of aftershocks.

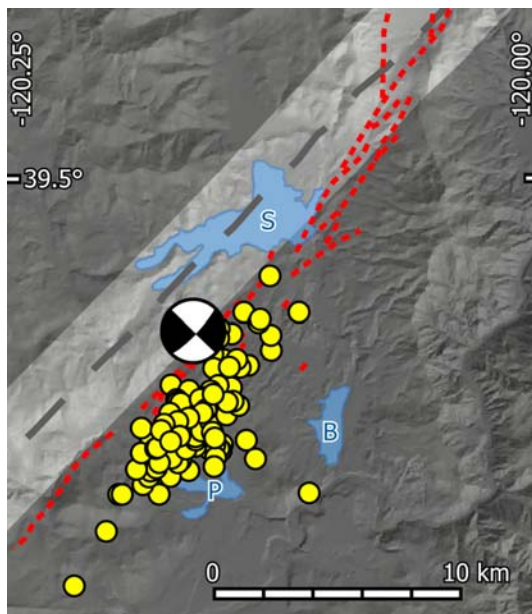


Fig 3. Focal mechanism, seismo-lineament (light gray swath), and trace of the mean nodal plane for inferred fault-plane solutions (dark gray dashed curve) of the M_L 6 Truckee earthquake of 12 September 1966. Red dashed curves are inferred strands of the DVFZ (US Geological Survey, 2014). Small circles are aftershock epicenters, from Greensfelder (1968). S=Stampede Reservoir, P=Prosser Creek Reservoir, B=Boca Reservoir.

Hawkins et al. (1986) indicated that the M_L 6 Verdi earthquake of 29 December 1948 and an earthquake sequence from January to September 1983 also occurred along the DVFZ. Lindsay (2012) and Reed (2013) applied SLAM to several earthquakes with epicenters in the vicinity of the DVFZ, including the M 4.0 event of 3 July 1983 and the M 3.2 event of 30 August 1992 (Figure 4). Hypocenter location data for the 1983 event are from the Northern California Earthquake Data Center (NCEDC, 2013), and the relocated hypocenter data for the 1992 event are from Waldhauser (2013). Horizontal uncertainties for both events are <0.54 km, and vertical uncertainties are ≤ 0.8 km. Focal mechanism solutions used to define the seismo-lineaments are from the NCEDC catalog (2013).

No ground deformation was reported for either of these minor events, although both were felt locally. Seismo-lineaments associated with both earthquakes correlate spatially with the DVFZ, as well as with the trend of aftershocks and ground deformation noted from the much larger M_L 6 earthquake of 1966 (Figure 4). SLAM provides the tools to recognize that the DVFZ is seismogenic based on data from recent magnitude 3.2 and 4.0 events, even without knowledge of the M_L 6.0 events of 1948 and 1966 along the same fault zone.

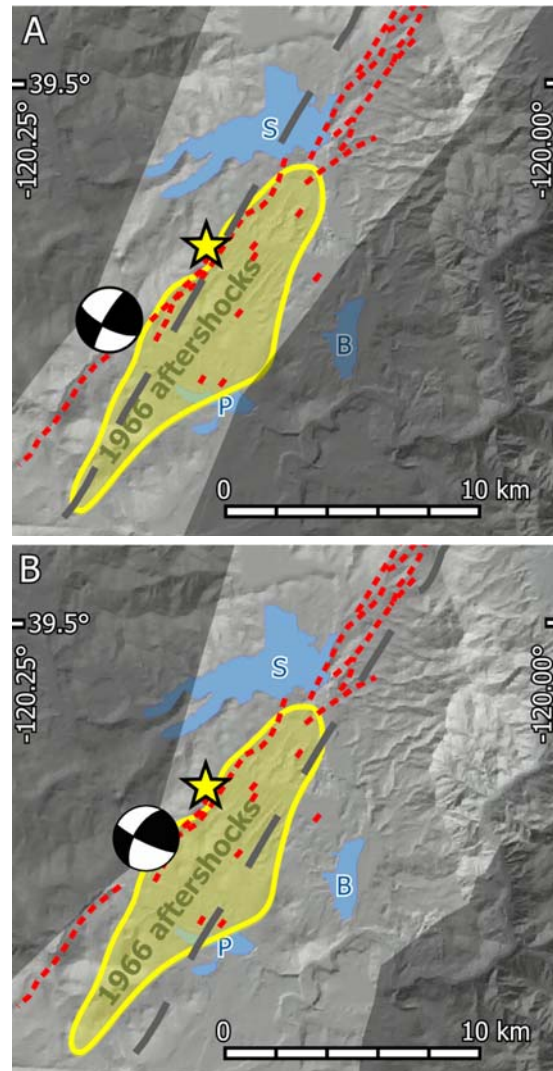


Fig 4. Focal mechanisms, seismo-lineaments (light gray), and traces of the mean nodal planes for inferred fault-plane solutions (dark gray dashed curves) for two minor earthquakes. [A] M 4 earthquake at 11.05 km depth on 3 July 1983. [B] M 3.2 earthquake at 5.344 km depth on 30 August 1992. The star marks the epicenter for the 1966 Truckee earthquake. Other symbols are the same as in Figure 3.

DISCUSSION

When well-located earthquake hypocenters coincide with a fault, and the slip characteristics defined by the corresponding earthquake focal mechanisms are compatible with slip indicators along the fault, it is



reasonable to conclude that the fault is seismogenic. SLAM provides several potential benefits for those who need to identify seismogenic faults. As seen in the DVZ example, SLAM can utilize data from small earthquakes to help identify seismogenic faults capable of large earthquakes. SLAM can be used along with traditional methods to help identify places where trench studies might produce useful information about suspected active faults. Seismo-lineament swaths might also be used to define survey tracks for airborne laser swath mapping (ALSM) along suspected fault trends. The combination of SLAM with ALSM to create bare-earth surface maps should be particularly useful in seismically active areas where forest cover has inhibited traditional geologic mapping, as is common in tropical and temperate rain forests.

The primary limitations in the application of SLAM to identify seismogenic faults are the availability and accuracy of hypocenter and focal mechanism data. The earthquake-seismology community should continue to create and routinely update searchable catalogues of relocated earthquakes (e.g., Waldhauser, 2013) and high-quality focal mechanism solutions, along with their uncertainty estimates. These data are only as good as the seismograph networks that collect them. The geoscience community should continue to stress the importance of building, maintaining, and improving seismograph networks in seismogenic areas worldwide, with appropriate shared/open-data policies, so that we can recognize earthquake hazards more effectively and assess the corresponding risks.

Acknowledgements: SLAM has been developed with assistance from Jeremy Ashburn, Brian Bayliss, Chris Breed, Bruce Byars, Ryan Campbell, David Cleveland, Jon Cook, Kelly Cronin, Jordan Dickinson, Daniel Lancaster, Ryan Lindsay, Mark Millard, Shane Prochnow, Tyler Reed, Stephen Secrest, Lauren Seidman Robinson, Keith Sverdrup and Lisa Zygo, with funds from AAPG, Baylor University, Colorado Scientific Society, Ellis Exploration, Ft. Worth Geological Society, Geological Society of America, GCAGS, Samson Resources, Roy Shlemon Scholarship Fund, Sigma Xi, and SIPES. I thank Ramon Arrowsmith for his helpful review.

References

- Cronin, V.S., (2010). A primer on focal mechanism solutions for geologists. Science Education Resource Center, Carleton College, accessible via http://serc.carleton.edu/files/NAGTWorkshops/structure04/Focal_mechanism_primer.pdf.
- Cronin, V.S., & K.E. Cronin, K.E., (2014). Revised geometry of nodal-plane uncertainty volume used in the seismo-lineament analysis method to locate seismogenic faults [abs.]. *Seismological Society of America Annual Meeting, Anchorage, Alaska*, accessible via http://www.seismosoc.org/meetings/2014/app/index.html#_14-698.
- Cronin, V.S., M.A. Millard, L.E. Seidman, & B.G. Bayliss, (2008). The Seismo-Lineament Analysis Method [SLAM] -- A reconnaissance tool to help find seismogenic faults. *Environmental & Engineering Geoscience*, 14(3) 199-219.
- Dziewonski, A.M., T.-A. Chou, & J.H. Woodhouse, (1981). Determination of earthquake source parameters from waveform data for studies of global and regional seismicity. *Journal of Geophysical Research*, 86, 2825-2852.
- Greensfelder, R., (1968). Aftershocks of the Truckee, California, earthquake of September 12, 1966. *Bulletin of the Seismological Society of America*, 58(5), 1607-1620.
- Hardebeck, J.L., & P.M. Shearer, (2002). A new method for determining first-motion focal mechanisms. *Bulletin of the Seismological Society of America*, 92, 2264-2276.
- Hawkins, F.F., R. LaForge, & R.A. Hansen, (1986). Seismotectonic study of the Truckee/Lake Tahoe area northeastern Sierra Nevada, California for Stampede, Prosser Creek, Boca, and Lake Tahoe dams. U.S. Bureau of Reclamation Seismotectonic Report 85-4, 210 p., plate I, scale 1:250,000.
- Kachadoorian, R., R.F. Yerkes & A.O. Waananan, (1967). Effects of the Truckee, California, earthquake of September 12, 1966. U.S. Geological Survey, Circular 573, 14 p.
- Lindsay, R.D., (2012). Seismo-lineament analysis of selected earthquakes in the Tahoe-Truckee area, California and Nevada. Waco, Texas, Baylor University, MS thesis, 147 p., accessible via <http://hdl.handle.net/2104/8441>.
- Millard, M.A., (2007). Linking onshore and offshore data to find seismogenic faults along the Eastern Malibu coastline. Waco, Texas, Baylor University, MS thesis, accessible via <http://hdl.handle.net/2104/5109>.
- Northern California Earthquake Data Center, (2013). Northern California earthquake catalog. Accessed 30 May 2014 via <http://quake.geo.berkeley.edu/ncedc/catalog-search.html>.
- US Geological Survey, (2014). Quaternary fault and fold database of the United States. Accessed 30 May 2013 via <http://quake.geo.berkeley.edu/ncedc/catalog-search.html>.
- Reasenber, P.A., & D. Oppenheimer, (1985). FPFIT, FPLOT, and FPPAGE: Fortran computer programs for calculating and displaying earthquake fault-plane solutions. U.S. Geological Survey, Open-File Report 85-739. Accessed 30 May 2014 via <http://pubs.er.usgs.gov/publication/ofr85739>.
- Reed, T.H., (2013). Spatial correlation of earthquakes with two known and two suspected seismogenic faults, north Tahoe-Truckee area, California. Waco, Texas, Baylor University, MS thesis, 96 p.
- Ryall, A., J.D. Van Wormer & A.J. Jones, (1968). Triggering of micro-earthquakes by earth tides, and other features of the Truckee, California, earthquake sequence of September, 1966. *Bulletin of the Seismological Society of America*, 58(1), 215-248.
- Shearer, P.M., (2009). Introduction to seismology [2nd ed.]. Cambridge, U.K., Cambridge University Press, 396 p.
- Stein, S., & M. Wysession, (2003). An introduction to seismology, earthquakes and Earth structure. Malden, Massachusetts, Blackwell Publishing, 498 p.
- Tsai, Y.-B., & K. Aki, (1970). Source mechanism of the Truckee, California earthquake of September 12, 1966. *Bulletin of the Seismological Society of America*. 60(4), 1199-1208.
- Waldhauser, F., (2001). HypoDD -- A program to compute double-difference hypocenter locations. U.S. Geological Survey Open-File Report 01-113.
- Waldhauser, F., (2009). Near-real-time double-difference event location using long-term seismic archives, with application to northern California. *Bulletin of the Seismological Society of America*, 99(5), 2736-2748, doi: 10.1785/0120080294.
- Waldhauser, F., (2013). Real-time double-difference earthquake locations for northern California. Accessed 6 August 2013 via <http://ddrt.ideo.columbia.edu>.
- Waldhauser, F., & W.L. Ellsworth, (2000). A double-difference earthquake location algorithm -- method and application to the northern Hayward Fault, CA. *Bulletin of the Seismological Society of America*, 90, 1353-1368.



INQUA Focus Group on Paleoseismology and Active Tectonics



paleoseismicity.org

NOTES



Progress in active bedrock normal fault investigations throughout the Mediterranean

Klaus Reicherter (1), Ioannis Papanikolaou (2), Jack Mason (1), Thomas Wiatr (1), Sascha Schneiderwind (1)

(1) RWTH Aachen University, Institute of Neotectonics and Natural Hazards, Lochnerstr. 4-20, 52064 Aachen, Germany

(2) Laboratory of Mineralogy & Geology, Department of Sciences, Agricultural University of Athens, 75 Iera Odos Str., 11855 Athens, Greece.

Abstract: Earthquakes in the Mediterranean larger than $M=5.5$ leave their imprint in the landscape as fault scarps. The majority of normal faults through this region comprise postglacial bedrock footwall scarps juxtaposed against Quaternary hanging-wall sediments. By using a combination of investigative techniques on both the footwall and hanging-wall, paleoseismologists are able to evidence individual paleoearthquakes and determine slip rates. Investigative techniques include t-LiDAR, geophysics, trenching and fault scarp dating. This information is then used to determine the seismic hazard of the individual fault. In this paper we provide a review of the state of the art in this field.

Key words: Bedrock normal fault, slip rate determination, geophysics, t-LiDAR, trenching, cosmogenic nuclide dating

INTRODUCTION

Decoding paleoearthquakes on normal bedrock fault scarps and their associated deposits on the hanging-wall is an important factor in estimating the seismic hazard potential of active fault zones. The Mediterranean region hosts many of these fault scarps with extensive outcrops of Mesozoic carbonate deposits of the Tethys. Typically the normal faults associated with the scarps are 15-30 km long, have a free-face height of several meters, slip rates of 0.3-1 mm/yr and recurrence periods of more than 1000 yrs. These normal faults occur in diffuse plate boundaries and back arc provinces and generate strong earthquakes from $5.5 \leq M \leq 7.0$. They are of great importance in terms of seismic hazards due to their proximity to human habitation. The last few destructive earthquakes in comparable tectonic settings demonstrated that these faults pose a significant threat due to their large number and long recurrence intervals.

POST GLACIAL SCARPS

The majority of the normal faults throughout the Mediterranean comprise bedrock fault scarps which are juxtaposed against Quaternary alluvial-colluvial or marine sediments (Figs. 1 and 2). These faults are easy to recognize as they offset smooth mountain slopes and have steeply dipping fault scarps that are several meters in height. These preserved fault scarps are coseismic and result from cumulative earthquake events on the individual fault. In the Mediterranean the common theory is that during glacial conditions the erosion rate of these bedrock fault scarps, and sediment deposition on the hanging-wall, was faster than the fault's slip-rate. This resulted in the bedrock fault scarp not being preserved in the landscape (Fig. 1a). In postglacial times, however, the improved climatic conditions reduced erosion rates allowing fault scarps caused by recurrent earthquakes to be preserved (Fig. 1b). Fault scarps can only be preserved when the slip rate is higher than the erosion rate (Benedetti et al., 2002; Papanikolaou et al., 2005; Reicherter et al. 2011). This is the situation we have throughout the Mediterranean and the preserved faults

are considered to be capable; a capable fault is defined as a fault that has significant potential to cause displacement at or near the ground surface (IAEA SSG-9, 2010). Normal fault scarps throughout the Mediterranean range in height from decimeters to many meters. Care must be taken when measuring scarp heights to estimate long-term throw rates as the height can be influenced by erosion and sedimentation; however, the preservation of many several-meter high scarps implies that regular seismic activity must have been occurring for a significant period since the last glacial maximum.

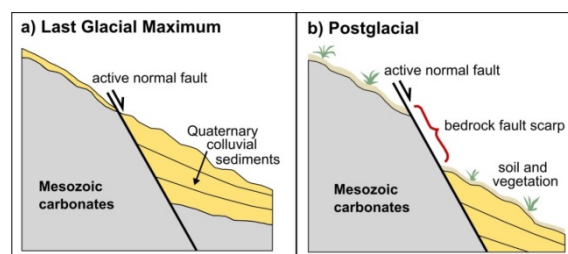


Figure 1: Geomorphology of a typical Mediterranean normal fault scarp with respect to climatic conditions (modified after Benedetti et al. 2002; Reicherter et al. 2011).

Not all of the normal faults throughout the Mediterranean juxtapose bedrock against Quaternary sediments. Many other faults are located in Tertiary - Quaternary sedimentary basins, and therefore do not have impressive morphological expressions. These faults are generally smaller in length and therefore can produce smaller magnitude earthquakes compared to the larger normal faults with exposed bedrock scarps (Wells and Coppersmith, 1994). The longest of these faults do pose a hazard if they are capable, and in order to determine this paleoseismological studies are needed on the individual faults. The techniques needed to study the larger bedrock faults are mentioned below; however, the same 'trenching study' techniques can be used for faults within sedimentary basins.



INVESTIGATION TECHNIQUES

Through studying the hanging-wall, fault scarp and footwall of these earthquake derived morphological features (Fig. 2), the reconstruction of prehistoric events in terms of their magnitude and intensity within an affected area is possible (Wells and Coppersmith, 1994; McCalpin, 2009). A review of the state of the art in this field is provided in the sections below:

Fault scarp dating and slip-rate determination

Dating of earthquake events is a central issue for paleoseismological studies. As many bedrock normal faults throughout the Mediterranean exhibit preserved fault scarps, it is possible to date when these scarps were first exposed to cosmic rays. This fault scarp dating technique, known as cosmogenic nuclide dating, has been carried out by various authors in central Greece (Sparta and Kaparelli fault, Benedetti et al., 2002, 2003), central Italy (Magnola-Velino fault, e.g., Palumbo et al., 2004; Schlagenhauf et al., 2011), the Hebgen Lake fault in Montana US (Zreda and Noller, 1998;), and northern Israel (Nahef East fault, Gran-Mitchell et al., 2001). In all of these studies the authors sampled and dated carbonate fault planes based on cosmogenic nuclide ^{36}Cl concentration. Locations on the fault plane where there is a rapid change in ^{36}Cl concentration define the sections that were exhumed by different earthquakes. These, therefore, define the paleo-ground levels or event horizons for each earthquake. When these event horizons are known, the ^{36}Cl concentrations can be transformed into ages that date each earthquake event. The distance between event horizons represents the amount of slip during each earthquake. This can then be used, in combination with empirical relationships (e.g., Wells and Coppersmith, 1994), to estimate the magnitude of paleoearthquakes. Event horizon determination is, therefore, the controlling factor when interpreting earthquake history. Fault scarps have also been relatively dated by correlating the enrichment/depletion of rare earth elements (REE). This technique has been successfully used on the Magnola-Velino fault in Italy by Carcaillet et al. (2008) and Manighetti et al. (2010). The Magnola-Velino fault was chosen as cosmogenic nuclide dating had already been undertaken on this fault and its Holocene earthquake history is known, which allowed correlations and comparisons to be made. The application of the ^{36}Cl dating technique relies hugely on sample site selection, and there are many pitfalls associated with this which need to be considered. A perfect sampling site would be a fresh bedrock scarp with no cemented colluvium attached to the fault plane, which is common in the Mediterranean region; the sampling site should be located away from nearby catchments and must show no evidence for any anthropogenic activity which may have contributed to the scarp's exhumation (see Fig 2).

Long term throw rates can be calculated using the height of exposed fault planes, assuming a post glacial exhumation date of 15 ± 3 ka. When undertaking this kind

of throw estimate, a great deal of care needs to be taken that the height of the fault plane used in the calculation is natural and has not been affected by processes such as erosion of cemented colluvium, human activity, or catchments as large throw-rate overestimations will result. Also, if these calculations are undertaken in areas where sedimentation is occurring, the throw-rate will be underestimated.

Hanging-wall investigations

The hanging-wall of normal faults throughout the Mediterranean are possibly the best place to focus paleoseismological studies, as within the hanging-wall sedimentary architecture is evidence for paleoearthquakes. The technique of paleoseismic trenching has been used for decades to identify earthquake event horizons and collect samples for dating paleoearthquakes. For normal faults where bedrock fault scarps are juxtaposed against Quaternary sediments, trenches can obviously only be excavated in the hanging-wall where no cemented colluvium is present. Within trench walls, sedimentary structures caused by coseismic earthquakes can be visualized very clearly, e.g., colluvial wedges, disrupted and displaced strata, grabens and half-grabens, sand blows, fissure fills, etc. Datable material within or buried under these sedimentary structures can provide dates for earthquakes, and with several generations of structures formed by different earthquakes, recurrence intervals for individual faults can be determined.

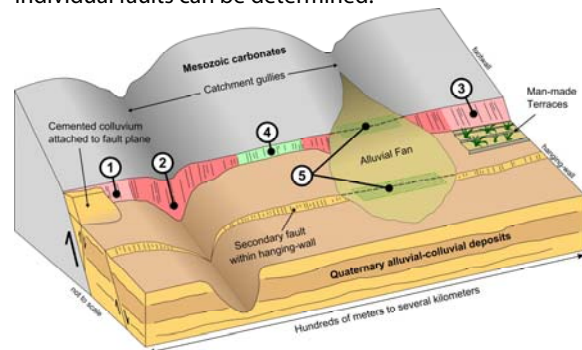


Figure 2. Sketch showing the features of a typical Mediterranean normal fault where paleoseismological investigations should be carried out. Fault scarp dating should be avoided at locations (1) due to presence cemented colluvium, (2) due to proximity to catchments, and (3) due to anthropogenic activity. Fault scarp dating should be undertaken at (4), and trenching investigations should be carried out where there is continuous sedimentation such as at alluvial fans (5).

Trench site selection is a major factor which will determine the quality of trenching results. An ideal trench site would have a continuous sediment record and contain sedimentary structures caused by recurrent earthquakes. Geophysical reconnaissance has been extensively used by many authors to determine good trench sites as sedimentary structures can be identified (e.g., Chow et al., 2001; Reiss et al., 2003) prior to the excavation and many surveys can be done in order to find optimum locations (e.g., Demanet et al., 2001;



Anderson et al., 2003; Alasset and Meghraoui, 2005; Grützner et al., 2012) since tectonogeomorphic features greatly vary along fault (Bubeck et al., 2014). In particular Ground Penetrating Radar (GPR) and Electrical Resistivity Tomography (ERT) have been used (e.g., Grützner et al., 2012). Previous work by many authors has shown that a large variety of sedimentary structures can be identified in GPR and ERT data. GPR in particular is ideally suited for imaging stratigraphic features of the shallow subsurface because it can detect contrasts in the dielectric properties by emitting high-frequency electromagnetic waves within the radiowave band into the subsurface (e.g. Daniels, 2004). Stratigraphic offset of sediments has been identified using GPR by many authors (e.g., Reicherter and Reiss, 2001; Anderson et al., 2003; Reiss et al., 2003; Alasset and Meghraoui, 2005) and a combination of GPR and ERT was used very successfully by Demanet et al. (2001) and Grützner et al. (2012) to image offset strata. Colluvial wedges have also been identified in GPR data by a number of authors (e.g., Chow et al., 2001; Christie et al., 2009; Denith et al., 2010); Reiss et al. (2003) identified event horizons beneath colluvial wedges indicating two co-seismic ruptures and post seismic sedimentation. Other structures that have been successfully imaged include small graben structures caused by antithetic faults (Christie et al., 2009), sand blows and fault related folding (Chow et al., 2001). Once a promising site has been identified using geophysics, a trench needs to be excavated (e.g., Grützner et al., 2012).

ERT measurements complete geophysical surveys by compensating for the handicaps of GPR studies. With GPR the electromagnetic waves are primarily influenced and attenuated by the moisture content of the subsurface materials (Daniel, 2004), but ERT rests on the electric conductivity of layers and is thus not limited by moisture, salinity or clays. Furthermore, ERT prolongs penetration depths commonly down to 25 – 30 m (e.g., McCalpin, 2009).

Rockfall wedges may be another indication of earthquake events (Reicherter et al. 2003). Rockfalls are usually quite localized when triggered by meteorological events; however, if the same rockfall wedges of similar thickness can be visualized over a large extent along a fault's strike, they are most likely formed due to earthquake shaking. This visualization can be done using geophysical techniques.

t-LiDAR

Terrestrial Light Detection and Ranging (t-LiDAR) has a wide range of applications with regards to active tectonics and paleoseismology. This remote sensing technique has been used by several authors to trace or map ruptured surfaces from recent earthquakes (Engelkemeir and Khan, 2008; Hunter et al., 2011). Other authors have used t-LiDAR to quantify the damage, side effects and urban structure changes related to strong events (Kayen et al., 2006; Pesci et al., 2010). These are descriptive approaches used to characterize, archive and document the surface ruptures as well as the primary and secondary effects of earthquakes. If the fault rupture is mapped along strike using t-LiDAR, high resolution morphological analysis can be performed with a high accuracy to characterize the fault in terms of tectonomorphology and slip distribution (Wilkinson et al., 2014). Wilkinson et al. (2010) used differential t-LiDAR to monitor the slip after fault ruptures and Karabacak et al. (2011) monitored aseismic surface creep along fault strike.

Wiatr et al. (*submitted*) carried out a long-range t-LiDAR investigation on various active bedrock faults on Crete. The authors describe a methodology (Fig. 3) for quantitatively determining areas along strike where the scarp has had minimal influence from erosion and sedimentation. These areas can then be confidently used for long-term throw rate calculations and also cosmogenic nuclide dating.

t-LiDAR data were also used in combination with the results of geophysical investigations on the near subsurface by Bubeck et al. (2014). Through studying the surface morphology (of the footwall, fault scarp, hanging-wall) and subsurface structures (sediment formations of the hanging-wall), the authors verified the presence of tectono-geomorphic features and determined their relationship with active extensional faulting. This multi-method approach is also useful to verify processes which modified the scarp height such as landslides in the hanging-wall. Up to now the application with t-LiDAR on naturally exposed bedrock scarps is rare; however it is slowly becoming more recognized as a valuable investigative technique.

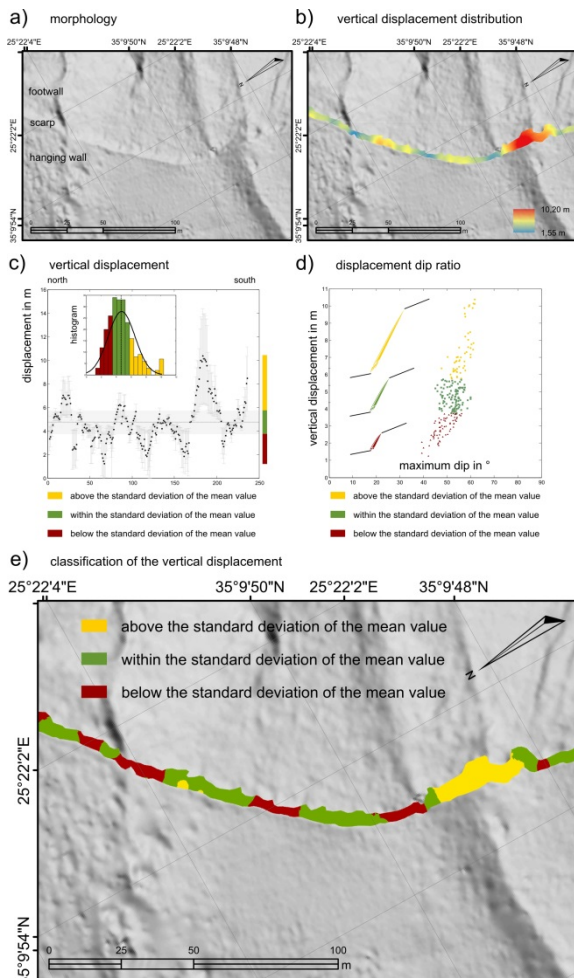


Figure 3: A simplified GIS workflow for the scarp analysis using the Kastelli fault in Crete as an example: a) morphology; b) the vertical displacement behavior along strike using near fault investigations such as scarp height profiling perpendicular to the fault plane (after Papanikolaou et al., 2005), and profiles of the vertical displacement along the detected fault segment (the vertical displacement are extracted from hundreds of cross sections); c) the histogram indicates a normal distribution of the vertical displacement and permits the mean value to be extracted within one standard deviation for all displacement results along each studied fault segment. This range of vertical displacement was chosen in order to split the displacement results into three groups: above, within, and below one standard deviation of the mean; d) linear regression between vertical displacement and dip of the detected fault segment (the subdivision is above (yellow), within (green) and below (red) one standard deviation from the mean); e) segmentation of the vertical displacement along the strike of the fault using GIS (based on c-d).

Other studies use t-LiDAR to produce high-resolution digital elevation models (DEMs) of active faults and earthquake ruptures (Kayen et al., 2006). These DEMs are used to determine the geometry of the fault scarp; fault slip rates can then be estimated using an exhumation date of 15 ± 3 ka (last glacial maximum). t-LiDAR data can also be used to determine the properties of surface roughness across non-weathered fault planes by using profiles perpendicular and parallel to the slip vector

(Candela et al. 2009). Wiatr et al. (*submitted*) carried out ruggedness analyses on naturally exhumed fault scarps on mainland Greece. The authors used the whole of the scanned scarp to determine structural changes over the scarp height and along strike. A methodology was produced to image surface features on the weathered fault plane which can be interpreted as being produced after exhumation from individual strong earthquakes.

CONCLUSIONS

A combination of techniques including t-LiDAR, geophysics, trenching and fault scarp dating must be used by paleoseismologists to determine the seismic hazards posed by individual faults throughout the Mediterranean. These faults are complex and are undergoing constant changes through erosion and sedimentation. Only when paleoseismologists understand these processes fully can reliable locations for sampling, trenching and slip-rate determination be chosen.

References

- Alasset, P.-J. & Meghraoui, M. (2005). Active faulting in the western Pyrenees (France): Paleoseismic evidence for late Holocene ruptures. *Tectonophysics* 409, 39–54.
- Anderson, K., Spotila, J. & Hole, J. (2003). Application of geomorphic analysis and ground-penetrating radar to characterization of paleoseismic sites in dynamic alluvial environments: an example from southern California. *Tectonophysics* 368, 25–32.
- Benedetti, L., Finkel, R., Papanastassiou, D., King, G., Armijo, R., Ryerson, F., Farber, D. & Flerit, F. (2002). Post-glacial slip history of the Sparta fault (Greece) determined by ^{36}Cl cosmogenic dating: Evidence for non-periodic earthquakes. *Geophys. Res. Lett.* 29, 1246.
- Benedetti, L., Finkel, R., King, G., Armijo, R., Papanastassiou, D., Ryerson, F.J., Flerit, F., Farber, D. & Stavrakakis, G. (2003). Motion on the Kaparelli fault (Greece) prior to the 1981 earthquake sequence determined from ^{36}Cl cosmogenic dating. *Terra Nova* 15, 118–124.
- Bubeck, A., Wilkinson, M., Roberts, G.P., Cowie, P.A., McCaffrey, K.J.W., Phillips, R. & Sammonds, P., (2014). The tectonic geomorphology of bedrock scarps on active normal faults in the Italian Apennines mapped using combined ground penetrating radar and terrestrial laser scanning. *Geomorphology*, (in press), <http://dx.doi.org/10.1016/j.geomorph.2014.03.011>
- Carcaillet, J., Manighetti, I., Chauvel, C., Schlagenhauf, A. & Nicole, J.M. (2008). Identifying past earthquakes on an active normal fault (Magnola, Italy) from the chemical analysis of its exhumed carbonate fault plane. *Earth Planet. Sci. Lett.* 271, 145–158.
- Candela, T., Renard, F., Bouchon, M., Brouste, A., Marsan, D., Schmittbuhl, J. & Voisin, C. (2009). Characterization of fault roughness at various scales: implications of three-dimensional high resolution topography measurements. *Pure Appl. Geophys.* doi: 10.1007/s00024-009-0521-2.
- Chow, J., Angelier, J., Hua, J., Lee, J. & Sun, R. (2001). Paleoseismic event and active faulting: from ground penetrating radar and high-resolution seismic reflection profiles across the Chihshang Fault, eastern Taiwan. *Tectonophysics* 333, 241–259.
- Christie, M., Tsofilas, G., Stockli, D. & Black, R. (2009). Assessing fault displacement and off-fault deformation in an extensional tectonic setting using 3-D ground-penetrating



- radar imaging. *Journal of Applied Geophysics* 68, Issue 1, 9 – 16.
- Daniels D.-J. (2004). *Ground Penetrating Radar*, 2nd Edition. IET Radar, Sonar, Navigation and Avionics Series 15.
- Demagnet, D., Renardy, F., Vanneste, K., Jongmans, D., Camelbeeck, T. & Meghraoui, M. (2001). The use of geophysical prospecting for imaging active faults in the Roer Graben, Belgium. *Geophysics* 66, 78-89.
- Denith, M., O'Neil, A. & Clark, D. (2010). Ground penetrating radar as a means of studying palaeofault scarps in a deeply weathered terrain, southwestern Western Australia. *Journal of Applied Geophysics* 72, 92 – 101.
- Engelkemeir, R.M., & Khan, S.D., (2008). Lidar mapping of faults in Houston, Texas, USA. *Geosphere*, 4 (1), 170-182, doi:10.1130/GES00096.1.
- Gran Mitchell, S., Matmon, A., Bierman, P.R., Enzel, Y., Caffee, M. & Rizzo, D. (2001). Displacement history of a limestone normal fault scarp, northern Israel, from cosmogenic ³⁶Cl. *J. Geophys. Res.* 106, 4247-4264.
- Grützner, C., Reicherter, K., Hübscher, C. & Silva, P. (2012). Active faulting and neotectonics in the Baelo Claudia area, Campo de Gibraltar (southern Spain). *Tectonophysics* 554-557, 241-259.
- Hunter, L. E., Howle, J. F., Rose, R. S., & Bawden, G. W., (2011). LIDAR-Assisted identification of an active fault near Truckee, California. *Bulletin of the Seismological Society of America*, 101, 1162-1181.
- International Atomic Energy Agency (IAEA) (2010). *Seismic Hazards in Site Evaluation for Nuclear Installations. Specific Safety Guide No. SSG-9.*
- Kayen, R., Pack, R.T., Bay, J., Sugimoto, S., Tanaka, H., (2006). Terrestrial-LIDAR Visualization of Surface and Structural Deformations of the 2004 Niigata Ken Chuetsu, Japan, Earthquake. *Earthquake Spectra*, 22: 147-162.
- Karabacak, V., Altunel, E. & Cakir, Z., (2011). Monitoring aseismic surface creep along the North Anatolian Fault (Turkey) using ground-based LIDAR. *Earth and Planetary Science Letters*, 304, 64-70.
- Manighetti, I., Boucher, E., Chauvel, C., Schlagenhauf, A. & Benedetti, L. (2010). Rare earth elements record past earthquakes on exhumed limestone fault planes, *Terra Nova* 22, 477-482.
- McCalpin, J. (2009). *Paleoseismology*, 2nd edition. International Geophysics Series Vol. 95. Academic Press.
- Palumbo, L., Benedetti, L., Bourlès, D., Cinque, A. & Finkel, R. (2004). Slip history of the Magnola fault (Apennines, Central Italy) from ³⁶Cl surface exposure dating: evidence for strong earthquakes over the Holocene, *Earth Planet. Sci. Lett.* 225, 163-176.
- Papanikolaou, I., Roberts, G. & Michetti, A. (2005). Fault scarps and deformation rates in Lazio-Abruzzo, Central Italy: comparison between geological fault slip-rate and GPS data. *Tectonophysics* 408, 147–176.
- Pesci, A., Loddo, F., Casula, G., Zampa, F., & Teza, G., (2010). Experience in mobile laser scanning by means of Lynx System in L'Aquila city. *Istituto Nazionale di Geofisica e Vulcanologia (INGV) report no. 133*, Sezione Bologna, Bologna, Italy, pp. 1-14.
- Reicherter, K., Jabaloy, A., Galindo-Zaldivar, J., Ruano, P., Becker-Heidmann, P., Morales, J., Reiss, S. & Gonzalez-Lodeiro, F. (2003). Repeated palaeoseismic activity of the Ventas de Zafarraya fault (S Spain) and its relation with the 1884 Andalusian earthquake. *Int. J. Earth Sci.* 92, 912-922.
- Reicherter, K., Hoffmann, N., Lindhorst, K., Krastel, S., Fernández-Steeger, T., Grützner, C., Wiatr, T. (2011). Active basins and neotectonics: morphotectonics of the Lake Ohrid basin (FYROM and Albania). *Z. dt. Geowiss.*, 162/2 217-234.
- Reicherter, K. & Reiss, S. (2001). The Carboneras Fault Zone (southeastern Spain) revisited with ground penetrating radar—Quaternary structural styles from high-resolution images. *Netherlands Journal of Geosciences*, 80, 129–138.
- Reiss, S., Reicherter, K. & Reuther, C.-D. (2003). Visualization and characterization of active normal faults and associated sedimentary structures by high-resolution ground penetrating radar (GPR). *Geol. Soc. London, Spec. Publ.* 211, 247-255
- Sagy, A., Brodsky, E.E. & Axen, G.J., (2007). Evolution of fault-surface roughness with slip. *Geology*, 35: 283-286.
- Schlagenhauf, A., Manighetti, I., Benedetti, L., Gaudemer, Y., Finkel, R., Malavieille, J. & Pou, K. (2011). Earthquake supercycles in Central Italy, inferred from ³⁶Cl exposure dating, *Earth Planet. Sci. Lett.* 307, 487-500.
- Wells, D.L. & Coppersmith, K.J. (1994). New empirical relationships among magnitude, rupture length, rupture width, rupture area, and surface displacement, *Bull. Seismol. Soc. Amer.* 84, 974-1002
- Wiatr, T., Papanikolaou, I., Fernández-Steeger, T., Reicherter, K. (submitted). Bedrock fault scarp history: Insight from t-LiDAR backscatter behaviour and analysis of structure changes
- Wiatr, T., Papanikolaou, I., Mason, J., Fernández-Steeger, T., Reicherter, K. (submitted). Normal bedrock fault scarp variation in an active region using long range t-LiDAR: Revisiting the fault scarps of Crete
- Wilkinson, M., McCaffrey, K. J., Roberts, G., Cowie, P. A., Phillips, R. J., Michetti, A. M., Vittori, E., Guerrieri, L., Blumetti, A. M., Bubeck, A., Yates, A. & Sileo, G., (2010). Partitioned postseismic deformation associated with the 2009 Mw 6.3 L'Aquila earthquake surface rupture measured using a terrestrial laser scanner. *Geophys. Res. Lett.* 37, L10309, doi:10.1029/2010GL043099.
- Wilkinson, M., Roberts, G.P., McCaffrey, K., Cowie, P.A., Faure Walker, J.P., Papanikolaou, I., Phillips, R.J., Michetti, A.M., Vittori, E., Gregory, L., Wedmore, L., and Watson, J., (2014). Slip distributions on active normal faults measured from LiDAR and field mapping of geomorphic offsets: an example from L'Aquila, Italy, and implications for modelling seismic moment release. *Geomorphology* /10.1016/j.geomorph.2014.04.026 (in press).
- Zreda, M., & Noller, J.S. (1998). Ages of prehistoric earthquakes revealed by cosmogenic chlorine-36 in a bedrock fault scarp at Hebgen Lake, *Science* 282, 1097-1099



INQUA Focus Group on Paleoseismology and Active Tectonics



paleoseismicity.org

NOTES



Late Quaternary evolution and potential for earthquake surface faulting along the Monferrato Arc, N Italy

Alessandro Maria Michetti (1), Livio Bonadeo (1), Fabio Brunamonte (1), Franz Livio (1), Gianfranco Fioraso (2)

- (1) Dipartimento di Scienza e Alta Tecnologia, Università degli Studi dell'Insubria, Via Valleggio 11, 22100, Como, Italy. Email: alessandro.michetti@uninsubria.it
(2) CNR – Istituto di Geoscienze e Georisorse, Torino, Italy.

Abstract: The Monferrato Arc is the westernmost arc of the Northern Apennines fold and thrust belt in the Po Plain foredeep. It belongs to the frontal sector of the most active mountain belt in Northern Italy. Since the historical and instrumental seismicity of this sector is moderate to low, the potential for earthquake surface faulting here has been overlooked and possibly underestimated. The objective of this work is to review the evidence for Late Quaternary active tectonics and capable faulting, based on: A) the reinterpretation of very detailed subsurface information collected by ENEL in 1980's for the Italian Nuclear siting program, including extensive seismic reflection investigations, boreholes, and trenching, B) new airphoto interpretation of the regional area, C) geomorphic and paleodrainage analysis, and D) field mapping. We conclude that the seismic landscape of the Monferrato Arc in terms of the maximum earthquake magnitude is not different from the other Quaternary tectonic structures of the Apennines arcs affecting the Po Plain foredeep; therefore coseismic surface faulting events along the Monferrato Arc should not be viewed as a surprise.

Key words: Monferrato Arc, Po Plain foredeep, seismic landscape, capable fault, earthquake surface faulting.

INTRODUCTION

The assessment of tectonic surface rupture hazard in regions of moderate historical seismicity is a crucial topic both in terms of understanding of recent landscape evolution and from the applied perspective (siting of critical facilities, safety of large metropolitan areas). The lessons learned after the 2010 Darfield is that most "unexpected" surface faulting events occurs in fact in areas characterized by poor or largely incomplete geological and geophysical database. In Italy, a similar debate has been triggered by the Emilia and Lombardia 2012 seismic sequence in N Italy (two main shocks of Mw ca. 6.0 along buried thrust faults). No unequivocal surface faulting has been identified during the 2012 seismic sequence due to the relatively low magnitude. However, available data show that the reference earthquake in the epicentral area is in the order of Mw 6.3 – 6.5 (e.g., Serva, 1990; Michetti et al., 2012; Vannoli et al. 2014). This is based on historical seismicity (several events with epicentral intensity MCS IX) and estimated rupture length for local Quaternary faults. Therefore, surface faulting hazard should be carefully evaluated for all relevant Quaternary tectonic structures of the Po Plain foredeep (e.g., Serva, 1990; Boccaletti et al., 2010; Picotti and Pazzaglia, 2008; Ponza et al., 2010; Galadini et al., 2012; Zerboni et al., 2014).

SEISMIC LANDSCAPE OF THE NONFERRATO ARC

Here we focus on the W sector of the foredeep. This is the area with the most controversial interpretation from the point of view of active tectonics and seismic potential. For instance, in the ITHACA catalogue of

capable faults (ITHACA, 2000), the official database for surface rupture hazard of the Geological Survey of Italy, available at <http://www.isprambiente.gov.it/en/projects/italy-hazards-from-capable-faulting>, the Monferrato Arc is regarded as a seismogenic structure with potential for surface faulting earthquakes; while in the DISS database (DISS WORKING GROUP, 2010) the catalogue of seismogenic sources compiled by INGV, <http://diss.rm.ingv.it/dissNet/>, the W Lombardia and Piemonte are essentially interpreted as areas lacking any evidence of active faulting and seismic sources with Mw > 5.5 (e.g., Vannoli et al., 2014).

In order to attack this issue, we conducted field investigation, geomorphic analyses and the revision of the large existing database of seismic reflection profiles covering the study area (for instance, see in Fig. 1 the available seismic reflection profiles in the PO1 and PO2 sites, as compiled by ENEL in 1984-1985) in order to assess the seismic landscape of the Monferrato Arc.

DISCUSSION AND CONCLUSIONS

Our investigations confirm that the Late Quaternary landscape evolution of the South-Central Piemonte is the result of the interaction between active tectonics and widespread phenomena of river avulsion and piracy, which affected virtually the whole Piemonte and nearby Liguria region. In fact, these dramatic changes in the regional drainage network are controlled by shortening and thrust fault growth, which started during Oligo-Miocene times and are still active with visible deformation rates (Carraro et al., 1995).

The development of the Apennines thrust fronts since Miocene gave rise to the progressive uplift of the Torino



and Monferrato Hills, and Casale - Valenza Palteaux (Fig. 2). The continuing deformation and displacement of the surficial deposits up to the Late Pleistocene to Holocene (Giraudi, 2014) allow us to regard the buried structures of the Monferrato Arc as potentially capable faults (IAEA, 2010). Therefore, based on the available data, the regional seismotectonic framework for the W Po Plain is comparable to the settings in the Emilia Arc or in the

Lombardia\Veneto S Alps, where several strong earthquakes have occurred (e.g., Modena 1212, Brescia 1222, Verona 1117). The seismic landscape of the Monferrato Arc thus includes potential surface faulting earthquakes, with M_{max} in the order of 6.0 – 6.5 (Michetti et al., 2012), and accompanied by considerable liquefaction and earthquake environmental effects.

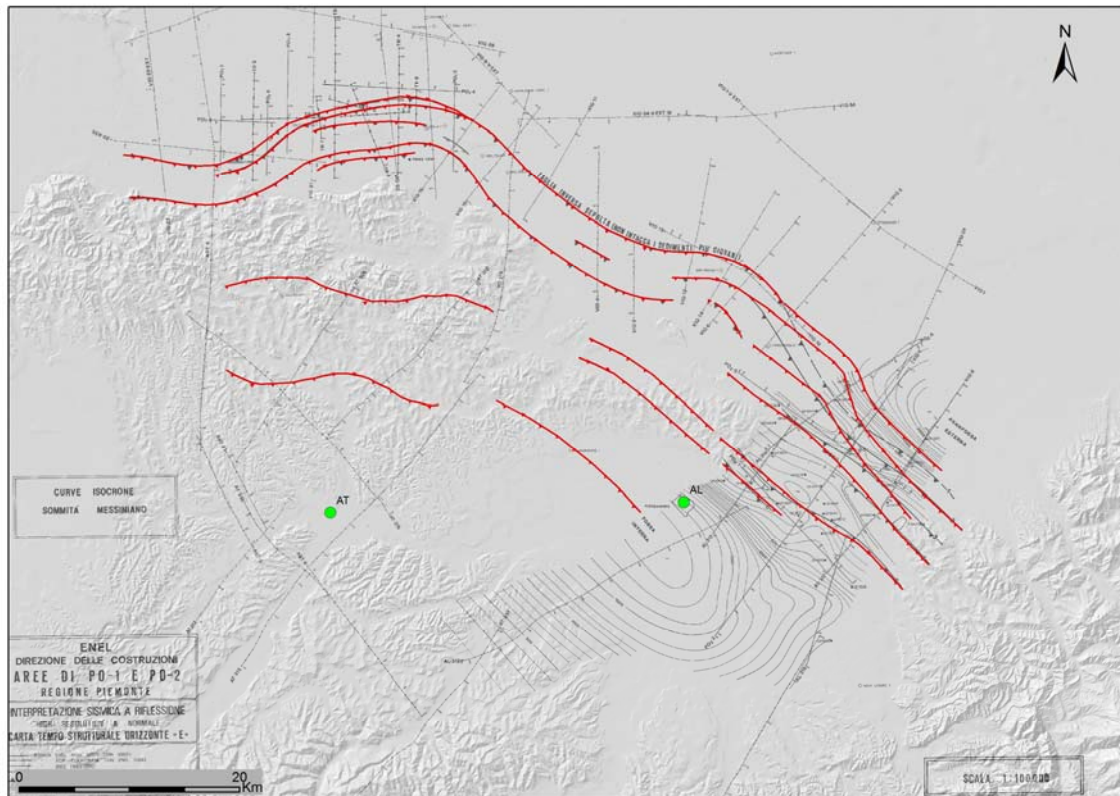


Fig. 1: Quaternary capable thrust faults showing evidence for capability in the Alessandria (AL) and Asti (AT) sector of the Monferrato Arc; in the background, the traces of the seismic reflection profiles that have been reinterpreted to map the potential for surface faulting in this area.

References

- Boccaletti M., Corti G. and Martelli L. (2010). Recent and active tectonics of the external zone of the Northern Apennines (Italy). *International Journal of Earth Sciences* Volume 100, Number 6 (2011), 1331-1348, DOI: 10.1007/s00531-010-0545-y
- Carraro F., G. Collo, M.G. Forno, M. Giardino, F. Maraga, A. Perotto and D. Tropeano (1995). L'evoluzione del reticolato idrografico del Piemonte centrale in relazione alla mobilità quaternaria. In: *Atti del Convegno "Rapporti Alpi-Appennino" e guida alle escursioni*, Peveragno (CN), 31 maggio-1 giugno 1994, Polino R. and R. Sacchi (Ed.), Acc. Naz. Sc., Roma, 14: 445-461.
- DISS WORKING GROUP (2010), Database of individual seismogenic sources (DISS), version 3.1.1: a compilation of potential sources for earthquakes larger than M 5.5 in Italy and surrounding areas. <http://diss.rm.ingv.it/diss/>
- Galadini F., E. Falcucci, P. Galli, B. Giaccio, S. Gori, P. Messina, M. Moro, M. Saroli, G. Scardia, A. Sposato (2012) – Time intervals to assess active and capable faults for engineering practices in Italy, *Engineering Geology*, 39–140, 50-65, ISSN 0013-7952, 10.1016/j.enggeo.2012.03.012
- Giraudi C. (2014), Quaternary studies as a tool to validate seismic hazard potential of tectonic structures: the case of the Monferrato thrust front (Vercelli Plain, NW Italy), *Alpine and Mediterranean Quaternary*, 27 (1), 2014, 5 - 28
- IAEA (2010). *Seismic Hazards in Site Evaluation for Nuclear Installations*. IAEA Safety Standard SSG-9 – Specific Safety Guide, 55 p., Vienna.
- ITHACA (2000) – ITHACA Italy Hazard from Capable Faults: a database of active faults of the Italian onshore territory. Michetti A.M., Serva L., and E. Vittori (eds.) Cd-rom and explication notes; last version available at http://www.mais.sinanet.isprambiente.it/ost/?LANG=en_US
- Livio F., A.M. Michetti, K. Mueller, L.Serva, G. Sileo, E. Vittori, R. Devoti, F. Riguzzi, C. Carcano, S. Rogledi, L. Bonadeo, F. Brunamonte and G. Fioraso (2012), Active compressional tectonics, Quaternary, *Journal of Geophysical Research*, accepted

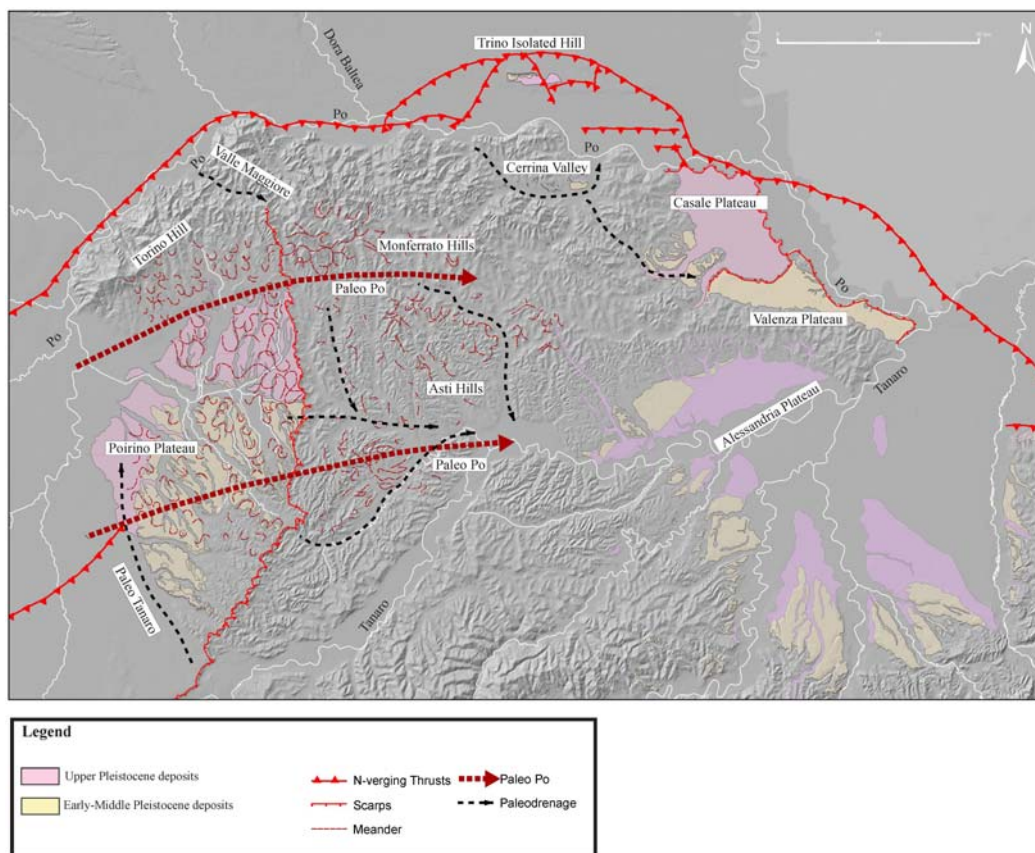


Fig. 2: Geomorphic map of the Monferrato Arc showing the Late Quaternary drainage diversion of the Po and Tanaro Rivers.

Michetti, A.M., F. Giardina, F. Livio, K. Mueller, L.Serva, G. Sileo, E. Vittori, R. Devoti, F. Riguzzi, C. Carcano, S. Rogledi, L. Bonadeo, F. Brunamonte and G. Fioraso (2012), Active compressional tectonics, Quaternary capable faults and the seismic landscape of the Po Plain (Northern Italy), *Annals of Geophysics*, 55(5), 969 - 1001.

Picotti, V. and F. J. Pazzaglia (2008), A new active tectonic model for the construction of the Northern Apennines mountain front near Bologna (Italy), *Journal of Geophysical Research: Solid Earth* (1978–2012) 113.B8 (2008).

Ponza, A., Pazzaglia, F.J. and V. Picotti (2010), Thrust-fold activity at the mountain front of the Northern Apennines (Italy) from quantitative landscape analysis, *Geomorphology*, 123(3), 211-231.

Serva, L. (1990), Il ruolo delle Scienze della terra nelle analisi di sicurezza di un sito per alcune tipologie di impianti industriali; il terremoto di riferimento per il sito di Viadana (MN), *Boll. Soc. Geol. Ital.*, 109, 375-411.

Vannoli, P., Burrato, P., & Valensise, G. (2014), The seismotectonics of the Po Plain (Northern Italy): tectonic diversity in a blind faulting domain. *Pure and Applied Geophysics*, 171(7), 1237-1250, 10.1007/s00024-014-0873-0

Zerboni, A., L. Trombino, C. Frigerio, F. Livio, A. Berlusconi, A.M. Michetti, H. Rodnight, C. Spötl (2014), The loess-paleosol sequence at Monte Netto: a record of climate change in the Upper Pleistocene of the central Po Plain, northern Italy, *Journal of Soils and Sediments*, 22 p., DOI 10.1007/s11368-014-0932-2



INQUA Focus Group on Paleoseismology and Active Tectonics



paleoseismicity.org

NOTES



Fault Displacement Hazard in urban areas in Italy: a first assessment

Guerrieri, Luca (1), Leoni Gabriele (1), Blumetti Anna Maria (1), Comerci Valerio (1), Livio Franz (2), Michetti Alessandro Maria (2), Vittori Eutizio (1) & Serva Leonello (3)

- (1) ISPRA, Geological Survey of Italy, Via Branconi 48, 00144 Roma, ITALY. Email: luca.guerrieri@isprambiente.it
(2) Dipartimento di Scienza e Alta Tecnologia, Università dell'Insubria, Via Valleggio, 11, 22100 Como, ITALY
(3) Consultant, Roma, ITALY

Abstract:

This paper provides a characterization of Fault Displacement Hazard (FDH) in Italy existing in the 73 most populated urban areas, with the aim to pinpoint the cities where this hazard is relevant and what directly threatens.

Despite the uncertainties in the location of the FDH areas, this study clearly shows that the problem is particularly evident in some cities located in Calabria and Sicily, in the inner sector of the Apennines and in Friuli. A more precise FDH zonation is recommended in these cities through detailed seismotectonic and paleoseismic investigations. Mitigation measures should be adopted for strategic settlements currently located in the FDH areas and the existing FDH should be taken into account in the areas that might be characterized by urban expansion in the next future.

Key words: Fault Displacement Hazard, urban areas, capable faults, Italy

INTRODUCTION

Fault Displacement Hazard (FDH) is a component of seismic hazard that puts the focus on the potential of coseismic tectonic surface rupture/deformation.

In Italy, FDH is a relevant issue that should not be disregarded although it is not yet properly taken into account in official seismic hazard maps and building codes. In fact, the Italian territory is characterized by:

- a great number of capable faults (i.e., faults able to produce significant ruptures or deformations at or near the topographic surface);
- a large urbanization, developed especially in the last decades, that has largely affected also areas in the proximity of capable faults.

This paper aims at providing a general indication of Fault Displacement Hazard in Italy in the 73 most populated urban areas (population > 60,000 inhabitants, up to about three million) with the aim to point out the cities:

- where this hazard does exist and is more relevant (in terms of maximum expected displacements) and
- what is directly threatened by surface faulting.

Of course, this is only a first zonation that shows where are the most critical areas: instead, a FDH assessment helpful for siting and land planning purposes, more detailed site investigations (Quaternary geology and paleoseismology) will be necessary, aimed at characterizing at larger scale the local pattern of capable faults and the age of last movements.

A MODEL FOR FAULT DISPLACEMENT HAZARD IN ITALY

In order to respond to the need of a specific knowledge regarding the Fault Displacement Hazard, the Italian Agency for Environmental Protection (ANPA, later APAT, now ISPRA) in the second half of the 1990s started the project ITHACA (ITaly HAZard from CApable faults). The project is aimed at building a tool for summarizing and making easily available information on capable faults,

based on published sources, field checks and *ad hoc* studies (for more details, see Comerci et al., 2013).

Currently, the ITHACA database contains about 2000 records (mapped in Fig. 1) including faults that exhibit at least one evidence of capability among the following: a) historical coseismic surface faulting; b) creep or surficial tectonic deformation; c) Late Pleistocene-Holocene paleoseismic evidence of ground rupture; d) displacement of Quaternary deposits/landforms. Moreover, the faults are classified according to the age of the last ascertained movement.

At the moment, the ITHACA database, although still incomplete and not homogeneous in terms of resolution and reliability of supporting data, is the most reliable tool for a first characterization of Fault Displacement Hazard in the entire Italian territory.

Among previous studies focused on this topic, Guerrieri et al. (2009) aimed at estimating the extent of urban areas exposed to surface faulting hazard within the ZS9 seismotectonic zonation of Italy. The analysis was conducted for each seismotectonic zone that was considered homogeneous also in terms of Fault Displacement Hazard, through the intersection of ITHACA and CORINE Land Cover databases. The results of the spatial analysis have been weighted through the introduction of a Fault Class parameter which takes into account the expected maximum displacement associated to capable faults in each zone. For this assessment a standard 300 m-wide buffer area around capable faults was considered.



INQUA Focus Group on Paleoseismology and Active Tectonics



paleoseismicity.org

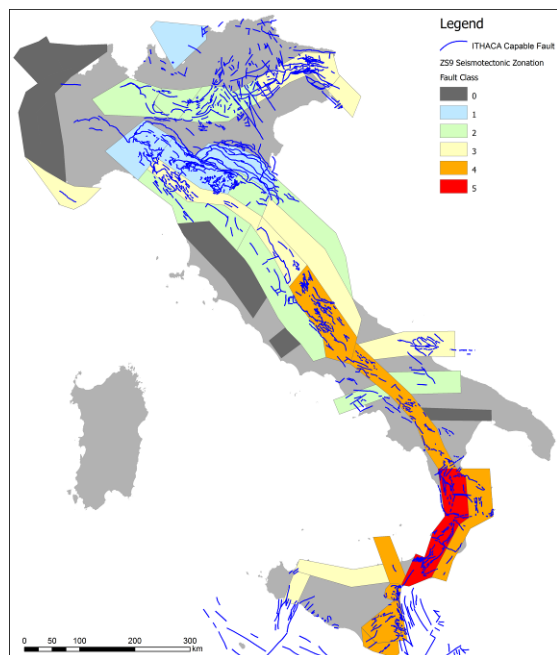


Fig. 1 – The ITHACA database (Comerci et al., 2013; <http://sqi1.isprambiente.it/geoportal/catalog/content/project/ithaca.page>) over the ZS9 seismotectonic zonation (Meletti and Valensise, 2004). According to the Fault Class parameter (Guerrieri et al., 2013), it is possible to evaluate maximum expected offsets: 1: 0-5 cm; 2: 5-20 cm; 3: 20-50 cm; 4: 50-150 cm; 5: up to 250 cm.

More recently, Guerrieri et al. (2013) proposed a more refined zonation of the area around the mapped capable faults, whose shape and width depend on the seismotectonic behaviour (i.e., type, style and amount of faulting) and the severity of the maximum expected earthquake. These two factors control also the amount of maximum expected surface displacements.

Five Fault Classes have been proposed: for each class, the maximum expected offsets and typical widths of the hazard zone in the footwall and in the hanging-wall of the master capable fault are provided. To this end, the capable faults recorded in ITHACA have been split into three main groups according to the prevalent fault kinematics (normal, reverse or strike-slip) and classified into different classes identified by specific maximum magnitude ranges (Fig. 3).

In order to take into account the uncertainties affecting the location of capable faults recorded in ITHACA, a standard minimum width value equal to 30 m has been introduced on both sides of the fault trace.

For normal faults (Fig. 2, above) surface primary ruptures (i.e., principal faulting, sensu Youngs et al., 2004) are expected to occur mainly in the hanging wall of the master fault: therefore, the model considers an asymmetric zone located mainly on the downthrown block, and width proportional to the maximum surface offset.

Conversely, in a compressive environment (Fig. 2, below) surface faulting features typically occur not only in correspondence to the main thrust but also at the hinge of the growing anticline, even with normal displacement,

for instance due to bending-moment faults. This zone may be located at a variable distance (up to some km) in the hanging wall of the main thrust. Thus, the width of hazard zone in the hanging wall of reverse faults has to be significantly larger than in the hanging wall of normal faults.

Concerning strike-slip environment, each individual fault segment should be managed as an independent source of Fault Displacement Hazard, locally with normal or reverse component. In this case, the hazard zone is symmetrical, 30 m wide, and expected width along principal faults (Petersen et al., 2011). Instead, when fault segmentation is not very well constrained, surface ruptures out of the 30m-hazard zone of the primary fault cannot be excluded.

Fault Class (with M_{max} ranges)	Normal faults		Examples
	Maximum expected offset (vertical)	Hazard zone width	
1 ($5.5 < M_{max} < 6.0$)	0-5 cm	HW: 50 m FW: 30 m	1997 Sept. 26, Colfiorito earthquake ($M_w = 6.0$)
2 ($6.0 < M_{max} < 6.3$)	5-20 cm	HW: 150 m FW: 30 m	2009 Apr. 06, L'Aquila earthquake ($M_w = 6.3$)
3 ($6.3 < M_{max} < 6.6$)	20-50 cm	HW: 300 m FW: 50 m	1915 January 13, Fucino earthquake ($M_s = 7.0$)
4 ($6.7 < M_{max} < 7.0$)	50-150 cm	HW: 250 m FW: 50 m	
5 ($M_{max} > 7.0$)	up to 250 cm	HW: 300 m FW: 100 m	

Fault Class (with M_{max} ranges)	Reverse faults		Strike-slip faults	
	Maximum expected offset (vertical)	Hazard zone width (*)	Maximum expected offset (horizontal)	Hazard zone width (**)
1 ($5.5 < M_{max} < 6.0$)	0-5 cm	HW: 100 m FW: 30 m	0-5 cm	FW: 30 m
2 ($6.0 < M_{max} < 6.3$)	5-20 cm	HW: 300 m FW: 30 m	5-20 cm	FW: 30 m
3 ($6.3 < M_{max} < 6.6$)	20-50 cm	HW: 400 m FW: 40 m	20-50 cm	FW: 30 m
4 ($6.7 < M_{max} < 7.0$)	50-150 cm	HW: 500 m FW: 50 m	50-150 cm	FW: 30 m

Fig. 2 – ITHACA capable faults have been classified into five classes according to the maximum magnitude range values. For each class, the following data are provided: the maximum expected offsets and typical width of the hazard zone in the hanging-wall (HW) and in the foot-wall (FW) of the master capable fault. Above: parameters for normal faults with some examples of documented surface faulting events. Below: the same parameters for reverse and strike-slip faults.



FAULT DISPLACEMENT HAZARD IN URBAN AREAS OF ITALY

In the frame of the ISPRA project “Quality of Urban Environment”, the FDH model proposed by Guerrieri et al. (2013) focused on the administrative territory of 73 Italian cities with population > 60,000 inhabitants, and in particular on the 45 cities that are crossed by capable faults (Fig. 3).

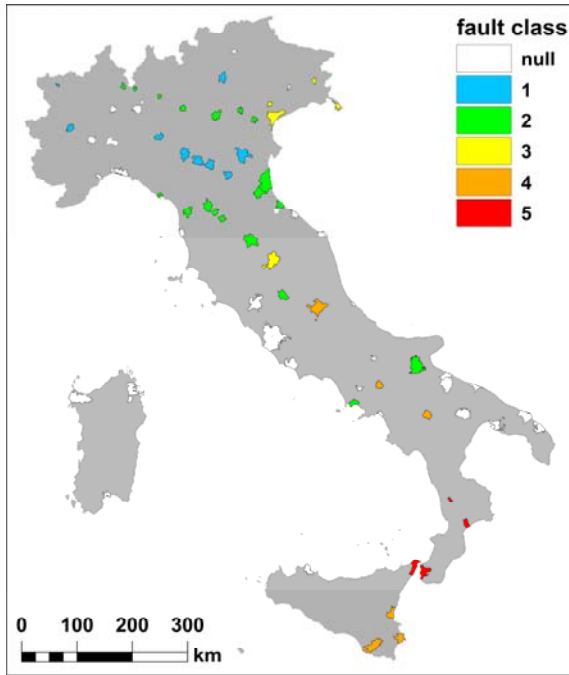


Fig. 3 – Fault Displacement Hazard in the administrative territory of 73 Italian cities with population > 60,000 inhabitants. More than 60% of the cities are affected by capable faults: maximum expected offsets are different according to the fault class (see text for more details).

Taking into account the maximum expected offsets, it is possible to state that Fault Displacement Hazard is very relevant:

- in four cities (Reggio Calabria, Messina Catanzaro and Cosenza), where offsets even larger than one meter are expected (class 5);
- in other six cities (Siracusa, L’Aquila, Ragusa, Benevento, Catania and Potenza), where maximum offsets are in the order of several decimeters up to one meter (class 4);
- in other five cities (Trieste, Udine, Perugia, Treviso and Venezia) where maximum displacements can reach 50 cm (class 3);

In the other 30 cities, Fault Displacement Hazard does exist but is much less relevant, as maximum displacements are in the order of some centimeters (19 cities) or lower (the remaining 11 cities).

In order to better characterize the Fault Displacement Hazard into these cities we have used the model proposed by Guerrieri et al. (2013). The total area

exposed to FDH in the 45 cities is equal to about 244 km², corresponding to 2.5 % of the study area. In particular the total area of class 5 risk areas is about 52 km², with a large contribution of Reggio Calabria (31 km²; 12% of the entire territory, see detail in Fig. 4, above) and Messina (14 km²; 7% of the entire territory). The total areas of class 4 and class 3 risk areas are respectively 68 km² (4.2%) and 15 km² (1.4%).

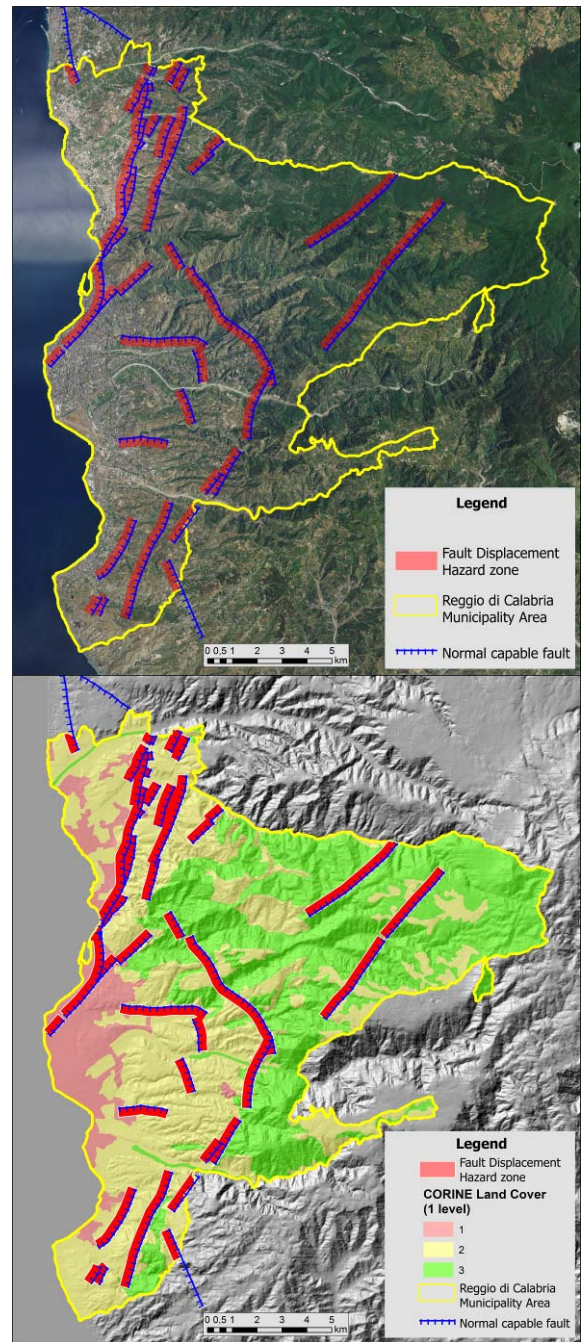


Fig. 4 – Above: Fault Displacement Hazard at Reggio Calabria mainly located in the hanging-wall of normal capable faults; Below: Land Cover distribution showing where FDH areas affect urban (code 1), agriculture (code 2) and natural (code 3) areas.



INQUA Focus Group on Paleoseismology and Active Tectonics



paleoseismicity.org

Considering the land cover/use of FDH areas (source: CLC 2006, EEA (2007)), only 17 % is already urbanized (class 1 of CORINE Land Cover). Conversely, most of the FDH areas (83 %) might still affect agricultural and natural areas, but might be theoretically affected by urban development in the next future (see map for Reggio Calabria in Fig. 4, below). The land cover affecting FDH areas for cities where FDH is relevant (Fault Class 3, 4 and 5) is reported in detail in Table 1.

Of course, these results cannot be taken as a Fault Displacement Hazard zonation, due to the large uncertainties introduced in the analysis by the low-resolution in the spatial location of some ITHACA capable faults and in the CORINE Land Cover (scale 1:100,000).

CONCLUSIONS

Despite the uncertainties in the location of the FDH areas, this study has clearly shown the Italian cities where Fault Displacement Hazard does exist and is relevant, in terms of maximum expected offsets and extension of risk area.

The problem is particularly evident in some cities located in Calabria and Sicily, in the inner sector of the Apennines and in Friuli.

More detailed seismotectonic and paleoseismic investigations are recommended in the municipality territory of these cities for a more precise FDH zonation in order to i) adopt mitigation measures for strategic settlements located in the FDH areas and ii) to take into account the existing FDH in the areas that could be characterized by urban expansion in the next future.

References

- Comerci V., Blumetti A.M., Di Manna P., Fiorenza D., Guerrieri L., Lucarini M., Serva L., Vittori E. (2013). ITHACA Project and Capable Faults in the Po Plain (Northern Italy). *Ingegneria Sismica*, Special Issue "Seismic risk in the Po Plain", Year XXX – n. 1-2 – January-June 2013, 36-50.
- EEA (2007) - CLC2006 technical guidelines. EEA Technical report No 17/2007, Copenhagen, Denmark. http://www.eea.europa.eu/publications/technical_report_2007_17
- Guerrieri L., Blumetti A.M., Di Manna P., Serva L. & Vittori E. (2009). The exposure of urban areas to surface faulting hazard in Italy: a quantitative analysis. *Boll.Soc.Geol.It. (Ital.J.Geosci.)*, Vol. 128, No. 1 (2009).
- Guerrieri L., Blumetti A.M., Comerci V., Di Manna P., Michetti A.M., Vittori E., and Serva L., (2013). Fault Displacement Hazard in Italy: input for siting of critical facilities and land planning. 4th International INQUA Meeting on Paleoseismology, Active Tectonics and Archeoseismology (PATA), 9-14 October 2013, Aachen, Germany, 91-94.
- Meletti C. and Valensise G. (2004) - Zonazione sismogenetica ZS9 - App.2 al Rapporto Conclusivo. Gruppo di Lavoro per la redazione della mappa di pericolosità sismica (Ordinanza PCM 20.03.03. n. 3274) – INGV <http://zonesismiche.mi.ingv.it/documenti/App2.pdf>
- Petersen M.D., Dawson T.E., Chen R., Cao T., Wills C.J., Schwartz D.P., and Frankel A.D. (2011) - Fault Displacement Hazard for Strike-Slip Faults. *Bull. Seism. Soc. Am.*, April 2011 vol. 101 no. 2 805-825, doi: 10.1785/0120100035.
- Youngs, R. R., Arabasz, W. J., Anderson, R. E., Ramelli, A. R., Ake, J. P., Slemmons, D. B., McCalpin J.P., Doser D.I., Fridrich, C.I., Swan F.H., Rogers A.M., Yount C.J., Anderson L.W., Smith K.D., Bruhn R.L. Knuepfer P.L.K., Smith R.B., dePolo C.M., O'Leary D.W., Coppersmith K.J., Pezzopane S.K., Schwartz D.P., Whitney J.W., Olig S.S. & Toro, G. R. (2004). A methodology for probabilistic fault displacement hazard analysis (PFDHA). *Earthquake Spectra*, 19, 191.

REF CLC

City	Fault Class	Total			Land cover of	Land cover of	Land cover of	FDH % Urban area
		Municipality Area	FDH area	FDH % area	FDH areas (CLC class 1)	FDH areas (CLC class 2)	FDH areas (CLC class 3)	
Catanzaro	5	112,7	4,7	4,2	0,6	3,2	1,0	12,3
Cosenza	5	37,9	2,0	5,3	0,0	1,3	0,7	0,3
Messina	5	213,8	14,3	6,7	2,7	4,8	6,8	19,1
Reggio di Calabria	5	239,0	30,9	12,9	3,8	18,6	8,5	12,3
Benevento	4	130,8	2,7	2,1		2,7	0,1	0,0
Catania	4	182,9	0,3	0,2		0,3	0,1	0,0
L'Aquila	4	473,9	37,6	7,9	1,2	5,7	30,7	3,2
Potenza	4	175,4	0,3	0,2		0,3		0,0
Ragusa	4	444,7	9,6	2,2	0,2	8,1	1,3	2,6
Siracusa	4	207,8	17,2	8,3	2,9	13,3	0,9	17,1
Perugia	3	449,5	7,2	1,6	0,4	5,5	1,3	6,1
Treviso	3	55,6	0,4	0,7	0,0	0,4		3,5
Trieste	3	85,1	5,6	6,6	1,6	0,8	3,2	28,3
Udine	3	57,2	1,8	3,1	0,6	1,2		34,3
Venezia	3	415,9	0,0	0,0		0,0		0,0

Table 1 – Fault Displacement Hazard in the administrative territory of 13 Italian cities with population > 60.000 inhabitants, crossed by capable faults with relevant expected offsets, ranging from tens cms up to more than one meter (Fault Class 3, 4 and 5) Areas are expressed in km². Land cover in FDH areas is based on CLC 2006 and points out urban (class 1), agriculture (class 2) and natural (class 3) areas.



INQUA Focus Group on Paleoseismology and Active Tectonics



paleoseismicity.org

NOTES



Correlation between fault activity and fault gouge color: toward the development of a new method for evaluating fault activity

Yukari Miyashita (1)

(1) Geological Survey of Japan, AIST, Central 7, Higashi 1-1-1, Tsukuba, Ibaraki 305-8567, Japan. Email: yukari-miyashita@aist.go.jp

Abstract: In order to establish a new method for evaluating fault activity, I analyzed relationship between fault activity and fault gouge characteristics. In particular, I focused on the color, clay mineral assemblage and chemical composition of fault gouges on active faults with different recurrence intervals. Trench excavation surveys, X-ray powder diffraction analysis, sequential selective extraction tests and color measurements of fault gouges were conducted. As the results, the fault gouge from the Otake fault showing 7-8 ky recurrence interval is mainly composed of illite and chlorite, and the gouge from the Hatakitoge fault with 41 ky or longer recurrence interval is mainly composed of halloysite. Color measurements revealed that white and greenish colors of gouges reflected the presence of chlorite, and beige and orange color gouges were derived from crystalline iron oxide. These results indicate that mineralogical and geochemical characteristics of fault gouges can distinguish clearly the difference of fault activity.

Key words: active fault, fault gouge, color measurement, fault activity

INTRODUCTION

One of the ultimate aims of paleoseismology is forecasting the next earthquake. The most effective approach to achieve this aim is reconstructing paleoearthquake recurrences by geomorphological and geological investigations, such as air-photo interpretations and trenching surveys.

During the last 15 years, however, Japanese islands have been suffered various inland earthquakes caused by unknown active faults, which were undetectable by geomorphological and paleoseismic investigations. The Western Tottori Prefecture earthquake in 2000 (Mw: 6.6) occurred where no active faults were not previously mapped, and presented a problem how to evaluate such active faults with ambiguous topography. Another important topic is how to evaluate the active faults without age-determinable sediments.

Kobayashi et al. (2003) and Kobayashi & Sugiyama (2004) suggested that areal distributions and color of fault rocks, especially fault gouges in the basement granite, might be effective indexes for evaluating 'fault maturity', based on the detailed field mapping and structural analysis of fault rocks in the Western Tottori area. Miyashita et al. (2011, 2012) and Manaka et al. (2012) analyzed mineral and chemical composition of fault gouges obtained from the Western Tottori area, and discussed about the correlation between 1) the composition and color of fault gouges, and 2) these fault gouge properties and recurrence intervals of each active fault. These results indicate that mineralogical and geochemical characteristics of fault gouges can clearly distinguish the difference of fault activity.

To verify the correlations between fault activity and mineralogical and chemical properties of fault gouges, I conducted trenching surveys and fault gouge analysis on the Iwakuni fault zone, Southwest Japan.

PALEOSEISMIC INVESTIGATIONS AND FAULT ROCKS SAMPLING

The Iwakuni fault zone is 44-km-long NE-SW trending right-lateral strike-slip faults located in Southwest Japan. I conducted trench excavation surveys on four sites. In this paper I present brief overview of two trenching surveys, which have the most valuable information to evaluate fault activity.

Based on the air-photo interpretations and field observations, the trace of the Otake fault is topographically clearer than that of the Hatakitoge fault. The result of trenching surveys show that the last surface rupturing earthquake of the Otake fault occurred after 2,800 years BP and that of the Hatakitoge fault occurred at least before 41,000 years BP, respectively.

Trench walls of the Otake fault exposed the fault fracture zone about 10-m-wide in basement sedimentary rocks consisting of the Jurassic accretionary complex and the Cretaceous porphyritic intrusive. Crosscutting relation of the fault plane to the Holocene sediments easily identified a fault plane, which slipped during the last event. The last fault plane is composed of 1-cm-thick fault gouge showing light gray, white and beige (Fig. 1a). In contrast, thick fault fracture zone was not exposed on the trench walls of the Hatakitoge fault, but several small fault zones accompanying 1-mm to 20-mm-thick fault gouges showing light green, white and orange were observed (Fig. 1b&c). I carefully sampled the fault gouges from each fault plane.



COLOR MEASUREMENTS OF FAULT GOUGES

I measured the color of the fault gouge samples by handy spectroradiometer. The first color measurement was conducted on the trench site at just after the

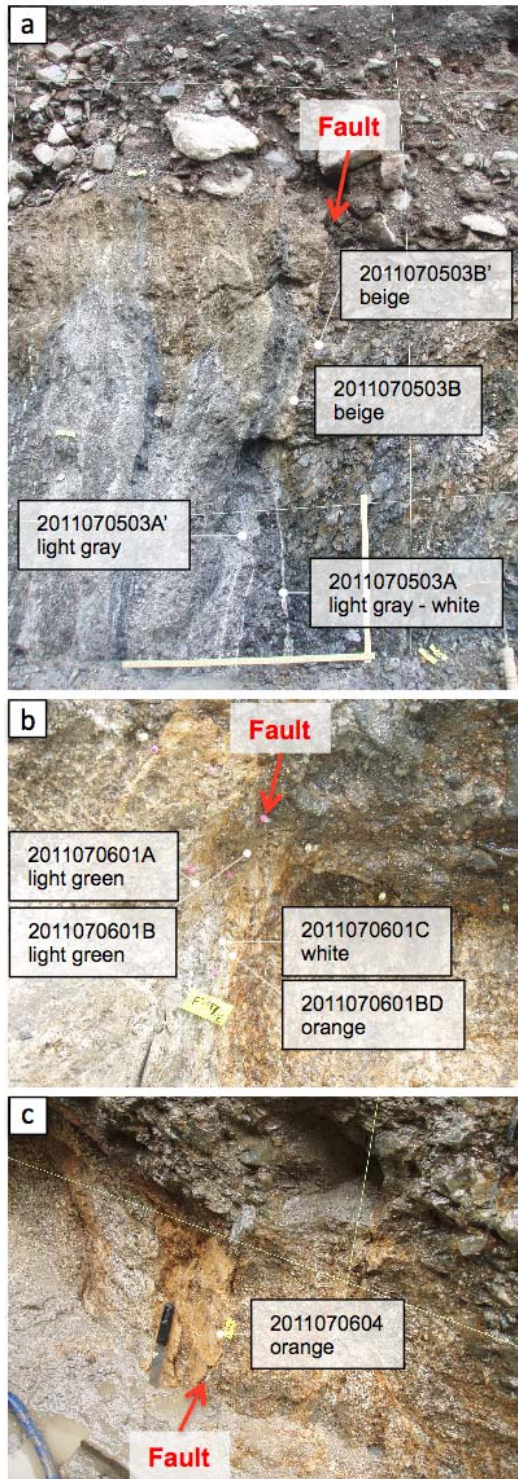


Fig. 1: Occurrences of the Otake fault (a) and Hatakitoge fault (b & c) on the trench walls. Sampling points, names and colors of fault gouges are shown.

sampling and the second measurement was conducted on the laboratory after air-drying. On the $L^*a^*b^*$ plot on $L^*a^*b^*$ color space, all of the Otake fault gouges and the Hatakitoge fault gouges showing light green and white were plotted same area. In contrast, the Hatakitoge fault gouges showing orange showed a different trend (Fig. 2). **MINERAL AND CHEMICAL COMPOSITIONS OF FAULT**

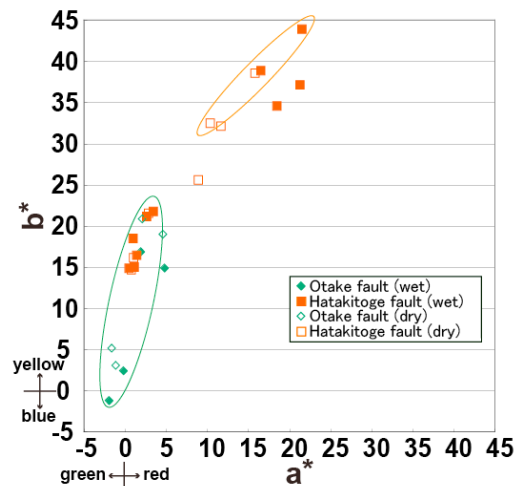


Fig.2: a^*-b^* diagram on the $L^*a^*b^*$ color system of the fault gouges from the Otake fault and Hatakitoge fault, Iwakuni fault zone, Japan.

GOUGES

The X-ray powder diffraction (XRD) analysis and sequential selective extraction tests of fault gouges were conducted. The sequential selective extraction tests consist of four steps, such as TAO extraction, CDB extraction, HCl extraction and HF extraction in order. The XRD analysis identified illite, chlorite, chlorite-smectite and smectite in the Otake fault gouges, by contrast, halloysite in the Hatakitoge fault gouges. Focusing on the Fe content of the sequential selective extraction tests, the Otake fault gouges and the Hatakitoge fault gouges were clearly distinguished, i.e. high Fe content of HCl extraction reflected presence of chlorite in the Otake fault gouges. On the sequential selective extraction tests, color measurements were also performed before and after each extraction steps. Remarkable points are: 1) after HCl extraction i.e. after chlorite dissolution, L^* value dramatically increases although a^* and b^* values do not change; 2) after CDB extraction both of a^* and b^* values drastically decrease although L^* value does not change, especially in beige and orange gouges; 3) the decrement of a^* and b^* values is larger on the samples showing originally high a^* and b^* values (Fig. 3).

DISCUSSION

The paleoseismic surveys of the Otake fault and Hatakitoge fault revealed that the last earthquake event occurred after 2,800 years BP and before 41,000 years BP, respectively. The long-term evaluation of the Iwakuni fault was reported that the last event of the Otake fault



was about 10,000–11,000 years ago (The Headquarters for Earthquake Research Promotion, 2004). The recurrence interval of the fault, therefore, is estimated

about 7-8 ky for the Otake fault and 41ky or longer for the Hatakitoge fault.

The results of the color measurements, XRD analysis and sequential selective extraction tests of the fault gouges indicate that both faults are clearly distinguished. It is possible to point out that the fault gouge properties reflect the fault activity.

Successive researches after the Western Tottori prefecture earthquake in 2000 revealed that correlation between characteristics of fault gouges, such as clay mineral assemblages, chemical compositions and color, and fault activity (e.g. Research Core for Deep Geological Environments, editor 2012).

The fault gouge properties described above and the correlation obtained from this study are consistent with the results of previous investigations of the Western Tottori. Accumulation of case studies for fault gouges showing various activities is needed to establish the method in the future.

Acknowledgements: I thank Dr. Mitsuo Manaka and Dr. Jun'ichi Itoh of the Geological Survey of Japan, Dr. Kenta Kobayashi of the Niigata University, Dr. Atsushi Kamei of the Shimane University, Dr. Keisuke Fukushi of the Kanazawa University for support of fieldwork and fruitful discussions. This study was mainly supported by Japan Nuclear Energy Safety Organization (2009-2011).

References

Kobayashi, K., Aizawa, Y., Umetsu, K., Oyama, A. & Yamamoto, R. (2003). Geological structure of the epicentral area of the 2000 Tottori-ken Seibu earthquake. *Annual Report on Active Fault and Paleoseismicity Researches*, Geological Survey of Japan/AIST, No.3, p.163-174. (in Japanese with English abstract)

Kobayashi, K. & Sugiyama, Y. (2004). Faults and fault rocks on aftershock area and surrounding area of the Western Tottori prefecture earthquake in 2000. *Chishitsu News* no.602, p.36-44. (in Japanese)

Manaka, M., Fukushi, K., Miyashita, Y., Itoh, J., Watanabe, Y., Kobayashi, K. and Kamei, A. (2012). Comparison of fault gouges in the aftershock area and the non aftershock area of 2000 Tottori-ken Seibu earthquake. *Jour. Geol. Soc. Japan*, Vol. 118, No. 8, p. 459-475. (in Japanese with English abstract and figure captions)

Miyashita, Y., Kobayashi, K., Kamei, A., Itoh, J., Manaka, M. & Fukushi, K. (2011). A new method for evaluating fault activity based on fault gouge properties: Occurrences and colors of fault gouge from western part of Tottori Pref. http://www2.jpgeu.org/meeting/2011/yokou/SSS032-P01_E.pdf

Miyashita, Y., Manaka, M., Itoh, J., Kobayashi, K., Kamei, A. & Fukushi, K. (2012). A new method for evaluating fault activity based on fault gouge properties. Abstracts Volume of 34th International Geological Congress. 29.3 #411

Research Core for Deep Geological Environments, editor (2012). Technical Report on the Review and Assessment Features, towards the Submission of the Preliminary Field Investigations of HLW Geological Disposals. Appendix 4. Geological Survey of Japan, AIST. <https://unit.aist.go.jp/dgcore/works/2012/GS/apdx4.html> (in Japanese)

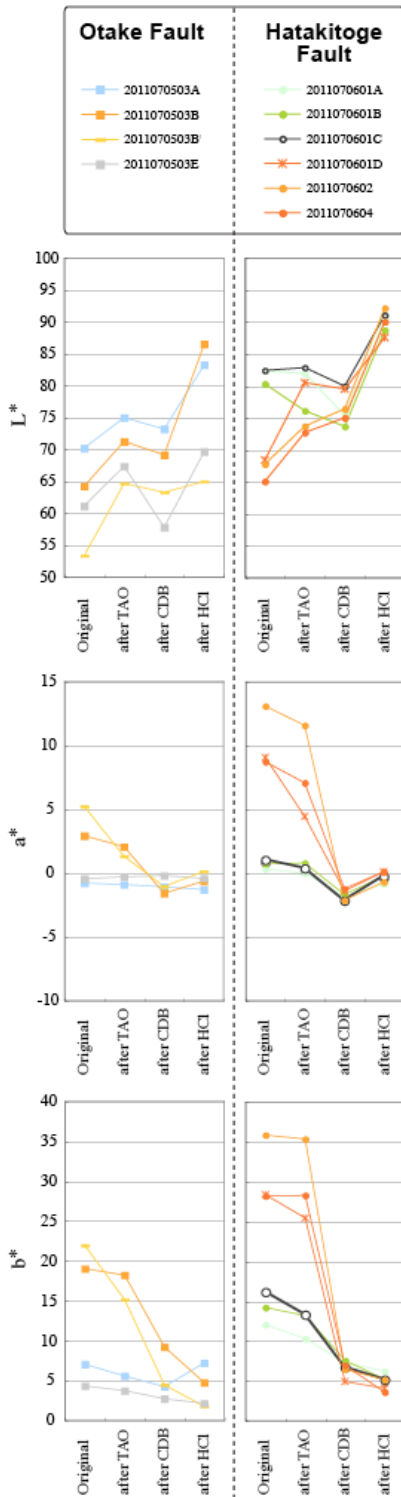


Fig. 3: Diagrams showing color changes at each step of the sequential selective extraction tests for fault gouges.



INQUA Focus Group on Paleoseismology and Active Tectonics



paleoseismicity.org

NOTES

Tuesday 23 September

Session Two: Remote Sensing and Geomorphology



High resolution topography and active faulting

J Ramón Arrowsmith (1)

(1) School of Earth and Space Exploration, Arizona State University, Tempe, AZ, 85287 USA.

Abstract: Active faulting can be characterized with topography sampling the ground once per meter or more. Such data come from traditional field survey and interpretation of stereo photography as well as airborne and terrestrial laser scanning and structure from motion. Applications of these data enhance efforts to map fault zones, reconstruct landscapes to infer offset, characterize surface process response to rock uplift, and quantify near-field coseismic displacements.

Key words: Tectonic geomorphology, earthquake geology, topography.

INTRODUCTION

Earthquake-related displacements of topography and subsequent surface process responses have meters of magnitude typically and occur across fault zones 10s to 1000s of meters wide and as much as 100s of km long. Given these spatial constraints, it is essential to have the right capability to measure the resultant features at the appropriate fine scale. High resolution topography samples the ground surface at least once per square meter and has decimeter local or preferably global accuracy. Analyses of high resolution topography in the study of active faulting can be divided into 4 classes: fault zone mapping, reconstructing surface deformation including offset, investigating geomorphic responses to active deformation, and differencing of repeat surveys for both fault and ground failure characterization.

In this contribution, I will briefly review high resolution topography and its applications to the study of active faulting, largely with a North American-centric perspective and one emphasizing research in which I have been engaged to some degree. Meigs (2013) provides a useful recent review.

GATHERING AND DISTRIBUTING HIGH RESOLUTION TOPOGRAPHIC DATA

Sampling the ground surface at a fine scale is an essential part of the earthquake geologist's toolbox. Early topographic data were gathered by tape and compass and plane table and alidade. Traditional photogrammetry and theodolite and laser range finder survey followed. LiDAR (Light Detection and Ranging) from both airborne and terrestrial platforms has revolutionized the accuracy, density, repeatability, and breadth of topographic survey in the last decade or so (Carter et al., 2007). Structure from Motion (Snavely et al., 2008) has recently made very fine topographic mapping with associated texture mapping accessible to many geomorphologists (James and Robson, 2012; Westoby et al., 2012; Fonstad et al., 2013).

LiDAR topography applied to active faulting initiated with the scans of the 1999 Hector Mine, California earthquake rupture (Hudnut, et al., 2002). That work led to important additional surveys including the ground breaking B4 San Andreas fault system scan (Bevis et al., 2005; <http://dx.doi.org/10.5069/G97P8W9T>) and the GeoEarthScope project (Prentice et al., 2009) both collected by the National Center for Airborne Laser Mapping in collaboration with the US Geological Survey and UNAVCO. These and many other data sets are now available for processing, analysis, and download via <http://www.opentopography.org/> (also with many tutorials and other documentation, Crosby et al., 2011).

Airborne laser swath mapping (ALSM) tends to provide a 2.5 dimensional (single z values for each x and y position) representation of topography with a few to tens of samples per square meter. It is usually represented by the regular sampling of a digital elevation model (DEM) at 0.25 to 1 m resolution and its various derived products (Figure 1A; slope, hillshade, contributing area, etc.). ALSM dataset coverage can be tens to hundreds of square km. Terrestrial laser scanning often is used to provide a more 3 dimensional representation from its tripod mounted perspective with 10s to 100s times higher shot densities and cm to dm resolution DEMs over usually less than 1 km² (e.g., Haddad et al., 2012). Both airborne and terrestrial LiDAR point clouds can be classified such that the vegetation and buildings can be separated from the ground returns. The latter may thus reveal important fault-related landforms below significant canopy (e.g., Haugerud et al., 2003; Sherrod et al., 2004; Kondo et al., 2008; Lin et al., 2012; and Langridge et al., 2014).

Finally, the Structure from Motion (SfM) technique allows for numerous photographs to be taken of a given target from multiple vantages and the scene structure (topography or 3D surface and even the camera positions) estimated. The images are also used to produce a seamless texture map to wrap on to the structural model or to assign color (R G, B) values to 3D points in the scene. SfM is valuable for mapping of fault zone topography or even paleoseismic trench



investigations using kite-, balloon-, drone-mounted, or hand held cameras (Johnson et al., 2014; Bemis et al., 2013; and Toké et al., 2013).

FAULT ZONE MAPPING

Classical mapping of fault zone landforms has been done in the field and with interpretation of aerial photography (Vedder and Wallace, 1970). The availability of high resolution topography along many active faults has been useful for uniform delineation of fault-related features and their relative activity (but does not supplant other approaches completely; Treiman et al., 2010). Many applications have been along strike-slip faults because of the availability of LiDAR data along the San Andreas Fault system in California (e.g., Arrowsmith and Zielke, 2009) and the Alpine Fault in New Zealand (Langridge et al., 2014). The tectonic landforms (ridges, troughs, offsets, scarps, benches, etc.) typically delineate blocks that comprise or bound the fault zone. They reflect the structural geology of the upper portion of the fault zone and their activity indicates where the next earthquake is most likely to slip.

RECONSTRUCTING SURFACE DEFORMATION

Where the fault slip rates are relatively high compared to the surface process rates, it is possible to reconstruct the landscape by backslipping faults and attributing the required displacements mostly to fault motion (e.g., Zielke and Arrowsmith, 2012). Cumulative offsets have been reconstructed using high resolution topography (airborne—e.g., Frankel et al., 2007; and terrestrial—e.g., Gold et al., 2011). High resolution topography has been particularly useful for reconstructing the fine scale offsets from a single or a few earthquakes (e.g., Salisbury et al., 2012; DePascale et al., 2014; Figure 1B). However, the tension between the ability to reconstruct many offsets by remote interrogation and the need for validation in the field is evident (Scharer et al., 2014). LiDAR scans following earthquake rupture enable clear mapping and offset reconstruction (e.g., Oskin et al., 2012; Quigley et al., 2012; Gold et al., 2013).

INVESTIGATING GEOMORPHIC RESPONSES TO ACTIVE DEFORMATION

Surface changes due to erosion and deposition may be similar in magnitude to the tectonic displacements. The resulting landforms reflect the geomorphic response to active deformation. High resolution topography enables the exploration of the responses at fine scales—that which is the most sensitive—the hillslopes and lowest order channels. Tectonic landforms such as the Dragon's Back pressure ridge along the San Andreas Fault in the Carrizo Plain have been illuminated using LiDAR-topography (Figure 1A; Hilley and Arrowsmith, 2008 and Hurst et al., 2013).

DIFFERENCING OF REPEAT TOPOGRAPHIC SURVEYS

Direct differencing of topographic data before and after earthquake displacements can reveal valuable information about the mechanical behaviour of the fault zone. Oskin et al., 2012 compared a LiDAR scan collected for regional topographic survey in 2006 (Glennie et al., 2014) with a high quality one collected in 2010 spanning the 2010 M7.2 El Mayor Cucupah earthquake and were able to demonstrate complex fault slip and block deformation patterns with only the vertical difference. Nissen et al., 2012 and Borsa and Minster (2012) compared portions of the B4 LiDAR dataset (Bevis et al., 2005) with synthetic displacements to explore optimal differencing methodology. Nissen et al., in press have been able to recover impressive 3D surface displacements using the Iterative Closest Point algorithm (Besl and McKay, 1992) on 50 m x 50 m samples from paired LiDAR datasets collected before and after the 2008 M6.9 Iwate Miyagi and 2011 M7.1 Fukushima-Hamadori Japanese earthquake ruptures. Finally, LiDAR differencing was used by Bray et al. (2012) to quantify the impact of liquefaction on critical infrastructure in Christchurch, New Zealand after the Feb 22, 2011 earthquake. They determined the repair rate for different pipe types as a function of angular distortion and lateral ground straining computed from repeat LiDAR surveys.

DISCUSSION

Increasing ease of access to previously gathered and new high and ultra high resolution topographic data along with the further refinement of analysis techniques and inevitable future earthquakes yield great opportunity and urgency in the study of high resolution topography and active faulting. Processing and filtering enhancements help us to find the signal in all of the data. For example, Hilley et al. 2010 used a wavelet approach to delineate and morphologically date fault scarps in high resolution topography. DeLong et al., 2010 analysed high resolution topography along the San Andreas Fault using spectral power approach to decompose the topographic signal into different wavelengths and orientations and evaluated the statistical significance of the periodic tectonic landforms along the fault zone. Finally, high resolution topography and their depiction of geomorphic and tectonic processes are a valuable asset in geoscience education.

Acknowledgements: Many thanks for numerous discussions with C. Crosby, G. Hilley, E. Kleber, T. Maruyama, E. Nissen, K. Okumura, M. Oskin, B. Salisbury, S. Saripalli, K. Scharer, Z. Wei, O. Zielke. Many thanks to the organizing committee for the PATA Days INQUA meeting and to Christoph Gruetzner for handling the review of this manuscript. The National Center for Airborne Laser Mapping has been a leader in the acquisition of research grade LiDAR topography. This work has been supported by the Southern California Earthquake Center, the US Geological Survey, and the US National Science Foundation.



References

- Arrowsmith, J. R., and Zielke, O., Tectonic geomorphology of the San Andreas Fault zone from high resolution topography: an example from the Cholame segment, *Geomorphology*, doi:10.1016/j.geomorph.2009.01.002, 2009.
- Bemis, S. P., Walker, L. A., Burkett, C., Devore, J. (2013). Use of 3D models derived from handheld photography in paleoseismology. Paper No. 47-9, *Geological Society of America Abstracts with Programs*. Vol. 45, No. 7, p.147.
- Bevis, M. and 18 others (2005). The B4 project: Scanning the San Andreas and San Jacinto fault zones (Abstract H34B-01), *Eos Trans. AGU* 86, no. 52 (Fall Meet. Suppl.), H34B-01.
- Besl, P. J., McKay, N. D. (1992). A method for registration of 3-D shapes. *IEEE Transactions on Pattern Analysis and Machine Intelligence* 14 (2), 239-256.
- Borsa, A., Minster, J. B. (2012). Rapid Determination of Near-Fault Earthquake Deformation Using Differential Lidar. *Bulletin of the Seismological Society of America*. 102, 1335-1347.
- Bray, J. D., O'Rourke, T. D., Cubrinovski, M., Zupan, J. D., Jeon, S. S., Taylor, M., Toprak, S., Hughes, M., van Ballegooy, S., Bouziou, D. (2012). Liquefaction impact on critical infrastructure in Christchurch, final report, US Geological Survey award number G12AP20034.
- Carter, W. E., Shrestha, R. L. and Slattton, K. C. (2007). Geodetic Laser Scanning, *Physics Today*, pp.41-47
- Crosby, C. J., Arrowsmith J. R., Nandigam, V., and Baru, C. (2011). Online access and processing of LiDAR topography data in *Geoinformatics: Cyberinfrastructure for the Solid Earth Sciences*, eds. G. R. Keller and C. Baru, Cambridge University Press.
- De Pascale, G. P., Quigley, M. C., & Davies, T. R. (2014). Lidar reveals uniform Alpine fault offsets and bimodal plate boundary rupture behavior, New Zealand. *Geology*, G35100-1.
- Fonstad, M.A., Dietrich, J.T., Courville, B.C., Jensen, J.L., and Carbonneau, P.E. (2013). Topographic structure from motion: A new development in photogrammetric measurement. *Earth Surface Processes and Landforms*, v. 38, p. 421-430, doi: 10.1002/esp.3366.
- Frankel, K.L., Dolan, J.F., Owen, L.A., Finkel, R.C., and Hoeft, J.S. (2007). Spatial variations in slip rate along the Death Valley-Fish Lake Valley fault system from LiDAR topographic data and cosmogenic ¹⁰Be geochronology: *Geophysical Research Letters*, v. 34, doi:10.1029/2007GL030549.
- Glennie, C., Hinojosa, A., Nissen, E., Kusari, A., Oskin, M., Arrowsmith, J. R., Borsa, A. (2014). Optimization of Legacy LiDAR Datasets for Measuring Near-Field Earthquake Displacements, *Geophysical Research Letters*, DOI: 10.1002/2014GL059919.
- Gold, R. D., Cowgill, E., Arrowsmith, J. R., Chen, X., Sharp, W., Cooper, K., Wang, X. (2011). Faulted terrace risers place new constraints on the late Quaternary slip rate for the central Altyn Tagh Fault, northwest Tibet, *Geological Society of America Bulletin*, v. 123, no. 5/6, p. 958-978, doi:10.1130/B30207.1.
- Gold, P. O., Oskin, M. E., Elliott, A. J., Hinojosa-Corona, A., Taylor, M. H., Kreylos, O., Cowgill, E. S. (2013). Coseismic slip variation assessed from terrestrial lidar scans of the El Mayor-Cucapah surface rupture. *Earth and Planetary Science Letters*. 366(3013):151-162.
- Haddad, D.E., Akciz, S.O., Arrowsmith, J.R., Rhodes, D.D., Oldow, J.S., Zielke, O., Toké, N.A., Haddad, A.G., Mauer, J., and Shilpakar, P. (2012). Applications of airborne and terrestrial laser scanning to paleoseismology. *Geosphere*, v. 8, p. 771-786, doi: 10.1130/GES00701.1.
- Haugerud, R.A., Harding, D.J., Johnson, S.Y., Harless, J.L., Weaver, C.S., Sherrod, B.L. (2003). High-resolution Lidar topography of the Puget Lowland, Washington—a bonanza for earth science. *GSA Today*, Geological Society of America 13 (6), 4-10.
- Hilley, G. E., and Arrowsmith J. R. (2008). Geomorphic response to uplift along the Dragon's Back pressure ridge, Carrizo Plain, California, *Geology*, v. 36; no. 5; p. 367-370; doi: 10.1130/G24517A.1.
- Hilley, G. E., Prentice, C. S., DeLong, S., Blisniuk, K., Arrowsmith, J. R. (2010). Morphologic dating of fault scarps using airborne laser swath mapping (ALSM) data, *Geophysical Research Letters*, 37, L04301, doi:10.1029/2009GL042044.
- Hudnut, K.W., Borsa, A., Glennie, C., and Minster, J.B. (2002). High-resolution topography along surface rupture of the 16 October 1999 Hector mine, California, earthquake (Mw 7.1) from airborne laser swath mapping. *Seismological Society of America Bulletin*, v. 92, p. 1570-1576, doi: 10.1785/0120000934.
- Hurst, M. D., Mudd, S. M., Attal, M., Hilley, G. (2013). Hillslopes record the growth and decay of landscapes, *Science*, 341, 868-871, doi:10.1126/science.1241791.
- James, M.R., and Robson, S. (2012). Straightforward reconstruction of 3D surfaces and topography with a camera: Accuracy and geoscience application. *Journal of Geophysical Research*, v. 117, F03017, doi: 10.1029/2011JF002289.
- Johnson, K., Nissen, E., Saripalli, S., Arrowsmith, J. R., McGarey, P., Scharer, K., Williams, P., Blisniuk, K. (2014). Rapid mapping of ultra-fine fault zone topography with Structure from Motion. *Geosphere*, v. 10; no. 5; p. 1-18; doi:10.1130/GES01017.1.
- Kondo, H., Toda, S., Okamura, K., Takada, K., Chiba, T. (2008). A fault scarp in an urban area identified by LiDAR survey: a Case study on the Itoigawa-Shizuoka Tectonic Line, central Japan. *Geomorphology* 101, 731-739.
- Langridge, R.M.; Ries, W.F.; Farrier, T.; Barth, N.C.; Khajavi, N.; De Pascale, G.P. (2014). Developing sub 5-m LiDAR DEMs for forested sections of the Alpine and Hope faults, South Island, New Zealand : implications for structural interpretations. *Journal of Structural Geology*, 64: 53-66; doi: 10.1016/j.jsg.2013.11.007.
- Lin, Z., Kaneda, H., Mukoyama, S., Asada, N., Chiba, T. (2013). Detection of subtle tectonic-geomorphic features in densely forested mountains by very high-resolution airborne LiDAR survey, *Geomorphology* v. 182, p. 104-115.
- Meigs, A. (2013). Active tectonics and the LiDAR revolution, *Lithosphere*, v. 5, p. 226-229, doi:10.1130/RF.L004.1.
- Nissen, E., Krishnan, A. K., Arrowsmith, J. R., Saripalli, S. (2012). Three-dimensional surface displacements and rotations from differencing pre- and post-earthquake Lidar point clouds, *Geophysical Research Letters*, v. 39, L16301, doi:10.1029/2012GL052460.
- Nissen, E., Maruyama, T., Arrowsmith, J. R., Elliott, J. R., Krishnan, A. K., Oskin, M. E., Saripalli, S., Coseismic fault zone deformation revealed with differential LiDAR: examples from Japanese Mw 7 intraplate earthquakes, *Earth and Planetary Science Letters*, in press.
- Oskin, M., Arrowsmith, J.R., Corona, A.H., Elliott, A.J., Fletcher, J.M., Fielding, E., Gold, P.O., Garcia, J.J.G., Hudnut, K.W., Liu-Zeng, J., Teran, O. J., Complex surface rupture of the El Mayor-Cucapah earthquake imaged with airborne lidar: *Science*, v. 335, p. 702-705, 2012.
- Prentice, C. S., Crosby, C. J., Whitehill, C. S., Arrowsmith, J. R., Furlong, K. P., Phillips, D. A. (2009). GeoEarthScope LiDAR illuminates northern California's active faults. *EOS Transactions of the American Geophysical Union*, v. 90, no. 7, p. 55, 2009.
- Quigley, M., Van Dissen, R., Litchfield, N., Villamor, P., Duffy, B., Barrell, D., Furlong, K., Stahl, T., Bilderback, E., Noble, D. (2012). Surface rupture during the 2010 Mw 7.1 Darfield (Canterbury, New Zealand) earthquake: implications for fault rupture dynamics and seismic-hazard analysis, *Geology* 40 (1) p. 55-59.
- Salisbury, J. B., Rockwell, T. K., Middleton, T. J., Hudnut, K. W., (2012). LiDAR and Field Observations of Slip Distribution for the Most Recent Surface Ruptures along the Central San



- Jacinto Fault. *Bulletin of the Seismological Society of America*, 102 (2): 598 DOI: 10.1785/0120110068.
- Scharer, K. M., Salisbury, J. B., Arrowsmith, J. R., Rockwell, T. K., Southern San Andreas Fault Evaluation field activity (2014). Approaches to measuring small geomorphic offsets – challenges and recommendations for active fault studies, *Seismological Research Letters*, v. 85, no. 1, ppl 68 - 76.
- Sherrod, B.L., Brocher, T.M., Weaver, C.S., Bucknam, R.C., Blakely, R.J., Kelsey, H.M., Nelson, A.R., Haugerud, R.A. (2004). Holocene fault scarps near Tacoma, Washington, USA. *Geology* 32, 9–12.
- Snaveley, N., Seitz, S.N., and Szeliski, R. (2008). Modeling the world from internet photo collections. *International Journal of Computer Vision*, v. 80, p. 189–210, doi: 10.1007/s11263-007-0107-3.
- Toké, N.A., Salisbury, J. B., Arrowsmith, J. R., Kellum, L.T., Matheson, E., Carlson, J.K., Horns, D., Sato, T., Abueg, N., Anderson, J., and Selck, J. (2013). Documenting at least 1300 years of aseismic slip: en-echelon shear bands and small-scale ground cracking at the Dry Lake Valley Paleoseismic site along the central San Andreas Fault, 2013 SCEC Annual Meeting, poster #025.
- Treiman, J.T., Perez, F.G., and Bryant, W.A. (2010). Utility of combined aerial photography and digital imagery for fault trace mapping in diverse terrain and vegetation regimes: Final Technical report to U.S. Geological Survey, National Earthquake Hazards Reduction Program, award number 08HQGR0096, 57 p., <http://earthquake.usgs.gov/research/external/reports/08HQGR0096.pdf>.
- Vedder, J.G., Wallace, R.E. (1970). Map showing recently active breaks along the San Andreas and related faults between Cholame valley and Tejon Pass, California. U.S. Geological Survey Miscellaneous Geologic Investigations Map 1-574, scale 1:24,000.
- Westoby, M.J., Brasington, J., Glasser, N.F., Hambrey, M.J., and Reynolds, J.M. (2012). ‘Structure-from-Motion’ photogrammetry: A low-cost, effective tool for geoscience applications. *Geomorphology*, v. 179, p. 300–314, doi: 10.1016/j.geomorph.2012.08.021.
- Zielke, O., and J. R. Arrowsmith (2012). LaDiCaoz and LiDARimager -MATLAB GUIs for LiDAR data handling and lateral displacement measurement, *GeoSphere*, v. 8, no. 1, p. 206–221, doi:10.1130/GES00686.1.

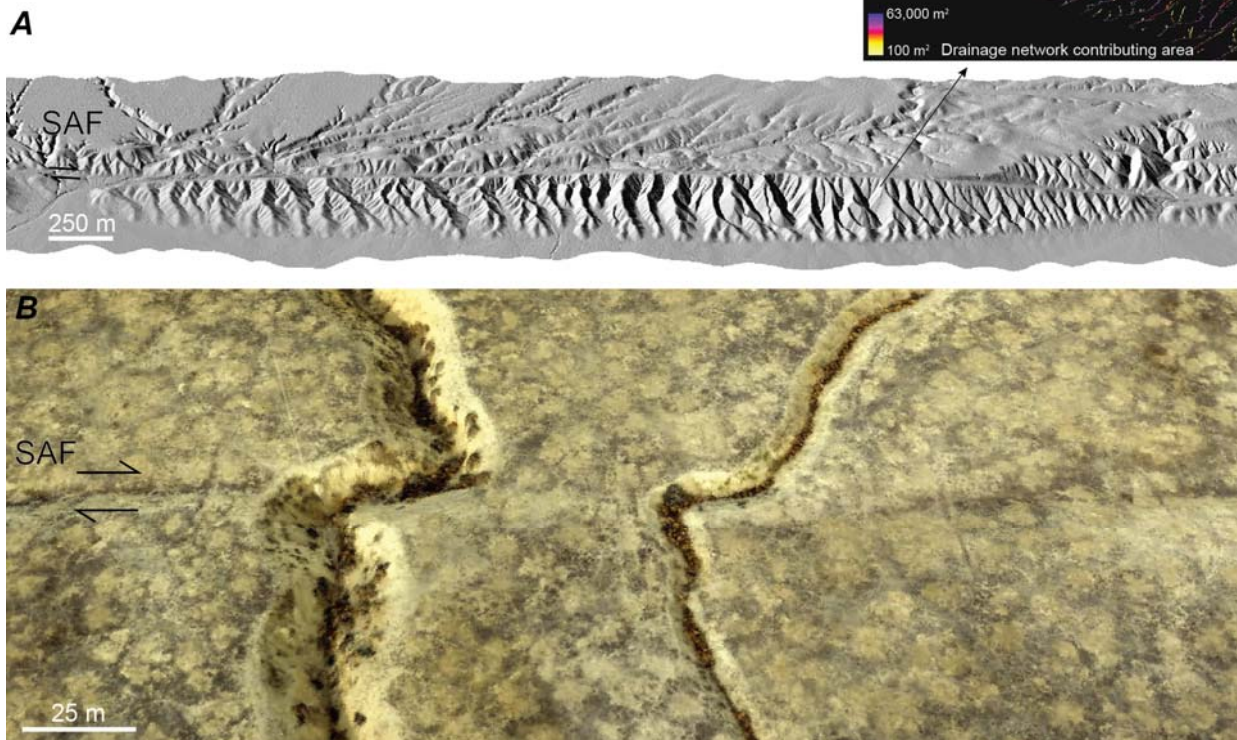


Fig. 1: High resolution topography and evidence of recent activity along the south-central San Andreas Fault (SAF). A) The Dragon's Back pressure ridge shows progressive landscape response to rock uplift and offset relative to a fixed uplift zone in the SE (Hilley and Arrowsmith, 2008). Inset shows drainage network in uplift zone. B) LiDAR topography (Bevis et al., 2005) processed at www.opentopography.org. B) Recent offsets along the SAF at Phelan Creeks. Image is from balloon aerial photography texture-mapped onto topographic model from Structure from Motion (Johnson et al., 2014).



INQUA Focus Group on Paleoseismology and Active Tectonics



paleoseismicity.org

NOTES



Lineament analysis using ASTER satellite images around the coastal area of Korean Peninsula

Weon-hack Choi(1), D. Inoue(2), M. Yanagida(3), Sung-il Cho(1), Dong-hee Park(1), Chun-joong Chang(1), Jae-woong Ryu(1)

- (1) Korea Hydro & Nuclear Power Co., Ltd. 1312-70 Yuseong-daero, Yuseong-gu, Daejeon, Korea (whchoi@khnp.co.kr)
- (2) Tokyo Electric Power Services Co., Ltd. 3-3 Higashiueno, 3-chome Taito-ku, Tokyo 110-0015, Japan
- (3) Hanshin Consultant Co., Ltd. 3-24-4-3F Minamitsuka, Toshima-ku, Tokyo 170-0005, Japan

Abstract: The lineaments are often related to faults and lithologic boundaries and in some cases to geomorphic relief. They can be helpfully utilized by investigating active tectonics as a preliminary data. In order to assess the distribution and activity of the lineaments around coast area of Korean Peninsula, we have interpreted lineaments using ASTER images. The lineaments range from 2 km to 50 km long and show a trend in NNW-SSE dominantly. The lineaments judged by the ASTER study ranked from La to Le. However, there are not many of La and Lb that have a high possibility to be active. We are going to recheck ASTER lineament existence and activity by aerial photographs and field investigations in the future.

Key words: Lineament, Active tectonic, ASTER Images, Fault

INTRODUCTION

The most observable features on satellite images and aerial photographs are the linear shapes, so-called lineaments. They appear as straight or curved lines of different lengths. They are often related to faults and lithologic boundaries and in some cases to geomorphic relief.

The objectives of this study are to interpret the lineaments along the coastal area of Korean Peninsula and to classify the activity order on the lineaments.

In this study, the lineaments were interpreted from the ASTER(Advanced Space borne Thermal Emission and Reflection Radiometer) satellite images. The activity order on the lineaments was classified by using the Table 1. The ASTER is the sensor with the 14 bands wavelengths that was loaded on the Terra satellite launched by NASA in 1999 (Abrams M. and Ramachandram S., 2003). The ASTER has the characteristic efficiency to view stereoscopic image using 760-860 nm near infrared wavelength band of vertical and backward view (VNIR band 3N(nadir), 3B(27.6 degrees from nadir). The height of satellite is 705 km above the earth surface; therefore resolution on this stereoscopic band is 15 meters. The ASTER images were enlarged to 1:100,000 scale in order to interpret the tectonic geomorphology. The area of one scene image covers 60 km x 60 km. In order to make a simple and easy interpretation, one scene is divided into six sheets. The width of one sheet is A3 size of 420 mm x 297 mm.

LINEAMENT ANALYSIS

The important technical points of ASTER image interpretation are to observe the large-scale topographical features arrangement and height differences of the mountains. The lineaments that indicate the active tectonics such as active faults, active flexures etc., are plotted whether the crustal movement is conceivable or not for the explanation of above large-scale cause. For example, when there are abrupt changes of mountain height, the fault may exist for the lifting up

the mountain.

When the piedmont line is composed of straight and steep slope, there may be the active tectonic relief such as potential or buried active faults. On the contrary, it might be interpreted as an alternative possibility to be explained as the results of the differential erosion process by interpreting surface texture of a mountain, valley density, and slope inclination etc. of surrounding mountains. The ASTER interpretation is more excellent than the aerial photograph interpretation for this judgment. Therefore, ASTER image interpretation can cover a wide range at a time and it is possible to compare the differences.

It is easy to observe the small fault scarps and offsets of small channels and ridges on the terraces by means of aerial photograph interpretation, but it is often difficult by means of ASTER interpretation. But it markedly excels in interpreting the sharp reverse scarplet when the height differences are more than 20 meters.

RESULTS AND INTERPRETATIONS

Eastern Korean Peninsula

The investigated area is along the eastern coast of the Korean Peninsula from the border of North Korea to Busan city. The study extent from the coast line is roughly 20 km into inland, because this study is to investigate active fault along the coastal line.

The 69 lineaments were interpreted at the eastern Korean Peninsula from the 20 sheets of ASTER images (Fig. 1; Area 2011). The long lineaments that do not suggest active fault are also picked up to illustrate old faults or geological boundaries. The lineaments have NNE-SSW orientation dominantly and range from 2 km to 30 km long.

The lineaments judged by the ASTER study ranked from La to Ld. Those of Le rank with longer lineament have been plotted on the sheets. The Le lineaments do not necessary to suggest to active faults but the results of some geological phenomena such as old faults, geological boundaries etc.



Table 1. Lineament interpretation criteria for the ASTER image.

Lineament rank	Definition	Terraces, small scale stream	Large scale valley and ridge	Mountain, hill, basin
La	Certain tectonic relief	<ul style="list-style-type: none"> The cliff and reverse scarplet in the same direction are admitted on the terrace surface and the talus slope in the lineament extension. There is surely a reverse inclination on higher terrace and a back of the hill. The lateral offsets are in plural valley and ridge systematically develop. 	This rank cannot be recognized in mountainous district geographical features alone. It is a conclusive evidence whether there is displacement in a terrace and a small-scale valley.	<ul style="list-style-type: none"> This rank cannot be recognized in mountainous district geographical features alone. It is a conclusive evidence whether there is displacement in a terrace and a small-scale valley.
Lb	Probable tectonic relief (50%)	<ul style="list-style-type: none"> The cliff and the reverse scarplet in the same direction are indistinctly admitted on the terrace surface and the talus slope in the lineament extension. The reverse inclination is presumed to a higher terrace and summit level of the hill. The lateral offsets are in plural valley and ridge systematically develop. 	Two or more big valley and ridge offsets.	<ul style="list-style-type: none"> There is discontinuity in big geographical features arrangement and the altitudinal distribution of the mountainous district, and needs assumption of tectonic movement to explain big geomorphology. There are basin and valley that continue straight, long and slenderly, and needs assumption of tectonic movement to explain big geomorphology. The foot of a mountain line is consecutively straight line and steep inclination, the tectonic relief is assumed.
Lc	Probable tectonic relief (20-30%)	<ul style="list-style-type: none"> Cliff as in same direction is admitted on terrace surface in lineament extension, locally. The reverse inclination is presumed to a higher terrace and a summit level hill 	A part of big valley and the ridge shift systematically offsets	<ul style="list-style-type: none"> There is highly discontinuity about big geographical features arrangement and altitudinal distribution of the mountainous district. However, the terrain feature is a little insufficient as the lineament. There are basin and valley that continue straight, long and slenderly, However, the terrain feature is a little insufficient as the lineament. The the foot of a mountain line forms a straight line and is a steep inclination. However, the terrain feature is a little insufficient as the lineament.
Ld	Low possibility of Tectonic relief (Because the possibility of the active fault cannot be denied, extract it for attention)	Scarp on the terrace surface and lateral offsets in a small-scale valley can't be admitted.	<ul style="list-style-type: none"> Offset is not admitted in a big valley and the ridge. There are a valley and a ridge that doesn't offset. 	<ul style="list-style-type: none"> There is highly discontinuity about big geographical features arrangement and altitudinal distribution of the mountainous district. However, the terrain feature is insufficient as the lineament. There are basin and valley that continue straight, long and slenderly, However, the terrain feature is insufficient as the lineament. The foot of a mountain line forms a straight line and is a steep inclination. However, the terrain feature is insufficient as the lineament.
Le	No tectonic relief (Erosional geomorphology correlating with old fault, bedding stratification, and intrusive boundary)	Scarp on the terrace surface and lateral offsets in a small-scale valley can't be admitted.	<ul style="list-style-type: none"> There is no systematical offset about the valley and the ridge. It offsets oppositely. 	<ul style="list-style-type: none"> There is no discontinuity about big geographical features arrangement and altitudinal distribution of the mountainous area though there is straight geographical feature. There are basin and valley that continues long and slenderly but the geographical features array bends, and it is regional. Though a foot of a mountain line forms straight line and step slope, the geographical features array bends, and regional.

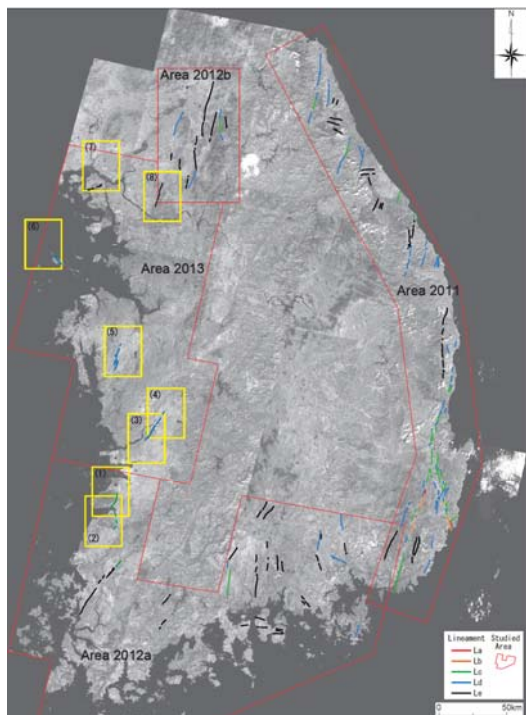


Fig. 1: Lineament map by ASTER images interpretation

Southern Korean Peninsula

The interpretation of ASTER images was carried out from Pusan city to Jindo island via Masan and Gwangyang of south coast line. The interpretation region to inland direction is generally about 30 km from the coast line, but the width differs scene.

The 23 lineaments were interpreted at the southern Korean Peninsula from the 11 ASTER scenes (Fig. 1; Area 2012a). The dominant orientation of the lineaments is NNE-SSW and NE-SW. The lineaments range from 6 km to 50 km long and ranks from Lc to Le activity. There are hills of peneplain remained blocks on the lower land with elevation less than 200 meter at southern Korean Peninsula. These hills are composed of close valley spacing.

Western Korean Peninsula

The interpretation region is from Jindo island to Imjin river of border line to North Korea. As results, the seven lineaments were interpreted. The lineaments have NNE-SSW orientation dominantly and range from 6 km to 26 km long (Fig. 1; Area 2013). The lineament rank is Ld and Le, except for the Buan lineament of Lc rank. The Ld and Le rank lineaments have little possibility to be active.



CONCLUSION

(1) Predominant orientation of the lineaments

Major geological structures of Precambrian gneiss, crystalline schist, granite etc. in Korean Peninsula are NNE-SSW direction. The large scale faults that separate big geological structure and divide Korean Peninsula with NNE-SSW direction, can be easily delineated by using small scale satellite image such as Landsat images. These faults are 200-400 km long. The dominant orientation of lineaments in this study area is also NNE-SSW that is the same as the geological structure. Fujita (1984) released the lineament map of Korean Peninsula using base map of Kim and So (1977) based on the Landsat satellite image. According to Fujita (1984), the dominant orientation of the lineament is from NNE to NE. The recent activity may be the inversion movement of the old faults. The lineament density along the eastern coast line of the Korean Peninsula is higher than southern and western coast line.

(2) Length of the lineaments

The active or probable active parts of faults with NNE-SSW orientation such as the Osipcheon fault, the Maupcheon fault and several lineaments interpreting by means of ASTER image do not continue long distance, as from 10 to 40 km long, comparing with the original fault length. The faults that divide geological distribution continue several hundred km by interpreting topographic maps. When ASTER images that correspond to the 1:100,000 scale topographic maps are used, lineaments are interrupted by the ridges or hills, and do not continue long.

(3) Lineaments activity

The Yangsan faults and the Ulsan faults are famous as the active faults. The Yangsan fault is right lateral fault and NNE-SSW orientation. Lineament that is located near the eastern coast is right lateral with NNE-SSW orientation. This is ranked as Lc rank. It is not confirmed that above faults have no evidences to be active, however there may be the possibility to be active, because they have clear topography as active faults. On the other hand, there are only three Ld rank lineaments, and all the others are Le rank lineaments in this study. The reason why they are judged to be Le rank is that there are no height differences across the lineaments or lineaments have smooth curves free from roughness due to the controlled by the schistosity or bedding plane.

(4) Uneven distribution of lineaments

This is definitely assumption in terms of geomorphologic situation, lineaments that are located along the eastern coast line do not continue to the inland. The faults are more than 100 km long from geological point of view, however lineaments do not continue long and distributed fragmentally. The lineaments to be active, including fragmental lineaments unevenly distribute, are limited at the east coast of Korean Peninsula.

(5) The long faults that form the geological structure

Why were the topographic features which correspond the long faults formed? This is the one solution that intermitted lineaments were formed by the erosion 240-247

process. On the other hand, the lineaments interpreted by the ASTER image are less than 40 km long. The NNE-SSW lineaments in this study are seven. The one is Lc and Ld, the five is Ld, the one is Le in the seven. These NNE-SSW orientation lineaments might be active, otherwise, they are the remnants that were moved during Neogene.

(6) E-W lineaments

There are seven E-W orientation lineaments. These lineaments seem that the distribution are systematical and the same separation between the lineament. But lineaments are from 5 to 34 km long. It is difficult to estimate the cause of the lineament formation. They may be formed by the joints, but if they were formed by joints, joints were too long. These lineaments might be formed by the differential erosion of different basement rock types.

FUTURE STUDY

The lineament rank should be regarded as commonly applicable for ASTER lineament for the practical use of engineering geology. However, this ASTER images interpretation study is preliminary step; hence analysis on the relationship between ASTER and aerial photograph lineaments concerning existence and rank is not yet carried out. We are going to recheck ASTER lineament existence and activity by aerial photographs and field investigations in the western coast area first (Fig. 1; yellow rectangle). The marine terraces of the extension of lineament by ASTER should especially reexamined by aerial photographs. It is very important for the judgments whether an individual lineament recognized by ASTER affects the deformation on the terraces or not. Hence, we interpreted the above area by means of ASTER image, based on the fact that we know the information of the fault outcrops, existence of lineaments and terrace deformation. ASTER sheet is very convenient to view the broad geomorphologic active tectonics in the view lights of the cause of geomorphology. We will use both precise lineaments map by aerial photographs of large scale and broad active tectonic map by ASTER of small scale.

Acknowledgements: This work was supported by the Radioactive Waste Management of the Korea Institute of Energy Technology Evaluation and Planning (KETEP) grant funded by the Korea Government Ministry of Trade Industry & Energy (2012171020001).

References

- Abrams, M., Ramachandram S. (2003). ASTER User Handbook. Jet Propulsion laboratory, Pasadena. CA. EROS Data Center, Sioux Fall 2003.
- Fujita K. (1984). 西南日本準大陸。アジアの変動帯ーヒマラヤアジアの変動帯ーヒマラヤと日本海溝の間ー, 67-88. 海文堂出版
- Kim, K. and So, J. (1977). A Study on the characteristics and the causes of earthquakes in Korea. Jour. Korean Institute of Mineral & Mining Engineers,14,



INQUA Focus Group on Paleoseismology and Active Tectonics



paleoseismicity.org

NOTES



Neotectonic evolution of the Ulsan fault system at the southeastern part of Korean peninsula

Weon-hack Choi(1), Daiei Inoue(2), Sung-il Cho(1), Dong-hee Park(1), Chun-joong Chang(1), Jae-woong Ryu(1)

- (1) Korea Hydro & Nuclear Power Co., Ltd. 1312-70 Yuseong-daero, Yuseong-gu, Daejeon, Korea (whchoi@khnp.co.kr)
 (2) Tokyo Electric Power Services Co., Ltd. 1-7-12 Shinonome, Koto-ku, Tokyo, Japan

Abstract: Many Quaternary faults along the Ulsan Fault System (UFS) have been reported and investigated with outcrop observation to clarify the neotectonic evolution and fault parameters such as length, displacement, slip rate and recurrence interval. In order to assess the activity of the UFS, we have interpreted lineaments and terraces using the large scale aerial photographs and conducted field surveys. The UFS is about 50 km long and trends NNW-SSE, from northern Gyeongju city to Ulsan city. The vertical slip rate of the UFS ranges between several hundredths of mm to 0.2 mm per year. The latest activity of this fault system was clarified at two localities by outcrop and trench investigation. The activity is estimated to have happened between 7,470 and 1,440 yBP from the northern to central part of the fault. The latest activity of the UFS differs depending on the segment.

Key words: Fault activity, Ulsan fault system, Lineament, Terrace, Slip rate,

INTRODUCTION

The UFS is about 50 km long and trending in NNW-SSE, located between northern Gyeongju city to Ulsan city (Fig. 1). The division of UFS into several segments is preliminary investigated based on the lineament geometry and certainty. Also, the UFS is interpreted as a reverse fault system that made the eastern mountain uplift. The continuity of its southern extension into the East Sea is not distinct.

The activity of the UFS was reported by Oh (1977) on the basis of the displacement of marine terrace near Bangeojin. Recently, new evidence of activity has been found at outcrops where Quaternary deposits are faulted (Ryoo, 1977; Okada et al., 1998; KIGAM, 1998). Okada et al. (1999), Kaneda et al. (1998) and Suzuki et al. (2005) confirmed the latest activity of the UFS by excavating trenches. These studies were concentrated on specific localities of UFS segments partly but there are little discussions for the activity along the whole extension of the UFS.

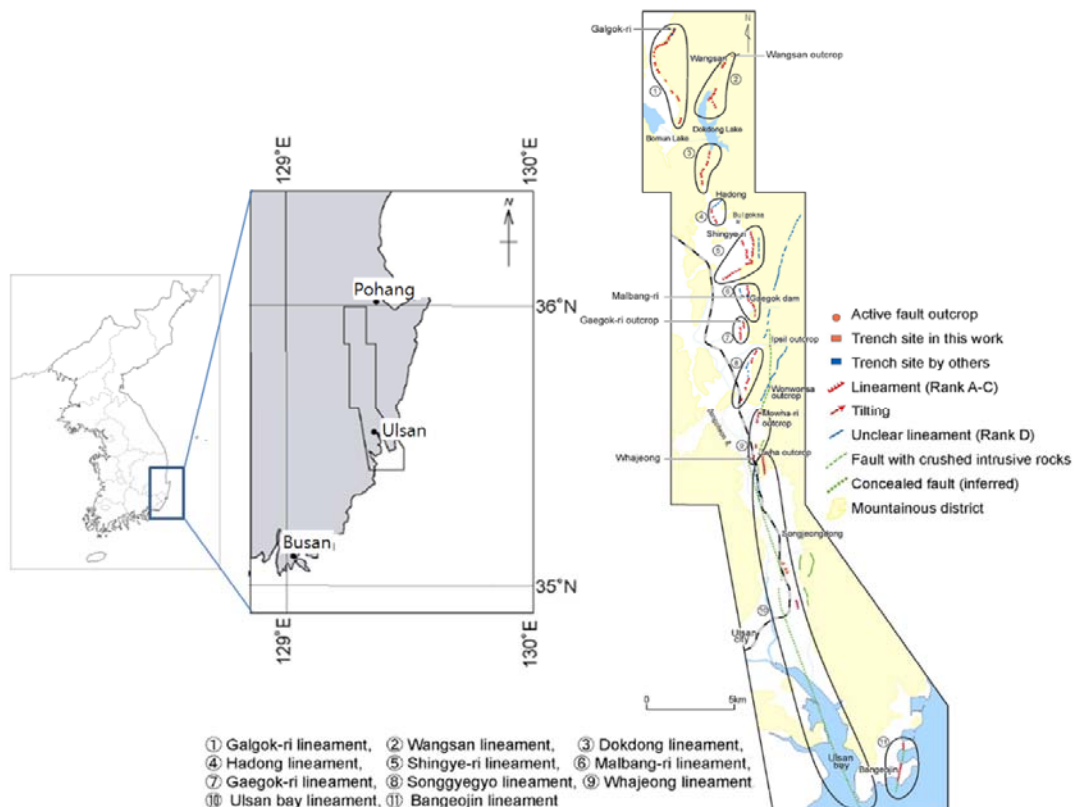


Fig. 1: Compiled lineament map along the Ulsan fault system.



The UFS is believed to be an active fault that moved in the late Quaternary. However, there have been scarce reports that dealt with the activity through its entire length, using integrated studies on lineament interpretation, slip rate, age of recent activity, and return period (Inoue and Choi, 2006). In order to assess the activity of the UFS, the ages of Quaternary marine terraces in this area are very important; however, several different opinions have been introduced, and they have not reached a close consensus. For example, the level of MIS 5e age terrace is different from 20m to 30m according to each studies (Oh, 1977, Inoue and Choi, 2006)

The objectives of this research are to interpret the aerial photographs along UFS in detail and to excavate trenches on the lineament, in order to clarify the property of the fault activity, such as the latest activity, slip rate etc. at each locality by means of ^{14}C dating and tephra chronology. Then the activity along the trace of UFS will be discussed on the basis of the above results. The division of UFS into several segments is preliminary investigated based on the lineament geometry and activity in order to estimate the magnitudes of earthquakes caused by the UFS.

We interpreted large scale (1:10,000) aerial photographs and extracted lineaments by geomorphologic features in the southern and northern part of the UFS. After a precise field survey for lineaments, four trench sites were selected on the lineament to elucidate the fault movement history.

TOPOGRAPHICAL AND GEOLOGICAL STUDIES

The aerial photographs study along the UFS, from Galgok-ri to Bangeojin was carefully carried out by using 1:20,000 aerial photographs, and the 1:10,000 aerial photographs that were enlarged from the 1:20,000 were used at the trench points.

The UFS occurs between the eastern mountain front and the western fluvial plain. The fault trace is not straight but irregularly undulated. There are fault scarps on the fluvial terraces and alluvial fan, and they sometimes make lineaments. The lineaments relating to UFS do not locate on a single line, but on several lines corresponding with the topographical feature such as mountain fronts, fault scarps and channel changes. The lineaments are sometimes discontinuous even between the mountainous area and fluvial plain, and the trends of lineaments change in places. Accordingly, the UFS is divided into 11 segments, based on the distribution and character of the lineaments and fault activity, named Galgok-ri(#1), Wangsan(#2), Dokdong(#3), Hadong(#4), Shingye-ri(#5), Malbang-ri(#6), Gaegok-ri(#7), Songyegyo(#8), Whajeong(#9), Ulsan Bay(#10) and Bangeojin(#11) areas, respectively from the north (Fig. 1).

RESULTS AND INTERPRETATIONS

Age determination of marine terrace

The marine terrace distribution along the southeastern coast of Korean peninsula was mapped. Three wide

terraces and several sub-terraces were discriminated on the map.

In order to reveal the ages of the marine terraces, tephra analyses of the sediments that lie directly above the deposits were carried out. Volcanic ashes originated from Aso, Ata and Aira volcanoes Kyushu, Japan were found at several points. The age of each terrace were determined by the volcanic ashes. It is concluded that the lowest wide marine terrace was formed during MIS 5e that is the large transgression period. It can be correlated to the world standard of marine isotope stages. Consequently, the ages of older and younger terraces can also be estimated by correlating them to the standard ages.

Activity of the Ulsan fault system

The lineament interpretation along the UFS from Gyeongju city to Ulsan city was made by the same methods used in Japanese style, because the geomorphologic features to detect active faults are similar. The UFS will probably be divided into three segments mainly by the feature of lineaments.

Most of Quaternary fault outcrops along UFS show reverse movement of east side up, and displacement from 1m to several meters, such as Wangsan, Galgok, Malbang, Gaegok and Ipsil sites. UFS is interpreted as reverse fault mainly based on east mountain area, high stream index change in east part, west side convex lineament shape and reverse Quaternary fault outcrops.

The latest activity of the fault system was clarified at two localities by outcrop and trench investigation. The latest activity at Galgok-ri located in the northern part of the fault occurred between 2,840 and 1,440 yBP. The activity is estimated to be between 7,470 and 2,990 yBP at Gaegok, located in the central part of the fault. The latest activity at the Wangsan, which is between Galgok-ri and Gaegok, is older than 7,000 yBP. The latest activity of the UFS differs among the localities.

The vertical slip rate of the UFS was calculated from the amount of vertical deformation and the ages of the terraces. It ranges between several hundredths of mm to 0.2 mm per year.

FUTURE STUDY

The activity of the UFS was studied during four years through the study of the terrace stratigraphy. However, many challenging tasks are still remaining for the engineering use in order to describe the activity of the UFS. Following points should be basically studied for evaluation of the earthquake scale, and time of the UFS. There are some contradiction of the ages among ^{14}C , OSL (Optically Stimulated Luminescence), tephra and geomorphologically estimated age. The Japanese tephra that fell in wide areas was used in this study and the tephra chronology was already established in Japan. The marine terrace stratigraphy has also been established using the tephra chronology. In order to solve the above contradiction, the fluvial terraces should also be carefully investigated to find primary ash falls in the sediments.



The UFS is possible to divide into segments by the topographical feature and the geological evidence. On the other hand, it is very difficult to determine the segmentation. This study revealed the latest activity of the UFS at the two places. Furthermore, especially the activity data of the southern part of UFS is very little. More data of activities should be increased not only in the northern part but also in the southern part of UFS.

The main body of the UFS is composed of low angle faults that build up the eastern mountain. However, the high angle faults form boundary between Quaternary deposits and basement rocks. The high angle faults with NS trend were recognized in the mountain. The relationship between the high angle and low angle reverse faults may show the slip partitioning or difference of faulting of UFS. The detailed field geological and geophysical investigation should be carried out with taking geological history into consideration.

Parallel lineaments are found at several points. The latest activity of the fault in them should be selected from the parallel faults. The seismic exploration for detecting geological structure, such as relationship of each parallel fault, structure, dip and dimension will be very effective.

Acknowledgements: This manuscript aims to introduce the active fault studies on UFS in Korea to foreign visitors and researchers who participate in 5th International INQUA Meeting on PATA and be summarized from the previous research results of "The Activity of the Ulsan Fault System Based on Marine Terrace Age Study at the Southeastern Part of Korean Peninsula (2006)". Also, this work was supported by the Radioactive Waste Management of the Korea Institute of Energy Technology Evaluation and Planning (KETEP) grant funded by the Korea

Government Ministry of Trade Industry & Energy (2012171020001).

References

- Inoue, D., Choi, W. H. (2006). The Activity of the Ulsan Fault System Based on Marine Terrace Age Study at the Southeastern Part of Korean Peninsula, CRIEPI Report : N05012, pp. 83.
- Kaneda, H., Okada, A., Takemura, K., Watanabe, Y., Suzuki, T., Naruse, T., Kyung, J. B., Ishiyama, T., Kawabata, D., Taniguchi, K. and Chae, Y. H. (1998). Trenching survey of Northern Ulsan Fault System in the southern part of Korea. Quart. Res. Annual Meeting, 28, 118-119 (in Japanese).
- Korea Institute of Geology, Mining and Materials (KIGAM) (1998). Final report of the re-evaluation to the design base earthquake considering the Yangsan fault. Korea Electric Power Corporation, pp.1964 (in Korean with English abstract).
- Oh, G. H. (1977). The geomorphic history of the southeastern coast of the Korean peninsula. Geographical review of Japan, 50, 12, 689-699 (in Japanese with English abstract).
- Okada, A., Watanabe, M., Suzuki, Y., Takemura, K., Ishiyama, T., Kawabata, D., Kaneda, H., Kyung, J. B. and Chae, Y. H. (1998). Activity Evaluation of the Active faults of the Ulsan fault system, southeast Korea. Proc. In Geographical Soc. of Japan, O-38 (in Japanese).
- Ryoo, C. R. (1977). Fault system in the eastern Korea: Gyongju horsetail structure as a new synthetic interpretation. Lee Y. And Kim, J. H. eds: Tectonic evolution of Eastern Asian continent, Geol. Soc. Korea of 50th Anniversary, Int. Symp. 22-27 (in English).
- Suzuki, T., Okada, A., Takemura, K., Kyung, J. B., Chae, Y. H., Kim, H. Y., Hirouchi, D., Ito, A., Oishi, K., Nakamura, Y., Naruse, T., Kitagawa, K. and Watanabe, M. (2005). Paleoseismic activity at the northern part of the Ulsan fault zone-Excavation study at Kalgoku-ri, Gyongju City, Southeast of Korea. Active Fault Research, 25, 147-152 (in Japanese with English abstract)



INQUA Focus Group on Paleoseismology and Active Tectonics



paleoseismicity.org

NOTES



Mapping of the Inabanga Fault in Bohol, Philippines using High Resolution LIDAR Imagery and Field Mapping Verification

Felix, Raquel (1,2), Lagmay, Alfredo Mahar Francisco (1,2), Norini, Gianluca (2), Eco, Rodrigo Narod (1,2)

- (1) National Institute of Geological Sciences, College of Science, University of the Philippines, Diliman, Quezon City 1101, Philippines. E-mail: raquel.felix@noah.dost.gov.ph, mlagmay@noah.dost.gov.ph, narod.eco@noah.dost.gov.ph
- (2) Nationwide Operational Assessment of Hazards, Department of Science and Technology, Philippines
- (3) Istituto per la Dinamica dei Processi Ambientali – Consiglio Nazionale delle Ricerche, Area della Ricerca CNR – ARM3 via Robert Cozzi 53, 20125 Milano, Italia. Email: gianluca.norini@cnr.it

Abstract: A M_w 7.2 earthquake devastated Bohol Island in the Central Philippines region on 15 October 2013 at 8:12 am. The temblor was associated with severe ground rupture, intense ground shaking and other earthquake hazards. Along with numerous landslides and sinkholes that formed during the event, the Bohol earthquake caused 222 deaths and massive destruction to infrastructure amounting to 1.64 million Philippine Pesos (US\$38.21 million). The source of the main shock is from an unmapped reverse fault with slight strike-slip component. Ground rupture of the Bohol event is best exposed in Barangay (village) Anonang, Municipality of Inabanga where a fault scarp 3-m high, with mean principal orientation of $N51^\circ E$ is observed. Thousands of inland and offshore aftershocks were recorded, which plots on a general $N55^\circ E$ trend, defining a plane about 100 km long. Using a 1-m resolution digital terrain model (DTM) derived from a Light Detection and Ranging (LiDAR) airborne survey after the earthquake, lineaments were identified and validated through field mapping to define the extent of the inland portion of the earthquake source. Other lineaments within the northern portion of Bohol Island were identified using the Lidar DTM to map out other possible structures in the region that may have been responsible for significantly large aftershocks with strike-slip movement as defined by focal mechanism solutions. Pre-event, 5-m resolution IfSAR DTMs mapped in 2012, were also used to determine changes in morphology after the 2013 temblor, including the identification of older fault scarps in Inabanga, where the newly-formed fault scarp is now seen. Results of this work can be used as reference for future studies to understand the tectonics of Bohol Island and the fatal 15 October 2013 earthquake to mitigate the impacts of future earthquake hazards in the area.

Key words: Bohol earthquake, Magnitude 7.2 earthquake, Inabanga Fault, Philippine earthquake

INTRODUCTION

A M_w 7.2 earthquake shook eastern Bohol, Philippines on 15 October 2013 at 8:12 am (local time) and resulted to 222 deaths and massive destruction of property amounting to 1.64 million Philippine Pesos (US\$38.21 million) (Lagmay, 2014, NDRRMC, 2013, PHIVOLCS, 2013). The main shock produced a 6.8 km-long ground rupture, best exposed in Barangay Anonang, Municipality of Inabanga. Although the reverse fault displacement of 3 m as seen in Inabanga is consistent with a M_w 7.2

earthquake (Coppersmith and Wells, 1994), the exposed rupture length is incomplete and may constitute only part of an approximately 90-100 km long fault defined by the distribution of epicenters associated with the 2013 Bohol Earthquake (Lagmay, 2013, Aurelio, 2013). Here, we map the surface rupture of the fault associated with the 2013 temblor and determine its possible land extent from lineament mapping using pre- and post-high-resolution Digital Terrain Models (DTM) derived from Interferometric Synthetic Aperture Radar (IfSAR) and Light Detection and Ranging (LiDAR) airborne

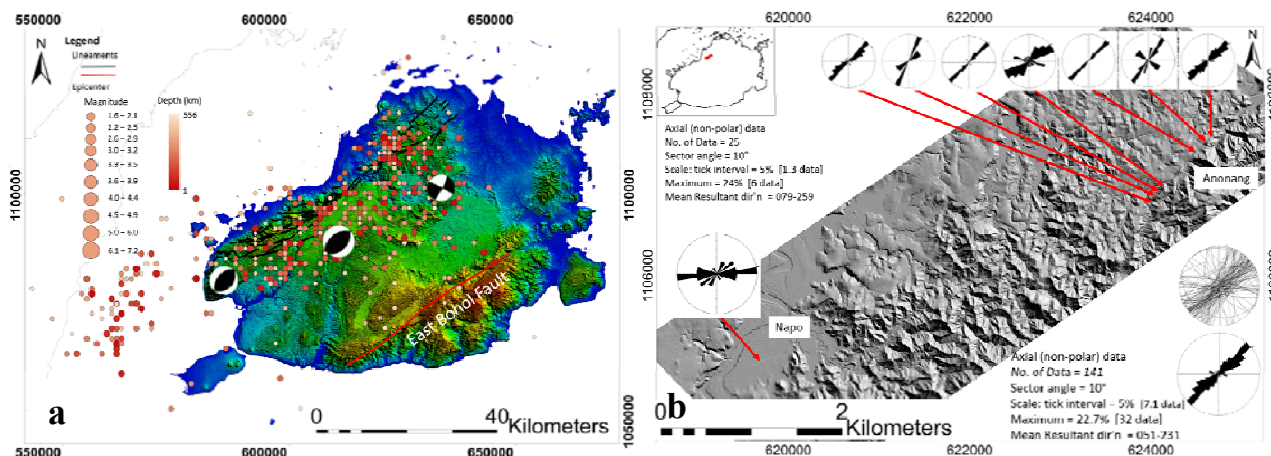


Fig. 1: (a) Lineament map using IfSAR-derived DTM of the Inabanga and East Bohol Fault. Colored circles represent epicenters related to the 2013 Bohol earthquake from October 15 to Dec 21, 2013 (source: PHIVOLCS). Beachballs are focal mechanism solutions of the mainshock and two other recorded aftershocks (source: Lagmay and Eco, 2013). (b) Rose diagrams for each field sites overlain on post 2013-earthquake LiDAR-derived DTM. The general readings for Barangay Napo and Barangay Anonang are shown on the lower left and lower right, respectively.



surveys, respectively (Figure 1). The results of field mapping of the fault at Inabanga and vicinities, herein referred to as the Inabanga fault, are also presented to define the field expression of the geometry and kinematics of the ground rupture plane. Shaded relief and slope-aspect maps (Figure 2) were processed from a post-2013 earthquake LiDAR-derived DTM with pixel size of 1 x 1 m. The sharp relief and linear surface shadows created in these maps facilitated the recognition of linear morphology and served as basis for the delineation of lineaments. To confirm which lineaments correspond to the fault rupture of the 2013 Bohol earthquake, field investigations were conducted on target sites selected from the processed lineament map. The field mapping comprised of measurement of the orientation of the fault plane, amount of surface displacement and identification of kinematic structures present on the ground surface and within the fault rupture plane. All measured joints and faults in each structural station were shown as rose and cyclograph diagrams and plotted against the lineament map. The pre- 2013 earthquake DTM with pixel size of 5 x 5 m was also processed to interpret lineaments present prior to the development of the 2013 ground rupture. This map was compared with the post-2013 earthquake DTM to identify lineaments coincident or near the location of the 2013 ground rupture and also to determine the direction of gross movement of the ground surface in

North Bohol.

RESULTS

Lineament analysis using the shaded relief images and slope-aspect (Figure 2) maps show that there are five major trends found. These are shown as different colored arrows in Figure 2. The discussion on each of the trend is shown below.

(a) The most prominent lineament orientation is NE-SW. This lineament orientation is of the same orientation as the ground rupture that formed during the 2013 Bohol earthquake and the East Bohol Fault located in the southern portion of the island (Figure 1a), originally believed to have been responsible for the 2013 temblor.

(b) There are also numerous NW-SE trending lineaments. They are most evident on the mountainous area in the southwestern tip and northeastern area of the LiDAR image as incised valleys.

(c) The NNE-SSW lineaments have longer continuity of lineaments on the southwest than on the northwest. Parallel valleys mostly define lineaments that were identified along or near the coast. Linear ridges, river valleys and fault scarps, define others with the same NNE-SSW orientation.

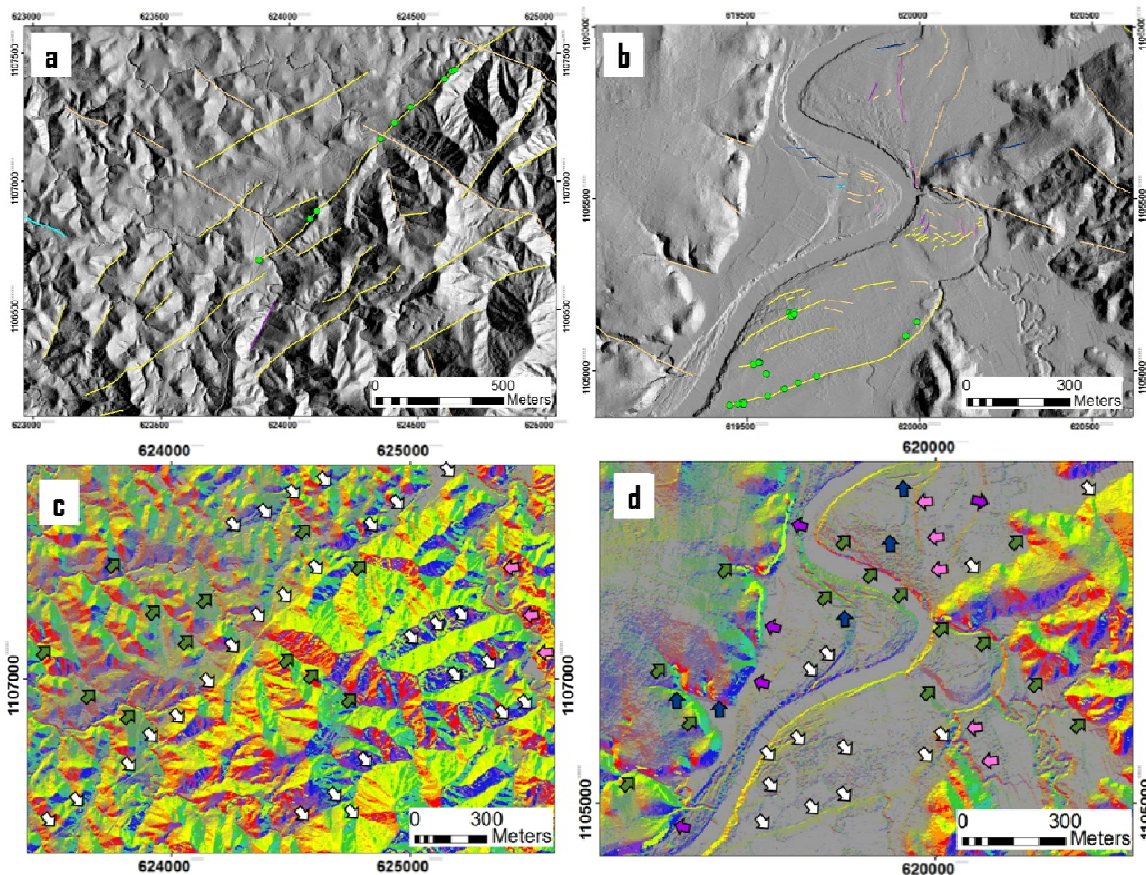


Fig. 2: Shaded relief images and corresponding slope aspect maps and their interpretations. Figure (a) is in Barangay Anonang while figure (b) is in Barangay Napo. Both villages are in the municipality of Inabanga.



(d) There is a consistency on the number of NNW-SSE trending lineaments over the study area. Massive landslides were observed along one of these lineaments in the southwestern mountainous area, beside the main NE-SW trend of the Inabanga fault. The NNW-SSE trends are also defined as valleys and scarps.

(e) There are few E-W trending lineaments in the area. The most distinctive is the grouped E-W lineaments cross-cutting the folded features located in the southwest of the LiDAR image in relatively lowland areas beside mountainous terrain.

Pre-2013 earthquake DTMs show a prominent lineament structure consistent with the location and orientation of the Inabanga Fault (Figure 1). This structure is part of a network of NE-SW trending faults about 4 km wide with an onshore extent of 66 km from the northeast to the west coast of Bohol Island. The lineament trace is segmented because of the quality of the DTM but the structures are nonetheless clearly evident. The post-2013 earthquake DTM also clearly shows the lineament coincident with the ground rupture.

Field Measurements

Field measurements made in structural stations along the rupture zone are consistent with the orientation of the lineaments identified from the DTMs. The 1.8 km-long rupture zone in Barangay Anonang, Inabanga, which has maximum vertical displacement of 3 meters and indicators of right-lateral oblique-slip movement, has a mean strike direction of N51°E. The angle of pitch of slickenlines in the exposed scarp is 60 degrees (Figure 3a). Older slickensides with chattermarks (Figure 3b) in some places of the Inabanga fault plane indicate nearly horizontal movement of this fault. Further southwest in Barangay Napo, municipality of Inabanga, ground rupture with a more east-west direction and having

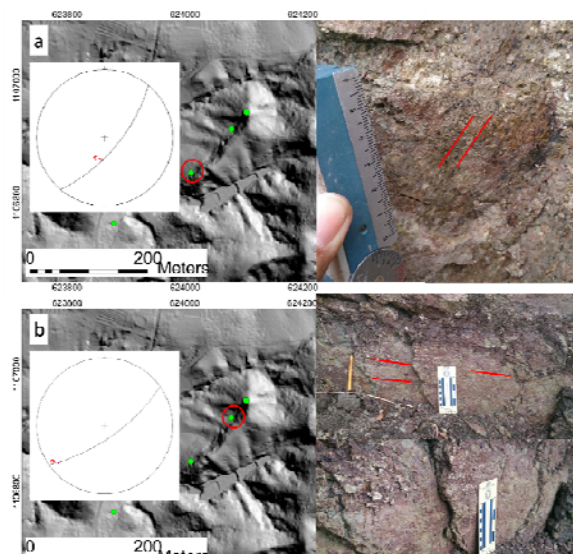


Fig. 3: Outcrops with slickenlines showing angle of pitch ranging from 3-60 degrees.

vertical displacement that range from 0.1-0.5 meters

have left-lateral oblique-slip sense of movement. The sense of movement of the rupture was determined from horizontal displacement of structures as seen in plan view.

DISCUSSION

The pre-2013 and post 2013 Bohol earthquake DTMs clearly shows major NE-SW lineaments traversing the northern portion of the island. This lineament is coincident with the 1.8 km ground rupture, first seen and best exposed as a 3 m-high nearly vertical scarp in the municipality of Inabanga. The lineament evidence along with the observation of older kinematic indicators, such as the presence of nearly horizontal and sub-vertical slickenlines, suggest that the 2013 ground rupture took place along a major structure that already existed with surface manifestation. Morphological evidence, such as ground rupture taking place at the boundary of hilly terrain and gently sloping ground, further supports this observation (Figure 4).

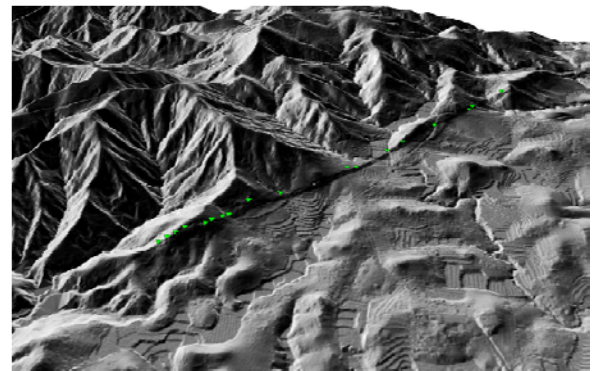


Fig. 4: LiDAR-derived DTM showing the ground rupture lineament between the hilly terrain and gently sloping ground.

The USGS focal mechanism solution for the 2013 Bohol mainshock is dominantly for reverse faulting but also indicates minor lateral sense of movement (Comcat, 2013). The style of faulting derived from the estimated moment tensor has two nodal planes (table 1) and is consistent with the fault rupture in terms of fault orientation. The scarp found at Inabanga also exhibits the lateral sense of motion described by the focal mechanism solutions.

Plane	Strike	Dip	Rake
Nodal plane 1	238°	46°	103°
Nodal plane 2	39°	46°	77°

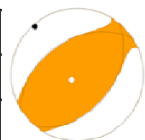


Table 1: Two nodal planes derived from the estimated moment tensor for the 2013 Bohol mainshock. On the right is the focal mechanism solution from the estimated moment tensor (Comcat, 2013).

Many fracture sets were measured along the Inabanga fault rupture plane. These are consistent with the 5 major lineament sets identified in the DTMs (i.e. NE-SW, WNW-ESE, E-W, NNE-SSW, NNW-SSE). The dominant orientation is the NE-SW trending fault with a mean principal orientation of N51°E. The next major lineament



orientation is at an acute angle relative to the mean principal orientation (refer to rose diagram and lineament interpretations in Figure 1b) and may represent Riedel fracture sets of the main shear.

Further to the southwest in Barangay Napo (see Figure 2b and 2d), ground rupture is observed but have much less vertical displacement and a more east-west directed strike orientation compared to those observed in Barangay Anonang, municipality of Inabanga. These faults are also oblique-slip faults but with a slight left-lateral sense of movement. Since they have a different orientation and are not continuous with the major lineament in north Bohol nor coincident with the main ground rupture found at Barangay Anonang in Inabanga, it is possible that these faults are Riedel shears of the main fault rupture. However, there is also the possibility that the observed left-lateral sense of movement is an artifact of lateral spreading.

Focal mechanism solutions of aftershocks that are strike-slip in nature must represent strike-slip faults traversing the subsurface of Bohol Island. These were not investigated in detail in this study but are important because they may be key in understanding the stress regime, tectonics and earthquakes of the central Visayas region. Identification of the lineaments is very important because these may be sites of surface ground rupture. This is clearly seen from the pre-2013 earthquake DTM where lineaments identified corresponded to the actual fault rupture in 2013. It is important that faults in the area, both mapped and unmapped, be understood for disaster preparedness and mitigation against earthquake hazards.

CONCLUSIONS

The Inabanga fault is a NE-SW trending, oblique fault showing reverse slip and minor lateral displacement. It has the approximate extent of 66 km onshore – a measurement starting from the northernmost NE-SW trending lineament going towards west of the island in Loon. The remaining several km from the expected rupture length of 100 km is offshore.

This paper shows the initial results of an on-going study of the Inabanga fault. The lineament interpretations from pre- and post-2013 high resolutions DTMs and the field mapping of structures within the zone of the Inabanga ground rupture can be used as reference for researchers doing related field studies on this newly discovered fault.

Acknowledgements: The LiDAR data is acquired from Disaster Risk and Exposure Assessment for Mitigation - Light Detection and Ranging (DREAM-LIDAR) Project, a component of Project NOAH.

This study is supported by Project NOAH (Nationwide Operational Assessment of Hazards) and by the province of Bohol headed by Gov. Edgardo Chatto. We would also like to thank Dr. Carlo Arcilla, Director of the University of the Philippines National Institute of Geological Sciences, for the

assistance. Special thanks to the geologists of Project NOAH landslide component who participated with the fieldwork.

References

- Aurelio, M.A., Rimando, J.M., Taguibao, K.J.L., Dianala, J.D.B. and Berador, A.L., (2013). Seismotectonics of the Magnitude 7.2 Bohol Earthquake of 15 October 2013 from Onshore, Earthquake and Offshore Data: A key to Discovering Other Buried Active Thrust Faults? In *Geocon 2013. Manila, Philippines: Geological Society of the Philippines*.
- Baliatan, E.G. (2014). Effects of Tectonic Structures on the Formation of Irosin Caldera, Philippines (M.Sc. thesis). University of the Philippines Diliman
- Campbell, J.B. (1996). Introduction to Remote Sensing, 2nd edition. *Taylor and Francis Group*. 0748406638, 9780748406630.
- Comcat.cr.usgs.gov. M7.1 – 4 KM SE of Sagbayan, Philippines (BETA). Available: http://comcat.cr.usgs.gov/earthquakes/eventpage/usbookdb4#scientific_moment-tensor
- Dost.gov.ph. DREAM come true – DOST-UP project wins geospatial excellence award. Available: <http://www.dost.gov.ph/>. Accessed: August 13, 2014.
- Dream.upd.edu.ph. Data Acquisition Component. Available: <http://dream.upd.edu.ph/about-us/data-acquisition/>. Accessed August 13, 2014.
- Dream.upd.edu.ph. Data Processing Component. Available: <http://dream.upd.edu.ph/about-us/data-processing/>. Accessed August 13, 2014.
- Engelkeimer, R.M. and Khan, S.D., (2008). Lidar Mapping of Faults In Houston, Texas, USA. *Geosphere 4 (1)*, 170-182.
- Lagmay, A.M.F. and Eco, R., (2014). Brief Communication "The magnitude 7.2 Bohol earthquake, Philippines." *Natural Hazards Earth System Sciences. In press*.
- Norini, G., G. Groppelli, L. Capra, and E. D. Beni, (2004). Morphological analysis of Nevado de Toluca volcano (Mexico): new insights into the structure and evolution of an andesitic to dacitic stratovolcano. *Geomorphology*, 62, 47-61.
- Oceanservice.noaa.gov. What is LIDAR? Available: <http://oceanservice.noaa.gov/fact/lidar.html>. Accessed April 21, 2014.
- Phivolcs.dost.gov.ph. Philippine Institute of Volcanology and Seismology 2013. Available: <http://www.phivolcs.dost.gov.ph/>. Accessed May 28, 2014.
- Toth, C., Brzezinska-Grejner, D.A., Bevis, M., (2006). High-resolution Airborne LIDAR/CCD Mapping of San Andreas Fault. In 3rd IAG / 12th FIG Symposium 2006. Baden, Austria: Research Group of Engineering Geodesy of Institute of Geodesy and Geophysics Vienna University of Technology.
- Wheeler, R.L., (2014). Earthquake catalog for estimation of maximum earthquake magnitude, Central and Eastern United States-Part A, Prehistoric earthquakes. *U.S. Geological Survey Open-File Report 2014-1025-A*, 26 p. Available: <http://dx.doi.org/10.1333/ofr20141025A>. Accessed August 30, 2014.
- Yu-Chang, C., Yue-Gau C., Tian-Yuan S. and Chung H. (2007). Active Fault Mapping Using Airborne LiDAR Technique: Case Study of the Hsincheng Active Fault, Taiwan. *Journal of Asian Earth Sciences* 31, 303-316.
- Zachariassen, J. and USGS Western Region Earthquake Hazards Team. (2008). Detailed Mapping of the Northern San Andreas Fault using LIDAR Imagery. *U.S. Geological Survey (California)*. 05HQGR0069.

Tuesday 23 September

Session Three: Archeoseismology



What can we learn about paleo-earthquakes from the anisotropy of magnetic susceptibility?

Shmuel Marco (1), Tsafir Levi (2), Ram Weinberger (2)

(1) Department of Geosciences, Tel Aviv University, Tel Aviv 6997801, Israel. Email: shmulikm@tau.ac.il

(2) Geological Survey of Israel, 30 Malkhe Yisrael Street, Jerusalem 95501, Israel. Email: tsafir@gsi.gov.il; rami.weinberger@gsi.gov.il

Abstract: The magnetic susceptibility of sediments is anisotropic. It can be described by three orthogonal principal axes of an ellipsoid, which correspond to the maximum, intermediate and minimum magnetic susceptibility. The magnetic fabrics may develop during depositional and/or subsequent deformation processes. We show how analyses of the anisotropy can be applied to identifying seismites, reconstruct the flow direction of earthquake-induced injections of liquefied clastics and how the stress orientation in fault rocks can be recovered in order to reconstruct the palaeo-focal-plane solution and damage zones near fault planes.

Key words: anisotropy of magnetic susceptibility, paleoseismology, deformation, Dead Sea Fault

Introduction

The magnetic susceptibility X is the ratio of induced magnetization M of a material to an applied magnetic field H ($M=XH$). The bulk magnetic susceptibility of rocks is primarily determined by their composition. The anisotropy of magnetic susceptibility (AMS) is commonly described by three orthogonal principal axes, k_{\max} (k_1), k_{int} (k_2), and k_{\min} (k_3), which correspond to the maximum, intermediate and minimum magnetic susceptibility.

The AMS mainly depends on the mineral shapes and their arrangement in the material (fabric), compositions and concentrations. The magnetic fabric, which is manifested in the measured orientation of the principal axes, may develop under different geological environments: 1) depositional processes, 2) flow, and 3) subsequent deformation. Generally, the principal AMS axes are coaxial with the directions of the principal stress axes. Therefore, in cases of known depositional conditions we can identify the 'Deformation fabrics' and determine the directions of the principal stress axes.

We show how the AMS analyses can be applied to reconstruct the flow direction of earthquake-induced injections of liquefied clastics, and how the stress orientation in fault rocks can be recovered in order to reconstruct the palaeo-focal-plane solution. These results, as well as previous ones (e.g., Marco et al., 1998; Marco et al., 1997; Mörner and Sun, 2008) can serve as a tool for recording invisible deformation caused by past earthquakes. The term "seismomagnetization", which was suggested by Mörner and Sun (2008) can be adopted.

Case studies

Clastic dikes (Fig. 1) can be formed either passively by filling of open fissures with sediments, or actively by injection of liquefied clastics into fractures that were formed in response to loading stresses (Marco et al., 2002). We discovered that passively silt-filled dikes, are characterized by oblate AMS ellipsoids and vertical k_3 . On the other hand, dikes that contain sediment connected to a source layers are characterized by a triaxial AMS ellipsoids in which the k_1 axes are well

grouped subhorizontal and parallel to the dike walls and k_2 are well grouped and in many cases subvertical. Field evidence and AMS analyses indicate that most of these dikes were emplaced by injection inferred to be due to seismically triggered fluidization. The magnetic fabrics and their parameters along the dikes and possible grain imbrications along dike walls support organization of grains under high strain rates. We therefore argue that the AMS provides a petrofabric tool for identifying seismites and inferring their flow kinematics in complex geologic areas (Levi et al., 2006a; Levi et al., 2006b; Levi et al., 2008).

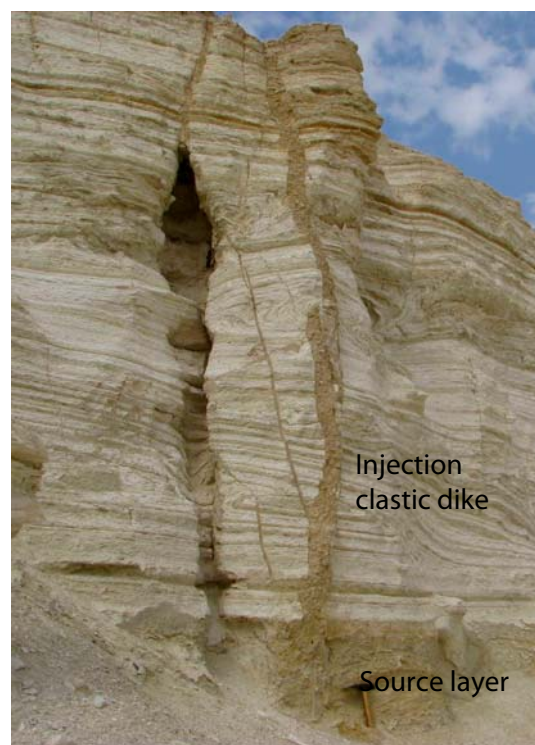


Figure 1. A clastic dike filled with material that was injected about 5 m upward from a silt layer at the bottom. Hammer is 30 cm long.

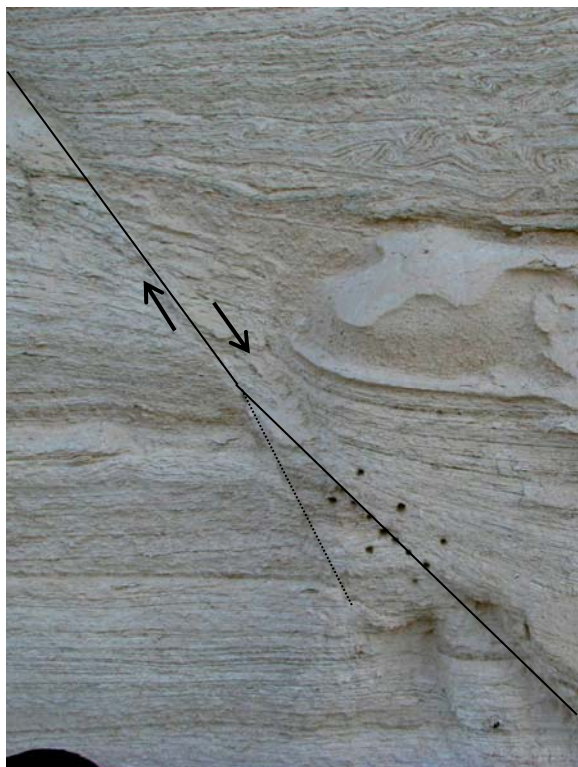


Figure 2. A fault that offsets laminated lacustrine Lisan Formation section. The layers are warped (dragged) near the fault. Width of image is about 1 m.

In addition to flow, the AMS also reflects the inelastic permanent strain preserved in the rocks. Therefore, the tectonic stresses that induce fracturing and faulting leave their mark on the AMS in the vicinity of the ruptures. We demonstrate how AMS can be applied to distinguish between the effect of remote and local strain fields, determine the size of the related inelastic damage zone, and resolve the fault-plane solutions of past earthquakes. The AMS fabrics were explored within the seismically active Dead Sea Fault zone, next to late Pleistocene normal faults that offset lacustrine rocks and exhibit total displacements of up to ~3.5 m (Fig. 2). We detected 'Depositional fabrics' that are characterized by scattered maximum and intermediate principal AMS axes a few meters away from the fault planes. In contrast, within tens of centimeters from the fault planes we find 'Deformation fabrics' that are characterized by well-grouped AMS axes, in which one of the principal axes is parallel to the strike of the adjacent fault.

Variations in the AMS fabrics and magnetic lineations define the size of the inelastic damage zone around the faults. The deformation-triggered magnetic fabrics and the associated inelastic deformation zones are compatible with coseismic dynamic faulting and the effects of the local strain field during earthquakes. Most of the AMS fabrics show a conspicuous similarity to that of the fault-plane solutions, i.e. the principal AMS axes and instantaneous strain ellipsoids are coaxial. These results suggest a novel application of the AMS method for defining the shape and size of the damage zones surrounding dynamic faults and for determining the full tensor of the local strain field (Levi et al., 2014).

Acknowledgements: We are grateful to the Israel Science Foundation for funding the study through grants No. 1245/11 and 1736/11, and to Geological Survey technicians Moshe Arnon and Yaacov Rafael for their assistance during fieldwork. We thank N.A. Mörner for a constructive review.

References

- Levi, T., Weinberger, R., Aifa, T., Eyal, Y., and Marco, S., 2006a, Earthquake-induced clastic dikes detected by anisotropy of magnetic susceptibility: *Geology*, v. 34, p. 69-72.
- Levi, T., Weinberger, R., Aifa, T., Eyal, Y., and Marco, S., 2006b, Injection mechanism of clay-rich sediments into dikes during earthquakes: *Geochemistry, Geophysics, and Geosystems*, v. 7, no. 12, p. Q12009 (doi:10.1029/2006GC001410).
- Levi, T., Weinberger, R., Eyal, Y., Lyakhovsky, V., and Heifetz, E., 2008, Velocities and driving pressures of clay-rich sediments injected into clastic dykes during earthquakes: *Geophysical Journal International*, v. 175, no. 3, p. 1095-1107.
- Levi, T., Weinberger, R., and Marco, S., 2014, Magnetic fabrics induced by dynamic faulting reveal damage zone sizes in soft rocks, Dead Sea basin: *Geophysical Journal International*, v. Revised version in review.
- Marco, S., Ron, H., McWilliams, M. O., and Stein, M., 1998, High-Resolution Record of Geomagnetic Secular Variation from Late Pleistocene Lake Lisan Sediments (Paleo Dead Sea): *Earth Planet. Sci. Lett.*, v. 161, p. 145-160.
- Marco, S., Ron, H., Stein, M., and McWilliams, M. O., High-resolution paleomagnetic record from Late Pleistocene Lake Lisan Sediments: magnetization processes and paleosecular variation, *in* Proceedings Paleomagnetism and Diagenesis in Sediments, London, 1997, The Geological Society, p. 4.
- Marco, S., Weinberger, R., and Agnon, A., 2002, Radial clastic dykes formed by a salt diapir in the Dead Sea Rift, Israel: *Terra Nova*, v. 14, p. 288-294.
- Mörner, N.-A., and Sun, G., 2008, Paleoequake deformations recorded by magnetic variables: *Earth and Planetary Science Letters*, v. 267, no. 3-4, p. 495-502.



INQUA Focus Group on Paleoseismology and Active Tectonics



paleoseismicity.org

NOTES



Damages to the 9th century Prambanan temple caused by the 2006 Yogyakarta earthquake (Java, Indonesia)

Kázmér, Miklós (1), Hariyadi, Agus (2)

- (1) Department of Palaeontology, Eötvös University, Pázmány sétány 1/c, H-1117 Budapest, Hungary. E-mail: mkazmer@gmail.com
(2) Department of Architecture and Planning, Faculty of Engineering, Gadjah Mada University, Yogyakarta, Indonesia.

Abstract: An M 6.5 earthquake hit Yogyakarta on May 26, 2006. The region, considered aseismic, suffered high damages: 155,000 houses were destroyed. The Prambanan temple complex was among the severely damaged masonry buildings. Location and direction of damages have been investigated: displacement and falling directions of masonry blocks were surveyed. We reconstructed the direction of strong motion responsible for the damages. It is parallel to the strike of the causative fault (30°-210°).

Key words: archaeoseismology, Java, Indonesia, Middle Ages.

INTRODUCTION

There was an M 6.5 earthquake on 26 May 2006 at dawn in Yogyakarta sultanate on Java island, Indonesia (Fig. 1). The city of 4 million did not suffer considerable damage, but 150,000 houses collapsed in the surrounding rural area and further 200,000 were severely damaged. Six thousand people died.

The earthquake occurred in a sector of Java which have been considered aseismic (Luehr et al., 2008). There was no surface rupture and the causative fault could not be identified with any of the known faults (Setijadji et al., 2008). Twelve temporary seismic stations were operated for three months to record aftershocks (Walter et al., 2007). Engineering geological mapping provided explanation for the great damage caused: thick, loose succession of repeated mudflows, lahars, derived from nearby Merapi volcano amplified the shaking (Walter et al., 2008).

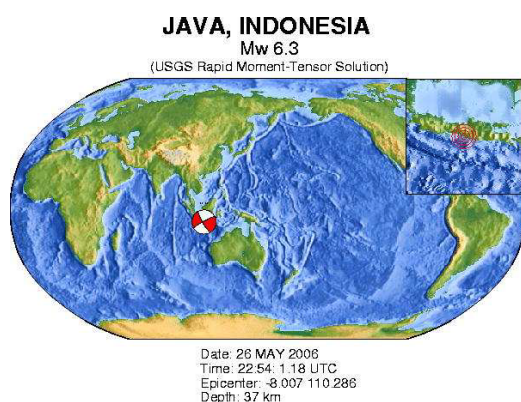


Fig. 1: Location and focal mechanism of the May 26, 2006 Yogyakarta earthquake

We carried out an archaeoseismological survey three year after the earthquake, supposing that Medieval Hindu masonry temples in the region preserved

earthquake-induced damages. The displacements – if caused by an earthquake of known focal mechanism – will be suitable for calibration of archaeoseismological studies, where the mechanism is unknown. The largest temple complex, Prambanan, suffered heavy damages in 2006. Restoration was in progress, and we were allowed to study the shrines before repairs covered the damages.



Fig. 2: Aerial view of the Prambanan temple complex.

PRAMBANAN

The Loro Jonggran temple complex (mentioned by the better-known name of the village Prambanan where it is located) was probably built during the first half of the 9th century (Fig. 2). The pervasive Hindu cultural influence and rule erected a multitude of temples at that time, including the UNESCO World Heritage site Borobudur 35 km to the NW. Prambanan has been a site for cultural and religious tourism (Jordaan, 1996) since its discovery by Sir Thomas Raffles, the then British governor of Java during the Napoleonic wars (Raffles,



1817). Excavation and surveying started at that time has been going on for two centuries (Tiffin, 2009): old temples are restored and long-forgotten ones are excavated from below thick volcano-sedimentary succession.

A modern restoration of Prambanan satisfying the needs of the tourist industry followed the grandiose aims set for Borobudur nearby. That, financed by UNESCO in the 1960s, was completely dismantled and re-built again, supported by a reinforced concrete structure (Soekmono, 1976). Therefore nothing can be seen on Borobudur which could offer any information on its twelve-century history in earthquake-stricken Indonesia. Fortunately, Prambanan's reconstruction was made in a financially less successful environment: only the external, carved stones were removed, a reinforced concrete layer constructed, and the carved stones replaced on select portions.

METHODS

Visibly recent damages on several buildings of the temple complex, considered to be made by the 2006 earthquake by Mr. Darmojo, the master builder, have been surveyed by compass and measuring tape, and documented on photographs. Restoration documentation prepared at various times was studied, commented by Mr. Darmojo. A manuscript map recording the surface deformations right after the 2006 earthquake was seen as well. Although the fallen masonry have mostly been removed by the time we visited the site, a few major pieces were located and their falling direction recorded. Observed damage features are also named as Earthquake Archaeological Effects (EAE - Rodríguez-Pascua et al., 2011), and are correlated to the intensity scale of Rodríguez-Pascua et al. (2013). We determined the shifting directions of masonry blocks as well. Recorded features were interpreted as parts of a strong-motion field, and principal directions were determined graphically (Angelier, 1984).

EARTHQUAKE ARCHAEOLOGICAL EFFECTS

The Shiva shrine of the Prambanan complex has excellent foundations: 8 m deep white tuff blocks, underlain by compacted sand down to 14 m. Groundwater level is at 11 m depth (Suryolelono, 2008).

Various damages were surveyed to determine the direction of the strong motion responsible for the displacement. The tip of the 14 m high Apit Utara shrine fell towards 120° for 7.7 m (Fig. 3) (EAE: impact block mark, I = VI-). The largest shrine, the 60 m high Shiva temple has a reinforced concrete mantle at the middle and upper levels, while the lower level has not been restored extensively. This unreinforced lower part suffered horizontal extension in 20-200° direction (Figs 4-5) (EAE: displaced masonry blocks in walls, I = IX-).



Fig. 3: Tip of Apit Utara temple fell towards 120° for 7.7 m.



Fig. 4: Shiva temple, sanctuary level. 45 mm shift towards 20°

Lower part of the Brahma temple was enclosed in reinforced concrete, while the middle and upper parts were left intact. There are centimetre-sized left-lateral displacements across several rows of masonry in the unreinforced level. We suggest that these are surface features of a left-lateral displacement zone, which runs diagonally across the monument (EAE: penetrative fracture of masonry blocks, I = VII-).

Tip of the Brahma temple fell towards 215° for 15 metres. (EAE: impact block mark, I = VI-).

Ground fissure

A 20 m long, several centimetre wide fissure extended in 15°-195° direction near Brahma temple. Further ground fissures were mapped regionally by Pramumijoyo and Sudarno (2008). Was there a higher water table, this ground fissure would have yielded liquefaction and sand volcano (EAE: liquefaction, I = VIII-).

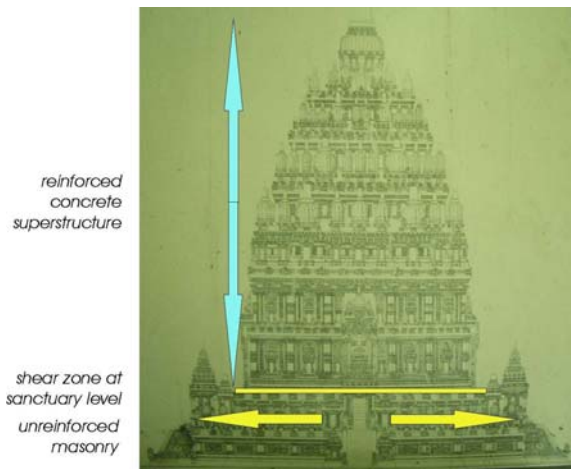


Fig. 5: Shiva temple as seen from the west (photo of an architectural drawing). A horizontal shear plane was formed between the top part containing a reinforced concrete core and the unreinforced bottom part. Horizontal arrows indicate the location of 10 cm extension due to seismic shaking



Fig. 6: Brahma temple: a NW-SE left-lateral fault cross-cutting the temple diagonally. A reinforced concrete wall surrounds the level below this floor. There was 4 mm left-lateral displacement.

DISCUSSION

Displacements are plotted in a single plot describing the strong motion stress field of the 2006 earthquake. Descriptors are falling directions, displacement of walls and ground fissures. The best descriptors are those

damages, where the displacement direction is the least constrained by the geometry of the building. Additionally, evidence of damages affecting major buildings are considered stronger than those affecting minor constructions (Fig. 8).

The least constraints are those which affected the falling directions of the tips of the Apit Utara and Brahma temples, both temples close to being centrally symmetrical. The top part can fall in any direction as dictated by shaking. Their falling direction is perpendicular to each other; i.e. both regular components of strong motion directions could affect them (Fig. 7).

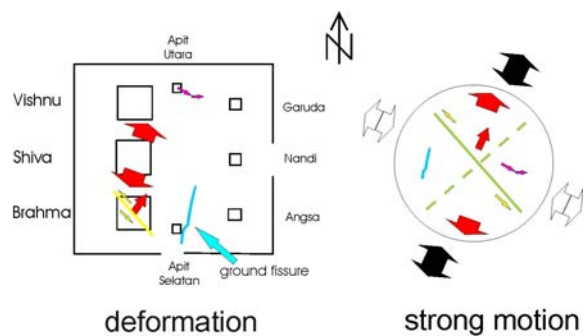


Fig. 7: Strong motion directions (black and white arrows) reconstructed from damaged temples

The causative fault of the 2006 Yogyakarta earthquake is a left-lateral strike-slip fault. Epicentre was at the SW termination, from where fracture spread towards NE, probably as far as indicated by the hypocentres of the aftershocks (Fig. 9). Prambanan complex is approximately at the hypothetical northeastern extension of the fault; this explains its major damage as compared to other temples nearby. Possibly the P-waves caused the extension of the unreinforced lower level of the Shiva temple. S-waves caused the jumping of the tip decorations off their tenons and subsequent fall.

Left-lateral strike-slip faulting of Brahma temple is also caused by P waves: these created the diagonal fracture across the building according to the Mohs planes. The left lateral displacement has no particular meaning: the shaking stopped at this particular moment. If stopped another second the displacement would have been right-lateral.

These suggestions serve a better understanding of the multitude of damage data recorded by archaeological monuments.

Acknowledgements: Supported by Hungarian Science Foundation OTKA grant K67583. Special thanks for the support of prof. Subagyo Pramumijoyo and Husein Salahuddin (Gadjah Mada University, Yogyakarta), director Haryana (Prambanan Complex, Klaten), master builder Darmojo, and Ditto Haryana. Comments of an anonymous reviewer improved the text. This study is part of IGCP Project 567 *Earthquake Archaeology: Archeoseismology along the Alpine-Himalayan Seismic Zone.*

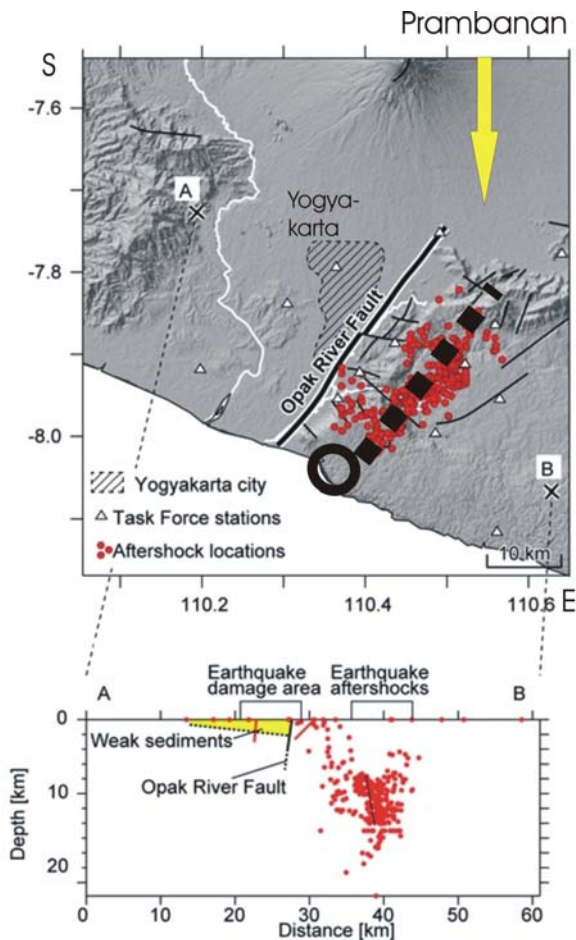


Fig. 8: Map of post-seismic activity after the May 26, 2006 earthquake (after Walter, 2008, modified). Black circle – epicentre. Hatched – Yogyakarta city. Triangles – temporary seismic stations. Small circles: epicentres of post-seismic activity. Hatched line: supposed azimuth of the causative fault. Prambanan is to the NE. Faults after Rahardjo et al. (1977). A-B profile: hypocentres of post-seismic activity compared to the location of the greatest damage. Unconsolidated sediments of the Opak River valley are mostly from lahars of Mt. Merapi volcano.

References

- Angelier, J., (1984). Tectonic analysis of fault data sets. *Journal of Geophysical Research* 89, 5835-5846.
- Jordaan, R. (ed.) (1996). *In Praise of Prambanan: Dutch Essays on the Loro Jonggrang Temple Complex*. KITLV Press, Leiden, p 259
- Luehr, B.-G., Walter, Th., Wassermann, J., Wang, R., Wagner, D., Anggraini, A., Parolai, S., Zschau, J., Prih Harjadi, P. J., Kirbani Sri Brotopuspito, (2008). The surprising Mw 6.5 Bantul earthquake 2006. *Geophysical Research Abstracts* 10, EGU2008-A-03153.
- Pramumijoyo, S., Sudarno, I., (2008). Surface cracking due to Yogyakarta earthquake 2006. In: *The Yogyakarta Earthquake of May 27, 2006*. Karnawati, D., Pranumijoyo, S., Anderson, R., Husein, S. (eds). Star Publishing Company, Belmont, CA, pp. 6-1 – 6-5.
- Raffles, T.S., (1817). *The History of Java*. London: Black, Parbury and Allen and John Murray, 2 vols.
- Rahardjo, Sukandarrumidi, W., Rosidi, H., (1977). *Geologic map of the Yogyakarta quadrangle, Java*, scale 1:100,000, 8 pp., Geological Survey of Indonesia, Ministry of Mines, Jakarta.
- Rodríguez-Pascua, M.A., Pérez-lópez, R., Giner-Robles, J.L., Garduño-Monroy, V.H., Reicherter, K. (2011). A comprehensive classification of Earthquake Archaeological Effects (EAE) in archaeoseismology: Application to ancient remains of Roman and Mesoamerican cultures. *Quaternary International* 242, 20-30.
- Rodríguez-Pascua, M.A., Silva, P.G., Pérez-López, R., Giner-Robles, J., Martín-González, F., Perucha, M.A. (2013). Preliminary intensity correlation between macroseismic scales (ESI07 and EMS98) and Earthquake archaeological effects (EAEs). In: PATA days – Seismic Hazard, Critical Facilities and Slow Active Faults. *4th International INQUA Meeting on Paleoseismology, Active Tectonics and Archeoseismology (PATA)*, Grützner, C., Rudersdorf, A., Pérez-López, R., Reicherter, K. (eds.), 9-14 October 2013, Aachen, Germany, pp. 221-224.
- Setijadji, L. D., Barianto, D. H., Watanabe, K., Fukuoka, K., Ehara, W., Sudarno, I., Shimoyama, S., Susilo, A. Itaya, T., (2008). Searching for the active fault of the Yogyakarta earthquake of 2006 using data integration on aftershocks, Cenozoic geohistory and tectonic geomorphology. In: *The Yogyakarta Earthquake of May 27, 2006*. Karnawati, D., Pranumijoyo, S., Anderson, R., Husein, S. (eds.). Star Publishing Company, Belmont, CA, pp. 4-1 – 4-23.
- Soekmono, (1976). *Chandi Borobudur – A Monument of Mankind*. Van Gorcum, Assen-Amsterdam, The UNESCO Press, Paris, 60 p.
- Suryolelono, K.B., (2008). Investigation of the Prambanan temple after the May 27, 2006 Yogyakarta earthquake. In: *The Yogyakarta Earthquake of May 27, 2006*. Karnawati, D., Pranumijoyo, S., Anderson, R., Husein, S. (eds.). Star Publishing Company, Belmont, CA, pp. 16-1 – 16-9.
- Tiffin, S., (2009). Java's ruined *candis* and the British picturesque ideal. – *Bulletin of SOAS* 72 (3), 525-558.
- Walter, T.R., Lühr, B., Sobiesiak, M., Gresser, H., Wang, R., Parolai, S., Wetzell, H.-U., Zschau, J., Milkereit, C., Günther, E., Wassermann, J., Behr, Y., Anggraini, A., Sri Brotopuspito, K., Harjadi, P., (2007). Soft volcanic sediments compound 2006 Java earthquake disaster. *Eos, Transactions, American Geophysical Union* 88 (46), p. 486.
- Walter, T.R., Wang, R., Luehr, B.-G., Wassermann, J., Behr, Y., Parolai, S., Anggraini, A., Günther, E., Sobiesiak, M., Gresser, H., Wetzell, H.-U., Milkereit, C., Sri Brotopuspito, P.J.K., Harjadi, P., Zschau, J., (2008). The 26 May 2006 magnitude 6.4 Yogyakarta earthquake south of Mt. Merapi volcano: Did lahar deposits amplify ground shaking and thus lead to the disaster? *Geochemistry, Geophysics, Geosystems* 9 (5), Q05006, doi:10.1029/2007GC001810.

Wednesday 24 September

Session Four: Paleoseismology



Surface faulting without earthquakes; sackung and salt tectonics

McCalpin, James (1)

(1) GEO-HAZ Consulting, Inc., Box 837, Crestone, Colorado 81131 USA. Email: mccalpin@geohaz.com

Abstract: Using high-resolution DEMs (LiDAR) we can now detect very subtle fault and fold scarps. But not all such scarps represent coseismic deformation. "Shallow-Rooted", non-seismogenic faulting can create linear fault and fold scarps, which are morphologically similar to coseismic fault scarps. Two common scarp mechanisms are deep-seated gravitational spreading (sackung) and salt flow or dissolution in the subsurface. In the past decade, trenching has been tried to differentiate non-seismic from coseismic scarps, in the belief that non-seismic scarps are produced by creep (gravitational sackung or salt flow). Surprisingly, most trenches show evidence of episodic displacement, even for clearly gravitational and salt faults. For assessing Seismic Hazards, we need to develop more rigorous methods to distinguish between coseismic and non-seismic fault scarps, because the former generate both ground motion hazards and surface rupture hazards, whereas the latter generate only surface rupture hazard. Case histories are described from the USA, Slovak Republic, Andorra, and Spain.

Key words: fault scarps, LiDAR, salt tectonics.

INTRODUCTION

Seismic hazard investigations in the past decade have identified linear fault scarps within the regulatory study area, but it is sometimes unclear whether the scarps are the result of coseismic surface faulting, or of some other non-seismic process (Hanson et al., 1999; McCalpin, 2003). A critical facility clearly must not be sited across such scarps regardless of their origin, due to the potential for future surface fault rupture. But if the scarps were produced by non-seismic faults, then there is no corresponding hazard from earthquake ground motion, which is a very significant matter for designing critical facilities.

The two non-seismic faulting mechanisms described herein are deep-seated gravitational spreading (sackung; Fig. 1) and salt flow and dissolution.

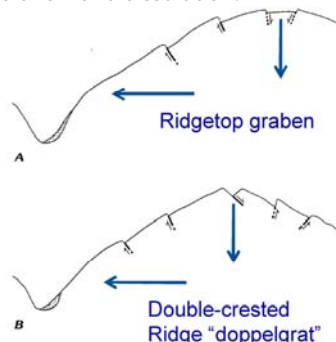


Fig. 1. Schematic cross-section of sackung scarps. Arrows show direction of rock movement.

Published literature implies that both processes should produce slow, creeping movement (e.g., Hanson et al., 1999). So trenching the scarps was attempted to see if the near-surface fault movement appeared to be slow creep deformation or rapid, episodic faulting. The former would be indicated by folding (rather than faulting), incremental increase in folding/displacement

downsection, stratigraphic onlap, and subtle angular unconformities. The latter would be indicated by brittle faulting, fissuring, colluvial wedges, and strong angular unconformities.

SCARPS PRODUCED BY SACKUNG

Sackung (also called deep-seated gravitational spreading) produces linear scarps on high ridges (Figs. 1 and 2). Normally the scarps are restricted to the upper 1/3 of the ridge landform, trend parallel to contours, face upslope, are very short in relation to their height, and occur in swarms. However, they may also be single long scarps that resemble coseismic fault scarps.



Fig. 2. Antislope scarp on Mt. Chabenc, Slovak Republic.

To date, only one trench across a sackung scarp has exposed evidence for creep displacement (McCalpin and Irvine, 1995). All the rest (e.g. Gutierrez et al. 2005; McCalpin et al., 2011; Carbonel et al., 2013) have exposed normal faults dipping steeply into the ridge, with associated colluvial wedges and fissures that have abrupt upward terminations, indicative of rapid, episodic displacement (e.g., Fig. 3).

Results of worldwide trenching studies indicate that sackung scarps form during episodic, decimetre- to meter-scale faulting events. The trigger mechanism could be earthquake shaking, such as in the 2002 M7.9



Denali earthquake, Alaska (Jibson et al., 2004), or periodic groundwater rise due to climatic events.

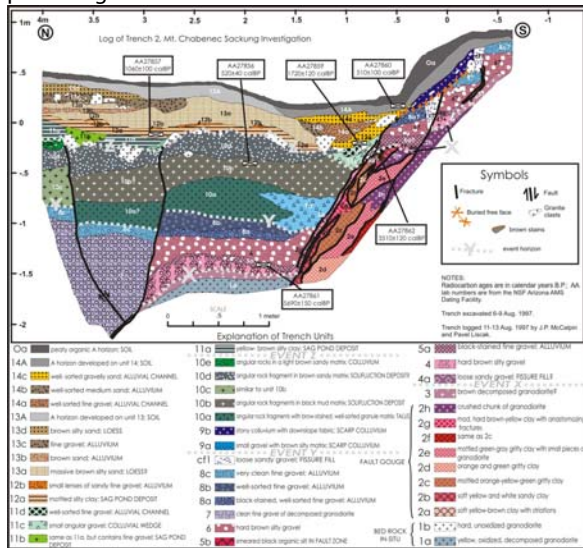


Fig. 3. Sackung trench on Mt. Chabenec, Slovak Republic.

SCARPS PRODUCED BY SALT TECTONICS

The term “salt tectonics” means faulting and folding caused by the flowage and/or dissolution of salt in the subsurface (Hudec and Jackson, 2011). Salt-related faults can occur in all different tectonic environments (extensional, compressional, strike-slip), but herein I will only describe those I have worked on in extensional continental environments.

Joes Valley graben; Are the faults seismic?

The Joes Valley graben in central Utah lies in the transition zone between the extensional Basin and Range Province to the west, and the weakly compressional Colorado Plateau to the east (Fig. 4). The graben is unusually narrow (3 km) for its length (84 km) and depth (1 km).

In the 1980s a seismic hazard study was performed for the Joes Valley Dam, including multiple trenches. Based on the evidence of episodic, meter-scale Quaternary displacements in the trenches, the graben faults were considered to be coseismic.

During the following 30 years seismic reflection lines were collected across the Wasatch Plateau and Joes Valley Graben by oil companies. These deep reflection surveys were interpreted by some authors to show that the graben-bounding faults terminate at a depth of about 3 km in a thin evaporite formation, and do not continue downward into the crystalline basement rocks. If this interpretation was correct then the faults could probably not generate earthquakes large enough to cause damage.

I was employed by the U.S. Bureau of Reclamation in 2013 to consult on this controversy (McCalpin, 2013). LiDAR data revealed small fault scarps that had been overlooked in the 1980s study (Fig. 5).



Fig. 4. Google Earth image of the Joes Valley graben (between arrows) disrupting the eastern slope of the Wasatch Plateau, Utah. The Joes Valley Dam lies close to the eastern margin fault.

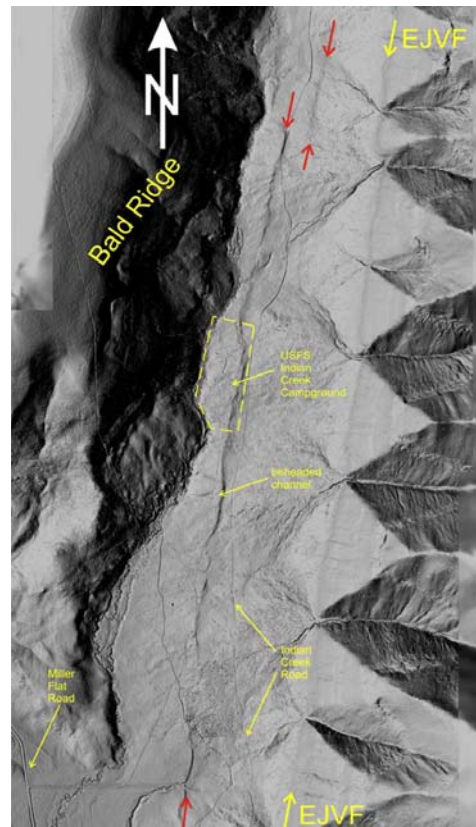


Fig. 5: LiDAR image of the Indian Creek scarps (between red arrows), in relation to the graben-bounding East Joes Valley fault (EJVF, between yellow arrows).



No new trenches were dug, because trench evidence was considered to be inconclusive with respect to the origin of the fault scarps. Instead, morphologic and structural parameters of the faults (length, width, displacement, slip sense, etc.) were compared to those of known coseismic and non-seismic faults. The existence of oblique slickenlines on the faults, and similar length: width: displacement ratios to coseismic faults, and dissimilarities with known salt tectonics faults, indicated that the conservative conclusion is that the faults are coseismic.

Moab valley trench

Ongoing work by the University of Zaragoza and American collaborators on salt-related Quaternary faulting (e.g., Gutierrez et al, 2012a, b, in press), resulted in trenching the eastern margin fault of the famous Moab salt-anticline valley in Utah, USA (Fig. 6).



Fig. 6: View of Moab Valley, Utah, from the eastern margin. Arrow points to outcrop of the evaporites.

Although this salt-collapse valley is widely considered to be aseismic, a trench on the eastern margin fault revealed evidence for episodic displacement (Guerrero et al, submitted-2014). Thus, evidence for episodic fault displacement on this salt-collapse fault cannot be used as proof that the fault is coseismic.

Grand Hogback monocline, scarps and trench

The down-to-the-west Grand Hogback monocline in the central mountains of Colorado was formed as a drape fold over a buried thrust fault during the late Cretaceous Laramide Orogeny (Kirkham et al., 2002). The folded Cretaceous and Jurassic formations overlie the Pennsylvanian-age Eagle Valley Evaporite, which is now exposed at the surface east of the monocline and has experienced severe dissolution and collapse in the past 10 Ma.

Cretaceous strata in the center of the monocline have been disrupted in the past 10 Ma by a series of 19 parallel, down-to-the-west fault scarps (Fig. 7). Individual bedding-plane faults associated with relaxation or "unfolding" of the Grand Hogback monocline offset Miocene basalt as much as 90 m, late Tertiary to early Quaternary basaltic gravel as much as 30 m, and Holocene (?) and Pleistocene debris-flow deposits about 3 m. Trenching in 2013 confirmed that the scarps are the result of episodic displacements (Gutierrez et al, 2014).

Gutierrez et al. (2014) concluded that the deepest flexural-slip faults had a downdip width of 7.5 km. The western 8 faults (out of 19 total faults) are shown with a downdip width of 2.5 km or less. The easternmost fault flattens and dies out at the toe of the monocline at a depth of 5 km. As with all flexural slip faults (whether created by folding or unfolding), displacement is greatest at the ground surface and decreases downward, reaching zero displacement at the fold axis or hinge line.

Rio Seco (Spain); monocline, scarps and trenches

This study in central Spain (Iberian Range) focused on the gravitational structures developed on the NW flank of Los Mansuetos mesa and along the Rio Seco Creek, where dissolution of Triassic evaporites has caused the downward flexure of the overlying Mio-Pliocene formations. The progressive migration of the dissolution front to the south has produced a synform and a monocline over the dissolved evaporites. The crest of the monocline is affected by a keystone graben 1.7 km long with conspicuous geomorphic expression (Fig. 7).



Fig. 7. Downslope part of the Quaternary keystone graben on the crest of the Rio Seco monocline. Thin red lines in foreground show faults in cross-section; red lines with hachures indicate antislope scarps in the graben. Red evaporites outcrop at bottom center.

Gutierrez et al (2012a) excavated three trenches across antislope scarps of the graben. Geometrical relationships in two of the trenches indicated late Holocene episodic displacement, with as many as 3 events. Some deduced parameters of the antislope scarps are clearly different from those expectable for tectonic faults in this intraplate area. These include anomalously high apparent vertical slip rates (0.6 to 1 mm/yr), anomalously short average recurrence of faulting events (1.2 to 2 ka), and high displacement per event values (>65 cm) for surface ruptures that are less than 200 m long.

Implications for Seismic Hazard Assessment

There is disagreement about whether shallow-rooted faults created by sacking or salt tectonics can generate significant earthquakes. Some authors (e.g. Gutierrez et al., 2014) have estimated the maximum earthquake magnitude of such faults from empirical regressions based on historic surface-rupturing earthquakes (e.g., Wells and Coppersmith, 1994). For example, for the deepest of the Grand Hogback faults, they use maximum scarp length (25 km) to estimate a magnitude of M6.7 and use fault area to estimate a magnitude of M6.4.



However, the authors acknowledge that a previous study (Unruh et al., 1993) proposed a maximum fault length of 8 km and depth of 6 km, resulting in a maximum credible earthquake of M5.0.

When estimating earthquakes magnitudes from fault length and fault area regressions, one should consider the difference in slip gradients on shallow-rooted, flexural-slip faults, compared to planar faults that penetrate the lower seismogenic crust. The Wells and Coppersmith (1994) data set is composed mostly of steeply-dipping, planar coseismic faults that had their largest slip amounts in the lower part of the fault plane, where confining stresses are highest and rocks are strongest. Slip decreased upward. This geometry permits a lot of crustal stress to accumulate before failure. However, shallow-rooted flexural-slip faults have the opposite geometry; the largest slip amounts occur at the surface (where confining stress is smallest and rocks are weakest), and the slip then decreases with depth, finally reaching zero in the fold axis, where the confining stress is greatest and rocks are strongest. This geometry, it seems to me, will result in a much smaller release of energy (for a given amount of slip on a given fault area) than for a planar, deeply-penetrating fault. So using the published regressions between magnitude, length, area, and displacement derived from coseismic faulting (such as Wells and Coppersmith, 1994) for estimating earthquake magnitudes on shallow-rooted flexural-slip faults seems not to have a firm physical justification, because kinematics are so different (opposite) for these two different types of faults.

Acknowledgements: I am indebted to my colleagues Francisco Gutierrez, Jesus Guerrero, and Pedro Lucha (University of Zaragoza, Spain) for their leadership in trenching fault scarps formed by sackung and salt tectonics. Bob Kirkham originally recognized the significance of these scarps over shallow-rooted faults, and their implication to seismic hazards.

References

- Carbonel, D., Gutiérrez, F., Linares, R., Roqué, C., Zarroca, M., McCalpin, J., Guerrero, J., and Rodriguez, V., 2013, Differentiating between gravitational and tectonic faults by means of geomorphological mapping, trenching and geophysical surveys. The case of Zenzano Fault (Iberian Chain, N Spain): *Geomorphology*, v. 189, p. 93-10.
- Guerrero, J., Bruhn, R.L., McCalpin, J., Gutiérrez, F., and Willis, G., 2012b, Interstratal karstification and late Quaternary active faulting in Moab collapse salt valley, SE Utah (USA): *Actas de la XII Reunión Nacional de Geomorfología*. Sociedad Española de Geomorfología, Santander, p. 417-420.
- Guerrero, J., Bruhn, R.L., McCalpin, J., Gutierrez, F. and Willis, G., submitted-2014, Interstratal karstification and late Quaternary active faulting in Moab collapse-salt valley, SE Utah (USA). Tectonic faults versus salt-dissolution faults.
- Gutiérrez, F., Acosta, E., Ríos, S., Guerrero, J. and Lucha, P., 2005, Geomorphology and geochronology of sackung features (uphill-facing scarps) in the Central Spanish Pyrenees: *Geomorphology*, DOI:10.1016/j.geomorph.2005.01.012
- Gutiérrez, F., Carbonel, D., Guerrero, J., McCalpin, J.P., Linares, R., Roque, C., and Zarroca, M., 2012a, Late Holocene episodic displacement on fault scarps related to interstratal dissolution of evaporites (Teruel Neogene Graben, NE Spain): *Journal of Structural Geology*, v. 34, p. 2-19.
- Gutiérrez, F., Linares, R., Roqué, C., Zarroca, M., Galve, J.P., Carbonel, D., and Rosell, J., 2012b, Investigating gravitational grabens related to lateral spreading and evaporite dissolution subsidence by means of detailed mapping, trenching and electrical resistivity tomography (Spanish Pyrenees): *Lithosphere*, v. 4, p. 331-353.
- Gutierrez, F., Carbonel, D., Kirkham, R.M., Guerrero, J., Lucha, P. and Matthews, V., 2014, Can flexural-slip faults related to evaporite dissolution generate hazardous earthquakes? The case of the Grand Hogback Monocline of west-central Colorado: *Geol. Soc. Amer. Bull.*, in press.
- Hanson, K.L., Kelson, K.I., Angell, M.A., and Lettis, W.R., 1999, Techniques for identifying faults and determining their origins. U.S. Nuclear Regulatory Commission. Washington, contract report NUREG/CR-5503, 186 p. and appendices.
- Hudec, M. R., and Jackson, M. P. A., 2011, The salt mine: a digital atlas of salt tectonics: The University of Texas at Austin, Bureau of Economic Geology, Udden Book Series No. 5; AAPG Memoir 99, 305 p.
- Jibson, R.W., Harp, E.L., Schulz, W., and Keefer, D.K., 2004, Landslides Triggered by the 2002 Denali Fault, Alaska, Earthquake and the Inferred Nature of the Strong Shaking: *Earthquake Spectra*, Vol. 20, No. 3, p. 669-691.
- Kirkham, R.M., Streufert, R.K., Kunk, M.J., Budhan, J.R., Hudson, M.R., and Perry, W.J. Jr., 2002, Evaporite tectonism in the Lower Roaring Fork river valley, West-Central Colorado, in Kirkham, R.M., Scott, R.B., and Judkins, T.W., eds., Late Cenozoic evaporite tectonism and volcanism in west-central Colorado: Geological Society of America Special Paper 366, p. 73-99.
- McCalpin, J.P., 2013, Evaluation of the Quaternary history of the Joes Valley fault zone, Huntignton North Dam, Utah: unpublished report submitted to U.S. Bureau of Reclamation, Denver, CO by GEO-HAZ Consulting, Inc., Job No. 2143, 30-APRIL-2013, 63 p.
- McCalpin, J.P. and Irvine, J.R., 1995, Sackungen at Aspen Highlands Ski Area, Pitkin County, Colorado: *Environmental and Engineering Geoscience*, v.1, no. 3, p. 277-290.
- McCalpin, J.P. and Hart, E.W., 2003, Ridge-top spreading features and relationship to earthquakes, San Gabriel Mountains Region, Southern California - Part B: Paleoseismic investigations of ridge-top depressions, in Hart, E.W. (ed.), *Ridge-Top Spreading in California; Contributions toward understanding a significant seismic hazard*: California Geological Survey, CD 2003-05, 2 CD-ROMs.
- McCalpin, J.P., 2003, Criteria for determining the seismic significance of sackungen and other scarplike landforms in mountainous regions, in Hart, E.W. (ed.), *Ridge-Top Spreading in California; Contributions toward understanding a significant seismic hazard*: California Geological Survey, CD 2003-05, 2 CD-ROMs
- McCalpin, J.P., Bruhn, R.L., Pavlis, T.L., Gutierrez, F., Guerrero, J. and Lucha, P., 2011, Antislope scarps, gravitational spreading, and tectonic faulting in the western Yakutat microplate, south coastal Alaska: *Geosphere*, v. 7, no. 5, p. 1143-1158
- Wells, D.L., and Coppersmith, K.J., 1994, New empirical relationships among magnitude, rupture length, rupture width, rupture area and surface displacement: *Bulletin of the Seismological Society of America*, v. 84, p. 974-1002.



INQUA Focus Group on Paleoseismology and Active Tectonics



paleoseismicity.org

NOTES



Great earthquakes in the western Transverse Ranges of southern California on the Pitas Point-Ventura thrust system

Thomas Rockwell (1), Kate Wilson (2), Lynn Gamble (3), Mike Oskin (4), Erik Haaker (1)

- (1) Geological Sciences, San Diego State University, San Diego, CA 92182 trockwell@mail.sdsu.edu
- (2) GNS, P.O. Box 30368, Lower Hutt 5040, New Zealand <http://www.pata-days.org/>
- (3) Anthropology, University of California, San Barbara, CA 93106 gamble@anth.ucsb.edu
- (4) Earth and Planetary Sciences, University of California, Davis, CA 95616 meoskin@ucdavis.edu

Abstract: Slip on the Pitas Point thrust produces uplift and folding of the Ventura Avenue anticline (VAA) in the western Transverse Ranges of southern California. Rapid convergence has resulted in 2.7 km of uplift on the VAA over the past 200-300 ka, with as much as 320m in the past 45-50 ka, indicating a long-term uplift rate of 6-7 mm/yr. We mapped four Holocene marine terraces between Carpinteria and Ventura. The most recent emergence event uplifted a Chumash Indian village at Pitas Point by 5-6 m about 900 years ago; this 1st terrace is nearly continuously preserved towards the fold crest where its elevation increases, reaching an altitude of 7-8 m, which implies 9-10 m of slip on the causative fault at depth. Radiocarbon dates on marine shells and culturally derived charcoal indicate terrace emergence at about 0.9 ka, 1.9 ka, and 4.2-4.7 ka, with the 4th (highest Holocene) terrace slightly older than 6.5 ka.

Key words: Holocene marine terraces, Transverse Ranges

INTRODUCTION

The Transverse Ranges are a major fold-and-thrust belt in southern California that accommodate as much as 10 mm/yr of shortening (Donnellan et al., 1993a, b; Meade and Hagar, 2005). The highest rates of convergence are recorded in the Ventura Basin area, and are also noted by high geologic rates (Rockwell et al., 1984, 1988; Rockwell, 1988). Although the historical record is devoid of large earthquakes for the Ventura Basin region (Toppozada et al., 1981), paleoseismic studies document the occurrence of large earthquakes on some major thrust faults onshore (Dolan and Rockwell, 2001).

structural relief in the past 200-300 ka (Rockwell et al., 1988), with a late Pleistocene to present uplift rate of 6-7 mm/yr at Pitas Point (data from Palmer, 1960 reinterpreted by Lajoie et al., 1979, 1982). This high rate of uplift has produced an emergent Holocene marine terrace sequence between Ventura and Carpinteria (Fig. 2), which is the focus of this study.

In this study, we acquired vintage stereo aerial photography from the late 1920's through the 1950's to map the emergent marine terraces from Pitas Point to Punta Gorda; the imagery predates most of the modern landscape development and disturbance. We collected marine fauna from three of these uplifted

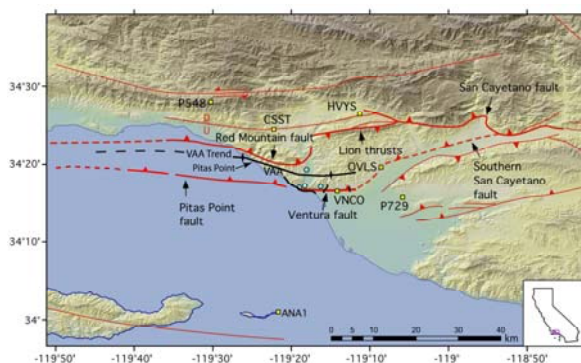


Fig. 1: Map of the Ventura Basin region showing the locations of the Ventura Avenue anticline, the Pitas Point-Ventura thrust, and the San Cayetano reverse fault.

A major structure in Ventura Basin that apparently accommodates a majority of the motion at the coast is the Ventura Avenue anticline and associated Ventura-Pitas Point thrust (Fig. 1). Uplift on the hanging wall of this coupled thrust-anticline system has produced 2.7 km of

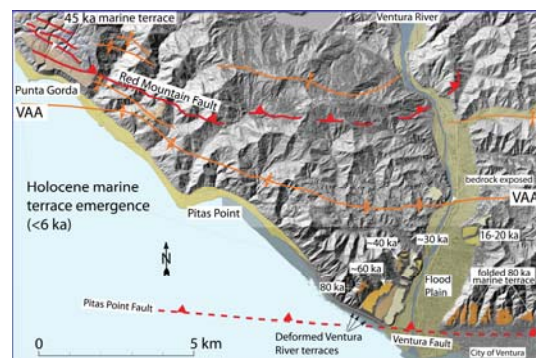


Fig. 2: Map of emergent Holocene terraces between Ventura and Punta Gorda (yellow). The Ventura Avenue anticline and Pitas Point-Ventura thrust are shown where they trend offshore. Terraces to Ventura River (orange) are from Rockwell et al., 1988.

terraces for radiocarbon dating and, combined with limited dates and results from archeological studies, provide ages of the past three emergence events,



which we infer to represent large, coseismic uplifts of the coastal zone.

HOLOCENE TERRACE SEQUENCE

The coastal terraces were mapped on the early aerial imagery with the specific purpose of resolving the elevations of the relic shorelines, which were then surveyed with differential GPS. We recognize the presence of four Holocene terrace remnants in the 1928 Fairchild imagery in the vicinity of Punta Gorda (Fig. 3), and a similar number on the lee side of Pitas Point in 1940's vintage imagery (Fig. 4). The terraces are well expressed, and each is separated by a 1 to 6 m-high terrace riser.

Archeological excavations at VEN27 in the 1970's (Gamble, 1983), located principally on the 2nd emergent terrace at Pitas Point, support the timing and magnitude of uplift for the most recent event. Notably, house pits were emplaced along a paleo-beach face of the first emergent terrace. The midden deposits interfingered with the beach deposits, and an archeologic trench excavated through the paleobeach revealed shoreface gravel against the village deposits (Fig. 6), both indicating that this was the beach at the time of occupation. As there are no other recognized shorelines in the 300 m to the

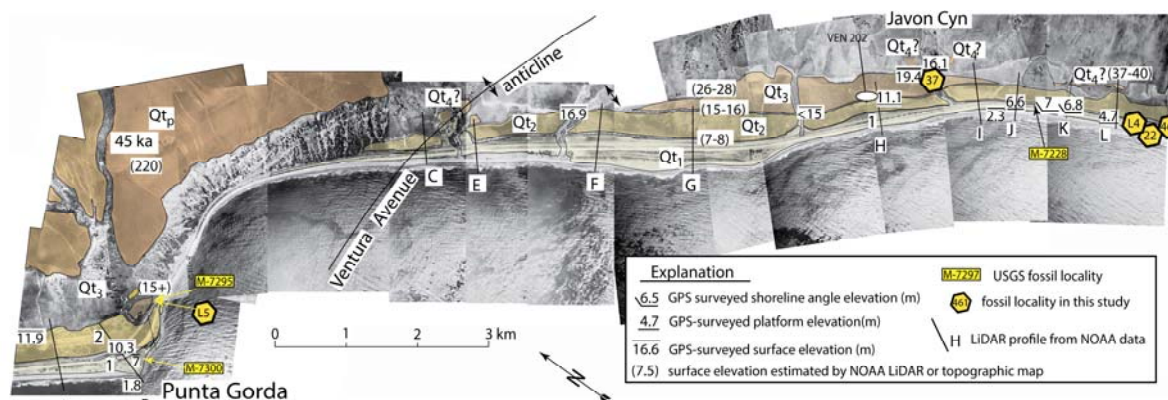


Fig. 3. Map of Holocene marine terraces from Punta Gorda eastward to nearly Pitas Point. Upper map shows the terraces relative to the modern topography, whereas the lower map shows the environment in 1928; this is the base upon which the mapping was completed. NOAA coastal LiDAR data aided with elevations (above msl) of preserved terrace remnants. Fossil localities are shown in yellow, with boxes showing USGS collection sites and stars showing our sites.

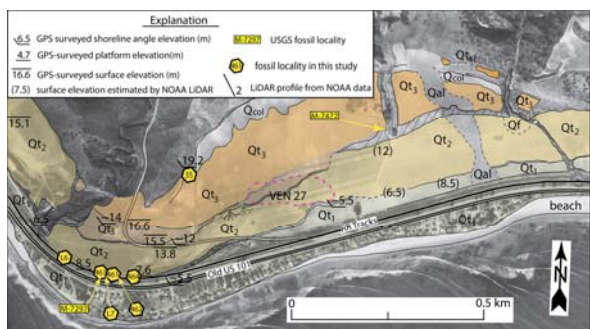


Fig. 4. Map of Holocene marine terraces at Pitas Point, using 1950 stereo aerial photographs as the base. Yellow boxes are USGS sample localities, yellow circles are sample localities from this study. The location of VEN 27 is indicated.

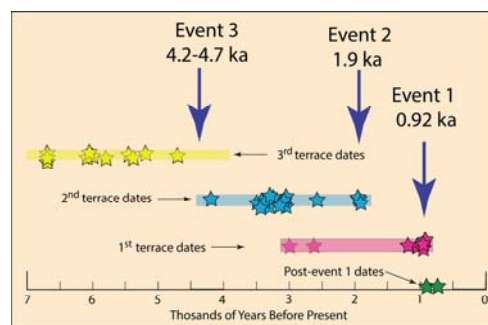


Fig. 5. Radiocarbon dates (stars) determined on mollusks and charcoal from the first three emergent marine terraces from Pitas Point to Punta Gorda. The uplift event ages are interpreted to have occurred at about 4.2-4.7 ka, 1.9 ka, and 0.92 ka.

The lowest three terraces have excellent lateral continuity between Punta Gorda and Pitas Point, whereas the fourth terrace appears to only be locally preserved as small remnants. The lowest emergent terrace (Qt1) is almost continuously preserved from east of Pitas Point to west of Punta Gorda and reaches a maximum surface elevation of about 7-8 m above msl near the axis of the VAA. The terrace deposits may be as much as 2 m thick, where exposed in roadcuts and railroad track cuts. Radiocarbon dating of mollusks recovered from the first terrace (Fig. 5) indicate that emergence occurred in the past millennium, and probably about 900 years ago.

modern beach, the sandy beach deposits south of the site are interpreted as the first emergent terrace. Furthermore, the terrace upon which the site rests is mapped and interpreted as the second emergent terrace. The site was originally surveyed in feet, with a datum of MLLW, and shows the first emergent terrace shoreline to be at 7.6 m elevation (surveyed as 25 ft), whereas the fore-edge of the second terrace is at 8.7 m (29 ft) (Fig. 7). The trench (Fig. 6) shows that the marine deposits are on the order of 2 m thick, indicating a shoreline elevation for terrace 1 of about 5-5.5 m at VEN 27 at Pitas Point.

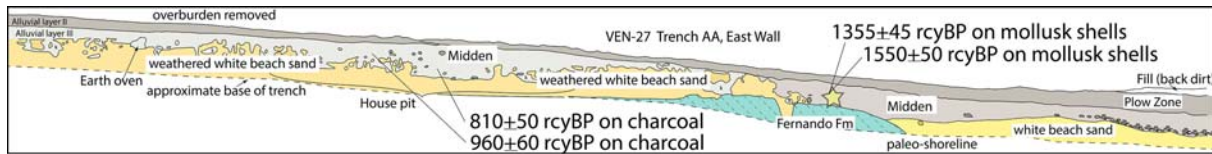


Figure 6. Log of trench C from VEN 27 archeology investigation at Pitas Point (Gamble, 1983). The VEN 27 midden deposits are shown to interfinger with littoral deposits, and several house pits were excavated into the terrace 2 deposits above the beach face. Radiocarbon dates are reported as uncalibrated ages: the two from the midden that buries the lower marine terrace are determined on shell, whereas the two from the VEN 27 midden house pit are on charcoal.

Two radiocarbon dates on detrital charcoal from the village yielded calibrated ages of about 1100 to 1000 AD (Fig. 6). Two additional dates on mollusk shells from the midden deposits below the shoreline, which must post-date terrace uplift, date to the same period. The eight radiocarbon dates on mollusks collected from the first terrace range in age from about 500 to 1200 AD. Together, the simple

The fourth terrace is only preserved near the mouths of a few canyons and reaches reported elevations near 40 m (Lajoie et al., 1979), although we could establish elevations only as high as about 30 m, which we infer to have occurred after sea level stabilized 6-7 ka BP. The surveyed terrace elevations are summarized in Fig. 8, showing the elevations as a function of distance from the fold crest.

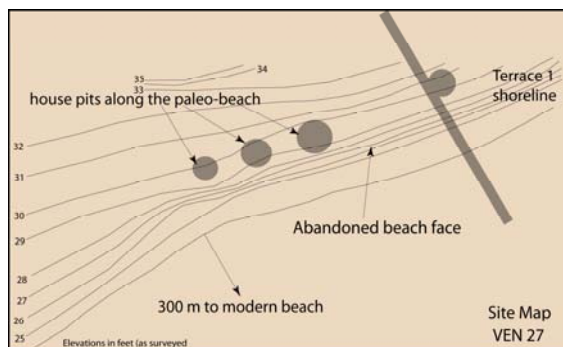


Fig. 7. Topographic map from transit survey data of VEN 27 archeological site. The shoreline for the first emergent terrace was recognized as a paleo-beach as early as the mid-1800's by coastal surveys. This survey used MLLW as the base elevation, which is slightly lower than MSL.

explanation is that the village was abandoned at the time of emergence around AD 1100 during an uplift event of at least 5 m at Pitas Point.

Similarly, the second emergent terrace was mapped from Pitas Point westward to Punta Gorda on the vintage aerial photography. The fore-edge of the terrace is exposed in a railroad cut at Pitas Point where it is rich with marine fauna. Radiocarbon dates on mollusks from this and other localities yield ages that range from about 100 AD to 2200 BC, with a couple of much older outliers (Fig. 5), suggesting that the second emergent terrace was actively cut between 1900 and 4200 years ago. Maximum surface elevations of this terrace reach to about 17-18m, and taken together with an assumed littoral deposit thickness of 2-3 m, indicates 14-16 m of emergence in the past 1900 years. The third terrace is well-preserved between Pitas Point and Punta Gorda and reaches a maximum surface elevation of 27m. Again, assuming a 2-3 m of littoral and colluvial sediments near the paleo-shoreline, we interpret this to represent about 24-25 m of uplift. This terrace is dated with a dozen radiocarbon dates on mollusks that range in age between 4.7 and 6.5 ka, so we infer it to have been uplifted at the time between the age ranges of the second terrace and third terraces, or between 4.2 and 4.7 ka.

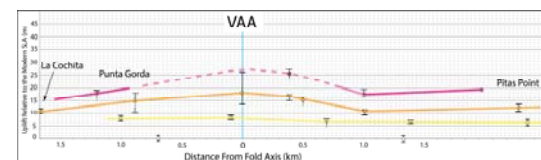


Fig 8. Elevations of emergent Holocene terraces from Pitas Point westward to La Conchita.

DISCUSSION

Uplift on the crest of the Ventura Avenue anticline is interpreted to be on the order of 7-8 m per event. The underlying geometry of the Pitas Point fault, with a dip of 50-60°, implies as much as 10 m of slip on the fault at depth. This magnitude of slip is typically associated with thrust earthquakes in the M7's, such as the Chi Chi earthquake in 1999 Taiwan (Mw7.8) and the 2010 Wenchuan earthquake in China (Mw7.9). This, in turn, requires large source dimensions.

Hubbard et al. (2014) have shown that the Ventura-Pitas Point fault may connect with the San Cayetano fault to the east. The hanging wall of this system is represented by the Ventura Avenue trend, which continues in the offshore to the west to nearly Point Conception. This provides a 180 km-long, continuous zone of thrust faulting and folding that can provide the source region that is sufficiently large to produce earthquakes in the magnitude range suggested by a 10 m displacement.

If we are correct that the terrace and village abandonment occurred about 900 years ago, and that the preceding event occurred about 1900 years ago, then the simple interpretation is for the occurrence of large earthquakes at these times. Similarly, terrace Qt2 is estimated to have been the active beach from about 4200 years to 1900 years ago, based on the many radiocarbon dates determined on mollusks from this terrace. This implies that it became active



about 4200 years ago, or slightly earlier, which we interpret as the age for the abandonment of terrace Qt3, which is dated as Young as 4.7 ka. Taken together, this allows us to interpret the length of time between two of the uplift events to have been about 1000 years and ~2500 years, and the time lapse since the most recent uplift event to be about 900 years. These estimates are consistent with the late Pleistocene uplift rate of 6-7 mm/yr, which independently would suggest an average recurrence of 8 m uplifts to be about 1100 years.

References Cited

- Dolan, J.F. and Rockwell, T.K., 2001, Paleoseismologic evidence for a very large ($M_w > 7$), post-1660 A.D. surface rupture on the eastern San Cayetano fault, Ventura County, California: Was this the elusive source of the damaging December 21, 1812 earthquake? *Bulletin of the Seismological Society of America*, 91, (6), 1417-1432.
- Donnellan, A., B. H. Hager, and R. W. King (1993a), Discrepancy between geological and geodetic deformation rates in the Ventura Basin, *Nature*, 366, 333-336.
- Donnellan, A., Hager, B., King, R. and Herring, T. (1993b). Geodetic measurement of deformation in the Ventura basin region, southern California. *Journal of Geophysical Research* 98 (B12): doi: 10.1029/93JB02766. issn: 0148-0227.
- Gamble, L., 1983, The organization of artifacts, features, and activities at Pitas Point: A coastal Chumash village. *Journal of California and Great Basin Anthropology*, 5, (1), 103-129.
- Hubbard, J., J.H. Shaw, J. Dolan, T.L. Pratt, L. McAuliffe, and T.K. Rockwell, et al., 2014, Structure and seismic hazard of the Ventura Avenue anticline and Ventura fault, California: Prospect for large, multi-segment ruptures in the Western Transverse Ranges, *Bulletin of the Seismological Society of America*,
- Lajoie, K.R., Kern, J.P., Wehmler, J.F., Kennedy, G.L., Mathieson, S.A., Sarna-Wojcicki, A.M., Yerkes, R.F., and McCrory, P.F., 1979, Quaternary marine shorelines and crustal deformation, San Diego to Santa Barbara, California: in Abbott, P.L. (ed.) *Geologic Excursions in the Southern California Area*, Geological Society of America Guidebook, 3-15.
- Lajoie, K.R., Sarna-Wojcicki, A., and Yerkes, R.F., 1982, Quaternary chronology and rates of crustal deformation in the Ventura area, California: in *Neotectonics in Southern California*, GSA Cordilleran Section fieldtrip guidebook, 43-52.
- Meade, B.J. and Hager, B.H., 2005, Block models of crustal motion in southern California constrained by GPS measurements. *Journal of Geophysical Research* 110, B03403, 19 p.
- Palmer, L.A., 1960, Marine terraces of California, Oregon, Washington. Ph.D. dissertation, University of California, Los Angeles.
- Rockwell, T.K., 1988, Neotectonics of the San Cayetano fault, Transverse Ranges, California. *Geological Society of America Bulletin* 100, 500-513.
- Rockwell, T.K., E.A. Keller, M.N. Clark, and D.L. Johnson, 1984, Chronology and rates of faulting of Ventura River terraces, California. *Geological Society of America Bulletin*, 95, 1466-1474.
- Rockwell, T.K., Keller, E.A., and Dembroff, G.R., 1988, Quaternary rate of folding of the Ventura Avenue anticline, western Transverse Ranges, southern California: *Geological Society of America Bulletin*, 100 (6) 850-858.
- Sawai, Y., Jankaew, K., Martin, M.E., Prendergast, A., Choowong, M., Charoentitirat, T., 2009, Diatom assemblages in tsunami deposits associated with the 2004 Indian Ocean tsunami at Phra Thong Island, Thailand, *Marine Micropaleontology*, 73 (1-2), 70-79.
- Topozada, T.R., Real, C., R. and Parke, D.L., 1981, Preparation of isoseismal maps and summaries of reported effects for pre-1900 California earthquakes: California Division of Mines and Geology Open File Report 81-11 SAC, 181 p.



INQUA Focus Group on Paleoseismology and Active Tectonics



paleoseismicity.org

NOTES



Reconstruction of a lateral offset paleo-channel on the Kego fault, western Japan

Azuma, Takashi

National Institute of Advanced Industrial Science and Technology, Tsukuba, 305-8567, Japan. E-mail: t-azuma@aist.go.jp

Abstract: This study focuses on the reconstruction of an offset paleo-channel on the Kego fault. The Kego fault is a left lateral active fault and locates in a major city, so that it is important to evaluate the magnitude of earthquakes from this fault. A paleoseismological trench survey was conducted at Kamiori on the southern part of the Kego fault. In the trench, fluvial sediments during Holocene - the last glacial period were exposed, and 25 sections were observed with interval of 30-50 cm along the strike of fault trace in order to reconstruct a shape of paleo-channel. As a result, this paleo-channel has been offset by the Kego fault one or twice and amount of offset is estimated ca. 4-5 m. This indicates the possibility of occurrence of M 7.5 earthquake on this fault, based on the empirical formula between slip per event and magnitude of earthquake.

Key words: Kego Fault, amount of lateral displacement, paleoseismological trench survey, Japan.

INTRODUCTION

This study focuses on the reconstruction of an offset paleo-channel crossing a left lateral fault. It is important to measure the amount of slip per faulting event based on the paleoseismological study, in order to evaluate the timing of faulting events and magnitude of earthquakes from active faults. But it is very difficult to measure amount of lateral offset in single trench.

There are some previous studies showing amount of offset on lateral faults by analysis of observation of multiple trenches or three-dimensional trenches. This study presents one of the examples of a measurement of offset paleo-channel based on the trenching survey on the Kego fault, a left-lateral fault in the northern Kyushu, western Japan.

Affected area and previous studies

The Kego fault is a left lateral active fault in urban area of Fukuoka (Hakata) City. It located along the geological boundary between granite and Paleocene and also along the topographic boundary between hills and alluvial plain. Because this city is one of the most populated and industrial cities in Japan, it is very important to evaluate the timing of faulting and magnitude of earthquakes from this fault.

Excepting the earthquake (M 7.0) in the west offshore of Fukuoka Prefecture in 2005, earthquake activities are very quiet in the northern Kyushu area. Epicenter of the 2005 earthquake located to the north of the Kego fault and its mechanism is left-lateral slip. It was one of the reasons that the Kego fault was focused on in the paleoseismological study and in the governmental earthquake research program.

Paleoseismological study on the Kego fault started in 1990's. A trench survey showed that the last faulting event occurred after 17 ka at the Osano site, in the most southern part of this fault (Shimoyama et al., 1999). AIST

group conducted trench surveys on the Kego fault and showed that the last faulting event occurred after 4 ka at the Kamiori site in the southern part of this fault (Miyashita et al., 2007). Though this fault is identified as a left-lateral fault, most of information on the slip amount is only vertical displacement measured on the trench wall and estimated from the drilling survey.

Method of paleoseismological trench survey

A paleoseismological trench survey at Kamiori site showed the existence of paleo-channel. Another trench was excavated at the Kamiori site. Direction of the new trench was along the strike of the Kego fault. It was excavated from the north wall of the previous trench and set back with 30-50 cm intervals. In the trench, fine fluvial sediments during Holocene-the last glacial period are exposed.

26 sections across the fault and 2 sections along the strike of the fault trace were observed and 26 samples were obtained for the radiocarbon dating in the trench. The outline of a paleo-channel crossing the fault was reconstructed based on the distribution of channel deposits in the trench.

OBSERVATION ON THE TRENCH WALLS

On the north wall of the previous trench at the Kamiori site, channel deposits contacted peaty silt with a high angle fault. Channel deposit contained charred materials dated 12-8 ka, whereas the age of peaty silt was older than 14 ka. That means that the channel downcut in the peaty silt around 12-8 ka and then faulting event occurred. Channel deposits began to distribute on the NE side of fault between the KOR-10 and KOR-24. On the SW side of the fault, distribution of channel deposits between KOR-10 and somewhere in the previous trench. From the observations of all of the trench walls, amount of the offset of paleo-channel are estimated as 4.4-5.6 m caused by left-lateral faulting.

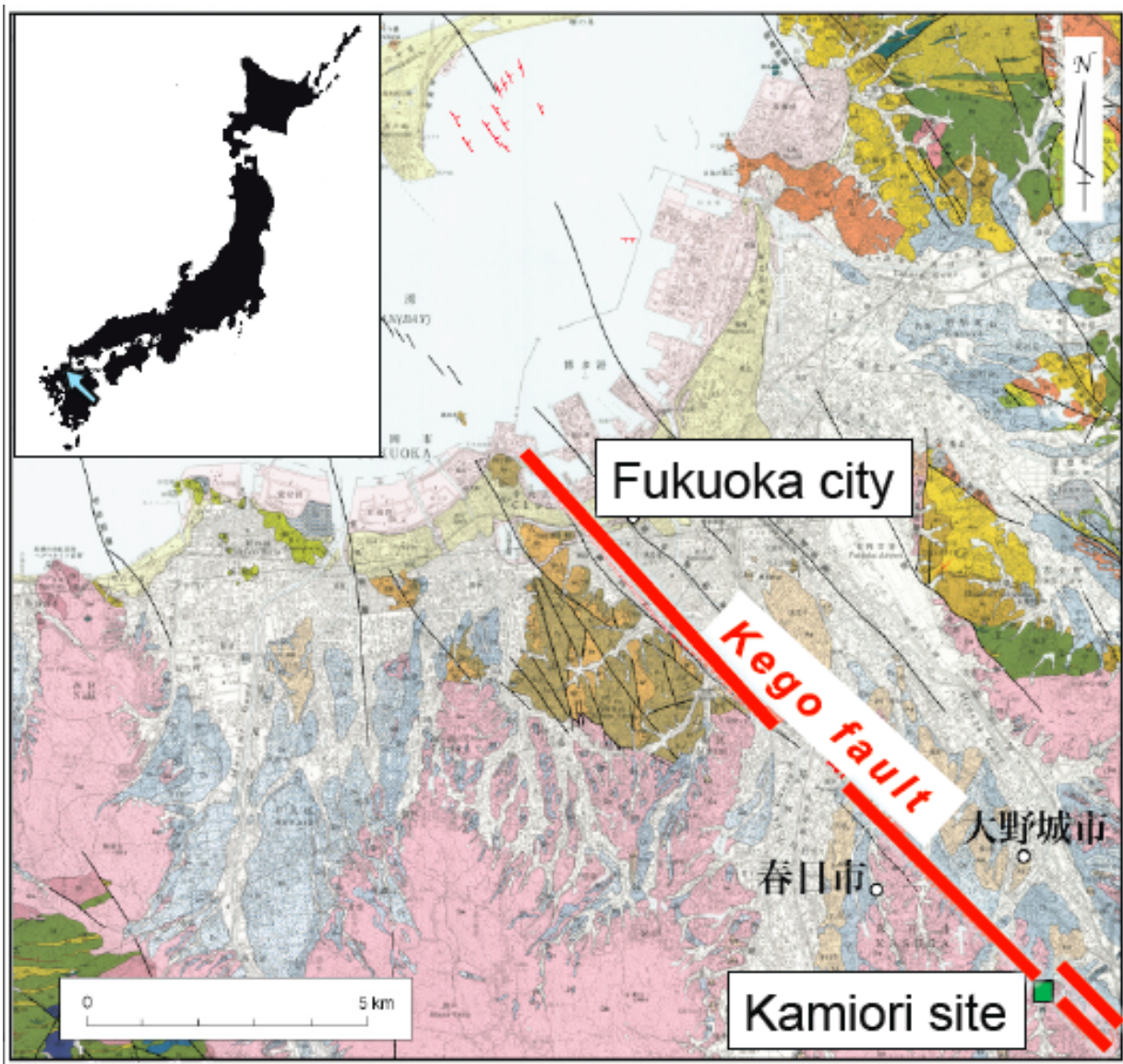


Figure 1: Map of the Kego fault. Base map is a 1:50,000 geological map of "Fukuoka" district (Karakita et al., 1994).

DISCUSSION

From a result of observation of trench wall, the axis and side walls of the paleo-channel deposits has been offset ca. 4.6-5.4 m. Activities of the Kego fault after production of the paleo-channel occurred once or twice based on the observation of the previous trench at Kamiori (Miyashita et al., 2007). This indicates that the offset had produced by one or two fault events and amount of slip per event ranges 2.3 m in minimum and 5.4 m in maximum. This result means the possibility of occurrence of earthquake larger than M 7.4 on this fault, based on the empirical formula between slip per event and magnitude of earthquake in Japan (Matsuda, 1975).

Acknowledgements: This survey was supported by the research project of seismic design for nuclear power plants in JNES in 2007.

References

- Karakida, Y., Tomita, S., Shimoyama, S., Chijiwa, K. (1994) Geology of Fukuoka district. Quadrangle Series, 1:50,000. Geological Survey of Japan, 192p. (in Japanese with English abstract)
- Matsuda, T. (1975) Magnitude and recurrence interval of earthquakes from a fault. Zisin 2, vol. 28, 269-283.
- Miyashita, Y., Azuma, T., Nikaido, M., Okazaki, K. (2007) Paleoseismological study on the Kego fault – A result of a trenching survey at Kamiori, Dazaifu City-. Gekkan Chikyu, no. 29, 133-138.
- Shimoyama, S., Matsuda, T., Chida, N., Sugiyama, Y., Iso, N., Matsumura, K., Suzuki, S., Mogi, T., Okamura, M., Matsuyama, N., Kuroki, M. and Katsume, Y. (1999) Trenching survey of the Kego fault, at Osano, Dazaifu City, Fukuoka Prefecture. Active Fault Research, no. 18, 55-64. (in Japanese with English abstract)

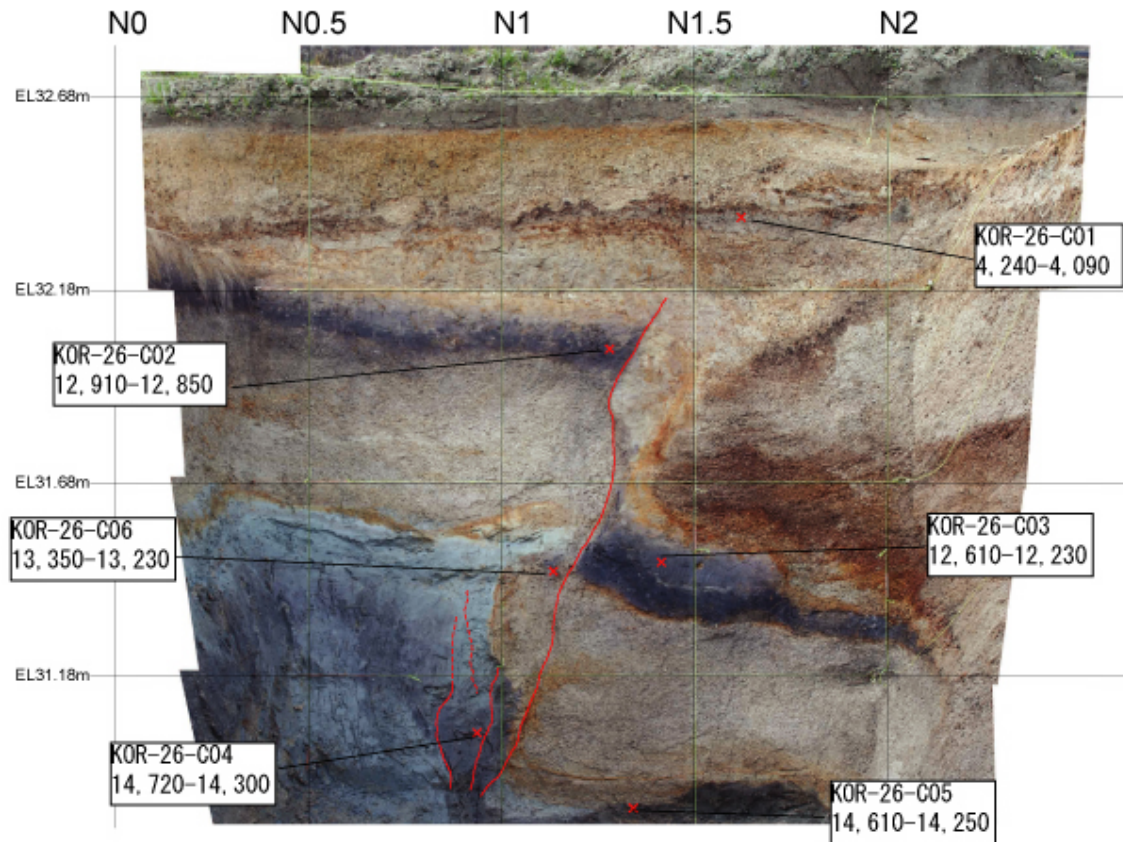


Figure 2: Photo of the trench wall of KOR-26 at the Kamiori site on the Kego fault. Size of grid is 0.5 m. Number in the box shows a ^{14}C age by the AMS dating.



INQUA Focus Group on Paleoseismology and Active Tectonics



paleoseismicity.org

NOTES



Important Issues Solved and Unsolved on the Paleoseismology of the North Anatolian Fault

Koji Okumura (1)

(1) Graduate School of Letters, Hiroshima University, 1-2-3 Kagamiyama, Higashihiroshima, 739-0045 Japan. Email: kojiok@hiroshima-u.ac.jp

Abstract: *Paleoseismological investigation has been conducted on the North Anatolian fault since late 1980s and advanced greatly after the 1999 Kocaeli earthquakes. However, we have not learned enough to understand the entire seismic cycles and the nature of recurring earthquakes. The problems left for further studies are summarized as follows. (1) Incomplete historic catalogs exerted too much influence on the interpretation of paleoseismological records. Geological data should be taken as primary information on earthquake records. (2) We learned about the variability and repeatability of coseismic slips over earthquake cycles on few of the 20th century segments. Much more studies on past coseismic slips are needed. (3) There are few reliable facts on the repeatability of segmentation and rupture sequence, but there is only optimistic and loosely constrained inference on the repetition of the 20th century westward-migration. (4) The data on cumulative offsets and slip rates over multiple earthquake cycles are still sparse. The information on cumulative offsets and slip rates in 1000 years have been reasonably reconstructed in a few paleoseismological sites. However, the cumulative offsets and slip rates in 1000 to 10000 years are known at very few sites and reliability is still not very high. It is necessary to conduct intensive and larger-scaled studies on the past history of ruptures and their natures.*

Key words: *The North Anatolian fault, recurrence time, characteristic slip, paleoseismology, historic earthquake.*

1. Incomplete historic catalogs

The completeness of historic catalogs are seldom questioned by paleoseismology though it is the only way to supplement incomplete historic records. Many paleoseismological works just confirm catalogs based on historic records. However, the excavation of 1944 and 1939 segments exposed evidence of earthquakes without any historic reference. (Okumura et al., 1993). Historic records are unreliable during periods of warfare and disruption. Historic records are reliable only 500 years even in Japan and it is presumably the case for Turkey before the fall of the Byzantine Empire.

Completeness of historic earthquake catalogs must be examined by geologic records. The historic records on large earthquakes from the North Anatolian fault are tested in trenches on the segment that ruptured in 1944. Previous results indicated 3 historic and 1 geologic events in past 1000 years with characteristic ~5 m slip and quasi-periodic recurrence every 200-280 years (Kondo et al, 2005a; 2005b, 2010).

The author and the collaborators excavated seven new trenches at the Ardiçli paleoseismic site, located about 15 km east of Gerece, to resolve displacement on a Byzantine-aged channel and the times of the offsets. The channel appears to have been excavated to drain the site and allow mining of clay to make bricks and tiles. A kiln is adjacent to the channel. The V-shaped channel thalweg is offset 13.5±1.5 m, and based on many cross-fault trenches, represents slip in the past three surface ruptures. Dating of pine cones, wood, and charcoal in the channel deposits and in the stratified sediments outside the channel suggest that this channel was cut in the 11th-13th century AD. The surface rupture that initially offset

the channel postdates the historically-reported earthquake in 1035 AD and predates the one in 1668.

The surface geomorphology records displacement from two more recent events. The 1944 surface rupture in this region produced 4-5 m of slip based on offset field boundaries and small channels. Older fluvial channels and rills in this area show about 10 m of displacement. We dated the fill from a 10 m-offset channel, and place the penultimate event as younger than about 1650 AD, which must correspond to the well-documented earthquake in 1668. From our previously reported work, we resolved 22-26 m of displacement for the past five surface ruptures on a 6th-century channel. Together, these data argue for fairly characteristic slip for the past five earthquakes. The interval between events ranges from around two centuries to four centuries, and there is no apparent correspondence between elapsed time and the amount of displacement. These observations might be inconsistent with the time- and slip-predictable models of earthquake recurrence.

2. Variability and repeatability of coseismic slips

The variability and repeatability of slip-per-event have been studied by Kondo et al. (2005a) on the 1944 segment and further studies are ongoing on the 1943, 1942, and 1939 segments. Kondo et al. (2010), interpreted the small slip in 1942 is related to the east-to-west rupture of the 1939 earthquake rupturing the continuous strand along Kelkit Çay in the east toward the Amasya branch in the west. Large slip on the 1942 from west may trigger the rupture on the Kelkit Çay strand in east. Slip variability might be related to the changing rupture direction across a large jog or segment boundary in the slip surface.



The North Anatolian fault is usually regarded as a simple shear zone with a constant GPS slip rate of 20 to 25 mm/yr. However, geologic data indicate the fault system is much more complicated. Geologic slip rates are significantly smaller than GPS slip rates and recurrence intervals are different among 20th century segments. The most reliable slip rate estimates come from the 1944 segment. Estimated cumulative slips are 14 m for 3 earthquake cycles in 910 years, and 21 to 23 m for 5 cycles in 1550 years. The slip rate is about 15 mm/yr. On the 1943 segment 10 to 15 mm/yr is estimated in Aslancayir. In Erzincan a higher slip rate of 20 mm/yr in the past 750 years is estimated. Recurrence intervals are 150–250 yr (historic) in Marmara, 300+/-30 yr on 1944 segment, 280–600+ years on 1943 segment, and 180–220 years in east of Erzincan. The slip-rate and event frequency are high on the 1939 segment and farther east, and in Marmara region. They are evidently low on the 1943 segment. If we consider the bifurcation of the fault into Bursa, Iznik-Mekece, and Izmit-Marmara strands, the high activity of the Marmara segment is remarkable. Geometry and tectonic settings may explain the variability. The area in east of Erzincan is under regional NS compression. Main 1939 segment (Erzincan–Niksar) has almost pure strike slip without extension. There are no pull-apart basins, which were the result of inaccurate fault mapping. Regional uplift and rapid lowering of erosional base level prevail along the 1939 segment. The Amasya branch that ruptured over 100 km in 1939 is a significant structure that takes certain amount of the slip and distributes it into the central Anatolia. The 1943 and 1944 segments consist of simple and straight strands without large steps, discontinuities and bifurcations. The Bolu-Mudrunu duplex is the most complicated with compressional 1999 Duzce segment and short 1957–1967 segments. The rupture pattern and history differ greatly across this Bolu-Mudrunu area. 1999 and Marmara segments consist of WNW transtensional and EW less tensional strands. Realization of the complexity and variability will lead us to

more realistic understanding of the seismic cycles on the fault.

3. Repeatability of segmentation and rupture sequence

Judging from the rupture history in and around the 1944 segment, the extent of seismic ruptures differ from one event to another. Kondo et al. (2005a) hypothesized characteristic slip in each behavioral segment and combination of the behavioral segment as a segment of an earthquake. Okumura (2006) recognized stationary and variable segment boundaries based on structural significance or size of discontinuity affecting rupture propagation.

Through a review of segmentation models of the Median Tectonic Line fault system in Shikoku, following two main issues were recognized. Firstly, the segmentation model based on the geometry and distribution of vertical movements cannot confine segments because the model mixes up spatial phenomena of various size and magnitude. Secondly, the chronological constraints in geologic data on past earthquakes are too poor to define the segments. In this paper, the author examined the 20th century segmentation of the North Anatolian fault from the view points of the size of the segmentation boundaries and their stability through time. The area between the eastern end of the 1999 Izmit earthquake ruptures and the western end of the 1944 rupture, namely the Bolu-Mudurnu Gap is a 70 km long and 25 km wide discontinuity of the North Anatolian fault system. This area is regarded as a gap because the rupture history to the west (16th century, 18th century, and 20th century) is completely different from that to the east (14th? century, 1668, and 1939–1944), and because the size of earthquake inside the gap is much smaller than the earthquakes on both sides. If we take this gap as a segment boundary, it has been stable over a few earthquake cycles. On the other hand, the other minor

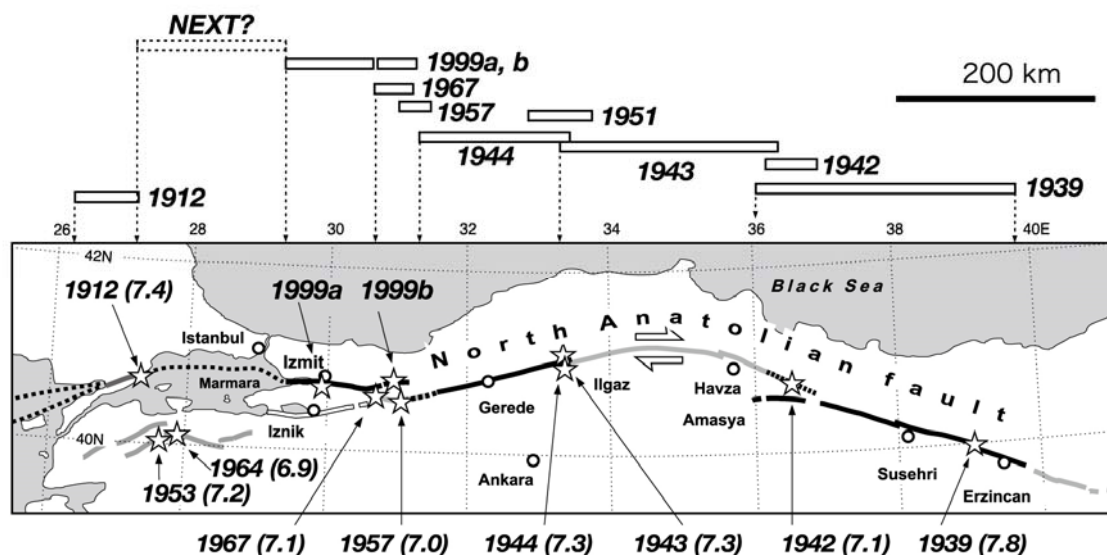


Fig. 1 20th century rupture sequence, epicenters, and paleoseismological sites on the North Anatolian fault.



segment boundaries have not been stable over earthquake cycles. Especially, the segment boundaries less than a few kilometers in width or in length like the 1943 and 1944 boundary did not behave as a boundary in former series of earthquakes. Okumura et al. (2000) estimated the amount of the subsided mass in a small pull-apart formed in 1999 Izmit earthquake and estimated the depth of the pull-apart structure is around 3 to 5 times of the width. If the dimension is similar to the larger pull-apart, a jog less than several kilometer wide does not affect the most part of the seismogenic fault. Therefore, the larger segment boundaries remain stable over time. On the Median Tectonic Line, only the gaps around the Okamura fault has significant size and coincide with a paleoseismological segment boundary. The area between the Komatsu fault and the Iyo fault may be taken as a large area of discontinuity.

4. Cumulative offsets and slip rates in 1000 years

The discrepancy between geologic and geodetic slip rate along the North Anatolian fault has been more evident as solid incremental (Kondo et al. 2010) and cumulative (Kozaci et al. 2009, Okumura et al. 2010) slip rate data are accumulated. The strain transient effect (Kozaci et al. 2009) could be a plausible cause for the discrepancy. At the same time, the seismicity, crustal deformation, and active structures indicate significant amount of distributed tectonic strain far inside the Anatolian micro plate. The accumulation and release of the distributed strain may affect the seismic cycle of the plate boundary. However, there is almost no quantitative information on the earthquakes and faults in central Anatolia. Considering the magnitude of the discrepancy, it is important to understand the intra-plate tectonics and to prepare for the seismic hazard in less active intra-plate areas. For this purpose, the author carried out detailed survey of the Amasya fault. Amasya fault is the only major branch of the North Anatolian fault in Central Anatolia. While the main strand of the North Anatolian fault steps at the Niksar basin, the Amasya fault is the westward continuation of the North Anatolian fault along the Kerkit River valley in the east. The fault extends to southwest over 250 km into the Anatolian microplate. In 1939 about 100 km long eastern portion of the Amasya fault ruptured together with the 200 km long main strand between Niksar and Erzincan. The location and slip distribution of the 1939 ruptures, as well as slip-rate and paleoseismicity on the Amasya fault have been studied very little. Preliminary fault mapping between 36 E and 37 E was done with Google-Earth satellite photos and 1939 rupture locations were confirmed on site by interviews to aged local people. Cumulative slip measurement and slip-rate estimation were conducted in east of Canbolat (37.6228 E) and east of Findicak (36.4572 E). At Canbolat, 11.4 m cumulative offset was measured on faulted hill slope. Assuming the periglacial origin of the slope formation, preliminary slip-rate estimate is around 1 mm/yr. At Findicak, offset terrace-riser indicate 7 to 8 m cumulative offset. The riser predates 2000–3000 year old terrace surface, and a rough estimate of the slip-rate is less than a

few mm/yr. Further investigation on paleoseismicity is strongly required.

5. Cumulative offsets and slip rates in 1000 to 10000 years

The cumulative offset and slip-rate in thousands of years has been very poorly studied until now. Only Kozaci et al. (2007) examined 2000 to 3000 year long-term slip-rate on the 1943 segment. Otherwise, long-term slip-rate has been discussed on very low resolution data for uncertain time periods only. These estimates have little to do with better understanding of fault behavior and earthquake recurrence. We really need more intensive studies on high-resolution long-term slip-rate of the North Anatolian fault. The discrepancy between geodetic and geologic slip rates (Okumura, 2006) is another important issue to be further investigated.

The geologic and geomorphic history of Anatolia during the Late Holocene, or a few millennia since the chalcolithic age have not been studied in details except for certain time horizons indicated by rather limited archaeological or historical markers. Otherwise, the Late Holocene environmental changes in Anatolia has not been revealed diachronically. It is mostly due to the paucity of chronological constraints such as radiocarbon dates and cosmogenic nuclide dates, and to limited distribution of continuous fine sediments bearing microfossils. On the other hand, paleoseismologists have conducted trenching studies of the North Anatolian fault since 1990 and 1999 Kocaeli earthquake further promoted geological research of the fault. There are many successful trenches that exposed fine sediments containing datable organic materials, however the section covers usually less than 1000 years and 2000 years at most. Since the purpose of paleoseismological trenching is to know the timing and slip of past earthquakes paleoenvironmental analyses are not common, but several sections with tens of fine radiocarbon dates are the best source of information on sedimentation, erosion, and fluvial activities.

Around Gerede, in north of Ankara, paleoseismology of the 1944 segment has been studied very much into details (Okumura et al., 1990, 1994, 2003, 2009; Kondo et al., 2010). Repeated trenching in an ideal sedimentary and tectonic condition demonstrated 6 unequivocal rupture events in 1500 years. In the Gerede area along the North Anatolian fault, which lies on the southern foot of ~3000 m mountains between the fault and the Black Sea, formation of extensive alluvial fan and fluvial terrace surfaces took place around 1.5 ka (Okumura et al., 1993; Kondo et al., 2010). This deposition episode of fluvial gravels is followed by deposition of finer sediments until around 16th century A.D. Between 16th century A.D. and 1668 Great Anatolian earthquake, most streams in this area started incision after about 1000 years of stability or local aggradation. Therefore, it is rather easy to find out streams offset by one or two events but rather difficult to find more offset on the surface because of the burial of the channel before 1668. In summary, in Gerede area rapid deposition of gravels occurred in 5th century and



aggradational condition lasted until 16th century. Then, degradation has been prevailing until present day.

In recent years, cosmogenic nuclide dating of alluvial deposits enabled estimation of longer term slip-rate based on cumulative offset over 3000 years in central Anatolia on the 1943 segment. At Eksik, Kozaci et al. (2007 and 2009) applied ^{36}Cl dating on alluvial sediments to estimate ~3 ka slip-rate. Kozaci et al. (2007) measured 46 m offset of valley walls derived from deep incision and then dated the top of the valley fill to be 2.0 to 2.5 ka by ^{10}Be and ^{14}C . They yielded a rather high slip rate of 20.5 ± 5.5 mm/yr by taking the termination age of valley fill as the age of incision. At Eksik, we can recognize three phases of fluvial activity. The incision indicates the first phase characterized by degradation. The second phase is aggradational and terminated before 2.0 to 2.5 ka. After the filling up, the top of the fill is now incised deeply, so the third degradational phase begun after 2.0 to 2.5 ka and continues until present. The timing of the first phase is not known, but applying the slip-rates acquired on 1942 and 1943 (Okumura et al., 2003; Kondo et al., 2010), 46 m offset could have been accumulated during 3000 to 4000 years.

At Taphtaköprü on the 1943 segment, Kozaci et al. (2009) reported a formative age of an alluvial fan at 3.0 to 3.5 ka. This may coincide with the degradational phase at Eksik which is located higher altitude and surrounded by steep mountain slopes while Taphtaköprü is located further down reach.

In the Erzincan Basin in the eastern Anatolia about 1300 year long records of sedimentation and faulting were exposed in a trench (Okumura et al., 1993). The aggradational condition lasted between 8th century A.D. and 13 century A.D. Later half of the 2nd millennium is characterized by incision except for modern alluvial fans. The timing is slightly different from Gereede area, but the long term tendency is similar.

Up to now, such well-dated sedimentary and erosional histories are limited. Studies on fluvial terraces and deposits of Late Holocene will bring perspective into the diachronic change of fluvial activities in Anatolia.

Acknowledgements: This short report is based on the abstracts reported by myself in various scientific meetings. The field investigations, laboratory analyses, and discussions have been conducted together with my collaborators who are listed in the reference list below.

References

- Kondo, H., Awata, Y., Emre, O., Dogan, A., Ozalp, S., Tokay, F., Yildirim, C., Yoshioka, T., and Okumura, K. (2005a): Slip Distribution, Fault Geometry, and Fault Segmentation of the 1944 Bolu-Gerede Earthquake Rupture, North Anatolian Fault, Turkey. *Bull. of the Seism. Soc. of Amer.*, v. 95, p. 1234-1249, doi:10.1785/0120040194
- Kondo, H., Awata, Y., Emre, O., Ozaksoy, V., Yildirim, C., and Koji Okumura (2005b): Characteristics of Repeated Faulting Behavior along the 1944 Bolu-Gerede Earthquake Rupture, North Anatolian Fault, Turkey. *Geographical Sciences*, 60, 213-219.
- Kondo, H., Ozaksoy, V., and Yildirim C. (2010): Slip history of the 1944 Bolu-Gerede earthquake rupture along the North Anatolian fault system: Implications for recurrence behavior of multisegment earthquakes, *J. Geophys. Res.*, 115, B04316, doi:10.1029/2009JB006413.
- Kozacı, Ö., Dolan, J. F., Finkel, R. C., and Hartleb, R. D. (2007): Late Holocene slip rate for the North Anatolian fault, Turkey, from cosmogenic ^{36}Cl geochronology: Implications for the constancy of fault loading and strain release rates, *Geology*, 35(10), 867-870, doi:10.1130/G23187A.1.
- Kozacı, Ö., Dolan, J. F., and Finkel, R. C. (2009): A late Holocene slip rate for the central North Anatolian fault, at Tahtaköprü, Turkey, from cosmogenic ^{10}Be geochronology: Implications for fault loading and strain release rates, *J. Geophys. Res.*, 114, B01405, doi:10.1029/2008JB005760.
- Okumura, K. (2005): Progress in On-fault Paleoseismology: Dating and Date Analyses. *Geographical Sciences*, 60, 167-174.
- Okumura, K. (2006): Segmentation model of a long fault zone based on the size and temporal stability of the segment boundaries. Abstract T34B-06 presented at 2006 Fall Meeting, AGU, San Francisco, Calif.
- Okumura, K. (2010): Intraplate Deformation of the Anatolian Micro Plate on the Amasya Branch Fault in Central Anatolia, Turkey. Abstract T33A-2207 presented at 2010 Fall Meeting, AGU, San Francisco, Calif.
- Okumura, K., Rockwell, T. K., Duman, T., Tokay, F., Kondo, H., Yildirim C., and Özaksoy, V. (2003): Refined slip history of the North Anatolian fault at Gereede on the 1944 rupture, Abstract S12B-0384 presented at 2003 Fall Meeting, AGU, San Francisco, Calif.
- Okumura, K., Awata, Y., Toda, S., Sugai, T., Furuhashi, T., Ozalp, S., Dogan, A., Emre, Ö., Duman, T., and Haraguchi, T. (2000): Formation of a Coseismic Pull-Apart Basin on the North Anatolian Fault Associated with the August-17-1999 Izmit (Kocaeli) Earthquake. Abstract S51A-08 presented at 2003 Fall Meeting, AGU, San Francisco, Calif.
- Okumura, K., Rockwell, T. K., Akçiz, S. O., Wechsler, N., Aksoy, E. M., and Ishimura, D. (2009): Slip History of the 1944 Rupture Segment on North Anatolia Fault Near Gereede, Turkey: Constraints on Earthquake Recurrence Models, Abstract S41A-1897 presented at 2009 Fall Meeting, AGU, San Francisco, Calif.
- Okumura, K., Yoshioka, T., and Kusçu I. (1993): Surface faulting on the North Anatolian fault in these two millennia, *U.S. Geol. Surv. OFR*, 94-568, 143-144.
- Okumura, K., Yoshioka, T., Kusçu, I., Nakamura, T., and Suzuki (1994), Y., Recent Surface Faulting on the North Anatolian Fault East of Erzincan Basin, Turkey — a Trenching Survey, *Summaries of Researches Using AMS at Nagoya University*, V., 32-48.
- Okumura, K., Yoshioka, T., Kusçu, I., (1990): Trenching Survey of the North Anatolian Fault at Ardicli, East of Gereede, Turkey-an Initial Report. *Active Fault Research*, 8, 9-15.



INQUA Focus Group on Paleoseismology and Active Tectonics



paleoseismicity.org

NOTES



Persia as a Paradise for Paleoseismological Studies, Example: Paleoseismologic and Geodynamic Issues, NW Iran

Shahryar SOLAYMANI AZAD (1&3), Khaled HESSAMI (2), Herve PHILIP (3), Jean Francois RITZ (3), Stephane DOMINGUEZ (3)
Mohammad Reza ABBASSI (2), Mohammad FOROUTAN (4), Esmaeil SHABANIAN (5)

- (1) Seismotectonics & Seismology Department of Geological Survey of Iran
- (2) Seismotectonics Department of International Institute of Earthquake Engineering & Seismology, Iran
- (3) University of Montpellier II, France
- (4) University of Paris VI, France
- (5) Institute of Advanced Studies in Basic Sciences Zanjan University, Iran

Abstract

Iran belongs to the central portion of the Arabia-Eurasia collision zone. Consequently, strong-moderate earthquakes (mostly with long recurrence intervals), as a part of total tectonic deformation, strike this domain. In most cases, the well-preserved coseismic surface faulting features (according to low rate of erosion) and more than 2500 years long history of the seismically active Persia makes it to a suitable domain to perform paleoseismological studies. In this study, to prepare more reliable data to assess the seismic hazard for the highly populated region of Iran we focus our study on two seismogenic fault zones of the Mousa-North Tehran (E-striking), in Tehran capital city and the North Tabriz (SE-striking) in Tabriz metropolis within NW of Iran where several historical seismic records have been well-documented. Preliminary results reveal different seismic behavior for the eastern and western sectors of the faults especially in terms of slip-rate and kinematic. Moreover, the results could be used to better understanding of the geodynamics of the NW Iran.

Key words: Paleoseismology, geodynamics, Tehran, Tabriz, NW Iran

Introduction

Iran is part of the Alpine Himalayan orogenic belt that extends over more than 10000 km from west Europe to Southeast Asia (e.g. Stöcklin et al., 1968). It is actively deforming in response to the northward motion of the Arabian plate that collides with Eurasia. As indicated by GPS measurements (e.g. Vernant and Chéry, 2006; Reilinger et al., 2006) the general direction of crustal motion in Iran, compare to Eurasia fixed, is toward the north at 23–25 mm/yr. The GPS strain field can be divided into several areas: the central Iranian plateau appears to move N355°E at 14 mm/yr. while north of Tabriz, the Talesh and Armenia move N10°E at 12 and 8 mm/yr respectively. A part of deformation (5-6 mm/yr) seems to be accommodated across the Alborz Range, which have partitioned generally to N-S compression and E-W horizontal shearing. In response, strong to moderate earthquakes (with mostly long return periods) strike this mainly intraplate region. According to historical seismicity catalogues (e.g. Ambraseys and Melville 1982; Berberian, 1994; Berberian and Yeats 1999), at least 450 destructive earthquakes were reported in Iran since 600 BC (Solaymani Azad et al., 2011a). Comparison of historical and instrumental earthquake catalogues of Persian territory reveals an intraplate tectonic regime and then, long return periods for most of strong seismic events. In the last decades, strong earthquakes ($M > 6.5$) occurred at a similar rate, each five to six years in average (Silakhor ($M_s = 7.4$, 1909), Salmas ($M_s = 7.4$, 1930), Torud ($M_s = 6.5$, 1953), Lar ($M_s = 6.7$, 1960), Buin Zahra ($M_s = 7.2$, 1962), Dasht-e-Bayaz ($M_s = 7.4$, 1968), Qir ($M_s = 6.9$, 1972), Khorghu ($M_s = 7.0$, 1977), Tabas ($M_s = 7.7$, 1978), Qayen ($M_s = 7.1$, 1979), Rudbar-Manjil ($M_s = 7.3$, 1990), Sefidabeh ($M_s = 6.1$, 1994), Ardebil

($M_s = 6.1$, 1997), Birjand ($M_s = 7.3$, 1997), Fandoga ($M_w = 6.6$, 1998), Avaj ($M = 6.6$, 2002), Baladeh ($M = 6.3$, 2003), Bam ($M = 6.7$, 2003), Zarand ($M = 6.4$, 2004), Tuchahi ($M = 5.9$, 2010), Negar ($M = 5.8$, 2010), Rigan ($M = 6.7$, 2010), Arasbaran ($M = 6.4$ and $M = 6.3$, 2012) and Sistan ($M = 7.7$, 2013)). The sources of all of these seismic events are well identified now and correspond to active reverse or strike-slip faults mainly concentrated in the south of Iran (Zagros fold-and-thrust belt), eastern Iran and north-west of Iran (Alborz ranges and Talesh-Azerbaijan region). However, it is important to point out that for some of these events, the seismic source was unknown before the occurrence of the earthquake because active fault mapping of Iran is still incomplete (Solaymani Azad et al., 2011a). Mostly shallow moderate-strong earthquakes of Iran together with low erosion rate within arid Persian territory help to have well-preserved surface faulting features for both instrumental and historical events.

Arid Persian territory contains a number of cities and villages which have been localized and then developed near the valleys within mountain fronts to supply water. In most cases, the mountain fronts in turn have mainly formed by active structural zones. The well-preserved coseismic surface faulting features and more than 2500 years long history of the seismically active Persia makes it to a suitable domain to conduct paleoseismological studies. To assess the seismic hazard for all Iranian cities, especially based on detailed and then expensive paleoseismological investigations, the large and highly populated regions (such as; NW Iran) have logically the priority. Within high-populated region of the NW Iran, Tehran and Tabriz cities are located in well-studied areas where several destructive historical seismic events have



been documented. In this domain, the main seismogenic sources are known as the Mosha-North Tehran fault, in Tehran and the North Tabriz fault in Tabriz regions (Fig. 1).

The Mosha (Dellenbach, 1964) and North Tehran (Rieben, 1955; Tchalenko et al., 1974; Berberian et al., 1985) fault system are mainly reverse ~E-striking faults with a structural junction zone in east of Tehran city. In addition, Quaternary markers and structural evidence reveal active sinistral faulting features concentrated along the fault zones (e.g. Tchalenko et al., 1974; Trifonov et al., 1996; Solaymani Azad et al., 2003; Ritz et al., 2006; Landgraf et al., 2009; Solaymani Azad et al., 2011b; Shabanian et al., 2012; Ghassemi et al., 2014).

The North Tabriz fault as another main geological structure of the NW Iran (Eftekharneshad, 1975; Nabavi, 1976) locates at the immediate vicinity of the Tabriz metropolis. This dextral active fault was the seismic source of at least three historical damaging events (e.g. Berberian and Arshadi, 1976; Berberian 1997; Karakhanian et al., 2002; Hessami et al., 2003; Solaymani Azad, 2009; Solaymani Azad et al., in press; Tectonophysics).

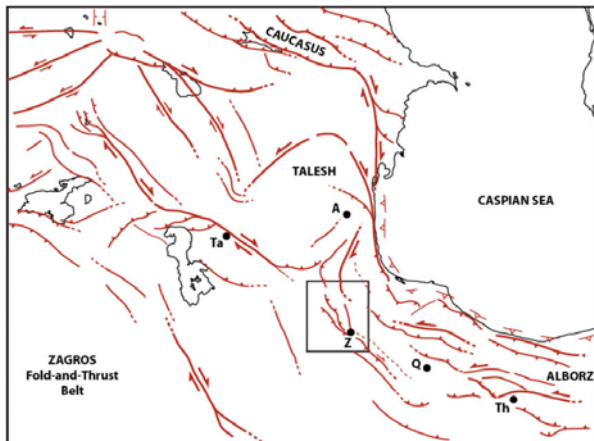


Fig. 1: Active faulting within NW of Iran (after Solaymani Azad, 2009). Note to the Left and right-lateral fault zones of the Mosha-North Tehran and North Tabriz in eastern and western portions of the domain. Ta: Tabriz, Th: Tehran, and Z: Zandjan.

In the present study, we summarize the paleoseismologic and morphotectonic characteristics of different sectors of the faults to investigate and compare the seismogenic behavior of them. In addition, the results could be used to better understanding of the geodynamics of the NW Iran.

Discussion

Tehran and Tabriz as the two high populated cities are located near-by the Mosha-North Tehran and North Tabriz fault zones at the eastern and western parts of the NW Iran, respectively. According to historical seismicity catalogues they were experienced a number of strong

seismic events. Within Tehran region, paleoseismological studies performed along the East Mosha-North Tehran fault system (e.g. Solaymani Azad et al., 2003; Ritz et al., 2006; Solaymani Azad, 2009; Solaymani Azad et al., 2011b; Ghassemi et al., 2014) revealed larger amounts of slip rate (i.e. 2-3 mm/yr) rather than western parts of the fault system (i.e. less than 1 mm/yr: e.g. Nazari, 2006; Ritz et al., 2012). According to morphotectonic and paleoseismologic studies within Tabriz region (Hessami et al., 2003; Solaymani Azad, 2009), the amount of detected Holocene strong paleo-seismic events along the western sector of the North Tabriz fault are significantly greater than the eastern sector of the fault zone (Solaymani Azad et al., in press; Tectonophysics).

Within central portion of the domain, the main morpho-structural result of this deformation pattern has been developed as N-S Talesh-Zandjan topographic reliefs. Despite of sparse paleoseismological investigations within NW of Iran, the slower active deformation in central portion of this domain could be compatible with longer return periods (more than 2 kyr; Berberian and Ghorashi, 1990) of strong earthquakes (e.g. Rudbar earthquake, 1990, M~7.3). According to historical (e.g. Ambraseys and Melville 1982; Berberian, 1994) and instrumental earthquake catalogues, Zandjan city as the greatest historic metropolis in southern part of this central domain can be considered as a seismic gap. Morphotectonic studies performed in Zandjan historically seismic gap (Solaymani Azad et al., 2011a) revealed an intraplate active fault network which is capable to produce strong-moderate earthquakes with return periods over two thousand years.

Conclusion

The features of active deformation in eastern and western sectors of the NW Iran show respectively left and right-lateral faulting evidence along roughly E-striking structural zones such as Mosha-North Tehran and North Tabriz faults. Paleoseismological studies along the eastern and western parts of the fault zones have been revealed different amounts of coseismic deformation rate, which decrease to the central portion of the domain. Logically, this deformation pattern could be compatible with longer return periods of strong earthquakes observed within this intraplate region.

Acknowledgment

We appreciate all notional and international colleagues and research organizations that helped us to prepare a basic and surely, more reliable data set for seismic hazard assessments of the high populated cities of Persia.

References

- Ambraseys, N. and Melville, C. P., 1982, A history of Persian earthquakes, Cambridge Earth Science Series, Cambridge University Press, London.



- Berberian, M., and Arshadi, S., 1976, On the evidence of the youngest activity of the North Tabriz fault and the seismicity of Tabriz city, *Geol. Surv. Iran Rep.*, 39, 397–418.
- Berberian, M., Qorashi, M., Arzhang-ravesh, B., Mohajer-Ashjai, A., 1985. Recent Tectonics, Seismotectonics and Earthquake Fault Hazard Investigations in the Greater Tehran Region: Contribution to the Seismotectonics of Iran: Part V: Geological Survey of Iran, report 56, p. 316.
- Berberian M. and Ghorashi M., 1990, The June 20, 1990 Rudbar-Tarom (NW Persia) catastrophic Earthquake; a preliminary field reconnaissance report, 1st Int. Conf. on Seis. and Eq. Eng. (SEE 1), Proc. Vol. 3, pp 3-53, Tehran, Iran.
- Berberian, M., 1994, Natural hazards and the first earthquake catalog of Iran, vol. 1: Historical hazards in Iran prior 1900, I.I.E.S. report.
- Berberian, M., 1997, Seismic sources of the Transcaucasian historical earthquakes. In S. Giardini and Balassanian, S. (Eds.), *Historical and prehistorical earthquakes in the Caucasus*. Kluwer Academic Publishing, Dordrecht, Netherlands, pp. 233–311.
- Berberian, M., and Yeats, R. S., 1999, Patterns of historical earthquake rupture in the Iranian plateau, *Bull. Seismol. Soc. Am.*, 89, 120–139.
- Dellenbach, J., 1964. Contribution à l'étude géologique de la région située à l'est de Téhéran (Iran). *Faculté des Science de l'Université Strasbourg (France)*, 117 pp. (in French).
- Eftekharneshad, J., 1975, Brief history and structural development of Azarbaijan. Geological Survey of Iran, Internal Report, 8P.
- Ghassemi, M.-R., Fattahi, M., Landgraf, A., Ahmadi, M., Ballato, P., Tabatabaei, S., 2014, Kinematics link between the Eastern Mosha Fault and the North Tehran Fault, Alborz range, northern Iran, *Tectonophysics*, 622, 81-95.
- Hessami, K., Pantosi, D., Tabassi, H., Shabaniyan, E., Abbassi, M.-R., Feghhi, K., and Soleymani, S., 2003, Paleoeearthquakes and slip rates of the North Tabriz fault, NW Iran: Preliminary results, *Ann. Geophys.* 46, 903–915.
- Karakhanian, A., Djabashian, R., Trifonov, V., Philip, H., Arakelian, S., and Avagian, A., 2002, Holocene-historical volcanism and active faults as natural risk factor for Armenia and adjacent countries. *J. Volcanol. Geotherm. Res.*, 113 (1–2), 319–344.
- Landgraf, A., Ballato, P., Strecker, M.R., Friedrich, A., Tabatabaei, S.H., Shahpasandzadeh, M., 2009. Fault-kinematic and geomorphic observations along the North Tehran Thrust and Mosha Fasham Fault, Alborz mountains Iran: implications for faultsystem evolution and interaction in a changing tectonic regime. *Geophysical Journal International* 177, 676–690.
- Nabavi, M. H., 1976. Preface to geology of Iran, Geological survey of Iran, p. 109 (in Persian).
- Nazari, H., 2006. Analyse de la tectonique récente et active dans l'Alborz Central et la région de Téhéran: Approche morphotectonique et paléoseismologique. *Faculté des Sciences et des techniques du Languedoc l'Université Montpellier II (France)*. 246 pp. (in French).
- Rieben, E.H., 1955. The geology of Tehran plain. *American Journal of Science* 253, 617–639.
- Reilinger, R. E., McClusky, S., Vernant, P., Lawrence, S., Ergintav, S., Cakmak, R., Ozener, H., Kadirov, F., Guliev, I., Stepanyan, R., Nadariya, M., Hahubia, G., Mahmoud, S., Sakr, K., ArRajehi, A., Paradissis, D., Al-Aydrus, A., Prilepin, M., Guseva, T., Evren, E., Dimitrova, A., Filikov, S. V., Gomez, F., Al-Ghazzi, R. and Karam, G., 2006, GPS constraints on continental deformation in the Africa- Arabia-Eurasia continental collision zone and implications for the dynamics of plate interactions, *J. Geophys. Res.*, 111, B05411, doi: 10.1029/2005JB004051.
- Ritz, J.F., Nazari, H., Salamati, R., Shafeii, A., Soleymani, S., Vernant, P., 2006. Active transtension inside Central Alborz: a new insight into the Northern Iran–Southern Caspian geodynamics. *Geology* 34, 477–480.
- Ritz, J.-F., Nazari, H., Balescu, S., Lamothe, M., Salamati, R., Gassemi, A., Shafei, A., Ghorashi, M., Saidi, A., 2012, Paleoeearthquakes of the past 30000 years along the North Tehran Fault (Iran), *Journal of Geophysical Research*, Vol. 117, B06305, doi: 10.10292012JB00091, 47.
- Shabaniyan E., Acocella, V., Gioncada, A., Ghasemi, H., Bellier, O., 2012, Structural control on volcanism in intraplate post collisional setting: late Cenozoic to Quaternary examples of Iran and Eastern Turkey, *Tectonics*, 31: doi: 10.1029/2011TC003042. issn:0278-7407.
- Soleymani Azad, Sh., Feghhi, Kh., Shabaniyan, E., Abbassi, M.R., Ritz, J.F., 2003. Preliminary Paleoseismological Studies on the Mosha Fault at Mosha Valley. *International Institute of Earthquake Engineering and Seismology*. 89 pp. (in Persian).
- Soleymani Azad, S., 2009, Evaluation de l'aléa sismique pour les villes de Téhéran, Tabriz et Zandjan dans le NW de l'Iran, *Approche morphotectonique et paléoseismologique*, PhD thesis, University of Montpellier (in French and English).
- Soleymani Azad, S., Dominguez, S., Philip, H., Hessami, K., Foroutan, M., Shahpasand Zadeh, M., Ritz, and J.-F., 2011a, The Zandjan fault system: Morphological and tectonic evidence of a new active fault network in the NW of Iran, *Tectonophysics*, 506, 73–85.
- Soleymani Azad, S., J.-F. Ritz, and M. R. Abbassi (2011b), Left-lateral active deformation along the Mosha–North Tehran fault system (Iran): Morphotectonics and paleoseismological investigations, *Tectonophysics*, 497, 1-14, doi:10.1016/j.tecto.2010.09.013.
- Soleymani Azad, S., Philip, H., Dominguez, S., Hessami, K., Shahpasandzadeh, M., Foroutan, M., Tabassi, H., Lamothe, M., Paleoseismological and morphological evidence of slip rate variations along the North Tabriz fault (NW Iran), paper in press; *Tectonophysics*.
- Stöcklin, J., 1968, Structural history and tectonics of Iran: A review. *American Association of Petroleum Geologists Bulletin* 52, 1229–1258.
- Tchalenko, J.S., Berberian, M., Iranmanesh, H., Bailly, M., Arsovsky, M., 1974. Tectonic framework of the Tehran region, Geological Survey of Iran, Report n° 29.
- Trifonov, V.G., Hessami, K.T., Jamali, F., 1996. West-Trending Oblique Sinitral—Reverse Fault system in Northern Iran: IIEES Special Publication 75. Tehran, Iran.
- Vernant, P., and Chéry, J., 2006, Low fault friction in Iran implies localized deformation for the Arabia-Eurasia collision zone, *Earth Planet. Sci. Lett.*, 246, 197–206.



INQUA Focus Group on Paleoseismology and Active Tectonics



paleoseismicity.org

NOTES



Geometric and kinematic characteristics of the Mosha-North Tehran Fault system, Northern Iran

Sowreh Rezaei (1), Jin-Hyuck Choi (1), Shahryar Solaymani Azad (2), Young-Seog Kim (1)

- (1) Dept. of Earth & Environmental Sciences, Pukyong National University, Busan 608-737, South Korea. Email: Rsoureh@yahoo.com
(2) Seismotectonics & Seismology Dept., Geological Survey of Iran, Meraj Blvd., Azadi Sq., Tehran, Iran.

Abstract: The Mosha Fault (MF) and the North Tehran Fault (NTF), located at the southern part of the Central Alborz mountain range, northern Iran, are geometrically characterized by fault branching. Since these faults are considered as tectonically active faults based on historical seismicity records and located near the most populous city of Iran (Tehran), understanding the fault characteristics and the potential of earthquake hazard around this area is very important. In this study, we carried out preliminary field work based on geomorphologic and kinematic analyses to understand the deformation history and evolutionary characteristics of the Mosha-North Tehran Fault system. Our field observations indicate that both of the two faults underwent multiple slip events with different slip senses. The MF has mainly evolved by reverse reactivated strike-slip movements, whereas the NTF is characterized by multiple reverse reactivations with dip-slip senses. These results may indicate that the two faults have been linked kinematically as well as geometrically. Therefore, more detailed fault zone characterization and evolution studies should be carefully carried out to understand active tectonics and related seismic hazards around this area.

Key words: Mosha Fault, North Tehran Fault, fault system evolution, reverse reactivation

Introduction

The Mosha Fault (MF) and the North Tehran Fault (NTF) are the most important active faults, which are located near the Tehran metropolis at the southern part of the Central Alborz Mountain range (e.g. Dellenbach, 1964; Berberian, 1983; Allen et al., 2003). According to historical seismicity records (e.g. Ambraseys and Melville, 1982) and active tectonic features observed along this fault system (e.g. Ritz et al., 2003, Solaymani et al., 2003, Abbassi & Farbod, 2009), the Mosha and the North Tehran faults are significant seismic hazard zone of the capital of Iran, where around 15 million people live.

The Mosha fault is about 200 km long and is located between Firuzkuh to the east and Abyek to the west (e.g. Dellenbach, 1964). It can be divided into 3 parts; an eastern WNW- striking part (EMF), a central NW-striking part (CMF) and a western EW-striking part (WMF) (Fig. 1b). The central and western parts have almost a sinusoidal trace on map view and show thrust mechanism (e.g. Zanchi et al., 2006; Moinabadi & Yassaghi, 2007), while the eastern part has a linear trace and shows a left-lateral strike-slip motion associated with a normal component (e.g. Solaymani et al., 2011; Ritz et al., 2006).

The North Tehran fault is located between Karaj to the west and Ira area to the east (Fig. 1b) that Eocene formations of the Alborz range are thrust over Neogene and Quaternary sediments of the Tehran embayment (e.g., Tchalenko et al., 1974). It is more than 60 km long strikes E-W to ENE-WSW and is an oblique thrust or reverse fault with a left-lateral component (Alavi, 1996).

In this paper, we examined the kinematics of the Mosha and the North Tehran Fault based on geomorphic and field investigations. This study can contribute to a better understanding of the evolution and seismic hazards of these faults.

Geological setting

The Alborz mountain range is an active mountain belt that formed due to the closure of Paleotethys Ocean and was affected by Kimmerian and Alpine orogeny. It is located in the northern part of Iran and northern part of the Alpine-Himalayan orogenic belt in Western Asia. According to Vernant et al. (2004) GPS measurements along the Iran microcontinent indicate NNE-directed shortening with a rate of 5 ± 2 mmyr⁻¹, where the Alborz range accommodate almost one third of the intracontinental deformation in Iran. Also a wide range shearing is observed at a rate of 4 ± 2 mmyr⁻¹, which caused left-lateral motion on E-W striking structures (Fig. 1a). As a consequence of this stress regime, the relief has been increased to more than 3000 m alongside the North Tehran fault and over the Tehran plain, which is an indicator of strain accommodation in the Tehran region. Also the Mosha fault accommodates an important part of lateral shearing in the Alborz mountain belt (e.g. Allen et al., 2003; Vernant et al., 2004; Ritz et al., 2006).

Field observations

Geomorphic and kinematic characteristics are well expressed at the eastern part of the Mosha Fault (Fig. 2).

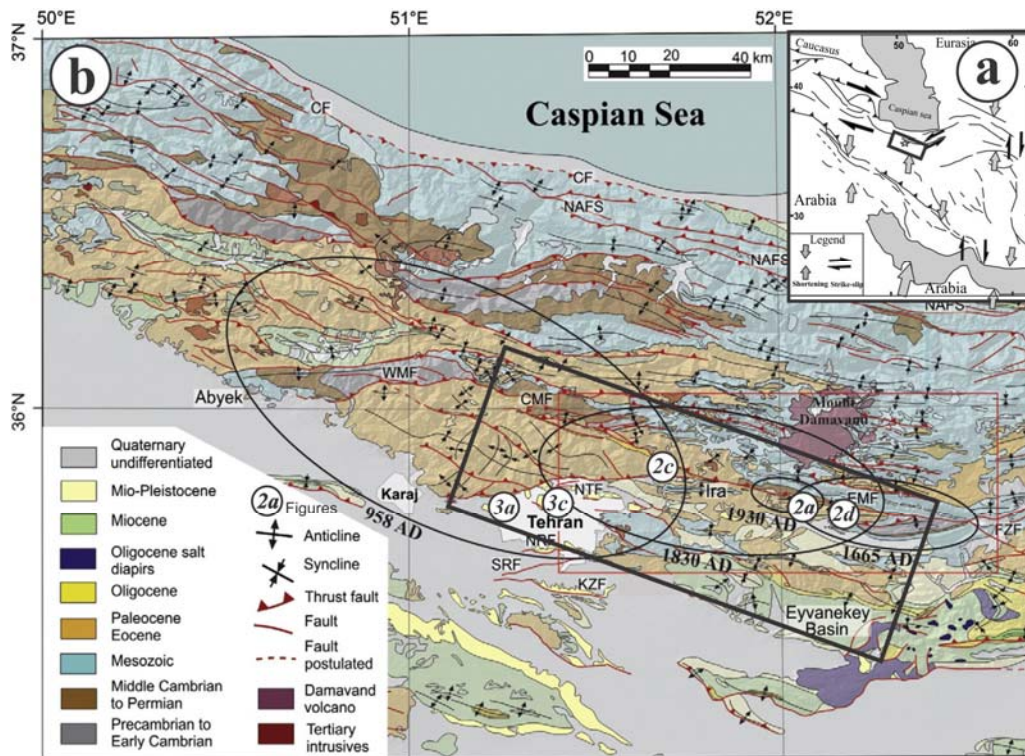


Fig. 1. a) Simplified tectonic map of the Middle East. Arrows show sense of relative motion (modified after Landgraf et al., 2009). The rectangle shows the location of the study area and the star shows the location of Tehran.

b) Central Alborz region and its major faults (modified after Ghassemi et al., 2014). Meisoseismal areas of historical earthquakes provisionally attributed to the NTF and EMF are shown by ellipses; data on the 958 AD Ray-Taleghan earthquake, and 1930 AD Ah-Mobarak Abad are from Ambraseys & Melville (1982); data on the 1830 AD Damavand-Shemiranat earthquake from Berberian & Yeats (1999). Location of pictures are shown by small white circles. The rectangle shows the study area. CF=Caspian Fault, CMF=Central Moshia Fault, EMF=Eastern Moshia Fault, FZF=Firuzkuh Fault, KZF=Kahrizak Fault, NAFS=North Alborz Fault System, NRF=North Ray Fault, SRF=South Ray Fault, WMF=Western Moshia Fault.

In Fig. 2a, the Moshia Fault is marked by a WNW-ESE trending lineament and a series of geomorphic features. In particular a large alluvial fan is cut by the fault indicating left-lateral movement. Towards the west and near the junction zone of MF and NTF, a ridge is also cut by the fault (Fig. 2c), indicating left-lateral movement (Fig. 1b). Several geomorphic markers indicate that the Moshia fault underwent left-lateral movement and this is what happens now. In Fig. 2d, the Moshia Fault zone is exposed on the N-S road-cut section, where the fault has a WNW-ESE trend and a sub-vertical dip. The fault core thickness is about 7 m and a high density of fractures is developed near the fault core. The Quaternary deposits are cut by faults with normal slip sense. Many field observations on the North Tehran fault indicate clear dip-slip movement (Fig. 3). Figure 3a shows a 12 m high N-S road-cut section of the NTF. Displaced layers along faults and field measurements are good indicators of normal faulting. Another 20 m high cross section in Abbasabad hills shows several dip-slip movements along faults (Fig. 3c and 3d). In this outcrop, Plio-Pleistocene sediments are affected by the fault and there is a time gap during sedimentation, which is distinguishable by a clear unconformity surface. Several events of dip-slip faulting before and after the unconformity are recorded along the faults. Field observations show several normal and reverse

movements along faults, which clearly indicates reverse reactivation along the North Tehran Fault.

Discussion

Most of faults are not always a straight single line but show complex geometry. Especially, many strike-slip faults show lateral geometric variation along strike such as bending, stepping, and branching. The kinematics of faults can be controlled by the geometry of faults and local dip slip movement can occur along strike-slip faults as illustrated in Fig. 4.

MF and NTF do not cross each other and the NTF geometrically merges into the MF showing a branch pattern. They underwent a dextral transpression stage under a NW-shortening (before Pliocene) and a later sinistral transtension stage under a NE-shortening with changing stress condition (from Pliocene to recent) (e.g. Landgraf et al., 2009), which may have inverted the kinematics of the Moshia and North Tehran Fault system. Although both MF and NTF underwent reverse reactivation, they show different movement patterns. MF shows strike-slip reverse reactivation that it reactivated from dip-slip to strike-slip fault (Fig. 2) and the NTF shows dip-slip reverse reactivation that the fault is reactivated from one type of

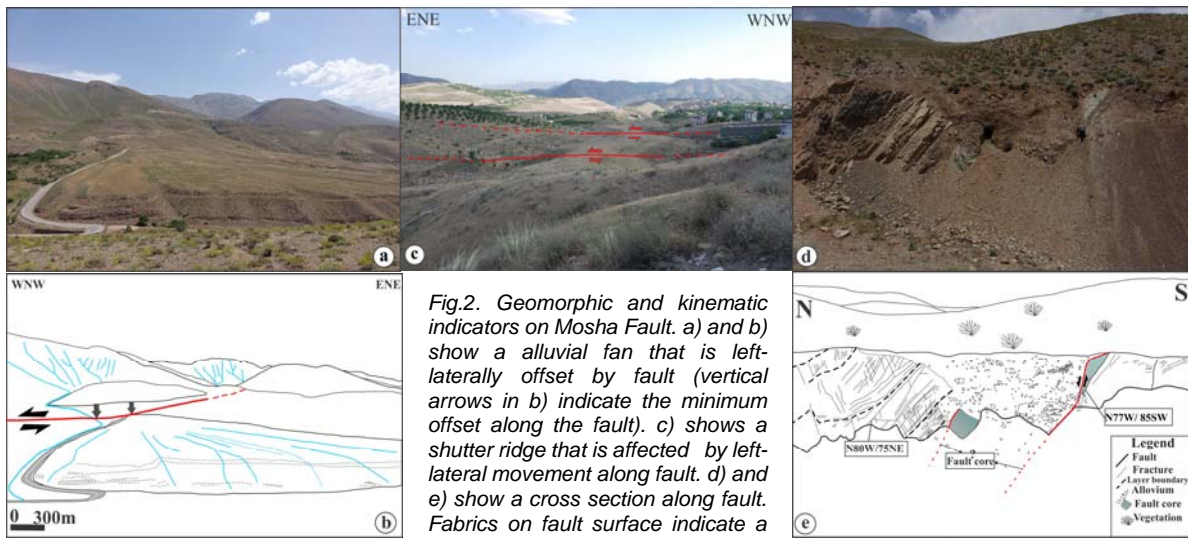


Fig.2. Geomorphic and kinematic indicators on Moshafault. a) and b) show a alluvial fan that is left-laterally offset by fault (vertical arrows in b) indicate the minimum offset along the fault). c) shows a shutter ridge that is affected by left-lateral movement along fault. d) and e) show a cross section along fault. Fabrics on fault surface indicate a clear normal component on fault.

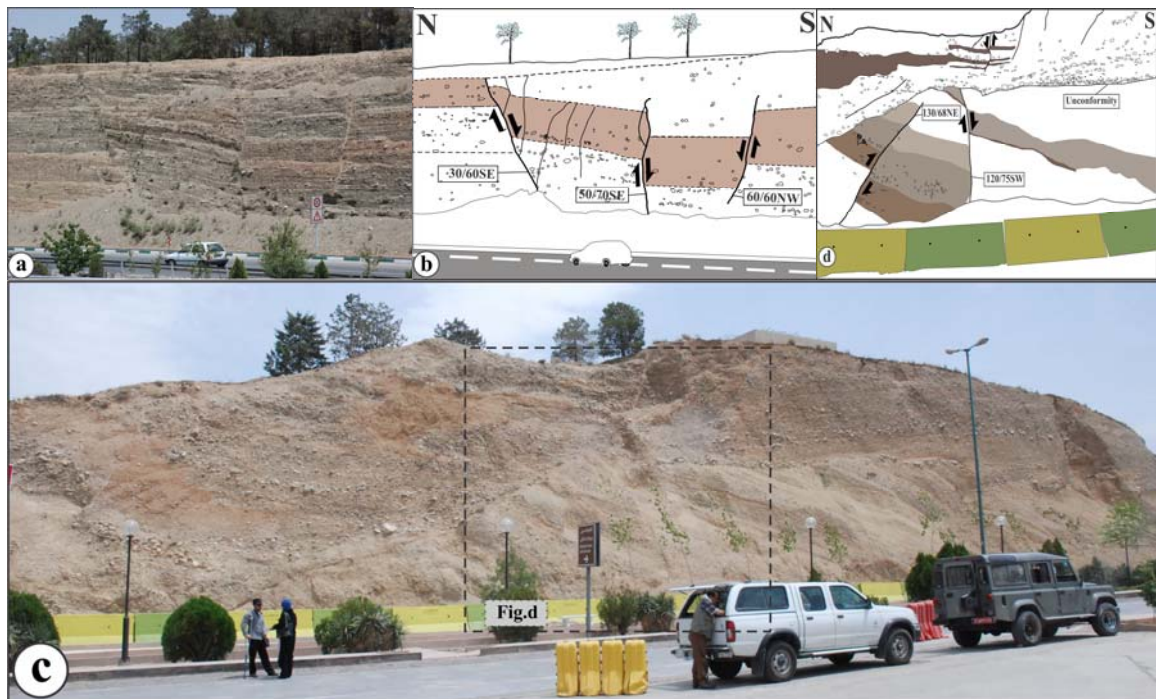


Fig. 3. Kinematic indicators on the North Tehran Fault. a) and b) show a road-cut section across faults. Bedding displacements along faults, mainly indicate a clear normal movement. c) shows a road-cut across fault in Abbasabad hills. d) is a detailed sketch of the Abbasabad road-cut section. The location of d) is shown in c) by dashed square. Several clear dip-slip faulting events are recorded along faults.

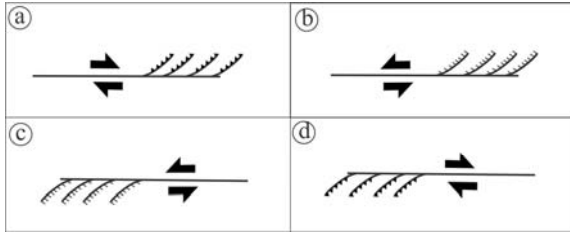


Fig. 4. Dip-slip movement along branches of strike-slip faults. a) and d) show dextral movement and b) and c) shows sinistral movement. Note that change of kinematic characteristics along the main fault can control the type of dip-slip faulting on fault branches.

dip-slip faulting to another type of dip-slip faulting (Fig. 3) depending on stress condition such as the strike of the fault relative to the maximum compressive direction. The main fault geometry and movement patterns along many faults based on field observations strongly indicate that they are kinematically linked. Therefore, we suggest that NTF and MF are one fault system and NTF is a playing fault of MF. Thus, the kinematic characteristics on NTF can be controlled by the kinematics along MF. Based on this interpretation, reverse faulting on NTF might occur when the Mosha Fault undergoes right-lateral movement (Similar as in Fig. 4d) and normal faulting might occur during left-lateral movement (similar to Fig. 4c).

Conclusion

Based on historical seismic events, MF and NTF are the main sources of seismic hazard to the most populous city of Iran. These two faults cut Quaternary deposits in many places indicating active faults. According to previous studies and our field observations, MF and NTF underwent reverse reactivation resulting in strike-slip reverse reactivation along MF and dip-slip reverse reactivation on NTF. Fault kinematic data and fault geometry indicate that these two faults behave as a fault system and NTF is a branch of MF. Therefore, the kinematic changes on MF can control kinematic characteristics of NTF.

Acknowledgements: We thank to all concerned staffs of Geological Survey of Iran (GSI) for preparing the best conditions for this research project.

References

Abbassi, M.R., Farbod, Y., 2009. Faulting and folding in Quaternary deposits of Tehran' piedmont (Iran). *Journal of Asian Earth Science* 34, 522–531.

Alavi, M., 1996. Tectonostratigraphic synthesis and structural style of the Alborz Mountain system in northern Iran, *J. Geodyn.*, 21, 1–33.

Allen, M.B., Vincent, S.J., Alsop, I., Ismail-zadeh, A., Flecker, R., 2003. Late Cenozoic deformation in the South Caspian

region: effects of a rigid basement block within a collision zone. *Tectonophysics* 366, 223–239.

- Ambraseys, N.N., Melville, C.P., 1982. *A History of Persian Earthquakes*. Cambridge University Press, London (219 pp.).
- Berberian, M., 1983. The southern Caspian: a compressional depression floored by a trapped, modified oceanic crust. *Canadian Journal of Earth Sciences* 20, 163–183.
- Berberian, M., Yeats, R.S., 1999. Patterns of historical earthquake rupture in the Iranian plateau. *Bulletin of the Seismological Society of America* 89, 120–139.
- Scholz, C.H., 1998. Earthquakes and friction laws. *Nature* 391, 37–42.
- Dellenbach, J., 1964. Contribution à l'étude géologique de la région située à l'est de Téhéran (Iran). Thesis Univ. Strasbourg (with maps, scales 1:500,000, 1:25,000 and 1:10,000). Mashhad Paleo-Tethys granitoids, Ferdowsi University of Mashhad, Iran (grant P/742-87/7/14).
- Ghassemi, M. R., Fattahi, M., Landgraf, A., Ahmadi, M., Ballato, P., Tabatabai, S., H., 2014. Kinematic links between the Eastern Mosha Fault and the North Tehran Fault, Alborz range, northern Iran. *Tectonophysics* 622, 81–95.
- Landgraf, A., Ballato, P., Strecker, M.R., Friedrich, A., Tabatabaei, S.H., Shahpasandzadeh, M., 2009. Fault-kinematic and geomorphic observations along the North Tehran Thrust and Mosha Fasham Fault, Alborz mountains Iran: implications for faultsystem evolution and interaction in a changing tectonic regime. *Geophysical Journal International* 177, 676–690.
- Moinabadi, M.E., Yassaghi, A., 2007. Geometry and kinematics of the Mosha Fault, south Central Alborz Range, Iran: an example of basement involved thrusting. *J. Asian Eart. Sci.* 29, 928-938.
- Ritz, J.F., Balescu, S., Soleymani, S., Abbassi, M.R., Nazari, H., Fegghi, K., Shabaniyan, E., Tabassi, H., Farbod, Y., Lamothe, M., Michelot, J.L., Massault, M., Che'ry, J., Vernant, P., 2003. Determining the Long-term Slip Rate Along the Mosha Fault, Central Alborz, Iran: Implications in Terms of Seismic Activity, S.E.E. 4 Meeting, Tehran, 12–14 May.
- Ritz, J.-F., Nazari, H., Ghassemi, A., Salamati, R., Shafei, A., Soleymani, S., Vernant, P., 2006. Active transtension inside Central Alborz: a new insight into the northern Iran southern Caspian geodynamics. *Geology* 34 (6), 477–480.
- Solaymani, Sh., Fegghi, Kh., Shabaniyan, E., Abbassi, M.R., Ritz, J.F., 2003. Preliminary Paleoseismological Studies on the Mosha Fault at Mosha Valley. *International Institute of Earthquake Engineering and Seismology*. 89 pp. (in Persian).
- Solaymani Azad, S., Ritz, J.-F., Abbassi, M.R., 2011. Left-lateral active deformation along the Mosha–North Tehran fault system (Iran): morphotectonics and paleoseismological investigations. *Tectonophysics* 497, 1–14.
- Tchalenko, J.S., Berberian, M., Iranmanesh, H., Bailly, M., Arsovsky, M., 1974. Tectonic framework of the Tehran region, Geological Survey of Iran, Report n° 29.
- Vernant, P. *et al.*, 2004a. Present-day crustal deformation and plate kinematics in the Middle East constrained by GPS measurements in Iran and northern Oman, *Geophys. J. Int.*, 157, 381–398.
- Zanchi, A., Berra, F., Mattei, M., Ghassemi, M.R., Sabouri, J., 2006. Inversion tectonics in central Alborz, Iran. *J. Struct. Geol.* 28, 2023–2037.

Wednesday 24 September

Session Five: Korean Active Tectonics



Review of paleoseismological studies in South Korea

Hee-Kwon Lee

Division of Geology and geophysics, Kangwon National University, Chuncheon, Kangwon 200-701, South Korea.
Email: heekwon@kangwon.ac.kr

Abstract: This paper reviews the studies on paleoseismology in South Korea over the past 20 years. Most of Quaternary faults have been reported along the Yangsan and Ulsan fault zones that define prominent lineaments in southeastern Korea. Dozens of trenches have been excavated along these fault zones and southeastern coastal region of Korean peninsula. Dozens of fault exposures cutting Quaternary fluvial, colluvial and marine terrace deposits have been studied. Some dating methods including C-14, Be-10, OSL, ESR were applied to constrain the age of Quaternary activities of many faults. These studies have supplied some reliable data on the Quaternary activities of many faults in South Korea

Key words: paleoseismology, Quaternary faults, trenches, terraces, dating

Introduction

Heavy industrial complexes including nuclear power plants have been constructed along the southeastern coastal region of the Korean peninsula. Most of the studies on paleoseismology have been focused Quaternary faults developed in this region. In order to overcome time limitations exhibited by instrumental and historic earthquake records, paleoseismic studies have been applied in South Korea. I present a short review on the study of Quaternary faults in this country. I do not herein intend to review all the undertaken studies

but present some case studies of paleoseismology in this country.

Studies on Quaternary fault in South Korea

A summary on the Quaternary faults in South Korea was provided by Kyung (2003, 2007) and Chwae and Choi (2007). Major tectonic deformation of southeastern region of the Korean peninsula was discussed in these papers. Kim et al. (2011) also summarised the research methods on active faults and limitations on these methods. Quaternary faults are recorded by multiple criteria in South Korea: Geomorphological features, primary fault plane, dating of fault gouge, offset of Quaternary deposits. The geographic locations of Quaternary faults are given in Fig. 1.

Quaternary faults in the Yangsan fault zone

A Quaternary fault was firstly reported by Okada et al. (1994) through trench study at the Wolpyung site on the Yangsan fault. This fault is the most prominent right lateral strike slip fault in the southeastern region of the Korean peninsula. After that, many trench studies have followed along this fault. Most of trenches have been practiced across the fault traces (lineaments) identified by geomorphic expression (Kyung, 2003). The fluvial terraces along the southern part of the Yangsan fault zone were divided into 4 levels (Qt1, Qt2, Qt3 and Qt4; Kyung, 2003).

The fault in the Wolpyung site forming the boundary between Cretaceous andesite and Quaternary alluvial fan deposit (Qt4), is exposed on the trench walls. The orientation of this fault is N25E/90. Dextral strike-slip movement with reverse component tend to be dominated (Okada et al., 1994, Kyung, 2003).

Quaternary alluvial sedimentary rocks (Qt4) are exposed in fault contact with granite in a small road cut at Sangchon-ri, Sangnam-myon (Kyung, 2003). The orientation of this fault is N23E/90 and is subparallel with

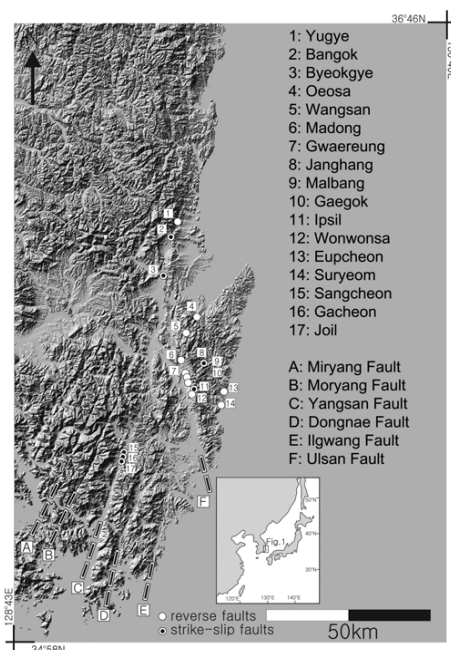


Fig. 1: Locations of Quaternary faults (1 to 17) discovered in the southeastern part of South Korea. A to F; lineaments representing major strike-slip faults in the Yangsan fault system (after Ree and Kwon, 2005).



the main trace of the Yangsan fault. This fault consists of 4 fault gouge bands and 1 microbreccia band. Each band has very sharp and planar fault planes in the both contacts. In the trench near this outcrop, the fault plane strikes N25E and dips 80 SE. Fault rock zone in this trench consists of 2 fault gouge bands and 1 microbreccia band. It suggests that the fault rock zone is very variable along the strike and dip directions and some fault gouge bands merge with the sharp fault planes. Dextral strike-slip movement with reverse component tends to be dominated. The deduced evolution of the fault rock zone in the Sangchon site using the ESR age data can be summarized as follows: at least 3 Ma years ago, a few meter wide cataclastic zone was formed during main active period of the Yangsan fault zone. The Quaternary alluvial sediments (Qt4) were deposited unconformably in this area. The localization of shear deformation by strain softening had occurred resulting in the development of the fault gouge band (770 ka). At about 660 ka ago, the new fault gouge band was added next to the older gouge band by a strain hardening process. At approximately 600 ka ago, a new gouge band and a microbreccia band were formed at both sides of a given fault rock zone. One of the main fault plane was reactivated and created the well foliated gouge band in about 410 ka ago.

Quaternary alluvial sedimentary rocks are exposed in fault contact with Cretaceous sedimentary rocks in the trench at the Shinhwa site. The orientation of the fault is N46E/70NW. The main gouge zone is typically 10 cm wide, and varies in strike and dip directions in trench surfaces. Dextral strike-slip movement with reverse component tend to be dominated.

Yang and Lee (2012) tested the consistency of ESR ages along the fault gouge zone developed on the same fault strand about 25 m long at the Kachon site. They found that ESR ages of three samples collected along the same band of fault gouge about 25 m in length show consistent ESR ages, equivalent doses and dose rates. Results of this ESR age estimates suggest that the fault strand in this site was formed before the Quaternary period and was reactivate at least two times within the Quaternary period.

The fluvial terraces along the northern part of the Yangsan fault zone were divided into 5 levels (Qt1, Qt2, Qt3, Qt4 and Qa). Qa represents the alluvium deposits of the latest Pleistocene to Holocene (Kyung, 2003). Fault gouges developed in the basement thrust over the alluvium deposits aged about 3298 by C-14 method. A layer of humic silt ranging from 1314 to 2356 B.P. by C-14 method was displaced by the latest thrust fault movement at the Yugye-ri site (Kyung, 2003).

Quaternary faults in the Ulsan fault zone

The NNW-SSE trending Ulsan fault passes through a long valley showing a distinct lineament. Quaternary reverse fault movements were reported along this fault. Kyung (2007) reported the average slip rate of the Ulsan fault ranges from 0.08 to 0.13 mm/yr by trench studies of the Malbang and the Kalgok sites.

The thrust fault developed at the outcrop on the northern wall of the Sagok reservoir in the eastern part of Malbang-ri, Waedong-up. The interbedded sequence of laminated sandstone, mudstone, and matrix supported conglomerate and massive very coarse sandstone on the hanging wall is folded forming the fault bend fold. The fault at the Malbang site moved at least 2 times within 500ka (Lee and Yang, 2007b).

The subhorizontal fault (NS/12W) is developed on the outcrop near the Wonwonsa temple. The medium light gray fault gouge at the floor fault is massive and about 20 cm thick at the Wonwonsa site. The thickness of fault gouge is various along the dip direction. The lenticular Quaternary sedimentary rock and the granite are exposed at the foot wall. The Quaternary conglomerate deposited on the granite unconformably on the hanging wall block thrust over the lenticular sedimentary rock and granite. The fault gouge zone is about 10-30 cm thick and branched and recombined on a scale of a few meters in the granite. ESR data for fault gouge suggest that the thrust fault at the Wonwonsa site was reactivated at least 4 times during the Quaternary period (Lee and Schwarcz, 2001).

The Ipshil fault is well exposed at the boundary between granite and andesitic rocks at the Ipshil-ri, Waedong-up, Korea. The exposures of the main fault rock zone consists of northern wall 2m high, and southern wall 2.0m high in the Ipshil creek. The fault rock zone of this fault consists of fault gouge, microbreccia and fault breccia. The andesitic rock near the fault is severely fractured. Anastomosing cataclastic shear bands are well developed in the granite near the fault rock zone. ESR data and geological structure in the fault rock zone indicate the evolution of the fault rock zone of the Ipshil site as follows; at least a few Ma years ago, anastomosing cataclastic shear band had formed in the damage zone of sheared granite. The localization of the shear deformation had formed the microbreccia zone about 1 m thick in the foot wall side and andesitic fault breccia in the hanging wall side. The main gouge zone was reactivated within the microbreccia zone in about 2 Ma ago. The microbreccia band located between the sheared granite and the main gouge zone at present is the relics of the older microbreccia zone. The last movement of the fault had occurred along one of the main fault surfaces in 1.4 Ma ago.

The Ihwa fault, forming the boundary between Tertiary granite and Quaternary deposits, is exposed on the wall of the Ihwa creek in Ulsan. The gouge zone 1-2cm thick branches and merges at the bottom of the creek. The central block about 20 cm thick, bounded by fault gouge, is composed of undeformed granite and basic dyke. Fault breccia is developed in a fractured granite and in contact with gouge zone but there is no evidence of deformation in the Quaternary alluvial sedimentary rocks, even near the fault gouge. The evolution of fault gouge zone deduced from ESR data is as follows; a fault breccia zone in granite cut by the fault zone was formed over 3 Ma ago. After the formation of this breccia zone in the granite, a basic dyke intruded along the breccia zone. A gouge zone was later formed between the basic dyke and fault breccia about 1.4 Ma



ago. A later gouge zone was formed between Quaternary deposits and the granite about 650 ka ago (Lee and Schwarcz, 2001)..

The Wangsan fault is exposed at Kyeongju, Korea. The Late Cretaceous to early Tertiary andesite is unconformably covered by Quaternary alternating conglomerate and sandstone deposits. The unconformity is cut by thrust fault which displaces a hanging wall block of about 30 m (Fig. 2; Ree and Kwon, 2005). Exposed at the surface of this fault is a light gray and brown fault gouge about 40-120 cm thick, but varying in thickness along strike and dip. Because the fault rocks cannot be generated along faults in unconsolidated sediments due to low confining stress near the surface, Lee and Yang (2003) consider that this fault gouge has been moved up along the fault on the Quaternary sedimentary rock of the footwall. They obtained ESR ages of 550ka and interpreted that this fault was reactivated prior to the deposition of the quaternary deposits (Lee and Yang, 2003). Cheong et al. (2003) reported the OSL ages ranging from 54 to 90 ka for the Quaternary deposits. These data suggest that this fault was reactivated at least 2 times during the Quaternary period and presents some potential seismic hazards to the heavy industrial complexes in the southeastern region of Korea.

Quaternary faults in the coastal area between Pohang and Ulsan

The Eupcheon Fault was discovered during the construction of a primary school in an area close to a nuclear power plant. Most of the research has been focused on the evaluation of the potential seismic hazards associated with this nuclear power plant (Kee et al., 2007; Kim et al., 2011). This fault zone was formed as a normal fault in the late Oligocene to early Miocene and

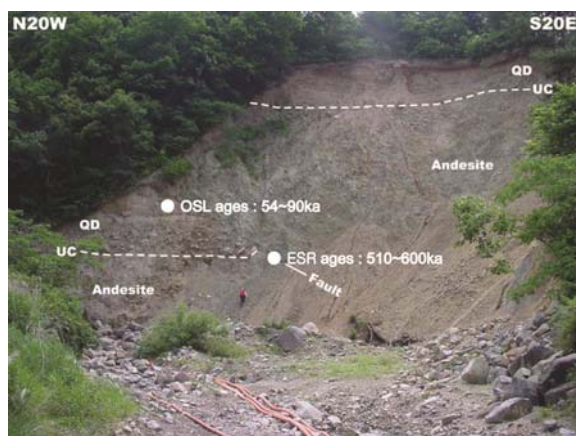


Fig. 2: Outcrop photograph of the Wangsan Fault showing ESR ages of fault gouge and OSL ages of sandstone. UC: unconformity. QD: Quaternary deposit (modified from Ree and Kwon, 2005).

It was then reversely reactivated during the Quaternary (Kim et al., 2011). Kim et al. (2011) identified four or five Quaternary faulting events upon the fault based on an interpretation of the trench logs including

an analysis of colluvial wedges, and measurements of displacement–distance relationships along the fault. And they estimated the amount of slip in the range of 0.7–1.8 m for each of the five identified faulting events and the earthquake magnitude in the range of M_w 5.4–7.4. Lee and Yang (2007a) studied temporal pattern of Quaternary activities of this fault, using ESR dating of fault gouges collected from basement. They suggested that this fault was reactivated at least five times during Quaternary period. These data indicate that long-term cyclic fault activity of this fault continued into the Quaternary. This fault presents some potential seismic hazards to the nuclear power plants in its vicinity.

Marine terraces

Marine terraces have been reported along the southeastern coastal region of the Korean peninsula. They were classified as T1, T2, and T3 with ages ranging from 127 ka to Holocene. The altitudes of inner edges are 0.5 m for T1, 10 m for T2 and 25-30 m for T3 in Daebo and Gori blocks. Whereas, the altitudes of inner edges are 4 m for T1, 20 m for T2 and 45 m for T3 terraces respectively in Wolsong block (Chwae and Choi, 2007). Aeolian dune sands are well preserved on top of each terrace surface, underlain by palaeo-beach sediments. OSL ages of the palaeo-beach sediments from T3 (127 ka) and T2 (73–80 ka) indicate that these terraces were formed during marine isotopic stage (MIS) 5e and MIS5a, respectively (Choi and Cheong, 2007; Choi et al., 2009). Uplift rates are 0.2 m/ka at the Daebo and Gori blocks and 0.3 m/ka at the Wolsong block indicating the middle Wolsong block was more active than the others (Chwae and Choi, 2007)..

Space-Time patterns of Quaternary fault activity in the southeastern part of the Korean peninsula

Lee and Yang (2007b) studied space-time patterns of Quaternary fault activity in southeastern part of the Korea, using ESR dating method. A plot of the distribution of ESR ages of the Wangsan fault zone shows that fault movements are clustered between 800 and 200 ka. That is, the fault movements appear to occur in active period, averaging 50 ka in length, separated by inactive periods of about 100 ka average length (Fig. 3). A plot of the distribution of ESR ages of the Ulsan fault zone and its vicinity shows that fault movements are clustered within 7 active periods (Fig. 4). Some faults in east side of the Ulsan fault were reactivated between 160 and 120 ka. Some strike-slip faults in the Wangsan fault zone and thrust fault in east side of the Ulsan fault were reactivated at 800 ka. Some thrust faults in the northern part of the Wangsan fault zone and east side of the Ulsan fault were reactivated between 500 and 700 ka. Some thrust faults in the southern part of the Wangsan fault zone and east side of the Ulsan fault were reactivated between 200 and 300 ka.

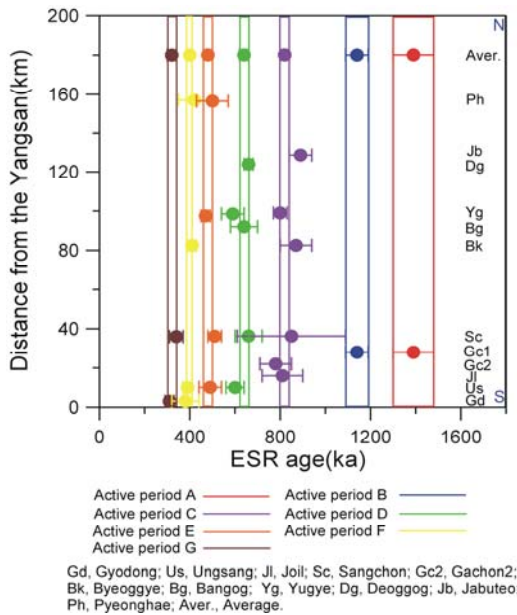


Fig. 3: Temporal pattern of Quaternary fault activities of the Yangsan fault (after Lee and Yang, 2007b).

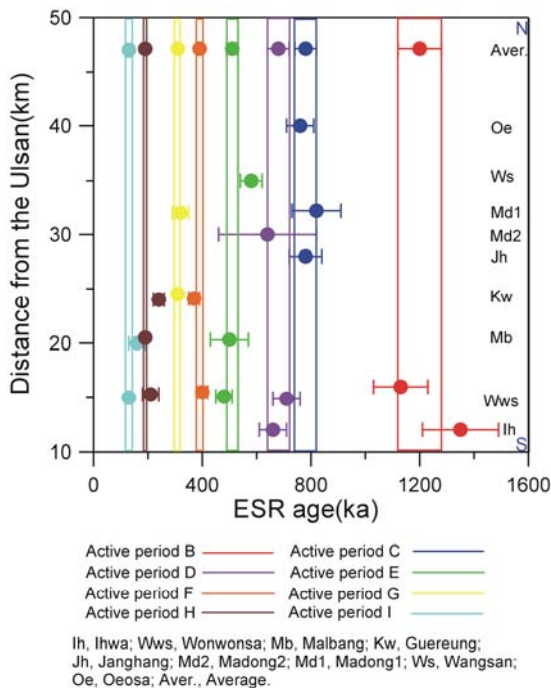


Fig. 4: Temporal pattern of Quaternary fault activities of the Ulsan fault (after Lee and Yang, 2007b).

References

Choi, J.H., Cheong, C.S. (2007) OSL dating of marine terrace sediments on the southeastern coast of Korea. In: *Quaternary Tectonics of Southeastern Korea* (Kee, W.S., Kihm, Y.H. Song, K. Y., eds). KIGAM, South Korea, 33-43.

Choi, J.H., Kim, J.W., Murray, A.S., Hong, D.G., Chngq, H.W. & C.S. Cheong (2009) OSL dating of marine terrace sediments on the southeastern coast of Korea with implications for quaternary tectonics. *Quaternary international*, 199, 3-14.

Chwae, U.C., Choi, S.J. (2007) Active Fault Study of Korea: the past, present and future. In: *Quaternary Tectonics of Southeastern Korea* (Kee, W.S., Kihm, Y.H. Song, K.Y., eds). KIGAM, South Korea, 1-31.

Kee, W.S., Kim, B.C., Hwang, J.H., Song, K.Y. & Y.H. Kihm (2007) The Eupcheon Fault SE Korea. In: *Quaternary Tectonics of Southeastern Korea* (Kee, W.S., Kihm, Y.H. Song, K.Y., eds). KIGAM, South Korea, 105-117.

Kim, Y.S. Kihm, J.H. & K. Jin (2011) Interpretation of the rupture history of a low slip-rate active fault by analysis of progressive displacement accumulation: an example from the Quaternary Eupcheon Fault, SE Korea. *Journal of the Geological society*, 168, 273-288.

Kim, Y.S. Jin, K., Choi, W.H. & W.S. Kee (2011) Understanding of active faults: A review for recent researches. *Journal of the Geological society of Korea*, 47(6), 723-752.

Kyung, J.B.(2003) Paleoseismology of the Yangsan Fault, southeastern part of Korean Peninsula. *Annals of Geophysics* 46(5), 983-996.

Kyung, J.B. (2007) Paleoseismological Characteristics of the Yangsan and Ulsan Faults since the Late Quaternary Time. In: *Quaternary Tectonics of Southeastern Korea* (Kee, W.S., Kihm, Y.H. Song, K.Y., eds). KIGAM, South Korea, 105-117.

Lee, H.K., Schwarcz., H.P. (2001) ESR dating of the subsidiary faults in the Yangsan fault system, Korea. *Quaternary Science Reviews*, 20, 993-1003.

Lee, H.K., Yang, J.S. (2003) ESR dating of the Wangsan fault, South Korea. *Quaternary Science Reviews*, 22, 1339-1343.

Lee, H.K., Yang, J.S., (2007a) ESR dating of the Eupchon fault, South Korea. *Quaternary Geochronology*, 2, 392-397.

Lee, H.K., Yang, J.S. (2007b) Temporal and spatial patterns of Quaternary fault activity in the Southeastern part of the Korean peninsula. In: *Quaternary Tectonics of Southeastern Korea* (Kee, W.S., Kihm, Y.H. Song, K.Y., eds). KIGAM, South Korea, 45-55.

Okada, A., Watanabe, M., Sato, H., Jun, M.S., Jo, W.R., Kim, S.K., Jeon, S.S., Chi, S.C. & K. Oike (1994) Active fault topography and trench survey in the central part of the Yangsan Fault, southeast Korea. *Journal of Geography*, 103, 116-126.

Ree, J.H., Kwon, S.K. (2005) The Wangsan Fault: One of the most "active" faults in South Korea? *Geoscience Journal* 9(3), 223-226.

Yang, J.S., Lee, H.K. (2012) ESR dating of fault gouge from the Gacheon 1 site on the Yangsan fault zone. *Journal of the Geological society of Korea*, 48(6), 459-472.

Acknowledgements: I thank all researchers for paleoseismology in South Korea for using their data to write this review paper.



INQUA Focus Group on Paleoseismology and Active Tectonics



paleoseismicity.org

NOTES



Earthquake characteristics in and around the Korean Peninsula and their tectonic implication

Myung-Soon Jun

Earthquake Research Center, Korea Institute of Geoscience and Mineral Resources, 124 Gwahang-no, Yuseong-gu, Daejeon, 305-350, Korea. Email: junms@kigam.re.kr

Abstract: In and around the Korean Peninsula, 21 intraplate earthquake source parameters since 1936 were analyzed to understand the characteristics of focal mechanisms and regional stress orientation and tectonics. These earthquakes are the largest ones from the last century and may represent the characteristics of typical earthquakes in this region. Focal mechanisms of these earthquakes show predominant strike-slip faulting with small amount of thrust components. The average P-axis is almost horizontal in ENE-WSW direction. This mechanism pattern and the direction of the maximum stress axis are very similar to the northeastern part of China and southwestern part of Japan. However they are quite different from the eastern part of East Sea. This may indicate that not only the subducting Pacific Plate from the east but also the indenting Indian Plate control focal mechanisms in the far east of the Eurasian Plate.

Key words: Intraplate earthquake, Korean Peninsula, Earthquake mechanism.

Introduction

Earthquakes in and around the Korean Peninsula are rather small in size with infrequent occurrence and show rather diffuse geographic distribution, which are typical characteristics of intraplate events. The occurrence of earthquakes in this region does not correlate with any known specific surface geologic features.

In Korea, instrumental earthquake recording has started in 1905. However, Korea has a 2000-year long history with more than 2000 documents which include not only earthquake information but also many other natural phenomena. Figure 1 shows the historical seismicity for 2000 years as well as instrumental seismicity since the 20 century.

Data Analysis

The focal mechanism of 21 ($M > 4.5$) shallow intraplate earthquakes in and around the Korean Peninsula since 1936 were analyzed (Fig. 2). Considering the low seismicity in the region, these earthquakes may represent and characterize the state of stress of the earth crust for the epicentral region. Nodal plane was obtained from the best double couple solutions of the moment tensor solutions. The majority of earthquake source mechanism in this region show predominant strike-slip faulting on steeply dipping nodal planes together with small amount of thrust components. In the Korean Peninsula, six earthquakes show predominant strike slip faulting while one event from the western central part of Korea shows normal faulting. In the Yellow Sea, six earthquakes show strike slip faulting and two events show thrust faulting. Along the eastern coast of the Korean Peninsula, from the East Sea (Sea of Japan), four earthquakes show strike slip faulting and two events show thrust faulting.

The seismogenic zones indicated by the deduced focal depths of earthquakes using the teleseismic short period waveform modelling from the Yellow Sea, the Korean Peninsula (Jun, 1990) and the western part of the East Sea (Jun, 1993) are very shallow and restricted

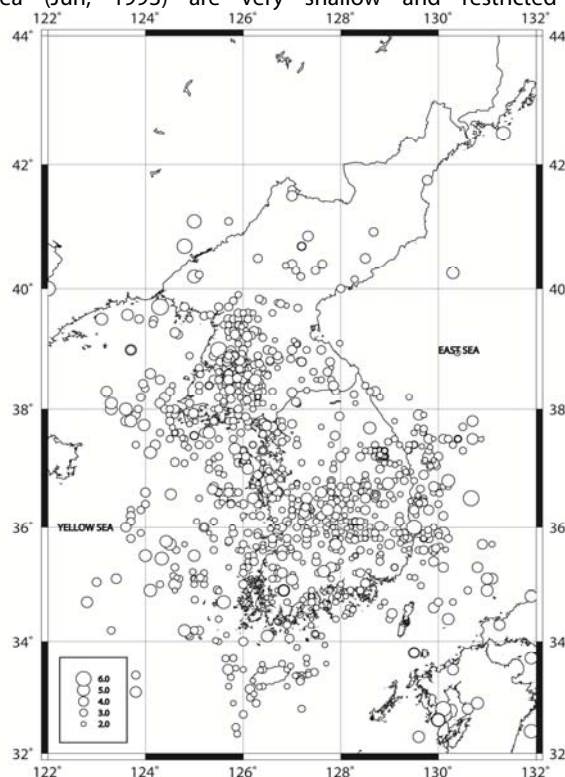


Fig. 1: Seismicity in and around the Korean Peninsula.

to the upper 10km of the crust. While focal depths from the southwestern part of the East Sea are deeper than 20 km (Jun, 1990). Since the depth of the crust in the southwestern part of the East Sea is about 15km which is the



half of the typical continental crust and the crust is probably being oceanic, these events from the SW of the East Sea might occur in the uppermost mantle.

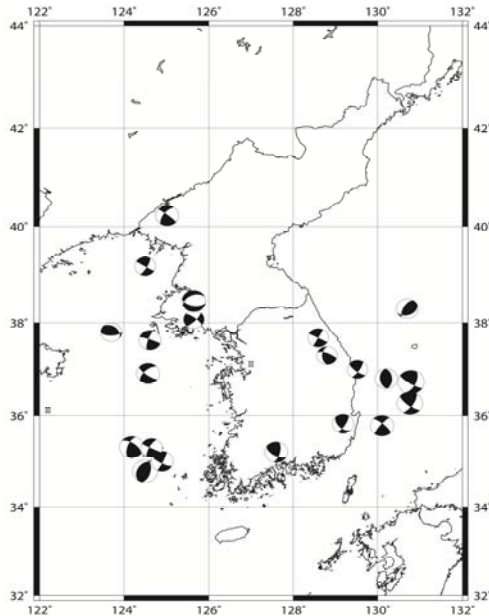


Fig. 2: Epicentral distribution of 21 studied earthquakes and their focal mechanisms.

I compared the earthquake source parameters in and around the Korean Peninsula with neighbouring regions. I used earthquake source parameters obtained by USGS using centroid moment tensor inversion since 1976 (U.S.

Geological Survey, 2010) from north-eastern China, the south-western part of Japan and the eastern part of the East Sea, which are also part of the Eurasian plate.

Used data are the shallow focus ($h < 60\text{Km}$), and their magnitude is larger than 6.5. From Figure 3, two major differences are evident from the pattern of earthquake mechanisms. The first difference is the faulting style. Thrust faulting is dominant in the eastern part of the East Sea, while strike slip faulting dominates around the Korean Peninsula, south-western part of Japan and in north-eastern China.

The horizontal projection of P-axis directions represent the directions of the horizontal maximum strain and also correspond to the directions of S_{Hmax} . Figure 4 shows the principal stress axes of the 21 studied earthquakes together with the neighbouring regions. Epicenters associated with strike-slip and normal-fault mechanisms are denoted by open circles and those associated with thrust-fault mechanism by solid circles. The horizontal projections of P-axis for strike-slip and thrust fault mechanism are indicated by lines through epicentral symbols. For normal faults, the T-axis is represented by outward pointing arrows.

Around the Korean Peninsula, the trend of P-axes is almost horizontal in ENE - WSW direction. In NE China and SW Japan, the P-axes trend ENE - WSW direction which are similar to that observed around the Korean Peninsula. By contrast, NW - SE trending P-axes with almost vertical T-axes are dominant in the eastern part of the East Sea.

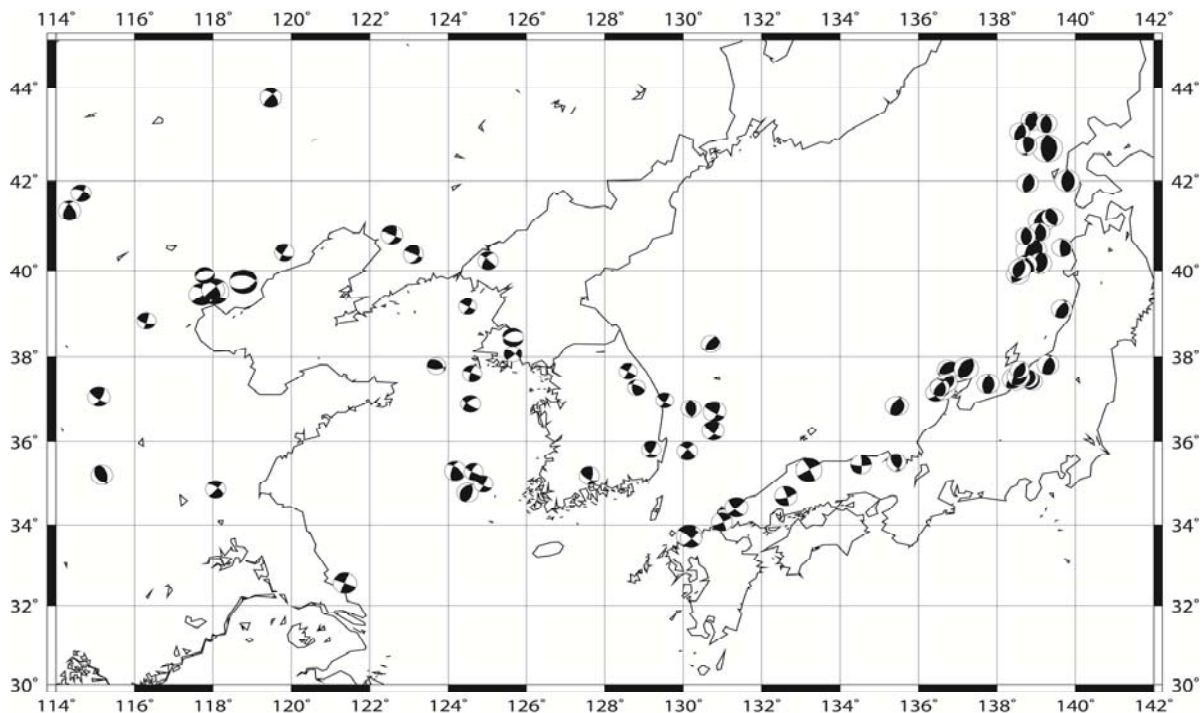


Fig. 3: Comparing earthquake mechanism in and around the Korean Peninsula with neighbouring regions.

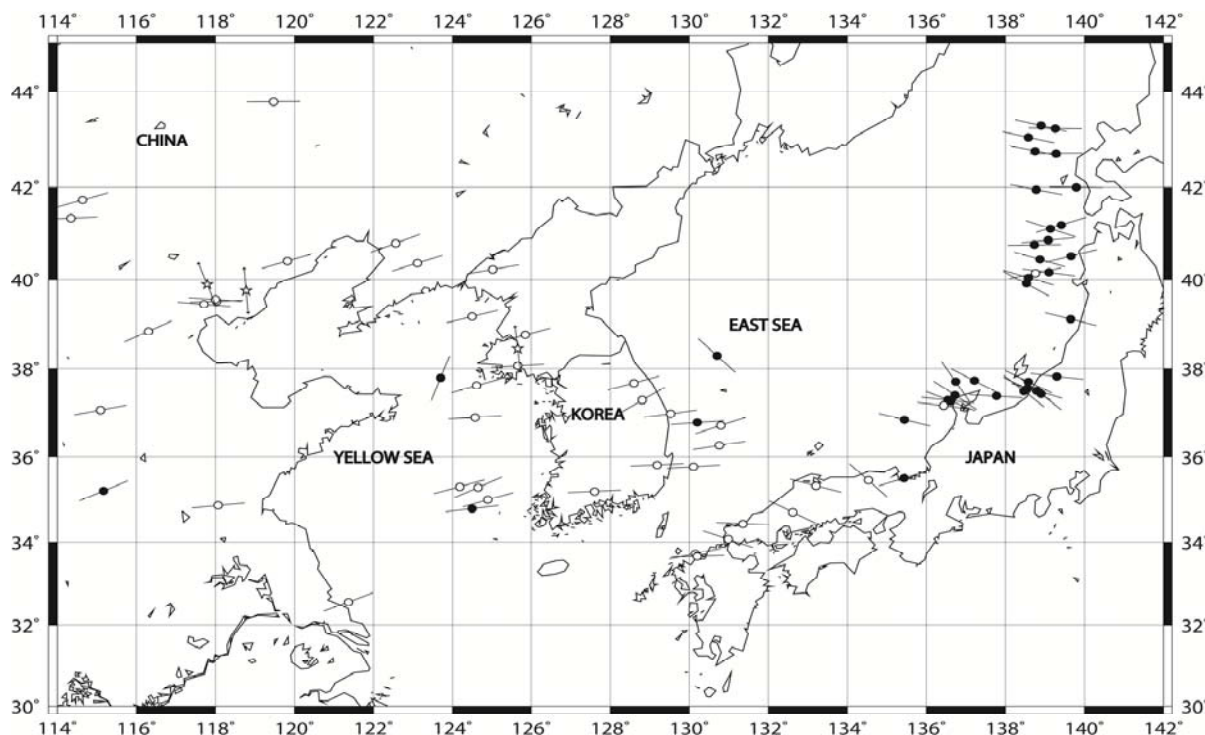


Fig. 4: Distribution of principal stress axes for the 21 studied earthquakes in and around the Korean Peninsula together with neighbouring region.

Discussion

The horizontal P-axis directions (ENE-WSW) in the Korean Peninsula and the north eastern part of China show different from those (NW-SE) of eastern part of East Sea. Chen and Nabelek (1988) proposed that the basin in the north eastern China was formed by the pull-apart process due to the dextral simple shear associated with the strike-slip fault system of NNE to NE trending, which was affected by the collision of the Indian Plate to the Eurasian Plate (Jolivet et al., 1990). Jin et al. (2006) also suggested that an estimated average azimuth of P-axis direction in this area is consistent with the orientation of the principal horizontal axis of the strain rate tensors obtained from GPS measurements. However, P-axis direction around the Korean Peninsula is different from the eastern part of the East Sea, and it implies that the stress field due to the subduction may not affect to the Korean Peninsula. Therefore, seismicity in and around the Korean Peninsula could be affected by the collision of the Indian Plate based on the earthquake characteristic analysis.

Acknowledgements: This work was supported by the Basic Research Project of Korea Institute of Geoscience and Mineral Resources funded by the Ministry of Science, ICT & Future Planning (MSIP, Korea).

References

- Chen, W.P., & J.L. Nabelek, (1988). Seismogenic strike-slip faulting and the development of the North China Basin. *Tectonics*, 7, 975-989.
- DeMets, C., R.G. Gordon & D.F. Argus, (2010). Geologically current plate motions. *Geophys. J. Int.* 181, 1-80.
- Jin, S., Li, Z.C., & Park, P.-H., (2006). Seismicity and GPS constraints on crustal deformation in the southeastern part of the Korean Peninsula. *Geosciences Journal*. 10, 491-497.
- Jolivet, L., P. Davy, and P. Cobbold (1990), Right-Lateral Shear Along the Northwest Pacific Margin and the India-Eurasia Collision, *Tectonics*, 9(6), 1409-1419
- Jun, M.S., (1990). Source parameters of shallow intraplate earthquakes in and around the Korean Peninsula and their tectonic implication. Doctoral Thesis, Uppsala University.
- Jun, M.S., (1993). Source properties of earthquakes in and around the Korean Peninsula. In 1993 Joint Conference of Seismology in East Asia, Tottori, Japan.
- U.S. Geological Survey, (2010). [http:// earthquake.usgs.gov/earthquakes/eqarchives/epi/epic_global.php](http://earthquake.usgs.gov/earthquakes/eqarchives/epi/epic_global.php).



INQUA Focus Group on Paleoseismology and Active Tectonics



paleoseismicity.org

NOTES



Optical dating of marine terrace sediments along the eastern coast of Korea, relevant to local crustal stability and Quaternary tectonics: Experiences and Expectations

Jeong-Heon Choi (1)*, Seongchan Hong (1), Seoyoung Heo (1), Sung-Ja Choi (2)

(1) Division of Earth and Environmental Sciences, Korea Basic Science Institute, Ochang Centre, Chungbuk 363-883, South Korea. *

Corresponding author: jhchoi@kbsi.re.kr

(2) Geological Mapping Department, Korea Institute of Geoscience and Mineral Resources, Daejeon 305-350, South Korea

Abstract: The formation ages of marine terraces along the eastern coast of Korea have long been the key issue for understanding Quaternary tectonics of the region. As some of these terraces, particularly those near the nuclear power plants, were cut by Quaternary faults with unknown age, establishing a chronological framework became critical for the assessment of local crustal stability of this area. Since the early 2000s, intensive works have been made to date Quaternary sediments covering each terrace platforms using the quartz OSL dating method, and the sedimentation ages corresponding to MIS 5a and 5e were suggested for 2nd (~18-25 m a.m.s.l) and 3rd (~40-50 m a.m.s.l), respectively. In this paper, we briefly summarise our efforts to OSL date marine terrace sediments during past decade, and explore future possibilities.

INTRODUCTION

Along the eastern coast of Korea, five to six flights of marine terraces are recognised (Lee, 1987; Kim et al., 1998). Controversially, these terraces are classified as 1st, 2nd, 3rd, 4th and 5th terraces at the elevations of < 5 m, 10-20 m, 20-40 m, 40-60 m and 70-80 m, respectively (Kim et al., 1998; Fig. 1).

Recently, the formation timing of these terraces have drawn considerable attention because some of these terraces and overlying Quaternary marine sediments were found to have been cut by Quaternary faults with unknown ages (Lee et al., 1999). Because these fault systems are located near heavy industrial complexes and nuclear power plants, the reliable assessment of the local crustal stability of this region is of importance not only for tectonics, but also for natural hazard prediction.

There have been, however, very few reports on the chronology of these terraces and faults (e.g. Choi, 2001; Lee and Yang; 2007), mainly due to the lack of suitable materials for dating; for instance, it is difficult to find charcoal or other organic materials for radiocarbon dating. Thus, recently, OSL (Optically Stimulated Luminescence) dating methods, which are to date time elapsed since last exposure to sunlight, are widely applied to date these marine terrace sediments; in this dating method, quartz grains, ubiquitous in almost all the sediments, are the usual target materials for dating.

While OSL dating marine terraces along the eastern coast of Korea, we observed several quartz OSL signal properties unsuitable for routine dating protocols, which we could later overcome through modification of experimental conditions and simple mathematical analysis. In addition, some quartz samples seemed to have depositional ages far beyond the usual datable age range of OSL method (> ~ 150 ka).

In this paper, we aim at briefly summarising our decadal experiences to OSL date marine terrace sediments, and further introducing future possibilities to extend the datable age range using luminescence techniques, particularly for dating marine sediments before last interglacial period.

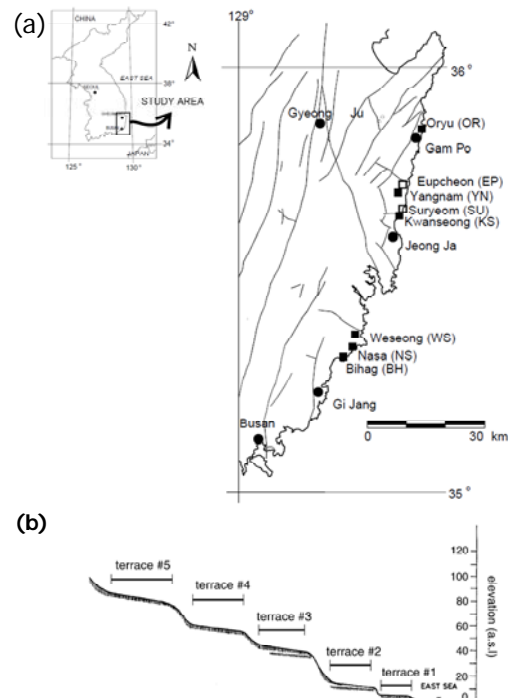


Fig. 1: (a) Location of marine terraces (modified from Choi et al., 2003a). Closed and open circles represent 2nd and 3rd terraces, respectively. Solid lines indicate tectonic faults with unknown ages. (b) Schematic view of marine terraces along the eastern coast of Korea (modified from Choi et al., 2003a)

OSL SIGNAL PROPERTIES OF QUARTZ GRAINS



2nd terraces

Quartz OSL signals are known to have several constituent components, each having different photoionisation cross sections, namely fast, medium, slow 1, slow 2, and so on, in the order of the size of photoionisation cross-section (Bailey et al., 1997; Singarayer and Bailey, 2003; Choi et al., 2006). The separation of these OSL signal components can be easily done by linearly modulating the power density of stimulation light source from 0 to maximum (LM-OSL, Linearly Modulated OSL; Bulur, 1996); in this study, the OSL signal stimulation was by blue-LEDs with wavelength of 470±30 nm and a maximum power density of 40 mW·cm⁻².

Of these components, when the conventional SAR (Single Aliquot Regenerative Dose; Murray and Wintle, 2000, 2003) protocol is applied, the fast OSL component ($\sigma = \sim 2.5 \times 10^{-17} \text{ cm}^2$) is known to be the best signal for estimating equivalent dose values (D_e , Wintle and Murray, 2006).

In a series of performance tests (i.e. dose recovery test, preheat plateau test and thermal transfer test, etc), we recognised that the conventional SAR protocol was not working properly for dating quartz grains from some of the 2nd terraces, for instance, those from Yangnam site. This was due to the presence of the ultrafast OSL component (Jain et al., 2008), which is thermally unstable and can be removed by heating the samples at 220°C or higher (Fig. 2).

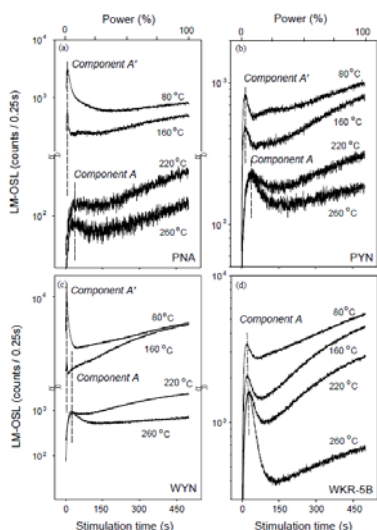


Fig. 2: LM-OSL curves in quartz from 2nd terraces. (a-c) Quartz samples PNA, PYN and WYN show distinguishable signature of component A¹ (ultrafast OSL component), (d) while this is not observed in the sample WKR-5B (from Choi et al., 2003a)

In addition, the fast OSL component in quartz grains from one of the 2nd terrace site, Oryu site, were observed to be contaminated by huge amount of slower

components (Fig. 3), which led to stratigraphically inconsistent OSL ages in our pilot scheme.

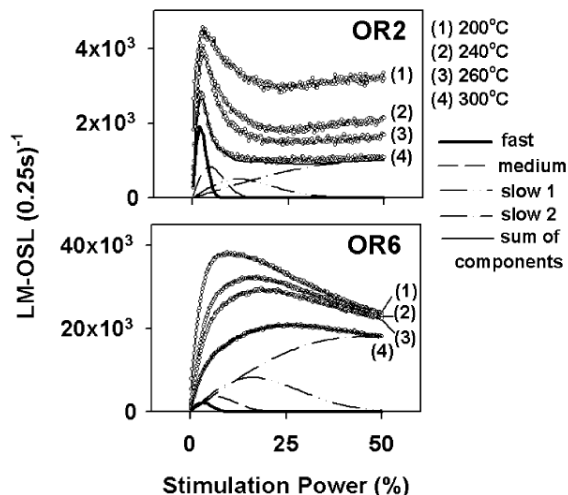


Fig. 3: LM-OSL curves in quartz from a 2nd terrace in Oryu site. The OSL signals in these samples are dominated by slower OSL components (from Choi et al., 2003b).

3rd terraces

Marine terrace sediments at the Suryum site are cut by a Quaternary reverse fault with unknown age, thus have been intensively investigated to figure out the recurrence interval of the fault and the timing of terrace formation (Fig. 4); Considering its elevation (~ 45-50 m a.m.s.l), it should be classified as 4th terrace (see the Introduction section). However, here we refer to this as 3rd terrace, because, in this area, no terrace platform was clearly observed between 2nd and the terrace at Suryum site.

Quartz grains from the Suryum site appear to have suitable OSL signal properties for dating as the samples passed through all the performance tests, the OSL signal being dominated by the fast OSL component. The OSL ages are in the range of ~60-90 ka (Choi et al., 2009) in single aliquot scale, made up of ~ 3000 sand-sized quartz grains.



Fig. 4: Suryum fault site. Quaternary marine terrace sediments were deposited on top of Tertiary volcanic. There were cut by a Quaternary reverse fault with unknown age.



OSL AGES OF 2nd and 3rd MARINE TERRACE SEDIMENTS

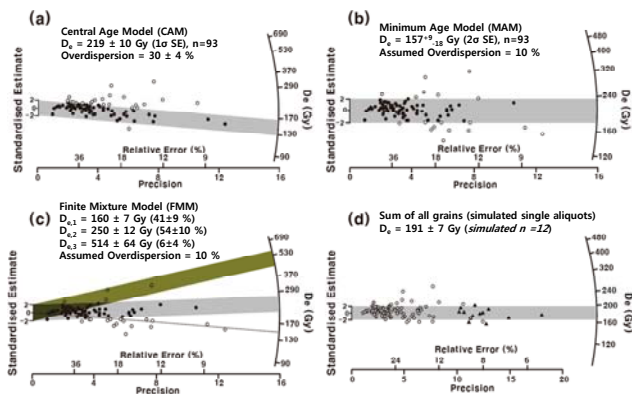
As indicated earlier, the ultrafast OSL component is thermally unstable and could be removed by increasing the test-dose preheating temperature up to 220°C in the SAR cycles. In case of marine sediments at Oryu site, we could pick up the fast OSL component only, through deconvolution of the LM-OSL curves.

After these experimental and mathematical modifications, we could obtain internally consistent OSL ages of ~60-70 ka from 2nd terrace sediments in the Gijang-Gampo area. This age range was, then, compared with OSL ages of 2nd terrace sediments from Pohang area (~50-70 ka), which is ~40 km to the north of Gampo (Fig. 1). Later, considering that the elevations of the 2nd terraces in Gampo-Jeong Ja area (~15-25 m) are systematically higher than those of Jeong Ja-Gijang (~7-12 m) area, Choi et al. (2008) proposed a “pop-up” model, in which, since at least MIS 5a, the middle part of the southeastern coast of Korea had uplifted more quickly than northern and southern parts.

The OSL ages of marine terrace sediments at Suryum site (~60-90 ka) are still controversial, because these ages are stratigraphically inconsistent with the ages of the lower 2nd terraces; In theory, located at higher elevations, the 3rd marine terraces should be older than the 2nd terrace. However, the OSL ages of both 2nd and 3rd terrace are indistinguishable.

Recently, based on single grain OSL dating, Heo et al. (in press) showed that quartz grains within the marine terrace sediments at Suryum site were of several age components (Fig. 5), presumably due to mixture of grains by post-depositional disturbance (e.g. roots or earthquake shock etc.). They also observed an OSL age component corresponding to MIS 7 (~190 ka) and concluded that it would be prudent not to exclude the possibility of its being MIS 7 terrace, although this will provoke further controversies over the absence of MIS 5 terrace in this region.

Fig. 5: The distribution of single grain D_e values of quartz from marine terrace sediments at Suryum site.



FUTURE WORKS TO EXTEND THE LUMINESCENCE AGE RANGE: CAN IRSL DATING BE AN ALTERNATIVE ?

The usual datable range of OSL method is limited by the concentration of defects in the crystal lattice that can accommodate electrons released by ionising radiation. It is well known that, although it varies from sample to sample, quartz OSL signal begins to be saturated at D_e values of ~200-300 Gy (~100-150 ka, assuming a dose rate of 2 Gy·ka⁻¹). Thus, many attempts have been made to extend the datable luminescence age range.

In this respect, dating with IRSL (InfraRed Stimulated Luminescence) signal in K-rich feldspar has long been one of the key issues for extending the luminescence age range, as this signal saturates at much higher doses, up to ~1000 Gy (corresponding to ~500 ka, assuming a dose rate of 2 Gy·ka⁻¹). However, anomalous fading of IRSL signal, which leads to significant age underestimation unless properly corrected, hindered its use for routine dating of Quaternary sediments (Wintle, 1973).

Recently, several works have successfully shown that there is no or negligible anomalous fading in post IR-IRSL signals measured at 290°C (e.g. Thomsen et al., 2008), and these signals could be applied to date sediments as old as 600 ka (Thiel et al., 2012).

Although there are still debates on the bleachability of the post IR-IRSL signal at deposition, this gives a new possibility to challenge for dating sediments older than MIS 7 period.

References

- Bailey, R.M., Smith, B.W., Rhodes, E.J., (1997). Partial bleaching and the decay from characteristics of quartz OSL. *Radiation Measurements* 27, 123-136.
- Bulur, E., (1996). An alternative techniques for optically stimulated luminescence (OSL) experiments. *Radiation Measurements* 26, 701-709.
- Choi, J.H., Duller, G.A.T., Wintle, A.G., Cheong, C.-S., (2006). Luminescence characteristics of quartz from the Southern Kenyan Rift Valley: Dose estimation using LM-OSL SAR. *Radiation Measurements* 41, 847-854.
- Choi, J.H., Kim, J.W., Murray, A.S., Hong, D.G., Chang, H.W., Cheong, C.-S., (2009). OSL dating of marine terrace sediments on the southeastern coast of Korea with implications for Quaternary tectonics. *Quaternary International* 199, 3-14.
- Choi, J.H., Murray, A.S., Jain, M., Cheong, C.S., Chang, H.W., (2003a). Luminescence dating of well-sorted marine terrace sediments on the southeastern coast of Korea. *Quaternary Science Reviews* 22, 407-421.
- Choi, J.H., Murray, A.S., Cheong, C.S., Hong, D.G., Chang, H.W., (2003b). The resolution of stratigraphic inconsistency in the luminescence ages of marine terrace sediments from Korea. *Quaternary Science Reviews* 22, 1201-1206.
- Choi, S.G., (2001). Tectonic movements indicated by the Late Pleistocene palaeoshorelines in the eastern coast of Korea. *Transactions, Japanese Geomorphological Union* 22-3, 265-275.



INQUA Focus Group on Paleoseismology and Active Tectonics



paleoseismicity.org

- Choi, S.J., Merritts, D.J., Ota, Y., (2008). Elevations and ages of marine terraces and late Quaternary rock uplift in southeastern Korea. *Journal of Geophysical Research* 113, B10403.
- Heo, S., Choi, J.H., Hong, D.G., Revisiting the OSL ages of marine terrace sediments at Suryum fault site, Gyeongju, South Korea: Single grain OSL dating. *Journal of the Petrological Society of Korea, in press.*
- Jain, M., Choi, J.H., Thomas, P.J., (2008). The ultrafast OSL component in quartz: Origins and implications. *Radiation Measurements* 43, 709-714.
- Kim, J.Y., Lee, D.Y., Choi, S.G., (1998). A research on Pleistocene stratigraphy. *Korean Journal of Quaternary Research* 4, 41-57.
- Lee, B.J., Ryoo, C.-R., Chwae, U., (1999). Quaternary faults in the Yangnam area, Kyungju, Korea. *Journal of the Geological Society of Korea* 35, 1-14.
- Lee, D.Y., (1987). Stratigraphical research of the Quaternary deposits in the Korean peninsula. *Korean Journal of Quaternary Research* 1, 3-20.
- Lee, H.K., Yang, J.S., (2007). ESR dating of the Eupchon fault, South Korea. *Quaternary Geochronology* 2, 392-397.
- Murray, A.S., Wintle, A.G., (2000). Luminescence dating of quartz using an improved single-aliquot regenerative-dose protocol. *Radiation Measurements* 32, 57-73.
- Murray, A.S., Wintle, A.G., (2003). The single aliquot regenerative protocol; potential for improvements in reliability. *Radiation Measurements* 37, 377-381.
- Singarayer, J.S., Bailey, R.M., (2003). Further investigations of the quartz optically stimulated luminescence components using linear modulation. *Radiation Measurements* 37, 451-458.
- Thiel, C., Buylaert, J.P., Murray, A.S., Elmejdoub, N., Jedoui, Y., (2012). A comparison of TT-OSL and post-IR IRSL dating of coastal deposits on Cap Bon peninsula, north-eastern Tunisia. *Quaternary Geochronology* 10, 209-217.
- Thomsen, K.J., Murray, A.S., Jain, M., Bøtter-Jensen, L., (2008). Laboratory fading rates of various luminescence signals from feldspar-rich sediment extracts. *Radiation Measurements* 43, 1474-1486.
- Wintle, A.G., (1973). Anomalous fading of thermoluminescence in mineral samples. *Nature* 245, 143-144.
- Wintle, A.G., Murray, A.S., (2006). A review of quartz optically stimulated luminescence characteristics and their relevance in single-aliquot regeneration dating. *Radiation Measurements* 41, 369-391.



INQUA Focus Group on Paleoseismology and Active Tectonics



paleoseismicity.org

NOTES



Distribution of Marine terraces and their tectonic implication, Southeastern Korea

Sung-ja Choi (1), Dorothy J. Merritts (2), Yoko Ota (3)

(1) Geological Mapping Department, Korea Institute of Geoscience and Mineral Resources, DAEJEON, S.KOREA

(2) Department of Earth and Environment, Franklin and Marshall College, PA, USA

(3) National Taiwan University

Abstract: From detailed GPS surveying and mapping of marine terraces and their former shoreline angles along the southeastern coast of the Korean Peninsula, we determine patterns of late Quaternary uplift over a coastal distance of ~100 km. The survey area is divided into three distinct parts named here the Daebo, Weolsung, and Gori regions from north to south based on relative differences in altitude of marine terrace platforms. In the Weolsung region, terrace inner edge altitudes are 3-5 m (T1), 19-24 m (T2), 30-35 m (T3b), 40-50 m (T3a), 65-70 m (T4), and 75-85 m (T5) above msl. In the Daebo and Gori regions, the inner edge altitudes of the five terraces are 0.5 m (T1), 9-11 m (T2), 18-22 m (T3b), 27-33 m (T3a), and 40-44 m (T4; locally as high as 50 m). The sequences of four to five terraces correlate with sea-level high stands as follows: T1 = 6 ka (i.e., Holocene? sea level high stand); T2 = 80 ka; T3b = 105 ka; T3a = 125 ka; and T4 = 200 ka. Using a paleo-sea level of +6 m for the 125-ka sea level highstand, the long-term uplift rates are 0.33 m/ka in the Weolsung region and 0.19 m/ka in the Daebo-Gori regions, respectively. The difference in uplift rate between them suggests local block tilting driven by the Ulsan fault and Gampo lineament. Persistent uplift that generated marine terraces is the result of a WNW to ENE maximum compressive stress.

Key words: marine terraces, southeastern coast of Korean Peninsula, MIS 5, uplift rate, block tilting.

Introduction

The Korean Peninsula located in the far eastern intraplate region of the Eurasian Plate is considered a stable continental area lying at least 550 km northwest of the Nankai Trough. Nevertheless, emergent flights of marine terraces occur extensively along the southeastern coast of the Peninsula. In this paper, we present the results of marine terrace mapping in locally active coastal region and assess variations in coastal uplift rates. We surveyed the former shorelines of coastal area 100km long and determined the rates and patterns of the late Quaternary uplift based on detailed Global Positioning System (GPS). This paper will present the local major faulting in the intraplate regime and define an independent crustal block with an isosceles triangle shape.

Result of Marine Terrace mapping

The survey area is divided into three parts based on the relative differences in elevation of marine terrace platforms; the Daebo, Weolsung, and Gori regions from north to south (Fig.1). The Daebo region extending southward 35 km from Homigot to Gampo consists of five well-expressed marine terraces that get narrower toward the south. The paleo-shoreline angle elevations of the five terraces are: ~1 m asl (T1), 9-11 m asl (T2), 18-22 m asl (T3b), 27-33 m asl (T3a), and 40-50 m asl (T4; locally as high as 50 m asl). The third T3 terrace in the Daebo is the broadest and best expressed of all the marine terraces on the Korean Peninsula. Sediment overlying terraces in the Daebo region is poorly developed and contains no fossils.

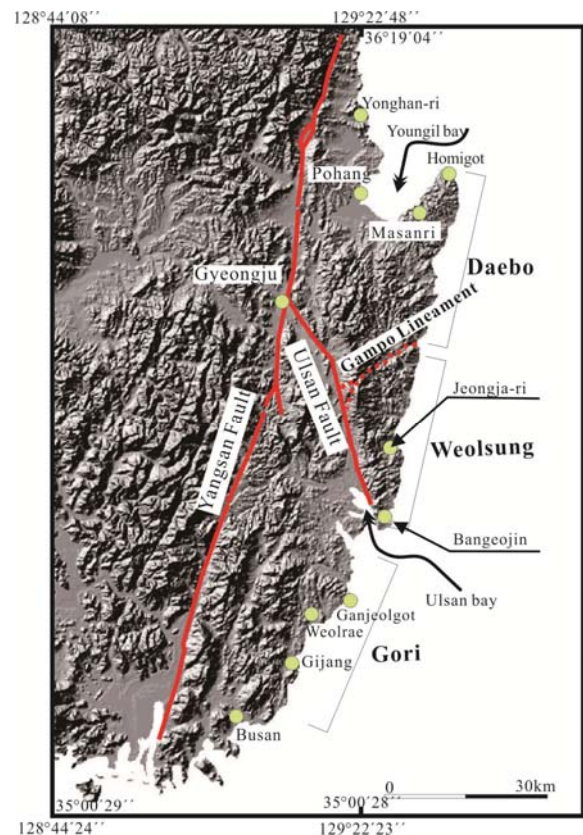


Fig. 1: Satellite image of the southeastern Korean Peninsula, showing Yangsan and Ulsan faults with the thick red line and three study regions.

The Weolsung region has been studied in the past because important industrial facilities had built since



1977. The central Weolsung region is 35 km long and contains six marine terraces: 2–5 m asl (T1), 19–24 m asl (T2), 30–35 m asl (T3b), 40–50 m asl (T3a), 60–70 m asl (T4), and 75–85 m asl (T5) (Fig. 2). Most of the platforms are covered by thick marine deposits overlain by younger fluvial sediments. Among them, the second terrace T2 and the third terrace T3 generally are broad and overlain by thick marine and fluvial deposits. There are several possible marine terraces above 90m asl, but they lack lateral continuity.

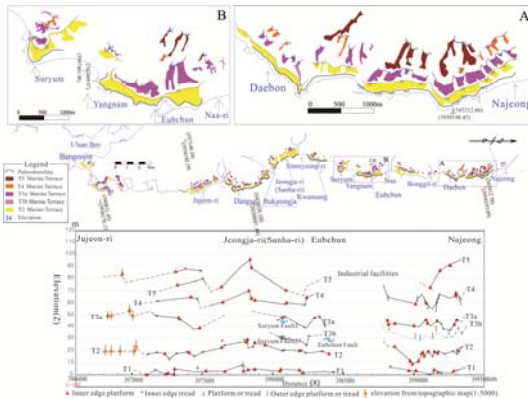


Fig. 2: Map of Marine terraces (middle) with detailed maps (A and B) and Profiles of former shoreline angle elevations (lower) in the Weolsung region.

In Gori region, which is 26 km long, four marine terraces occur along the Bangeojin to Gijang: ~0.5 m asl (T1), 8–11 m asl (T2), 17–22 m asl (T3b), 25–30 m asl (T3a), and 40–44 m asl (T4). The Gori region is composed of low relief similar in elevation to the lowest four terraces of the Daebo region. The terraces in the Gori region generally are more narrow and discontinuous than that in the Daebo region. The T3 terraces are classified into two; T3a and T3b. The Terrace T3b continuously is developed while the T3a is not extended to the south of Ganjeolgot.

Estimation of Marine Terrace Ages and its Tectonic implication

Twenty-four OSL dates from beach sands overlying the T2 platform in the Daebo, Welsung, and Gori regions yield ages that range from 72-84 ka. The T2 terrace is correlated with the 80 ka (~75 ka) (MIS 5a) highstand. At Masan-ri and nearby Ipam-ri in the Daebo region, the range of OSL ages for six dates on dune sand immediately above a thin layer of beach gravel on the T3a wave-cut platform is 119–99 ka, in agreement with the paleomagnetic age estimate of 117–111 ka for the same stratum at Masan-ri. Given that these are minimum estimates of the age of the terrace, we conclude that the T3a terrace most likely correlates with MIS 5e, the 125 ka sea level highstand. Using the 76–80 ka of T2 terrace, which has the best age control by OSL dating in this study area, and the assumption that uplift of the marine terraces is steady over a period of tens of thousands of years, we derive the following inferred ages for the other

four terraces: T1 = 6 ka (i.e., Holocene sea level highstand); T3b = 105 ka; T3a = 125 ka; and T4 = 200 ka. We estimated uplift rates of marine terraces in order to understand the cumulative vertical motion along the southeastern coastal area of the Korean Peninsula for the last Pleistocene. While elevations of original global paleo-sea level highstands are not uniform for different regimes, those of MIS 5e are generally agreed to be 6 m asl (Chappell and Shackleton, 1986). The inner edge elevation of the T3a is 40–50 m asl in the Weolsung region and 25–33 m asl in the Daebo–Gori regions. Using a paleo-sea level of + 6 m for 125 ka, the maximum and minimum uplift rates were estimated to be 0.27 m/ka and 0.35 m/ka for the Weolsung region, and 0.15 m/ka and 0.22 m/ka for the Daebo–Gori regions. Mean uplift rates of the Weolsung and Daebo–Gori regions are 0.31 m/ka (~0.3 m/ka) and 0.18 m/ka (~0.2 m/ka), respectively (Fig.3).

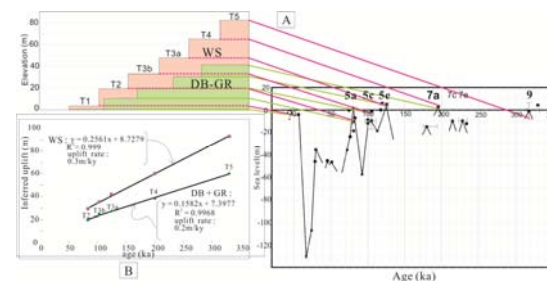


Fig. 3: (A) Global eustatic sea-level highstand elevations of the late Pleistocene (Chappell and Shackleton, 1986; Ludwig et al., 1996; Robinson et al., 2002; Kelly et al., 2005; Siddall et al., 2007). (B) Inferred uplift of each terrace plotted versus terrace age for the Weolsung and Daebo-Gori regions.

The uplift rates of the Weolsung and Daebo-Gori regions are similar to those of California and of the Ryukyu Island. However, they are located in active plate boundaries, for example the east Pacific Plate or the Nankai trench. The Korean Peninsula is far from the plate margins seen as the India-Eurasian collision belt or the Pacific and Philippine subduction zones. The vertical movements causing marine terraces result not only from the subduction or collision of regional plates but also from local movements on individual major faults (Ota and Omura, 1992; Zazo et al., 1999; Marquardt et al., 2004). We assume that plate tectonic motion has had a relatively insignificant influence over the uplifted flight of marine terraces in the Korean Peninsula. The local tectonic activity along the major Yangsan and Ulsan faults mainly resulted in uplift of five to six marine terraces along southeastern coastal area. Each marine terrace in the Weolsung region is slightly higher in altitude than its Daebo-Gori counterpart. This difference might be associated with structures separating crustal blocks. The structures are the Ulsan fault along the southwestern margin of the Weolsung region and a prominent Gampo lineament along the northern regional margin (Fig.1). The Quaternary faults are exposed on Ulsan fault. Gampo lineament showing a topographic discontinuity could be an active fault. The intersection of the Ulsan fault and Gampo fault lines



defines a crustal block as an isosceles triangle in the middle of the survey area.

In conclusion, the Korean Peninsula belongs to an intraplate regime where there is sufficient local tectonic activity to generate earthquakes. Vertical movements reflect an uplift rate of 0.2–0.3 m/ka which is similar to that at active plate boundaries in other areas, for example, California, northern Chile, the Ryukyu Islands, and the Strait of Gibraltar (Ota and Omura, 1992; Hanson et al., 1994; Zazo et al., 1999; Marquardt et al., 2004).

Acknowledgements: This work was funded from 1999 to 2006 by the Atomic Energy Fund of the Korean Ministry of Science (KINS) and supported by the Korea Institute of Geoscience and Mineral Resources (KIGAM).

References

- Chappell, J., and N. J. Shackleton (1986), Oxygen isotopes and sea level, *Nature*, 324, 137-140.
- Hanson, K. L., J. R. Wesling, W. R. Lettis, K. I. Kelson, and L. Mezger (1994), Correlation and ages of Quaternary marine terraces, south-central coastal California, in *Seismotectonics of the Central California Coast Ranges*, edited by I. B. Alterman, R. B. McMullen, L. S. Cluff, and D. B. Slemmons, pp. 45-71, Geological Society of America Special Paper 292, Boulder, Colorado.
- Kelly, M. J., R. L. Edwards., H. Cheng, D. Yuan, and Y. Wang (2005), Global and regional climate correlations during marine isotope stage 7 and termination III Using a stalagmite oxygen isotopic record from Dongge cave, China, *AGU, Fall Meeting*, abstract #PP21A-1555 [Online] <http://adsabs.harvard.edu/abs/2005AGUFMPP21A1555K>.
- Ludwig, K. R., D. R. Muhs, D. K. Simmons, R. B. Halley, and E. A. Shinn (1996), Sea-level records at ~80 ka from tectonically stable platforms: Florida and Bermuda, *Geology*, 24, 211-214.
- Marquardt, C., A. Lavenu, L. Ortlieb, E. Godoy, and D. Comte (2004), Coastal neotectonics in southern central Andes: uplift and deformation of marine terraces in northern Chile (27°S), *Tectonophysics*, 394, 193-219.
- Ota, Y., and A. Omura (1992), Contrasting styles and rates of tectonic uplift of coral reef terraces in the Ryukyu and Daito islands, southwestern Japan, *Quaternary International*, 15, 17-29.
- Robinson, L. F., G. M. Henderson, and N. C. Slowey (2002), U-Th dating of marine isotope stage 7 in Bahamas slope sediments, *Earth and Planetary Science Letters*, 196, 175-187.
- Siddall, M., J. Chappell, and E.-K. Potter (2007) Eustatic sea level during past interglacials, *Developments in Quaternary Science*, 7, 75-92.
- Zazo, C., P. G. Silva, J. L. Goy, C. Hillaire-Marcel, B. Ghaleb, J. Lario, T. Bardají, and A. González (1999), Coastal uplift in continental collision plate boundaries: data from the Last Interglacial marine terraces of the Gibraltar Strait area (south Spain), *Tectonophysics*, 301, 95-109.

Wednesday 24 September
Session Six: Seismic Hazard
Assessment for Critical Facilities



Earthquake databases in hazard assessment of critical facilities

Ruben Tatevossian

Institute of Physics of the Earth, Russian Academy of Sciences, Moscow 123995, Russia. Email: ruben@ifz.ru

Abstract: The IAEA considers compilation of the comprehensive earthquake database as first order task. However, compilation of the database is often treated as secondary technical procedure. Meanwhile the result strongly depends on this stage of work. No sophisticated computer program is able fully and truly compensate the lack of high quality data on earthquakes. In this paper we present materials and summarize the experience accumulated by the Institute of Physics of the Earth (Moscow) in seismic hazard assessment of pipe-lines in Siberia, Altai and South-East Europe (Serbia). Comprehensive databases have to include information starting from local high resolution instrumental network up to palaeo earthquake data. Before entering the database each data type has to be critically examined. One should be very careful to avoid mixing different data types at too early stages of the database compilation.

Key words: earthquake databases; critical facilities, seismic hazard assessment

INTRODUCTION

Seismic hazard assessment for critical facilities is mandatory requirement in several countries. Without being approved by corresponding authorities, no engineering part of projects can start. Assessment has to be done on the firm ground of comprehensive earthquake databases. This is crucial requirement for hazard assessment of critical facilities: nuclear power plants, pipe-lines (e.g. IAEA, 2010). However there is rather dangerous modern tendency in hazard assessment, which is based on sophisticated statistical analysis, generation of artificial earthquake catalogues instead of addressing the data. Thus, the result departs far from observed data toward models and concepts. We definitely stand on the position that real data plays the primary role and no sophisticated computer program is able fully and truly compensate the lack of high quality database.

The goal of this paper is to demonstrate what is understood by "comprehensive earthquake database" based on the experience accumulated during several projects of seismic hazard assessment carried by the Institute of Physics of the Earth (IPE, Moscow).

LOCAL NETWORK DATA

Data of local network is essential part of the comprehensive earthquake database. In the area the pipe-line crosses in Siberia (Fig. 1), there were no regional stations. In 2010 – 2011 more than 40 seismic stations were installed. They recorded ca. 300 local events from June 2010 to October, 2011 (Fig. 1), only 2 out of which were reported in regional catalogue of Siberia. In October 14, 2011 occurred strong (Mw6) earthquake recorded by the Global network. It followed by very active aftershock process. Local network recorded ca. 1300 seismic events (Fig. 2). The aftershock sequence was rather unusual; the strongest aftershock had magnitude 3.5 only. Only one (the strongest)

aftershock was reported in the Regional catalogue. Detailed analysis of the Skovorodino earthquake is given in (Bykova et al., 2014). In case of the Skovorodino earthquake, the local network not only provides directly useful data for seismic hazard assessment (location, strike-and-dip, and slip sense of a previously-unknown fault capable of generating at least Mw6 earthquakes) but also indicates the scope of future palaeoseismological detailed studies for realistic assessment of maximum expected magnitude and its return period. Therefore, local network data is not only important as the information source on the current seismic activity but also as a sort of "guidelines" for planning the further studies.

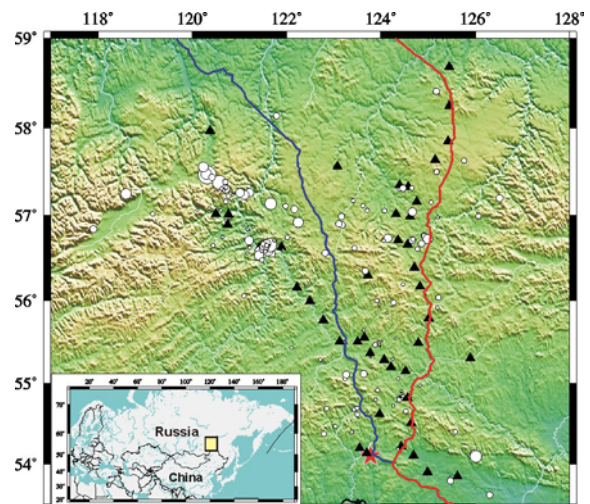


Fig. 1: Temporary seismic stations (triangles) in the pipe-line area in Siberia. The square in the inset shows the area. Epicenters of earthquakes recorded by the temporary network before October 14, 2011 (circles) and the main shock of the Skovorodino earthquake (star) are plotted. From two alternative pipe-line traces (shown in blue and in red) the red one was chosen based on the seismic hazard assessment.

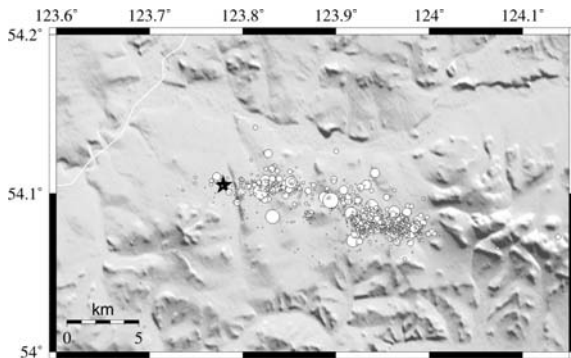


Fig. 2: The Skovorodino, October 14, 2011 earthquake (Mw6) and the shocks recorded by the local network in two months after the mainshock.

Local networks designed especially for hazard assessment of critical facilities are important also in regions with relatively good station coverage.

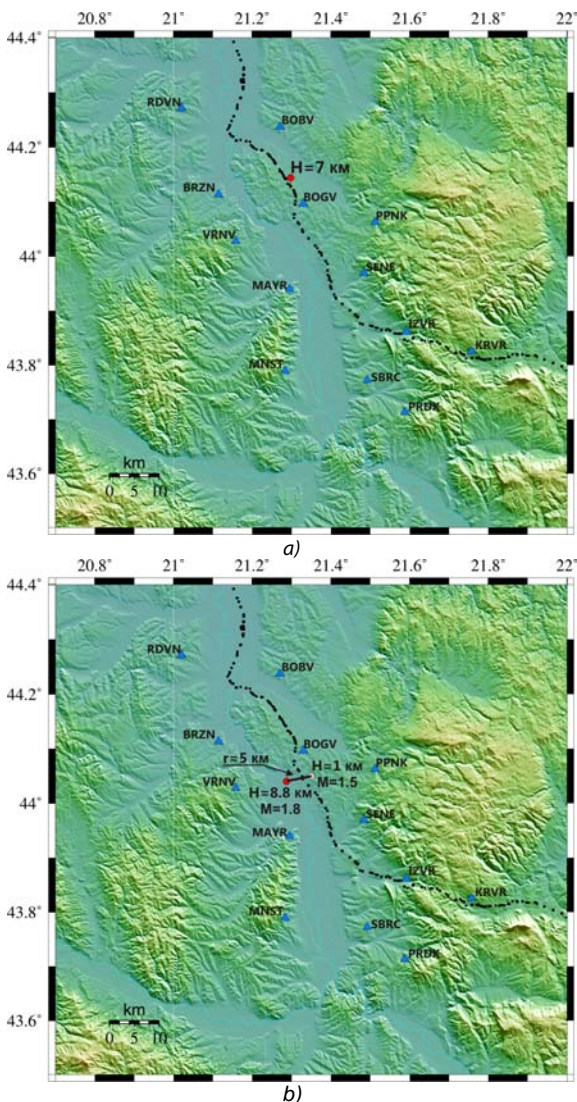


Fig. 3: Earthquake on 13.02.14 at 7:33 is missing in the Serbian regional catalogue (a); earthquake on 15.02.14 at 19:17 is located at much shallower depth in the regional catalogue (b).

In Serbia rather dense national seismic network is installed. The average spacing between stations is 50 km. For seismic hazard assessment denser temporary local network was organized by the IPE. The average spacing between stations is 15 km (Fig. 3). Thanks to denser station coverage in the vicinity of the pipe-line much more earthquakes were recorded. And what is even more important for seismic hazard assessment, the focal depth are better constrained.

USING PALAEOEARTHQUAKE DATA

Local network supplies precise but unfortunately very short-term information on earthquakes. The most long-term data follow from paleo earthquake studies.

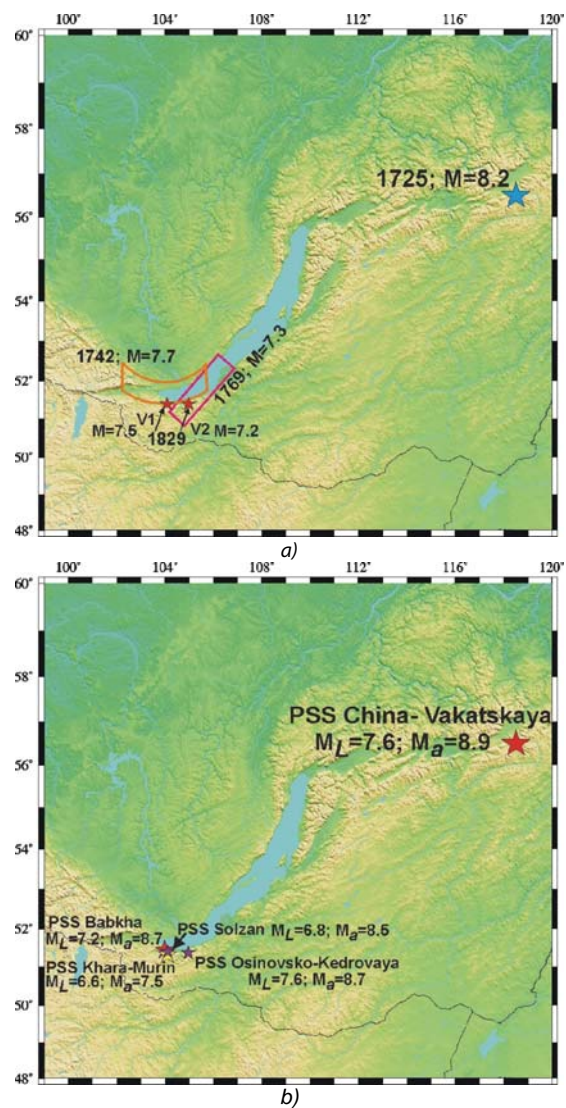


Fig. 4: (a) Four earthquakes in the Baikal region catalogue and (b) parameters of paleo-seismo-structures (PSS) used for their parameterization according to the New Catalogue ..., 1977.

Definitely, search for paleo earthquakes must be planned for hazard assessment of critical facilities regardless of the modern activity level, to obtain stable and well grounded result. Paleo earthquake data have to be included in the earthquake database as **independent**



component to be taken into account in hazard assessment. One should resist the temptation to combine paleo earthquake and historical (macroseismic) data at early stages of the analysis elaborating, so called, comprehensive solution. The following shows that it can lead to unjustified solutions.

In the earthquake catalogue of Baikal seismic region there are four earthquakes, which parameters are evaluated based both on paleo and macroseismic data (Fig. 4). Among these earthquakes is the largest one (M8.2), which determines the level of the seismic hazard in the region (so called the *Great Siberian Earthquake*).

These solutions were reported first time in the New Catalogue ... (1977) and then used in several projects including the current official Russian General Seismic Zoning map. It is believed that large magnitude is supported both by the macroseismic and geological data. But careful re-examination of historical data (dairies of German traveler Messerschmidt, the eyewitness of the earthquake, were checked) using modern approaches of verification demonstrated that macroseismic data do not correspond to the given solution. Details of this study can be found in the paper (Tatevossian et al., 2013). Actually, magnitude of the *Great Siberian Earthquake* is based on the PSS parameters only. Possible solutions compatible with macroseismic data are shown in Fig. 5 (from Tatevossian et al., 2013).

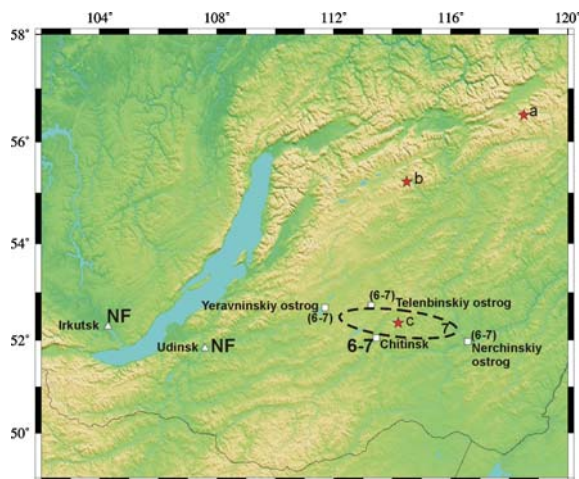


Fig. 5: Possible solutions for the “Great Siberian Earthquake” in 1725. (a) Solution from the New Catalog, M8.2; (b) alternative solution, M8.1 which at least not in contradiction with some of the macroseismic data; (c) solution corresponding to macroseismic data; M6.8.

DISCUSSION and CONCLUSION

In this paper only two components of comprehensive earthquake database for hazard assessment of critical facilities are considered. The complete database has to include also historical earthquakes and instrumental data from Global and regional seismological agencies. For the later data type one should be careful to ensure homogeneous magnitude calibration for all instrumentally recorded earthquakes. Often it is believed

that instrumental data is precise by definition and it is just enough to download the catalogues from the website.

Combination of different data types creates illusion of more reliable solution. Seismologists are well aware about the limitations and possible accuracy of parameters derived based on macroseismic information but they do trust the catalogue record because it is supported by geological data. The geologists, just the opposite, know problems of magnitude calibration of palaeo earthquakes, but the final solution is considered to be reliable, because it is supported by macroseismic information.

Clearly, the main obstacle in combining paleo and historical data is the incompatibility of their dating accuracy. Usually, it is believed that accuracy of dating in written historical documents is much more precise. In general it is true, but not always. Serious problems with dating of historical documents arise when studying cross-border earthquakes (Tatevossian et al., 2011) or during transition period when calendar is changed in the country (Tatevossian & Albin, 2010). Combining two uncertain pieces of information will only increase uncertainty of final conclusions but not reduce it.

Seismic hazard assessment is mandatory for critical facilities; it is required by the design codes in many countries. Without conducting proper probabilistic seismic hazard assessment projects can not pass licensing procedure in corresponding authoritative organizations. Of course, this is just beginning of the design process. Normally, engineers need much more information than just hazard level expressed in ground acceleration or macroseismic intensity. Moreover, when expected seismic loading is not very high (say, less than intensity 8) engineers do not care much about level of shaking. Crucial information for them is whether the pipeline trace will cross active or capable fault and what displacement could be associated with it. These topics are far out of the scope of the paper. My goal is to call attention to the problem of databases: their compilation is not a trivial task, because they have to cover very large time span, have to take into account wide range of magnitudes and spatial scales. There is a strong temptation to mix different data types from the very beginning and forget about the problem of databases.

Actually, when preparing this paper the intention was to share some of my thoughts and concern on the essence of earthquake databases for seismic hazard assessment of critical facilities illustrated by a few examples related to different time-scales. Data should govern conclusions and not models.

Acknowledgements: I'm grateful to PATA Scientific and Organizing Committees for invitation and financial support. The work was partly supported by the RFBR Grant 14-05-00258. It is my pleasure to express the gratitude to the Reviewer for valuable comments, which help me more clear to formulate the goal of the paper and understand what is left out of its scope.



INQUA Focus Group on Paleoseismology and Active Tectonics



paleoseismicity.org

References

- New Catalog of Strong Earthquakes in the Territory of the Soviet Union from Ancient Times till 1975. Kondorskaya NV, Shebalin NV (Eds), Nauka, Moscow, 535 pp. English edition published in 1982, Boulder, USA, 608 pp.
- Bykova, V.V., R.E. Tatevossian, L.D. Nikolayev, A.G. Mikhin, N.G. Mokrushina, (2014). The Skovorodino, 2011 earthquake. *Fizika Zemli, (in Russian), in press.*
- IAEA (2010) Safety Guide № SSG-9, Seismic Hazards in Site Evaluation for Nuclear Installations. Vienna.
- Messerschmidt, D.G., Forschungsreise Durch Sibirien, 1720 - 1727, Tagebuchzeichnungen: Mai 1724 – Februar 1725, Berlin, 1966.
- Messerschmidt, D.G., Forschungsreise Durch Sibirien, 1720 - 1727, Tagebuchzeichnungen: Februar - 1725 November, Berlin, 1968.
- Tatevossian, R., P. Albini, (2010). Information background of 11th–15th centuries earthquakes located by the current catalogues in Vrancea (Romania). *Natural Hazards // DOI 10.1007/s11069-009-9448-2*
- Tatevossian, R.E., P. Mäntyniemi, T.N. Tatevossian, (2011). On the earthquakes in the Northern Baltic Shield in the spring of 1626. // *Natural Hazards, 57:133–150*
- Tatevossian, R.E., N.G. Mokrushina, J.Ya. Aptekman, and T.N. Tatevossian, (2013). On the relevancy of the combination of macroseismic and paleoseismic data. *Seismic Instruments, 49, (2), 115–138.*



INQUA Focus Group on Paleoseismology and Active Tectonics



paleoseismicity.org

NOTES



Emerging Concepts in Probabilistic Seismic Hazard Analysis and the Use of the SSHAC Process for Assessing Uncertainty

William Lettis

Lettis Consultants International Inc., Walnut Creek, United States

Abstract: Emerging best practice is increasingly using probabilistic approaches to assess seismic hazard at nuclear facilities and other important structures throughout the world. Probabilistic seismic hazard analyses (PSHA) involved developing both a Seismic Source model (SSM) and Ground motion model (GMM) based on all available data, methods and models and that properly capture the range in aleatory variability and epistemic uncertainty in each input parameter. Seismic source models include a full description of both areal (or "background") sources and fault sources, including location, geometry, rate, magnitude distribution, and recurrence. Ground motion models include a description of applicable ground motion prediction equations applicable to the tectonic setting, style of faulting, and regional and site-specific crustal properties. The Senior Seismic Hazard Analysis Committee (SSHAC) developed explicit methods and guidance for developing SSM and GMM for input to PSHA that properly capture and quantify the center, body, and range of aleatory and epistemic uncertainty in technically defensible interpretations within the professional community. Four levels of SSHAC study (Level 1 to 4) are described with increasing complexity and scope with higher study level. Given the importance of seismic hazard to nuclear safety, a SSHAC Level 3 or 4 study is recommended to develop PSHA for nuclear facilities. This presentation will describe the essential steps in developing SSM and GMM for PSHA, and the use of the SSHAC methodology for assessing uncertainty in the SSM and GMM input parameters.

INTRODUCTION

Risk analysis for nuclear and other critical facilities requires a probabilistic assessment of seismic hazard. Probabilistic seismic hazard analysis (PSHA), in turn, requires as input a seismic source model (SSM) and ground motion model (GMM) that fully capture the range of aleatory variability and epistemic uncertainty in the model parameters. Aleatory variability describes the natural randomness in Earth processes that cannot be reduced through further data acquisition or knowledge. Epistemic uncertainty describes the uncertainty in Earth processes that can be reduced through further data acquisition, modeling, and knowledge. It should be noted that the deterministic approach to seismic hazard analysis (DSHA) does not explicitly incorporate either aleatory variability or epistemic uncertainty, and cannot be used for input to a probabilistic risk analysis for a critical facility. Thus, PSHA has replaced DSHA for modern assessments of seismic hazard for nuclear and other critical facilities, and represents current International Best Practice.

Explicitly capturing the full range of aleatory variability and epistemic uncertainty in SSM and GMM for input to a PSHA is not easy. Developing an acceptable SSM or GMM requires careful analysis, discussions with members of the professional community (both site-specific experts and experts on generic issues), and through documentation of the data, methods and models (including alternative models) that were used to construct the SSM and GMM. The objective in developing an acceptable SSM and GMM is to capture the full center, body and range of technically defensible interpretations (termed the CBR of the TDI) within the professional technical community.

Capturing the CBR of the TDI for seismic hazard analysis is not an activity performed by one person or small group of individuals that develop a "preferred" SSM or GMM. This activity requires soliciting input from knowledgeable experts throughout the informed technical community, and assessing this input through a formal, structured "evaluation" and "integration" process to develop an SSM and GMM that captures the CBR of the TDI.

The SSHAC process was explicitly developed to provide an acceptable approach to develop an SSM and GMM that captures the CBR of the TDI with a high level of both technical and regulatory confidence. The SSHAC process was first published in NUREG/CR-6372 (Budnitz et al, 1997) and has been updated with explicit implementation guidance in NUREG 2117 (NRC, 2012).

As shown on Figure 1, the SSHAC Level 3 process consists of a variety of work activities that fall under one of four main components: (1) Evaluation, (2) Integration, (3) Documentation, and (4) Peer Review, and is performed by a Technical Integration (TI) Team, supported by Resource and Proponent Experts, Hazard analysts, and a Participatory Peer Review Committee (PPRP). The four process components are summarized below. The analysis is "hazard-informed" whereby the hazard analyst iteratively performs sensitivity analyses throughout the study to inform the TI Team of those issues and parameters that are most significant to hazard.

EVALUATION

The process of evaluation involves the consideration of all data, models and methods proposed by the larger technical community that are relevant to seismic hazard



INQUA Focus Group on Paleoseismology and Active Tectonics



paleoseismicity.org

at a site. The process of evaluation includes: (a) identification of hazard-significant issues; (b) compilation of relevant data, models, and methods (e.g., published research papers, geologic and geophysical data); (c) collection and analysis of new data to address focused issues; and (d) evaluation of the data, models, and methods with respect to their impact on the SSM or GMM models. The overall goal of the evaluation process is to compile and evaluate all of the data that are relevant to the SSM and GMM. The data evaluation process is led by the TI Team, with specific input from the TI Team technical staff and Resource and Proponent Experts (REs and PEs). Most of the interactions between the REs and PEs and the TI Team occur at the formal project Workshops as shown on Figure 1. The PPRP is involved in the evaluation process through attending workshops, reviewing interim project documentation, and participating in field reviews and/or working meetings.

INTEGRATION

The process of integration involves developing an SSM and GMM model that represents the CBR of the TDI in light of the evaluation process (i.e., informed by the assessment of existing data, models and methods). Following the evaluation process, the TI Team integrates the relevant data, models, and methods to develop an SSM and GMM model that captures the CBR of the TDI. The process of integration typically includes: (a) developing a preliminary version of the model; (b) performing hazard sensitivity analyses to document the impact of model parameters on the seismic hazard at the frequencies of interest; (c) obtaining feedback from REs, PEs, and the PPRP on the preliminary model and hazard sensitivity; and (d) developing the final version of the SSM and GMM model. The PPRP is involved throughout the integration process through attending workshops, reviewing interim project documentation, and attending selected working meetings.

PEER REVIEW

A Participatory Peer Review Panel (PPRP) is an integral component of a SSHAC study. The overall goal of the participatory peer review is to ensure that the SSHAC process is adequately followed and that the technical results adequately characterize the CBR of the TDI. As described in NUREG 2117 (NRC, 2012b), the review is participatory in that it is a continuous process

throughout the study, and not a singular review at the end of the study. The PPRP is kept abreast of project developments through a combination of attending workshops, reviewing interim project documents, and attending selected field reviews and/or working meetings.

DOCUMENTATION

As described in NUREG 2117 (NRC, 2012), documentation is an integral component of a SSHAC study in that it provides a record of the final technical results, how they were reached, and how the SSHAC process was implemented. In addition, the documentation provides the basis for review by any pertinent regulatory officials, if needed. Documentation for a SSHAC study typically includes (1) a Final Report describing the technical judgments and rationale for the logic tree elements (i.e., nodes), parameters and weights, (2) Workshop summaries and presentations, PPRP letter reports and TI Team responses, (3) the GIS Geospatial Database, with summary tables describing the contents of the database and the reference library, (4) the project earthquake catalog, (5) source-specific Data Summary and Source Evaluation sheets, and (6) the final Hazard Input Document (HID).

Acknowledgements: This work was funded from 1999 to 2006 by the Atomic Energy Fund of the Korean Ministry of Science (KINS) and supported by the Korean Institute of Geoscience and Mineral Resources (KIGAM).

References

- Budnitz R.J., G Apostolakis, D.M. Boore, L.S. Cluff, K.J. Coppersmith, C.A. Cornell, and P.A. Morris. 1997. Recommendations for Probabilistic Seismic Hazard Analysis: Guidance on Uncertainty and Use of Experts – Main Report. NUREG/CR-6372, Vol. 1, U.S. Nuclear Regulatory Commission, Washington, D.C.
- Coppersmith, K.J., Bommer, J.J. 2012. Use of the SSHAC Methodology within regulated environments: Cost-effective application for seismic characterization at multiple sites. *Nuclear Engineering and Design* 245, 233-240.
- NRC (U.S. Nuclear Regulatory Commission). 2012a. Practical Implementation Guidelines for SSHAC Level 3 and 4 Hazard Studies. NUREG-2117, U.S. Nuclear Regulatory Commission, Washington, DC.

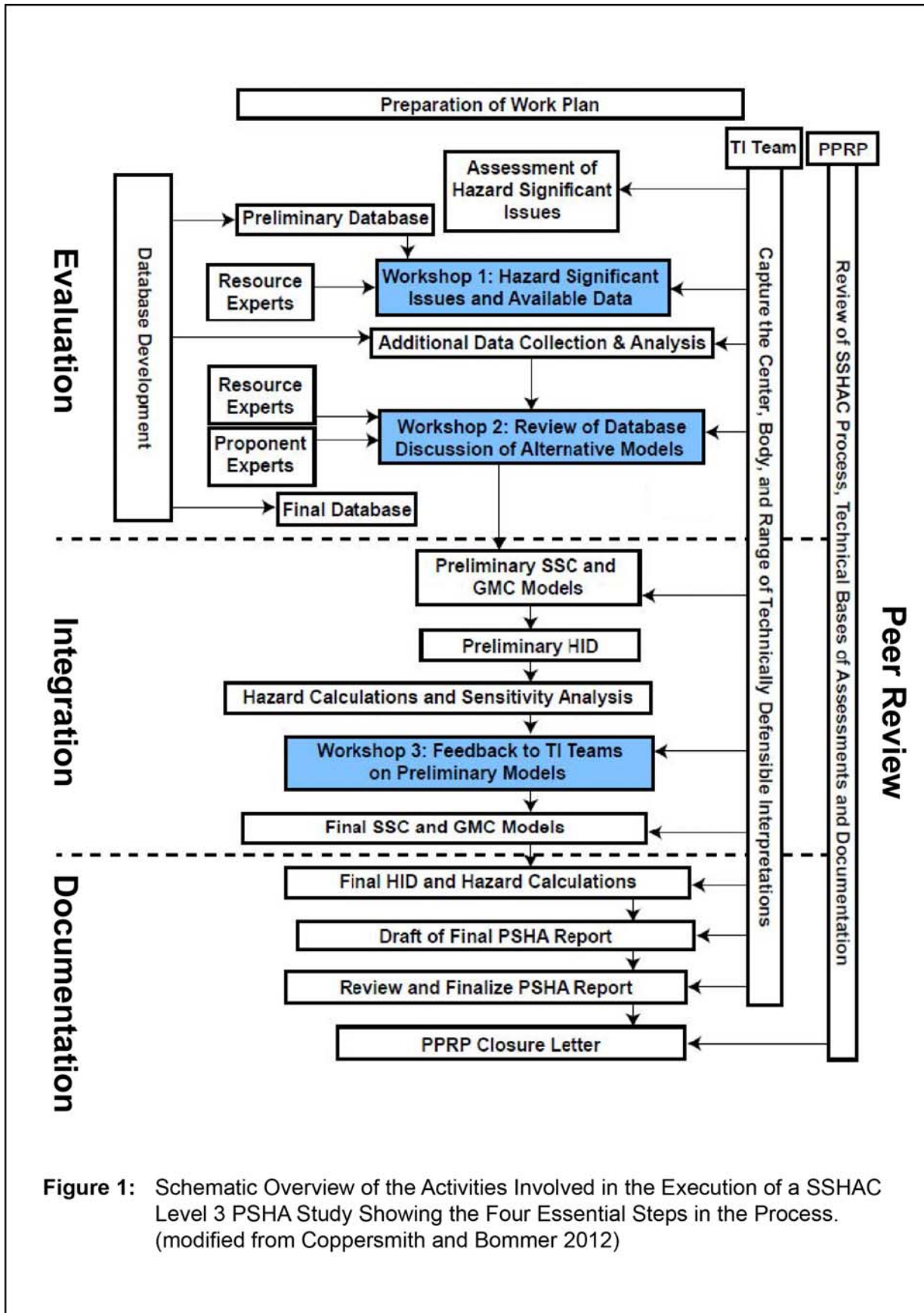


Figure 1: Schematic Overview of the Activities Involved in the Execution of a SSHAC Level 3 PSHA Study Showing the Four Essential Steps in the Process. (modified from Coppersmith and Bommer 2012)



INQUA Focus Group on Paleoseismology and Active Tectonics



paleoseismicity.org

NOTES

Wednesday 24 September

Session Seven: Secondary Effects of Earthquakes



Evaluation of seismic stability of coherent landslides: Analytical approach versus FEM

Koltuk, Serdar (1), Fernandez-Steeger, Tomas M. (1)

(1) Department of Engineering Geology and Hydrogeology, RWTH Aachen University, 52062 Aachen, Germany;
E-mails: koltuk@lih.rwth-aachen.de, fernandez-steeger@lih.rwth-aachen.de

Abstract: One of the major causes of landslides is earthquake loading. Conventionally, the evaluation of landslides under seismic load is performed by using pseudo-static and displacement-based methods. However, through recent advances in computational ability, numerical methods have become popular to evaluate the seismic stability of slopes. This study aimed to investigate the seismic stability of a two-dimensional slope model. For that purpose, the results obtained from pseudo-static and permanent displacement-based methods are compared with those obtained from finite element analyses. The results demonstrate that the displacements obtained from finite element analyses are larger than that obtained from displacement-based methods. Both pseudo-static method and FEM yield similar failure surfaces. However, a Rayleigh damping of 5% used in the numerical analyses leads to a significant decrease in the displacement of the slope, while no failure surface develops.

Key words: slope performance, seismic load, pseudo-static, finite element method, permanent displacement

1. Introduction

From a global perspective, earthquakes are a main cause of large destructive landslides, like the ones in Fig. 1. Landslides triggered by earthquakes can be grouped according to their fragmentation-placement and material type as: 1) disrupted slides and falls of rock and/or soil, 2) coherent slides, rock and/or soil masses with well-developed failure planes and 3) lateral spreads and flow slides due to liquefaction (Keefer, 1984).



Fig. 1: Landslides caused by earthquakes. At the left the 2001 Las Colinas slide in El Salvador and at the right a landslide dam NW of Jacmel triggered by the 2010 Haiti earthquake (source: USGS).

The main methods to investigate the stability of coherent slopes under seismic load fall into three categories: pseudo-static method, displacement-based method, and numerical methods. The approaches of those methods are briefly described in the following.

Pseudo-static method: This method ignores the dynamic nature of earthquakes and treats it as if it applied a static lateral force acting through sliding mass, in an out-of-slope direction (Terzaghi, 1950). For stability analysis, any limit equilibrium methods, such as ordinary method of slices or Swedish method, Bishop's simplified method, Janbu's method, Spencer's method, Morgenstern-Price's

method and so on, are used. The pseudo-static lateral force F_h is applied to each slice through its centroid, as shown in Fig. 2. The pseudo-static lateral force F_h is calculated by using Eq. (1)

$$F_h = \frac{W a_{max}}{g} \quad (1)$$

where W is the weight of slice, g is acceleration of gravity, a_{max} is maximum horizontal acceleration at ground surface that is induced by the earthquake. The maximum horizontal acceleration is commonly referred to as peak ground acceleration (PGA). The ratio a_{max}/g in Eq. (1) is called seismic coefficient k_h .

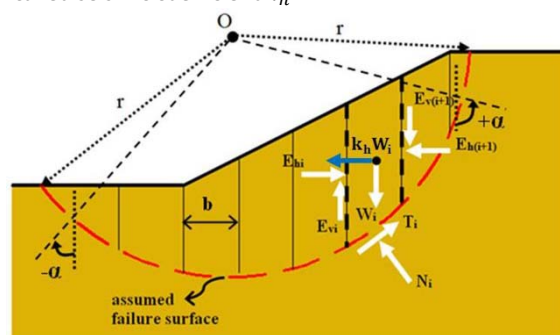


Fig. 2: The ordinary method of slices and forces acting on a slice under seismic loading.

Determination of seismic coefficient is the most important and difficult aspect of a pseudo-static analysis since a_{max} depends on local seismic activity, local soil conditions and topography, as well as the importance of facilities. Terzaghi (1950) suggested the following values: $k_h = 0.1$ for severe earthquakes, $k_h = 0.2$ for violent and destructive earthquakes, $k_h = 0.5$ catastrophic earthquakes. However, there are no sharp defined rules for the determination of the seismic coefficient for design.



The selection of k_h takes considerable experience and judgment (Kramer, 1996).

Displacement-based method: Newmark (1965) presented a technique for estimation of the displacements of slopes due to earthquake. This approach assumes that a slope will deform only if the factor of safety obtained from pseudostatic analysis is smaller than 1.0. In this case, the seismic coefficient is reduced until a factor of safety equal to 1.0 is reached. A horizontal acceleration that leads to a safety factor of 1 is referred to as yield acceleration. The sequence of an earthquake strong-motion record that exceed the yield acceleration are integrated to obtain the velocity-time history, and the velocity-time history is then used to obtain the cumulative displacement of the slope (see Fig. 3).

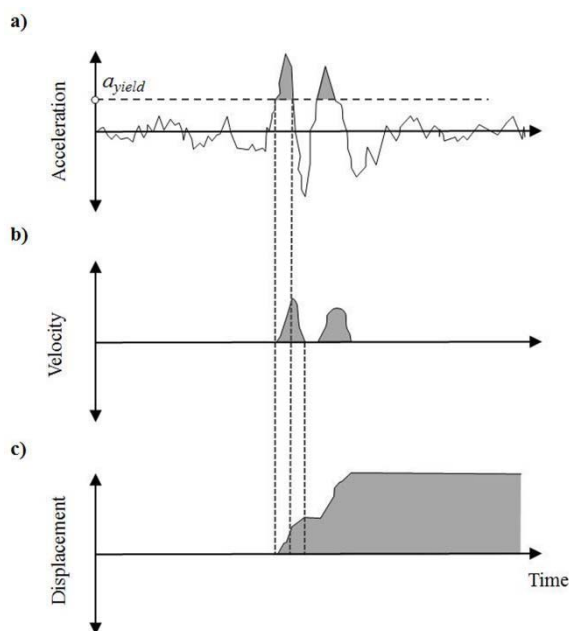


Fig. 3: Illustration of the Newmark Method: a) earthquake acceleration-time history; b) velocity-time history; c) displacement-time history (modified from Wilson & Keefer 1985).

Several simplified approaches have been developed utilizing the Newmark method (Makdisi et al., 1978; Ambraseys et al., 1988; Bray et al., 1998; Jibson, 2007). In this study, the Eq. 2 and 3, which were presented by Ambraseys & Menu (1988) and Jibson (2007) respectively, are used to evaluate permanent displacements induced by an earthquake.

$$\log d = 0.9 + \log \left[\left(1 - \frac{a_{yield}}{a_{max}} \right)^{2.53} \cdot \left(\frac{a_{yield}}{a_{max}} \right)^{-1.09} \right] \mp 0.3 \quad (2)$$

where d is slope displacement in cm. This equation is valid for earthquakes with surface-wave magnitude in the range of 6.6–7.2. It should be mentioned that the permanent displacement increases with increasing magnitude of earthquake due to increasing duration of seismic loading.

$$\log d = -2.71 + \log \left[\left(1 - \frac{a_{yield}}{a_{max}} \right)^{2.335} \cdot \left(\frac{a_{yield}}{a_{max}} \right)^{-1.478} \right] + 0.424M \mp 0.454 \quad (3)$$

where d is slope displacement in cm, M is moment magnitude of earthquake. This equation is valid for magnitude range of 5.3-7.6.

The question whether the calculated displacement is acceptable or leads to a failure is not easy to answer. According to Blake et al. (2002): "1) for slip surfaces intersecting stiff improvements (such as buildings, pools, etc.) median displacements should be maintained at < 5 cm; 2) for slip surfaces occurring in ductile (i.e., non strain softening) soil that do not intersect engineered improvements (e.g., landscaped areas and patios), median displacements should be maintained at < 15 cm; 3) for slip surfaces occurring in soil with significant strain softening (i.e., sensitivity > 2), if k_{yield} was calculated from peak strengths, displacements as large as 15 cm could trigger strength reductions, which in turn could result in significant slope destabilization. For such cases, the design should either be performed using residual strengths (and maintaining displacements < 15 cm), or using peak strengths with displacements < 5 cm". Critical displacement values suggested by further researchers are given in Tab. 1.

Table 1: Critical displacement induced by earthquakes.

Source	Displacement [cm]	Hazard level
California Geological Survey (2008)	0-15	unlikely serious movement
	15-100	slope failure
	> 100	damaging landslide movement
Miles et al. (2009)	< 2	very low
	2-5	low
	5-10	moderate
	> 10	high
Jibson et al. (2011)	< 1	low
	1-5	moderate
	5-15	high
	> 15	very high

It should be noted that the Newmark method may only be applied for slopes that will deform as a single massive block, and not for those cases where the sliding mass disintegrates and sections will tend to individually deform (such as slopes in cohesionless granular soils).

Numerical methods: The pseudo-static method is not applicable to soils that may change their shear strength during seismic loading. This means, this type of stability analysis cannot be applied to soils with high sensitivity and to soils in which large excess pore water pressure builds up, and therefore the loss of shear strength occurs due to cycling loading.

The finite element method (FEM) is a powerful numerical method, which is used as an alternative to the pseudo-static and displacement-based methods. The advantages of FEM to slope stability analysis over conventional methods can be given as follows: 1) no assumption needs



to be made in advance about the shape or location of the failure surface; 2) If the stress-strain properties of the soil are available, the finite element method gives information about the deformations of the slope; 3) the excess pore water pressures that are generated by earthquake within the slope can be determined.

2. Numerical Investigations

This study aims to compare established methods to investigate slope performance under seismic load. Results obtained from numerical FEM analysis are compared with those obtained from conventional pseudo-static and displacement-based methods.

The slope consists of a slightly overconsolidated cohesive soil, overlying a rock formation. Moisture unit weight of the soil is taken as 18 kN/m^3 . It is assumed that no groundwater level exists. Therefore, no excess pore water pressure occurs during seismic loading. Dimensions of the slope model and the soil parameters can be seen in Fig. 4. The factor of safety for the slope under gravity loading is determined as 1.25. Mohr-Coulomb material model is assigned to the soil, which requires two elastic (*Young's modulus* $E'_{ref} = 5,000, 10,000, 20,000 \text{ kPa}$; *Poisson's ratio* $\nu' = 0.3$) and three plastic parameters (*cohesion* $c' = 5 \text{ kPa}$; *friction angle* $\phi' = 25^\circ$; *dilatancy* $\psi = 0$).

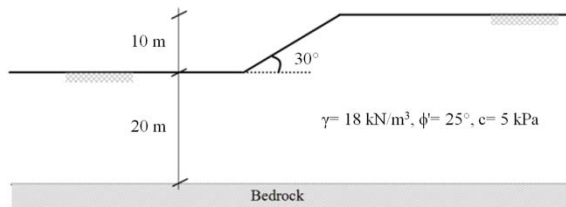


Fig. 4: Slope model and soil parameters.

The pseudo-static stability analyses are performed using Bishop's simplified method (1955), which ignores vertical forces $E_{v(i)}$ and $E_{v(i+1)}$ on the lateral boundaries of the slices (see Fig. 2). In order to apply Bishop's simplified method to the stability analysis of the model slope, the software GGU-Stability version 10 is used in which the failure surface is automatically searched. Subsequently, the permanent displacements due to seismic loading are determined by use of Eq (2) and Eq (3).

The dynamic numerical analysis of model slope has been carried out using the software Plaxis 2D version 2012, which is based on the finite element method. The analyses are performed in three stages: 1) in the first stage, the gravity acceleration of 9.81 m/s^2 is applied to the ground to obtain the initial stress conditions; 2) in the second stage, the model slope is generated through excavation; 3) in the third stage, dynamic analysis is performed using the acceleration-time record of Ahuachapan station / 4354a from El Salvador earthquake in 2001 (see Fig.5.) The moment magnitude and maximum horizontal ground acceleration were 7.6 and 2.1 m/s^2 , respectively.



Fig. 5: Acceleration-time history of the El Salvador earthquake (U.S.G.S.-N.S.M.P.).

A plain strain model of 15-noded triangular elements is used for numerical modeling. The mesh is refined in the slope zone where the stress concentration is expected to develop. The number of elements and nodes are 1.447 and 11.819 respectively. Figure 6 shows the dimensions and the boundary conditions of the numerical model. The vertical model boundaries of the soil model are chosen sufficiently far from the slope zone to avoid disturbances due to reflections. In addition to standard fixities boundaries, absorbent boundary conditions are applied at the vertical boundaries of the model to absorb outgoing waves. To convert the unit of displacement from cm to m, a prescribed horizontal displacement of 0.01 m is imposed at the base of the model since the displacement unit in the acceleration-time history is cm. The prescribed vertical displacement is kept to zero.

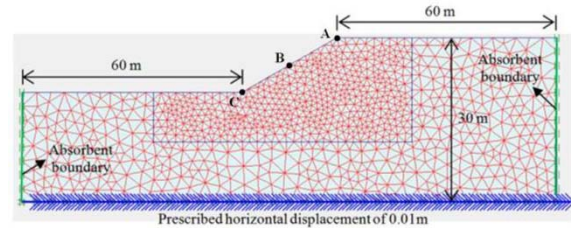


Fig. 6: Numerical model of the slope (Boundary conditions and model dimensions).

For three Young's moduli ($E'_{ref} = 5,000, 10,000, 20,000 \text{ kPa}$) and two Rayleigh damping ratios ($\xi = 0\% \text{ and } 5\%$), the stability of the model slope is examined under seismic loading given in Fig. 5 for a time interval of 33 s. As a result of numerical analyses, the time histories of the displacements at different locations of the slope (at points A, B, and C) and the potential failure surfaces are shown. However, the factor of safety is not determined since the value and the direction of the seismic force change with time.

3. Results and Discussions

For a horizontal seismic coefficient of 0.21, the pseudo-static analysis yields a factor of safety of 0.85. The most



probable failure surface developed under seismic loading is demonstrated in Fig. 7.

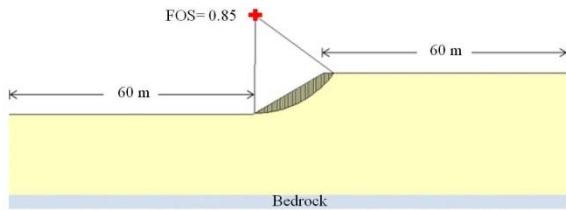


Fig. 7: Failure body obtained from pseudo-static analysis.

Yield horizontal seismic coefficient k_{yield} is determined as 0.115, and subsequently the permanent displacement of the slope is calculated according to Eq. (2) and (3) as 2.05 cm and 1.24 cm, respectively.

Acceleration-time and displacement-time histories for the slope obtained from numerical FEM analysis are shown in Fig. 8. The data clearly indicate that not only maximum acceleration but also duration control overall displacement. Another maybe surprising but never the less relevant point is that material damping parameters have a considerable influence on the distribution of acceleration and displacement over the slope height. Material damping is caused by the viscous properties of soil, friction and the development of plastic strains. The occurring plastic strains in dynamic analyses cause material damping. However, this damping is generally not sufficient to simulate the damping of real soils. Thus, an additional damping of 5% is used in this study by means of Rayleigh damping (Plaxis 2D, 2012). Unfortunately damping is usually not determined even so considerable research exists.

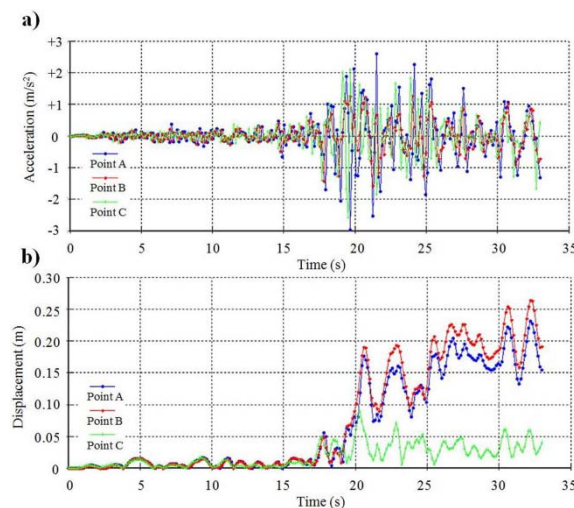


Fig. 8: Horizontal acceleration-time (a) and displacement-time (b) histories for $E_{ref} = 10.000$ kPa and $\xi = 0\%$.

The Comparison of the slope displacements obtained from FEM and permanent-displacement methods according to Ambraseys & Menu (1988) and Jibson (2007) is shown in Fig. 9. It is apparent from the figure that a large difference exists between the displacements obtained

from analytical and numerical methods. Moreover, they show an unexpected soil behavior, namely, the displacement does not decrease with increasing Young's modulus, but it increases. This is due to the fact that compression and shear wave velocities increase with increasing Young's modulus whereas the strength parameters of the soil are kept constant in the numerical analyses.

Finally, Figure 10 indicates that the displacement solely might provide misleading information regarding slope stability. It demonstrates deformed meshes and failure surfaces for various Young's moduli and a damping factor of $\xi = 0\%$. The displacement in point A (see Fig. 9) is according to all proposed values in Table 1 points out a slope failure. However, the shear zone in Fig. 10a is not continuous. This indicates that no slope failure occurs. Furthermore, no failure surface has developed in the cases with a Rayleigh damping of $\xi = 5\%$ although the displacements are sufficiently large according to Table 1.

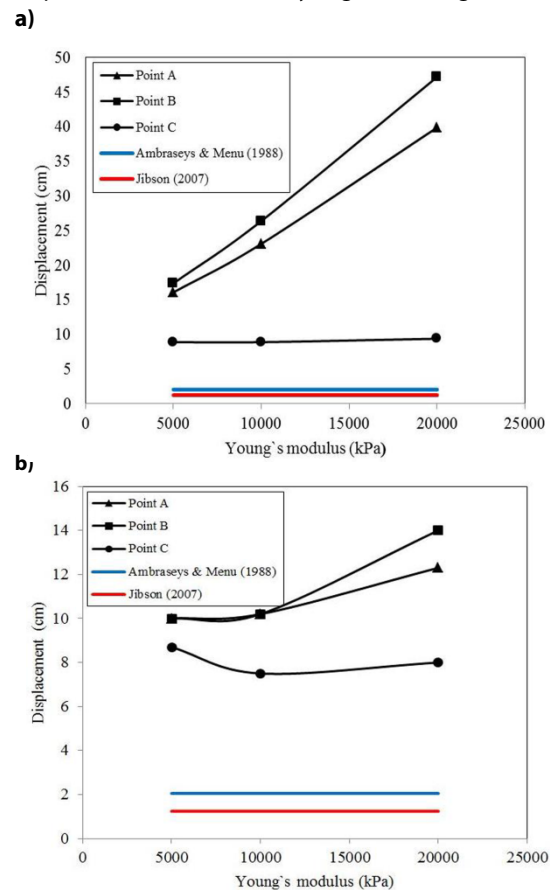


Fig. 9: Comparison of the slope displacements obtained from FEM and permanent-displacement methods: a) for a Rayleigh damping factor of $\xi = 0\%$; b) for a Rayleigh damping factor of $\xi = 5\%$.

4. Conclusions

Based on the results of conventional and numerical analyses, the following conclusions have been achieved:



- 1) Although the permanent displacements obtained from simplified methods are determined using the peak ground acceleration, finite element analyses give larger displacements.
- 2) An increase of Rayleigh damping from 0 % to 5 % causes a significant decrease in the displacement of the slope.
- 3) Both pseudo-static method and FEM for $\xi = 0\%$ give similar failure surfaces. However, no failure surface has developed for a Rayleigh damping of 5 %.
- 4) In contrast to pseudo-static method, the acceleration occurring over the slope is not constant, and the maximum displacement appears between the toe and the crest of the slope.
- 5) Mohr-Coulomb law is used in the FE analyses performed in this study. More qualitative results can be achieved by using advanced constitutive models, such as Hardening Soil Model with small-strain stiffness.

Finally, it should be pointed out that, in this study, the acceleration-time history of El Salvador earthquake in 2001 is used to compare different methods with each other with regard to permanent displacements. However, a further acceleration-time history may cause a more or less difference between the displacements obtained from FE and simplified approaches. Because the simplified approaches used to determine permanent displacements do not consider the frequency of acceleration-time histories and the duration of earthquakes. Additionally, further simplified methods, such as Makdisi & Seed's method (1978), may give larger displacement than those calculated according to Eqs. (2) and (3).

Acknowledgements: The numerical analyses performed in this study were supported by the Department of Geotechnical Engineering of RWTH Aachen University. This support is greatly appreciated.

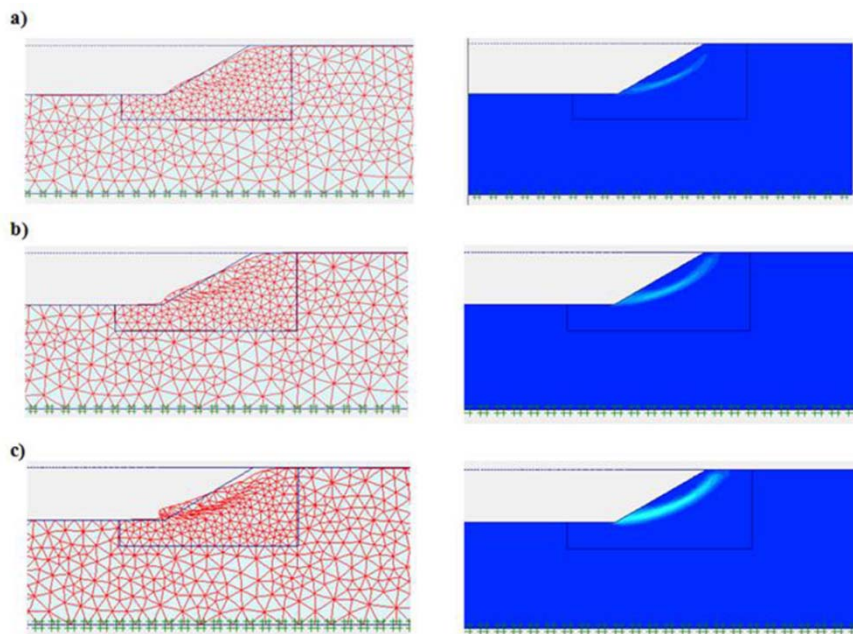


Fig. 10: Deformed meshes (left side) and failure surfaces (at the right): a) for $E_{ref} = 5.000 \text{ kPa}$; b) for $E_{ref} = 10.000 \text{ kPa}$; c) for $E_{ref} = 20.000 \text{ kPa}$.



References

- Ambraseys, N.N., Menu, J.M. (1988). Earthquake-induced ground displacements. *Earthquake Engineering and Structural Dynamics* 16, 985-1006.
- Baker R., Shukha R., Operstein V., and Frydman S. (2006). Stability charts for pseudo-static slope stability analysis. *Soil Dynamics and Earthquake Engineering*, 26, 813-823.
- Bishop A. W. (1955). The Use of the Slip Circle for the Stability Analysis of Slopes. *Geotechnique*, Vol. 5 (1), 7-17.
- Blake T.F., Hollingsworth R.A., Stewart J.P. (2002). Recommended procedures for implementation of DMG Special Publication 117-Guidelines for analyzing and mitigating landslide hazards in California. Southern California Earthquake Center.
- Bray J.D., Rathje E.M. (1998). Earthquake-induced displacements of solid-waste landfills. *Journal of Geotechnical and Geoenvironmental Engineering*, Vol. 124 (3), 242-253.
- California Geological Survey (2008). Guidelines for evaluating and mitigating seismic hazards in California. Special Publication 117A.
- GGU-Stability (2012). A Software Package for Slope Stability Analysis. Version 10, Civilserve GmbH, Steinfeld - Germany.
- Jibson R.W. (2007): Regression models for estimating co-seismic landslide displacement. *Engineering Geology*, Vol. 91, 209-218.
- Jibson R.W. (2011). Methods for assessing the stability of slopes during earthquakes-A retrospective. *Engineering Geology*, Vol. 122, p. 43-60.
- Keefer D.K. (1984). Landslides caused by earthquakes. *Geol. Soc. Am. Bull.*, Vol. 95, 406-421.
- Kramer S.L. (1996). *Geotechnical Earthquake Engineering*. Prentice Hall, Upper Saddle River, NJ.
- Makdisi F.I., Seed H.B. (1978). Simplified procedure for estimating dam and embankment earthquake-induced failures. *American Society of Civil Engineers, Journal of the Geotechnical Division* 104, 849-861.
- Miles S.B., Keefer D.K. (2009). Evaluation of Camel-comprehensive areal model of earthquake-induced landslides. *Engineering Geology*, Vol. 104, 1-15.
- Newmark N. (1965). Effects of earthquakes on dams and embankments. *Geotechnique*, 15(2), 139-160.
- Plaxis-2D (2012). *Finite Element Code for Soil and Rock Analyses*. Plaxis bv, Delft - the Netherlands.
- Terzaghi K. (1950). *Mechanisms of landslides. Application of Geology to Engineering Practice*. Geological Society of America.
- U.S. Geological Survey National Strong-Motion Project. http://nsmpr.wr.usgs.gov/data_sets/20010113_1.html
- Wilson R.C., Keefer D.K. (1985). Predicting the areal limits of earthquake-induced landsliding. Evaluating earthquake hazards in the Los Angeles region-An Earth science perspective. U.S. Geological Survey Professional Paper 1360, 316-345



INQUA Focus Group on Paleoseismology and Active Tectonics



paleoseismicity.org

NOTES



Long-term Forecast of Large Earthquakes: Lessons from the 2011 Tohoku Earthquake

Satake, Kenji (1)

(1) Earthquake Research Institute, the University of Tokyo, 1-1-1 Bunkyo-ku, Tokyo 113-0032 Japan. E-mail: satake@eri.u-tokyo.ac.jp.

Abstract: The 11 March 2011 Tohoku earthquake (M 9.0) was the largest instrumentally recorded earthquake in Japan. Numerous source models using various kinds of data show a common feature that a very large, several tens of meter, slip occurred east of the epicenter. The long-term forecast of large earthquakes, based on past data and characteristic earthquake model, failed to predict size and source region of this gigantic event, while the 30 year probability of an M ~7.5 earthquake was estimated as 99 % just west of the 2011 epicenter. The historical and paleoseismological data indicated that the 869 Jogan earthquake produced similar earthquake and tsunami damage in Sendai plain. One simple way to include such an infrequent gigantic earthquake in the existing characteristic model is a hierarchy supercycle model. Several factors must be incorporated to improve long-term forecasts of large earthquakes, including the estimation of probable maximum earthquake size.

Key words: long-term forecast, subduction zones, tsunami deposits, paleoseismology, the 2011 Tohoku earthquake

THE 2011 TOHOKU EARTHQUAKE AND TSUNAMI

The 11 March 2011 Tohoku earthquake was the largest earthquake instrumentally recorded in Japan. The Japan Meteorological Agency (JMA) named it “the 2011 off the Pacific coast of Tohoku earthquake” and provided source parameters of an epicenter at $38^{\circ} 06.2' N$, $142^{\circ} 51.6' E$, a depth of 24 km, a magnitude of M 9.0 and an origin time of 14:46:18.1 JST (GMT+ 9 hours). Here we call it “the 2011 Tohoku earthquake.”

The earthquake and tsunami caused devastating damage, including approximately 15,900 deaths and 2,600 missing, as well as serious damage to nearby Fukushima Dai-ichi Nuclear Power Station.

Numerous source models of the 2011 Tohoku earthquake have been proposed using seismic, land-based and marine geodetic, and tsunami data (see e.g., Tajima et al., 2013; Satake and Fujii, 2014 for a review). Although these models show common features such as a seismic moment or a general pattern of slip distribution, they also show differences in the exact location of the largest slip, the northern extent of the slip, as well as the duration of the tsunami source.

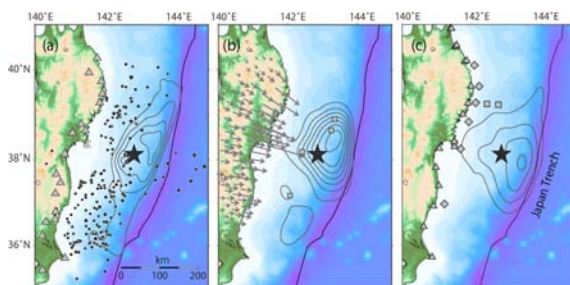


Fig. 1. Spatial distribution of coseismic slip for the 2011 Tohoku earthquake. The counter interval is 8 m. Black stars indicate the epicenter. (a) Solution from teleseismic body waves (Yoshida et al., 2011). Circles indicate aftershocks ($M \geq 5$) within 1 day after the mainshock. (b) Solution from land-based GPS and marine GPS/A data (Geospatial Information Authority of Japan, 2011). (c) Solution from tsunami waveform data (Satake et al., 2013).

The Centroid Moment Tensor (CMT) solution obtained by JMA (2012) indicates a seismic moment of 4.2×10^{22} Nm (moment magnitude M_w 9.0) and an underthrust faulting mechanism (strike 193° , dip 10° , and slip angle 79°) associated with subduction of the Pacific plate beneath Tohoku.

Seismic wave analysis resolves the temporal change of the source process very well. Many seismic wave studies (e.g., Ide et al., 2011; Yoshida et al., 2011) show a source duration of up to ~ 160 s, with most of the moment release limited to the first 100 s and a total moment of $\sim 4 \times 10^{22}$ Nm (M_w 9.0). Spatial distributions of slip differ somewhat from study to study but have the common feature that the largest slip of >20 m was estimated east of the epicenter, with considerable >10 m slip at both the shallowest part of the fault plane near the trench axis and the deeper part (Fig. 1a).

A land-based Global Positioning System (GPS) network recorded large coseismic displacements up to 5 m in horizontal and 1 m in vertical components (Ozawa et al., 2011). Inversion of land-based geodetic data indicates that the slip on the fault extends several hundred km with a maximum of 27 m near the epicenter.

Marine geodetic measurements begun before 2011 (e.g., Sato et al., 2011) detected large vertical displacements of up to 5 m and even larger horizontal displacements of up to 74 m. The joint inversion of land-based GPS data and marine geodetic (GPS/A) data yielded a coseismic slip of >50 m near the trench axis (GSI, 2011) (Fig. 1b).

Tsunami waveforms were recorded on many coastal and offshore tsunami gauges, such as bottom pressure gauges or GPS buoys, near Japan and around the Pacific Ocean. Inversion of tsunami waveforms also yielded a huge (50 to 70 m) slip near the trench axis (Fig. 1c). The tsunami waveforms require delayed tsunami sources along the Japan trench, north of the epicenter (Satake et al., 2013).



LONG TERM FORECAST BY JAPANESE GOVERNMENT

The occurrence of an $M\sim 9$ earthquake along Japan Trench was a surprise to the Japanese and global seismological communities. The long-term forecast made by the Earthquake Research Committee (ERC) of Japanese government failed to predict the size (M) and the source region of the Tohoku earthquake. Here we review the long-term forecast made by ERC before and after the 2011 Tohoku earthquake (ERC, 2009; 2011).

The ERC has annually publicized long-term forecasts of large earthquakes in and around Japan for the purpose of creating national seismic hazard maps. Long-term forecasts were made for individual segments of subduction zones or inland active faults based on dates and locations of past large earthquakes. Thirty-year earthquake occurrence probabilities are calculated by fitting a probability density function to the frequency distribution of inter-earthquake times. If earthquakes of similar size (“characteristic earthquakes”) recur more or less regularly and both the average recurrence interval and most recent event dates are known, the Brownian Passage Time (BPT) model is used to calculate time-dependent probabilities. “Characteristic earthquakes” are more broadly defined than the original definition (Schwartz and Coppersmith, 1984) or “repeating earthquakes”. If data indicate that temporal distribution is random, or if available data are insufficient to indicate regular occurrence, the Poisson process is assumed to calculate the time-independent probability.

The highest 30-year earthquake probability in Japan was calculated off Miyagi prefecture (called Miyagi-oki region), west of the 2011 Tohoku earthquake epicenter (Fig. 2). In this region, $M\sim 7$ earthquakes have occurred repeatedly since 1793 at an average interval of 37 years, although individual sequences are complex and cannot be modelled by a simple “characteristic earthquake” model. In the 1930s, three $M\sim 7$ earthquakes occurred: $M 7.1$ in 1933, $M 7.4$ in 1936 and $M 7.1$ in 1937. The 1978 earthquake of $M 7.4$ seemed larger than any of the 1930s earthquakes and possibly ruptured all three asperities. In 2005, another interplate earthquake of $M 7.2$ occurred that may be similar to the 1936 earthquake but smaller than the 1978 event. The 2005 earthquake was therefore not considered a “characteristic earthquake” in this region, or the sum of earthquakes in the 1930s or the 1978 earthquake. Because 34 years have passed since the last “characteristic earthquake” in 1978 (Fig. 2), the probability of a large $M\sim 7.5$ earthquake occurring between 2010 and 2040 was estimated at 99 % based on the BPT model.

Just to the east, in the southern Sanriku-oki region where the 2011 epicenter was located, the 30-year probability of an earthquake of $M\sim 7.7$ was estimated at 80-90 % based on the BPT model. The forecast stated that an earthquake that simultaneously ruptured these two regions –the Miyagi-oki and southern Sanriku-oki regions– would be $M\sim 8.0$. To the north, in the central Sanriku-oki region, no large earthquake occurrence was known to have occurred

hence probability could not be calculated. To the south, off Fukushima prefecture (Fukushima-oki region), swarm activity with a maximum M of 7.5 was recorded in 1938. Assuming that these were the only large earthquakes since the 1600s, the 30-year probability of an $M 7.4$ earthquake was estimated at $<7\%$ based on the Poisson model.

Along the Japan Trench, the ERC made long-term forecasts for two types of earthquakes – “tsunami earthquakes” and outer-rise normal-fault earthquakes.

“Tsunami earthquake” refers to one with relatively minor ground shaking but very large tsunami occurrence (Kanamori, 1972). Three tsunami earthquakes are known to have occurred along the Japan Trench –the Sanriku earthquakes in 1611 and 1896 and a Boso earthquake in 1677. The 30-year probability of a tsunami earthquake with tsunami magnitude $M_t 8.2$ was estimated at 20 % using the Poisson model and based on the fact that three tsunami earthquakes occurred somewhere along the Japan trench in the last 400 years.

A normal-fault earthquake occurs outside the trench axis, in what is often called the outer-rise region. The 1933 $M 8.1$ Sanriku earthquake was the only known great normal-fault earthquake and the 30-year probability of similar earthquake was estimated at 4-7 % based on the Poisson model.

The 2011 Tohoku earthquake was much larger than the forecast, both in magnitude and source area. The rupture started in the southern Sanriku region and propagated to the neighboring regions of central Sanriku, Miyagi-oki, southern Sanriku, and Fukushima-oki regions and parts of Ibaraki-oki and along the Japan Trench.

After the 2011 Tohoku earthquake, the ERC tentatively revised long-term forecasts, characterizing the 2011 event as an $M 8.4-9.0$ earthquake and estimating the recurrence interval at ~ 600 years based on paleoseismological studies. The ERC also considered the 2011 Tohoku earthquake to have a component similar to a tsunami earthquake and revised the 30-year probability of tsunami earthquakes to 30 % based on the four earthquakes occurring in the last 400 years (Fig.2).

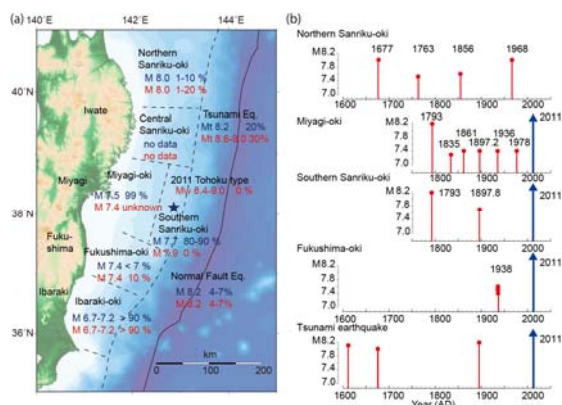


Fig. 2. (a) Segments along the Japan trench and the ERC 30-year probabilities of earthquake as of January 2011 in blue and as of January 2014 in red (ERC, 2009; 2011). (b) Magnitude-time plot of large earthquakes used for long-term forecasts.



THE 869 JOGAN EARTHQUAKE AND A SUPERCYCLE MODEL

While it was not considered in the long-term forecast of ERC (2009), the AD 869 Jogan earthquake is now considered to be a predecessor of the 2011 Tohoku earthquake. According to a historical document reporting this disaster recorded near Sendai, the strong ground shaking and the ensuing tsunami caused 1,000 fatalities. Tsunami deposits attributed to this earthquake have been found on the Sendai and Ishinomaki Plains (Minoura and Nakaya, 1991; Sawai et al., 2012). Tsunami deposits typically associate with the AD 915 ash layer from Towada volcano, and extend at least 1.5 km inland from the AD 869 shoreline, which is 1–1.5 km inland from the present coast. The tsunami deposits also indicate that several similar earthquakes occurred with recurrence interval of 500 to 800 years (Sawai et al., 2012).

The Jogan-type earthquake shows much longer recurrence interval than that of $M\sim 7$ earthquakes off Miyagi (Fig. 2). One simple way to reconcile this discrepancy is a supercycle model (Fig. 3). The average interval of $M\sim 7$ off-Miyagi earthquake with a typical slip of ~ 2 m is 37 years, meaning that the cumulative coseismic slip is about 6 m per century. Because the plate convergence rate is ~ 8 m per century, 2 m slips may remain unreleased. Such a difference has been interpreted as aseismic slip or coupling factors smaller than 1, but if this amount has accumulated at the plate interface, a slip of ~ 15 m could be released by an earthquake with a longer recurrence interval, e.g., ~ 700 years. This is similar to the 2011 earthquake slip amount in the deeper part near the source of past Miyagi-oki earthquakes. Along the trench axis, the slip deficit for 700 years exceeds 50 m, similar to the estimated slip near the trench axis. Although such a hierarchy in earthquake cycles may be too simple ignoring the variation in physical states of plate-boundary with depth, it can be tested using paleoseismological data before consideration for long-term forecast.

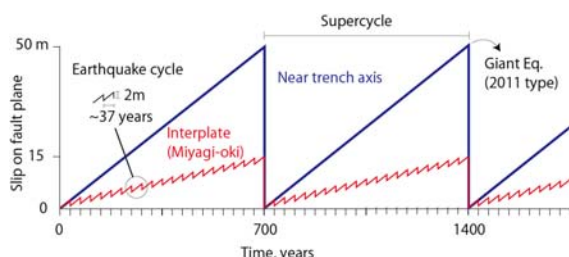


Fig. 3. Schematic model for earthquake supercycle off Miyagi in red and near the trench axis in blue. If accumulated slip is released by giant earthquakes such as the 2011 event, the recurrence interval or supercycle becomes about 700 years.

MAXIMUM SIZE OF LARGE EARTQUAKES

How big is the largest earthquake in individual subduction zones? Answering this question may require a global perspective (Satake and Atwater, 2007). Following the 2004 Sumatra-Andaman

earthquake of M 9.1 in the Indian Ocean, it was proposed that subduction zones worldwide could produce $M\sim 9$ earthquakes (McCaffrey, 2008). A similar proposal was made following the 2011 Tohoku earthquake which shows a return time of an $M > 9$ earthquake off Tohoku in the range of 300 to 400 years based on the moment conservation principle (Kagan and Jackson, 2013). Matsuzawa (2014) recently proposed that we should globally prepare for an $M\sim 10$ earthquake.

Various estimations of maximum earthquake size for Nankai trough have been recently made by different government committees. The Central Disaster Management Council in 2012 assigned M 9.1 as the maximum size of earthquake along the Nankai trough, then computed the ground shaking and tsunami inundation for several scenario earthquakes, and estimated the human and economic losses. The ERC recently (2013) revised the long-term forecast of Nankai trough earthquake; while the 30 year probability (60 – 70 %) is similar to the previous estimate (in 2001), they noted the size can be M 8 to 9, considering the variability of past earthquakes. The Nuclear Regulation Authority, established in 2012, assigned probable maximum earthquake magnitude of 9.6 for Nankai an Ryukyu troughs, 9.6 for Kuril-Japan trench, and 9.2 for Izu-Bonin trench (Fig. 4).

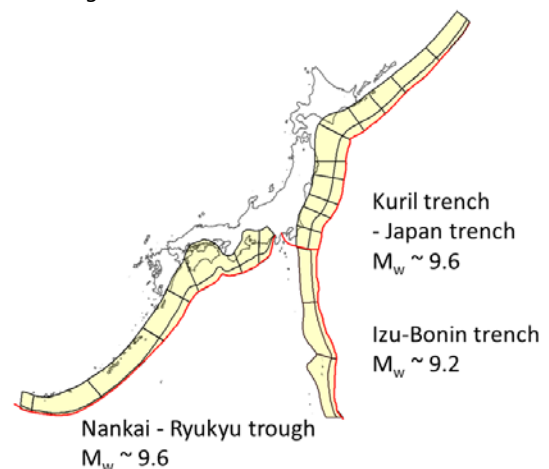


Fig.4 Possible source area and maximum size of interplate earthquake along three subduction zones around Japan, as estimated by Nuclear Regulation Authority in 2012.

IMPROVEMENT OF LONG-TERM FORECAST

Several other factors must be incorporated into long-term forecasts of large earthquakes. Paleoseismological data for hundreds to thousand years must be included to assess the recurrence of earthquakes. Monitoring plate coupling using land-based and marine geodetic data will provide important information on the state of stress on the plate interface. The greatest challenge, however, remains how to incorporate non-characteristic behavior. Studies of giant earthquakes in global subduction zones have shown such behavior (Satake and Atwater, 2007), so probabilistic estimates require detailed recurrence histories within the individual region. The occurrence of



giant earthquakes such as the 2011 earthquake may also influence probability in neighboring segments (Somerville, 2014). In fact, the several large $M > 7$ earthquakes occurring around the 2011 Tohoku earthquake source include normal-fault earthquake of $M 7.5$ on the east side of Japan trench and a few $M > 6$ earthquakes far from the source region.

Acknowledgements: This work was supported by KAKENHI (24241080).

References

- Earthquake Research Committee (2009). Long-term forecast of earthquakes from Sanriku-oki to Boso-oki (revised) (in Japanese). Headquarters for Earthquake Research Promotion, 63 pp.
- Earthquake Research Committee (2011). Long-term forecast of earthquakes from Sanriku-oki to Boso-oki (2nd version) (in Japanese). Headquarters for Earthquake Research Promotion, 70 pp.
- Geospatial Information Authority of Japan (2011). Crustal movements in the Tohoku District (in Japanese). *Rep. Coord.Comm. Earthq. Pred., Japan*, 86, 185-272.
- Ide, S., A. Baltay, and G. C. Beroza, (2011). Shallow Dynamic Overshoot and Energetic Deep Rupture in the 2011 Mw 9.0 Tohoku-Oki Earthquake, *Science*, 332, 1426-1429, doi:10.1126/science.1207020, 2011.
- Japan Meteorological Agency (2012). Report on the 2011 Off the Pacific Coast of Tohoku Earthquake by Japan Meteorological Agency (in Japanese with English summaries), *Technical Report of JMA*, No. 133, 479 pp.
- Kagan, Y.Y. and D. D. Jackson (2013). Tohoku earthquake: A surprise? *Bull. Seism. Soc. Am.*, 103, 1181-1194.
- Kanamori, K. (1972). Mechanism of tsunami earthquakes, *Phys. Earth Planet. Inter.*, 6, 246-259.
- Matsuzawa, T. (2014). The largest earthquakes we should prepare for. *J. Disaster Res.* 9 (3) 248-251.
- Minoura, K., and Nakaya, S. (1991). Traces of tsunami preserved in intertidal lacustrine and marsh deposits. *J. Geology*, 99, 265-287.
- McCaffrey, R. (2008). Global frequency of magnitude 9 earthquakes, *Geology*, 36(3), 263-266.
- Ozawa, S., T. Nishimura, H. Suito, T. Kobayashi, M. Tobita, and T. Imakiire (2011). Coseismic and postseismic slip of the 2011 magnitude-9 Tohoku-Oki earthquake. *Nature*, 475 (7356), 373-376.
- Satake, K. and B. F. Atwater (2007). Long-term perspectives on giant earthquakes and tsunamis at subduction zones, *Annu. Rev. Earth Planet Sci.*, 35, 349-274.
- Satake, K., Y. Fujii, T. Harada, and Y. Namegaya (2013). Time and slip distribution of coseismic slip of the 2011 Tohoku earthquake as inferred from tsunami waveform data, *Bull. Seism. Soc. Am.*, 103, 1473-1492.
- Satake, K. and Fujii, Y. (2014). Review: source models of the 2011 Tohoku earthquake and long-term forecast of large earthquakes. *J. Disaster Res.* 9 (3) 272-280..
- Sato, M., T. Ishikawa, N. Ujihara, S. Yoshida, M. Fujita, M. Mochizuki, and A. Asada (2011). Displacement above the hypocenter of the 2011 Tohoku-Oki earthquake. *Science*, 332(6036), 1395-1395.
- Sawai, Y., Y. Namegaya, Y. Okamura, K. Satake and M. Shishikura (2012). Challenges of anticipating the 2011 Tohoku earthquake and tsunami using coastal geology, *Geophys. Res. Lett.*, 39, L21309, doi:10.1029/2012GL053692.
- Schwartz, D.P. and K. J. Coppersmith (1984). Fault behavior and characteristic earthquakes: Examples from the Wasatch and San Andreas fault zones, *J. Geophys. Res.*, 89 (B7), 5681-5698.
- Somerville, P.G. (2014). A post-Tohoku earthquake review of earthquake probabilities in the Southern Kanto District, Japan, *Geosci. Lett.*, 1:10, doi:10.1186/2196-4092-1-10.
- Tajima, F., J. Mori and B.L.N. Kennett (2013). A review of the 2011 Tohoku-oki earthquake (Mw 9.0): Large-scale rupture across heterogeneous plate coupling, *Tectonophysics*, 586, 15-34.
- Yoshida, Y., H. Ueno, D. Muto, and S. Aoki (2011). Source process of the 2011 Off the Pacific Coast of Tohoku earthquake with combination of teleseismic and strong motion data, *Earth Planets Space*, 63, 565-569.



INQUA Focus Group on Paleoseismology and Active Tectonics



paleoseismicity.org

NOTES



Paleo- tsunami event reconstruction using sediment cores along the upper shelf of the eastern Mediterranean basin- Caesarea and Jisr Al-Zarka, Israel

Braun Y. (1), Tyuneleva N. (1,2), Ben-Avraham Z. (1), Goodman-Tchernov B.N. (1)

(1) Department of Marine Geo-science, The Leon H. Charney school of marine sciences, University of Haifa. yaelsyb@gmail.com

(2) Odessa I.I. Mechnikov National University

Abstract: Recent research argues for the presence of tsunami deposits offshore Caesarea Maritima, along the coast of Israel. The study presented here compares sediments identified offshore Jisr Al-Zarka, to the north of Caesarea, and presents at least three distinct tsunami events for the area.

A 2.19 m sediment core, from 15.3 m water depth off the coast of Jisr Al-Zarka, was collected and studied for paleo-environmental reconstruction and correlation of possibly tsunamigenic horizons. It was sampled at 1cm intervals for multi-proxy analysis including granulometry, micropaleontology, XRF, and FTIR measurements.

Two ^{14}C ages correlate to previously identified tsunamigenic layers from offshore Caesarea: 749CE; Santorini eruption of ca. 3.5ka; and one, previously unidentified, event at ca. 5.6-6ka is also present.

By comparing similar cores from different locations we reassert the validity of this approach for discovering, identifying and studying continuous records of paleo-tsunami events.

Key words: Paleo-tsunami, tsunamigenic, tsunamite

Introduction

Identifying distinct tsunami sediment layers continues to be a major preoccupation for tsunami researchers and advancements in the field are occurring constantly. Generally, tsunami deposits are recognized when certain conditions are met, particularly the presence of a laterally continuous, allochthonous, anomalous occurrence in an otherwise predictable or well-defined sedimentological setting. Therefore, in order to identify the distinct signature of tsunami sediment layers it is important to also understand the characteristics of the "normal" sediment sequence in a specific depositional setting. The south eastern Mediterranean continental shelf is part of the 650km long Nile littoral Cell and is dominated by siliciclastic quartz sands, derived from the Nile drainage basin. These sediments are transported along the Israel shoreline from the Nile Delta by a counter-clockwise long shore current that flows along the south eastern Mediterranean shores. Another main component of sediments in this region is carbonaceous sand derived from biogenic material, namely shell fragments (Zviely et al., 2007). Along the central coast of Israel (i.e. the area of Caesarea Maritima) the percentage of siliciclastics in the sand is approximately 92%. At -5m to -30m water depths, the average size of the siliciclastic grains is 0.12-0.16mm (Almagor, 2005 and references therein). In Caesarea specifically, the mode grain size measured in cores from -15msl was particularly conservative, varying only slightly from 169 micron.

Tsunamigenic deposits within this sedimentological framework have been identified offshore Caesarea Maritima. In these layers easily recognized coarse grained sediments were embedded in the sand, including whole and broken shells, rip-up clasts, archaeological material, beach-zone pebbles and even rafted organics or pumice (Reinhardt et al., 2006; Goodman-Tchernov et al., 2009). These deposits were then further analyzed by Goodman-Tchernov et al. (2009) in order to identify and define

tsunami deposits using a multi-proxy approach, which included looking into the smaller components of the sediment (e.g. grain-size distribution for particles smaller than 2mm and microfossil assemblages of foraminifera). In order to expand on these findings and continue to determine the lateral extent of these tsunamites, another sediment core (core 6) was extracted from a nearby location, offshore the village of Jisr Al-Zarka (Fig. 1).

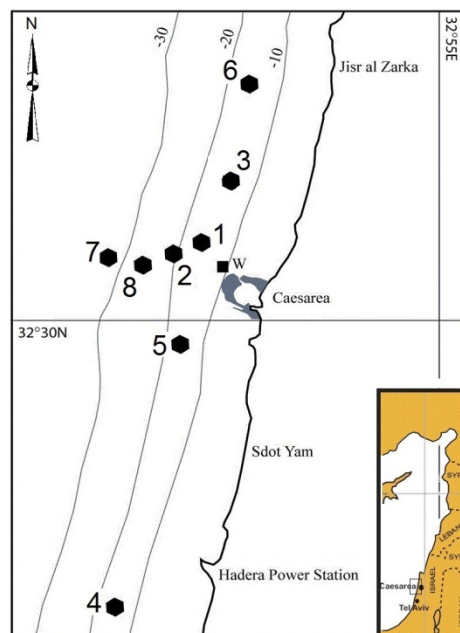


Figure 1: Location map of sediment cores 1-8 (marked as black hexagons) and Area W underwater excavation (marked as black square).

The tsunami sources for the events identified in the Caesarea cores vary. There are presumed far field events, like the tsunami waves caused by the Thera volcano



eruption in Santorini, Greece. There are also presumed near field events, such as the 749 CE tsunami, which is believed to be connected to the Dead Sea Fault earthquake. The sources of other events have not been clearly established to date, e.g. the 115 and 551 CE tsunamis. Our working assumption is that Jisr Al-Zarka, which is a mere 1km to the north of Caesarea (Fig. 1) would have been impacted by some, if not all, of the tsunami events that affected Caesarea. According to the bathymetric map shown in figure 1, the two sites are part of the same sedimentary basin. The stretch of shoreline itself cuts through a small sandstone ridge (known locally as Kurkar) that is partly underwater. This ridge is cut off to the north by the Taninim (Crocodile) stream and opens up to a sandy soil-rich trough, north of Jisr, known as the Kabara marsh, between the south western edge of Mt. Carmel to the east and the Kurkar ridge along the coast to the west. This marsh was dried up during the beginning of the 20th century. During the Byzantine period the area was dammed and the water was converted to a reservoir for Caesarea (Mart & Friedman, 2003 p. 34). The water that flows through Crocodile stream originates from the local "Yarkon-Taninim" aquifer and except for extreme flooding events flows at a very slow and steady pace through a flat terrain that cuts the sandy soil. In fact, most of the stream's water trickles into the sandstone aquifer rocks of the coastal plains, and never reaches the sea. The stream's outlet is blocked by a sandbank, causing the water to trickle into the sea and at times sea water actually flows into the stream, rather than the other way around. During flooding events the stream flows at a higher pace and transports colloids of clay and silt from the surrounding soil (Almagor, 2005).

Both Jisr Al-Zarka and Caesarea Maritima boast a significant history of human occupation (Almagor, 2005 and references therein) but as will be noted below, it is probably only the monumental harbour at Caesarea and its nearby structures that left their mark on the archaeological component of the later tsunamigenic sediment layers.

Methods

After extraction, the core was described, documented, photographed and sampled at 1cm intervals for multiproxy analysis that included granulometry, micropaleontology, XRF, and FTIR measurements. The aim of these analyses was to reconstruct the environmental trends and determine the general character and sedimentological history of typical background sediments versus anomalous horizons. Five articulated bivalves and 2 gastropods in pristine condition were extracted from key locations in the core for ^{14}C dating. These dating samples were chosen because the organisms that were housed in them are believed to have died and been buried in the location in which they were found with little transport post-mortem, thereby representing the age of that sediment within a reasonable window.

Results and Discussion

In core 6's "normal" sediment the dominant grain size is sand (125-250 micron). Shell fragments are embedded into the sand and are not larger than 4mm. In the upper part of the core (0-29cm) the mode grain size measured is similar to that of the -15m cores from offshore Caesarea, varying only slightly from 168 micron. Downwards into the core the mode grain size is consistently around 185 micron (Events 1,3,4 in Figs. 2,3). Most of core 6 is comprised of "normal" sandy sediments, typical of this environment. Within these sediments three distinct anomalous horizons were identified as tsunami events. A Principal Coordinate Analysis of similarity index for particle size distributions of Core 6 matrix sediments also shows a distinct clustering of the separate events.

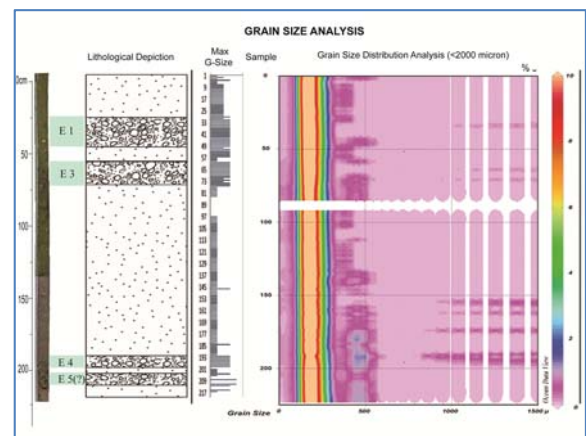


Figure 2: Core 6 description and grain size analysis results. Grain size distribution analysis is displayed in a particle-size distribution contour map of the core. Data were plotted using Ocean Data View Software (version 3.3.2). Identified tsunami events are marked as E1, E2 etc.

Although it cannot be completely negated, the anomalous horizons found in all the sediment cores mentioned here were not considered to represent storm events.

This assumption is based on a) the transport mechanism of sediments by strong storm waves can be similar to that of tsunamis but they should be more repetitive and the anomalous horizons in the core do not appear in a distinct pattern, b) no recently recorded storm events have been strong enough so as to create such distinct deposits, c) there are no known historical records of storm events available, d) the ages of these horizons match those of historically known tsunami and earthquake events. Even without a statistical analysis that can show the rarity of the chances of this compatibility, we do not consider it likely that it is random.

Event 1 was clearly noted at a depth of 29-49cm. At this depth fine grained sand was embedded with rare gravel (round flint), whole *Glycymeris* shells, shell fragments and an articulated *Glycymeris* shell at 40-43 cm. This shell was dated to ca. 658-781 CE and corresponds chronologically with a historically documented event at 749 CE (Amiran et al., 1994; Ambraseys & Synolakis, 2010). This event may be represented within the anomalous horizons identified



in all of the cores and trenches from Caesarea to the mixed layer that was dated to the late Byzantine period (ca. 4th-6th century CE) (Fig. 3). The layer was presumed to be the tsunamite caused by the 551 CE tsunami (Reinhardt et al., 2006; Goodman-Tchernov et al., 2009), but since pottery dating could not clearly distinguish between the two events, the later event may have mixed the previous tsunami sediments and re-embedded them both as one in Caesarea. This is further discussed in relationship to deposits found terrestrially and described in archaeological reports (Dey et al., in press).

The tsunamite in core 6 does not suggest such a mixing event, implying that the 551 CE tsunami either a) did not impact this portion of the shoreline, b) it impacted but did not leave a distinctive deposit, or c) its deposit was reworked/removed without any clear indication to differentiate it from the later event. Considering the domination of archaeological findings within this layer offshore Caesarea harbour that was identified by Reinhardt et al. (2006) as ship ballast, it is not surprising that an area less occupied at the time of the event may not have left a distinctive anthropogenic signature in the sediment. A further understanding of the dynamics of the 551 CE tsunami event may shed some light on the subject. The clear tsunamigenic horizon of the 115 CE event, recognized in all cores and trenches at Caesarea, is markedly lacking in core 6 (Fig. 3). This horizon of a thick layer of Glycymeris shells was found right outside Caesarea harbour, at the W areas (Fig. 1) (Reinhardt et al., 2006). The anomalous horizon is also very distinct farther north and south in cores 3 and 4 respectively (Goodman-Tchernov et al., 2009). Its absence from core 6 may be explained by an apparent hiatus that is clear in the very thin 10cm layer of sediments (49-59cm) between the first tsunamigenic horizon of ~1.3Ka and the second one of ~3.5Ka. According to the dating done for this study, those ten centimetres represent more than 2,000 years of sedimentation (Fig. 2). With the important exception of the Crocodile stream outlet, the two sites have near identical bathymetric settings (Fig. 1). Therefore, the stream must be taken into account as a possible explanation for the hiatus; either directly related to the increased inundation and intensified back-channel scouring which occurs during tsunami or even storm events or an outcome of rare flooding events. It should be noted though that during extreme flooding events, which happen every few years, the streams along the coast deposit a significant amount of debris that may contain sand from the river banks. This debris does, on occasion, accumulate as sandbanks off the stream outlets, which may survive for a few years at most. The silty and clayey materials in these floods are dispersed by the waves, creating plume like structures to hundreds of meters off the coast that may last a few weeks (Almogor, 2005 and references therein). It is therefore expected that flooding events actually add sediments to the surrounding area and not cause hiatuses in sedimentation. As it turns out, these flooding events do not seem to leave any distinctive mark on the sea floor even a few months after and have not been identified in any of the sediment cores that have been collected to date. As aforementioned, although

sediment scouring due to a storm event cannot be completely negated, it seems highly unlikely in this case, since this hiatus is an atypical sedimentation occurrence in the area and storms are expected to occur more often than tsunamis and in a somewhat repetitive pattern.

Event 3 (Fig. 2) was identified at a depth of 59-75cm, where fine grained silty-sand was embedded with round pebbles, whole Glycymeris shells, shell fragments and an articulated Glycymeris shell at 63-74cm. This shell was dated to ca. 3,582-3,400 BP and corresponds chronologically with tsunami waves produced during the Thera volcano eruption in Santorini, Greece, dated to ca. 3.5Ka (e.g. Yokoyama, 1978; Bruins et al., 2008). This anomalous horizon was also clearly identified in cores 1-4 (Fig. 3). As stated by Goodman-Tchernov et al. (2009), during this event (Late Bronze Age) no major settlement is known to have existed at this area and therefore no anthropogenic debris was found in any of the cores.

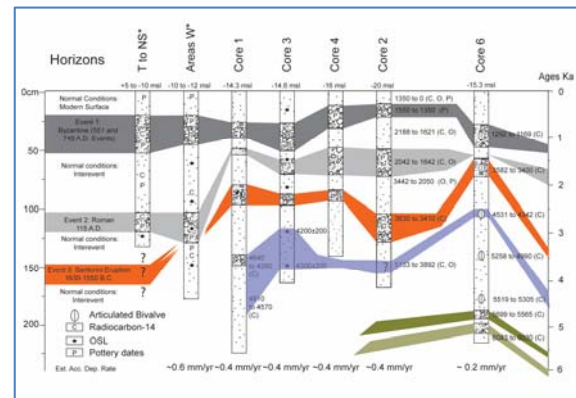


Figure 3: Stratigraphic correlation of cores 1-6 and Area W, as well as terrestrial nearshore excavation in Caesarea (T-NS).

Here we present a fourth and previously unknown tsunami event (Event 4- Fig. 2) that was identified at the downcore depth of 199-211cm. In this horizon the fine sand was embedded with shell fragments, whole shells, gastropod shells in pristine condition and at the bottom of the layer a 3cm Kurkar fragment that was covered with calcareous worm deposits. The pristine condition of the delicate gastropod shells and the worm deposits on the Kurkar pebble indicate that they were all buried very quickly. This layer may also represent two separate tsunami horizons since there is a three centimetre gap of "normal" sedimentation between 199 and 203 centimetres. The two separate ages obtained from the gastropod shell samples (ca. 5.6 ka from the sample taken at 192-193cm and ca. 6ka from the sample taken at 210-211cm) could imply that this separation of the two horizons into two separate events may have merit. Furthermore, the <2000 micron granulometric analysis (see Fig. 2), clearly shows a distinct change between the two horizons' matrixes. Yet, the principal coordinate analysis of similarity index for particle size distributions of Core 6 revealed that maybe those two horizons are not so different after all. Further analyses of other elements in the core are expected to yield a clearer picture of these



distinctions, or lack thereof. This anomalous horizon is much older than the horizons found to date. The sedimentation rate at this location appears to be nearly half (0.2mm/yr) of the calculated sedimentation rate calculated for the area with cores 1-4 (0.4mm/yr) (Fig. 3). Under these circumstances it is clear that this unique location afforded us a farther glimpse into the past within a ~2m core than would be expected. It will be interesting to find these horizons in other sediment cores so a comparison could be made. Such a comparison may give us answers as to the validity of our interpretation of this horizon and may dramatically enhance our physical evidence-based catalogue of tsunami events in the eastern Mediterranean.

Conclusions

At least three distinct tsunami events were identified in core 6, taken from offshore Jisr Al-Zarka.

Two tsunami horizons can be correlated to tsunami layers from offshore Caesarea; an event at 749 CE and the ca. 3.5ka tsunami caused by the Santorini eruption. The two, previously identified events at 115 and 551 CE were not identified in this core. The absence of some of the events and the appearance of others signifies the complexity of this approach and better helps our understanding of the effects of tsunamis on different sedimentological basins, as well as the dynamics of the events themselves.

A third event at ca. 5.6-6ka has not been previously identified. The tsunamigenic horizons that define it may in fact record two separate tsunami events. Further analyses of other tsunami indicators as well as a comparison with similar results from other cores may contribute to a better understanding of this layer. This event is significant in that, to our knowledge, it is the first and only evidence to date of a tsunami event along the eastern Mediterranean coast during the mid Holocene. If a correlation can be made to other paleo-seismological evidence from this time, we may even be able to define the extent and the implications of this event in a previously untapped line of research.

By comparing similar cores from different locations along the upper shallow continental shelf in the eastern Mediterranean basin, we reassert the validity of this approach for discovering, identifying and studying continuous records of paleo-tsunami events that occurred during the Holocene. Studies (e.g. Dominey-Howes, 2004) suggest that for tsunami events the sedimentological fingerprint, in the offshore and onshore environments, can vary greatly from place to place, even at very short distances, due to changes in bathymetry, coastal morphology and differing sediment regimes, as well as the type and direction of the waves themselves.

Therefore, changes in the appearance of these horizons are expected, and indeed welcomed since they are invaluable important for site specific paleo-environmental reconstructions. In learning to understand these variations we enhance our understanding of their effects on our surroundings.

Acknowledgements: We would like to thank Prof. Sarel Shalev from the University of Haifa for his help with XRF analyses, as well as Dr. Eli Shemesh and Nimer Tahafor for their invaluable help in the lab. We would also like to thank the Israel Scientific Foundation for the funding of this research.

References

- Almagor, G. (2005). The Mediterranean Coast of Israel. *GSI Report GSI/13/02* (in Hebrew).
- Ambraseys N., Synolakis, C., (2010). Tsunami Catalogs for the Eastern Mediterranean, Revisited. *Journal of Earthquake Engineering* 14, 309-330.
- Amiran, D.H.K., E. Ariei, & T. Turcotte, (1994). Earthquakes in Israel and Adjacent Area: Macroseismic Observations since 100 B.C.E. *Israel Exploration Journal* 44, 3/4, 260-305.
- Bruins, H.J., J.A. MacGillivray, C.E. Synolakis, C. Benjamini, J. Keller, H.J. Kisch, A. Klugel & J. van der Plicht, (2008). Geoarchaeological tsunami deposits at Palaikastro (Crete) and the Late Minoan IA eruption of Santorini. *Journal of Archaeological Science* 35, 191-212.
- Dey, H., N.B. Goodman-Tchernov, J., Sharvit, (in press). Archaeological evidence for the tsunami of January 18, 749 AD: A forgotten chapter in the history of early Islamic Qaysariyah (Caesarea Maritima, Israel). *Journal of Roman Archaeology*.
- Dominey-Howes, D.T.M., (2004). A re-analysis of the Late Bronze Age eruption and tsunami of Santorini, Greece, and the implications for the volcano-tsunami hazard. *Journal of Volcanology and Geothermal research* 130, 107-132.
- Goodman-Tchernov, N.B., H.W. Dey, E.G. Reinhardt, F. McCoy & Y. Mart, (2009). Tsunami waves generated by the Santorini eruption reached Eastern Mediterranean shores. *Geology* 37(10), 943-946.
- Mart, Y., Friedman D. (2003). Coastal sediments at Ma'agan Mikhael- their paleogeographic significance. In: The Ma'agan Mikhael Ship: The recovery of a 2400-year-old merchantman. Final Report, Volume 1. *Israel exploration Society & University of Haifa* (Linder, E. & Kahanov, Y.). 27-36.
- Reinhardt, E., B.N. Goodman, J.I. Boyce, G. Lopez, P. van-Hengstum, W.J. Rink, Y. Mart, & A. Raban, (2006). The Tsunami of 13 December A.D. 115 and the Destruction of Herod the Great's Harbor at Caesarea Maritima, Israel. *Geology* 34, 1061-1064.
- Yokoyama, I., (1978). The tsunami caused by the prehistoric eruption of Thera, in Thera and the Aegean World I: Santorini, Greece. *Second International Scientific Congress Part One*, 277-283.
- Zviely, D., E. Kit & M. Klein, (2007). Longshore sand transport estimates along the Mediterranean coast of Israel in the Holocene. *Marine Geology* 238, 61-73.



INQUA Focus Group on Paleoseismology and Active Tectonics



paleoseismicity.org

NOTES

Poster Presentation Abstracts



SEISMOTECTONICS AND ACTIVE FAULTS OF BALI ISLAND

A. Soehaimi (1), J.H Setiawan and Marjiyono(1)

(1)Geological Agency, Ministry of Energy and Mineral Resources Indonesia, 57 Diponegoro Street, Bandung, Corresponding email: s.asdani@yahoo.com.

The island of Bali is part of an active arc seismotectonic unit and is an earthquake prone area in Indonesia (Geological Research and Development Center, Department of Energy and Mineral Resource, 2004). Seismotectonics and active fault studies have been conducted in order to understand the seismogenetic condition and the potential earthquake hazard of this region. This island and surrounding areas are controlled by three main submarine seismotectonic zones; Bali Subduction Zone (South), Bali Back Arc Thrust Zone (North), and Lombok Strait Zone (East). Several destructive earthquakes ($M \geq 6$ Mb) have occurred in these seismotectonic zones. Seririt Earthquake (1976) occurred in-land in the northern part of Bali Island and had a thrust fault focal mechanism. Culik Earthquake (1979) located in-land in eastern Bali island had a left lateral strike slip fault focal mechanism. Both earthquakes affected the environment and human life in the region. Earthquake intensities in this region were influenced by the physical character of several lithological units of Pleistocene volcanic products (Seraya, Buyan – Bratan and Jembrana), Holocene volcanic products (Buyan – Bratan, Batur, Agung, Lesong, Tapak, Pohen, Adang, Batukau and Sengayang) and coastal alluvial deposits. Pleistocene volcanic products are consolidated and Holocene volcanic products are unconsolidated. According to Regional Seismic Hazard Map of Indonesia (Badan Standarisasi Nasional, 2012), Bali Island, has bedrock acceleration at short period $S_s = 0.8$ to $0.9g$ and at 1 second period $S_1 = 0.3$ to $0.4g$ (MCE_R , 2% in 50 years), and therefore is within a high seismic hazard zone. Moreover, those destructive earthquakes had maximum intensities of VIII (MMI Intensity Scale).

Keywords: Seismotectonics, Active Fault and Potential Seismic Hazard.

Introduction

Bali Island is one of the popular tourism destinations in the world. Tourists from many countries all over the world visit this island. Therefore, this island is densely populated and has important infrastructure facilities for tourism such as international airport, hotels, high way and harbours. According to tectonic framework, the island is located in the northern part of Sunda Subduction Zone and belongs to the Indonesian Earthquake Hazard Prone Region No. IX (Geological Research and Development Center, Department of Energy and Mineral Resource, 2004) and shown in figure 1. In order to know the seismogenetic conditions and the potential earthquake hazards of this region, seismotectonics and active fault studies have been conducted. Some methodologies have been applied in this study, such as research, evaluation and analysis of the primary and secondary geological and seismological data were used to evaluate the potential earthquake hazard.

Geology of Bali Island

Bali Island is described here in terms of geomorphology, lithology, and structure geology and active faults.

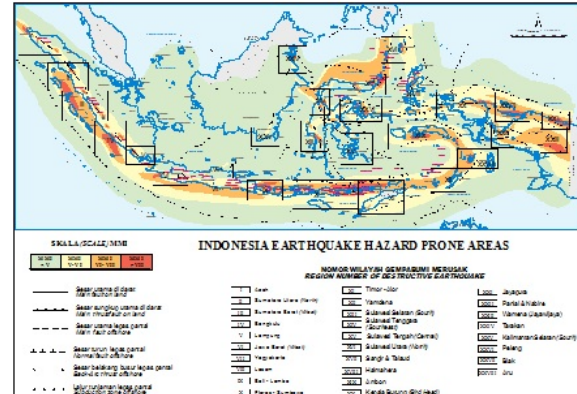


Figure 1. Indonesia Earthquake Hazard Prone Areas (Geological Research and Development Centre, 2004)

Geomorphology

The geomorphology of Bali Island can be divided into six geomorphological units: folded ridges, faulted hills volcanic cones, caldera and crater lakes, volcanic slopes and costal planes.

The folded ridge unit is located in western part of Bali Island and represents an east-west elongated ridge. This region consists of Tertiary Formations and old volcanic products such as breccia, conglomerate, lava and tuff. Faulted Hills is found in separate regions in the northwest, south and southeast of Bali Island. The hilliest have steep slope which are controlled by faults. The lithology of the hilliest area consists of marine sediment such as marl, sandstone, shale and limestone, breccia, lava and tuff. Volcanic cone consist of the volcanic cones of Agung, Lesong, Tapak, Pohen, Adang, Batukau and



Sengayang. These volcanic cones have steep slope which consist of breccia, lahar, agglomerate, lava and tuff. Some parts of these volcanoes cone have the steep slopes which are controlled by faults. Caldera and crater lakes are found in volcano of Batur and Buyan-Bratan. These lakes and calderas are formed of breccia, lava, tuff and lake deposits. Volcanic slopes are widely distributed throughout Bali Island, especially in central of Bali. The volcanic slopes can be divided into north region and south region and consist of breccia, lahar, agglomerate, lava and tuff. The costal plane area is located from west to east coast of northern Bali, from Singaraja to Gilimanuk. In south of Bali island, the coastal plane occupy the Negara District, south of Denpasar City (Kuta, Jimbaran and Benoa) and consist of coastal alluvial deposits.

Lithology

Bali island consist of Tertiary, Pleistocene, Holocene and recent lithological groups. Base on the geological map of Bali Island at a scale of 1: 250,000 (Purbo Hadiwidjoyo et al, 1998) these groups are:

Tertiary Lithology Group (Miocene – Pliocene) consisting of several formation such as the Asah Formation, Prapatagung Formation, Sorga Formation, Ulakan Formation and South Formation. Other lithology include in this group called as the Pulaki volcanic product. All of this group consist of marl, sandstone, shale, limestone, breccia, lava and tuff. This group is mostly physically hard and dense.

The Pleistocene lithology group consists of Seraya, Buyan-Bratan and Jembrana old volcanic products. The lithology of this group consists of breccia, conglomerate, lava and tuff. The breccia and conglomerate are mainly compact and dense; sometimes these rocks are comprised of soft and loose material. Tuff in this group is also comprised of loose material. The lavas are dense.

The Holocene lithology groups consist of young volcano products of Agung, Lesong, Tapak, Pohen, Adang, Batukau and Sengayang. The lithology of this group consists of breccia, agglomerate, lahar, tuff and lava.

The recent alluvial deposits group consist of coastal, river, and lake deposits. The lithology of this group mainly consists of loose gravels, pebbles, sands, shale and clay.

Structure Geology and Active Faults

Structure geology in Bali Island and surrounding areas consist of thrust faults, strike slip faults and normal faults. The Seririt active thrust fault (East – West direction) is located in north of this island. The main active left lateral strike slip fault (Northeast - Southwest direction) is located in central and eastern Bali. Normal faults which are generated in the tensional zone of the main fault and appear in and around volcanoes complex show a radiate pattern. Sub-marine active faults are located in northern, eastern and southern part of Bali Island. The northern part of this island has the Bali back arc thrust active fault, Lombok Strait right lateral strike slip active fault and South of Bali subduction zone.

Seismicity

The seismicity data from this region are taken from the NEIC, USGS from 1973-2014. This seismicity data divided can be into three class of magnitudes are 4 – 4.9, 5-5.9 and 6-7 Mb with four depth classes of 0-60 Km, 61-100 Km, 101-200 Km and 201-600 Km. These are based on the vertical hypocentre distributions which is shown on the seismotectonic map and seismicity profile (north-south direction) and shown in figure 2. The seismicity of this region can be divided into two seismogenic source zones. First is the South Bali subduction seismogenetic zone (Hindia-Australia Oceanic Plate) and second is the upper crust of Bali ccontinental seismogenic zone (Eurasia Continental Plate). The seismicity at the upper crust of Bali continental seismogenetic zone is associated with the in-land active faults of Bali Island, the Bali back arc thrust fault and the Lombok Strait right lateralstrike slip active fault.

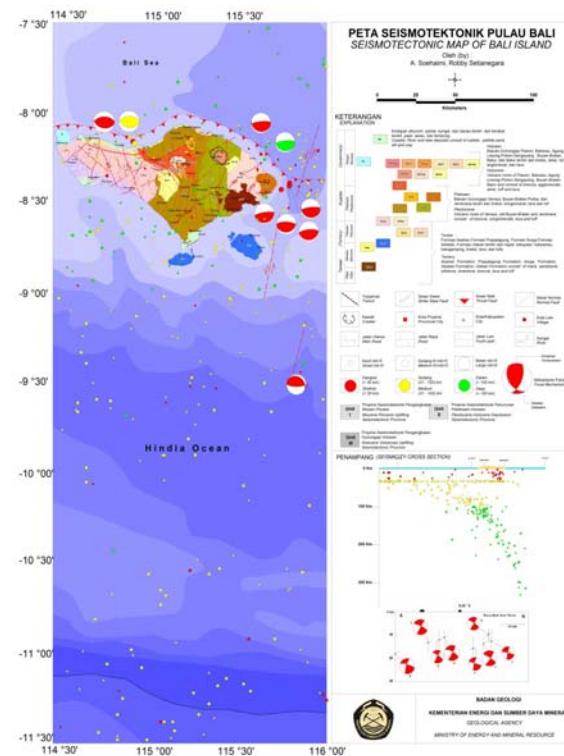


Figure 2. Seismotectonics map of Bali Island

Bali Island has historically been struck by more than 5 destructive earthquakes ($M \geq 6$ Mb). These earthquakes occurred in 1976, 1979, 1984, 2004 and 2013 and affected the environment and human life. The Seririt destructive earthquake of 1976 had the magnitude of 6.5 Mb and a depth of 40 Km. The epicentre of this event was located near Seririt city. The aftershock of this earthquake had the magnitude of 5.9 Mb with the depth of < 33 Km. In this event 559 people died, 850 people were seriously injured and more than 3000 people slightly injured (Governor Office of Bali Information Centre, 1976). The infrastructure damage consisted of elementary schools, intermediate schools and high



schools, temples and mosques, government offices, hospital (Puskesmas), major office, markets and houses, road and irrigation. The material loss estimated in three districts (Buleleng, Jembrana and Tabanan) was more than \$39 Million USD (Bali Pos, Juli 1976). The maximum intensity of this earthquake was felt in Seririt district and was VIII in the MMI Scale.

The Culik destructive earthquake of 1979 had a foreshock which occurred on 21 May 1979 with magnitude of 5.7 Mb at a depth of 76 Km. The main shock occurred on 30 May, 1979 with the magnitude of 6.1 Mb at a depth 25 Km. The aftershock on 21 June, 1979 had a magnitude of 5.1 Mb and a depth 33 Km. This was followed by another aftershock on 21 October, 1979 with the magnitude of 6.2 Mb at a depth 38 Km. In this event a maximum intensity of VIII of MMI Scale was felt. The last big earthquake occurred in this region occurred on 1 January, 2004. The epicentre of this earthquake was beneath the Hindia Ocean south of Bali Island, and there was no reported of damage.

Seismotectonics of Bali Island

The seismotectonics of Bali Island (Figure 2) is controlled by four main seismotectonic zones: South Bali Subduction Zone, North Bali Back Arc Thrust Active Fault Zone, Central and East Bali Active Fault Zone and Lombok Strait Active Fault Zone. The South Bali Subduction Zone is associated with mainly thrust fault earthquake focal mechanism. Base on the distribution of earthquake hypocentres, the subduction zone beneath Bali Island has the angle of 30°- 60°. The 30° angle of the Benioff zone shown by the earthquakes at depths of 0 - 100 Km, and the 30°- 60° angle Benioff zone is located below Bali island and proven by the earthquake at depths between 100 – 200 Km. The North Bali Back Arc Thrust Active Fault Zone is shown by shallow earthquake hypocentre and thrust fault focal mechanisms. The activity in these seismotectonics zone followed by other thrust fault in land and call as Seririt Active Thrust Fault. Other shallow earthquake hypocentres of Bali Island are associated with the Central and West Bali Left Lateral Strike Slip Active Fault and Lombok Strait Left Lateral Strike Slip Active Fault.

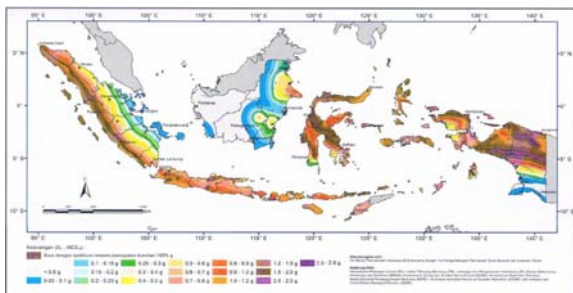


Figure 3. Bedrock acceleration at short period $S_s = 0.8$ to $0.9g$ in Bali island (Badan Standarisasi Nasional, 2012).

Potential Earthquake Hazard

The potential earthquake hazard for Bali Island is expressed by in the Indonesia Seismic Hazard Map, Badan Standarisasi Nasional (2012). In this map Bali island is located in a high- seismic hazard zone which has bedrock acceleration at short period $S_s = 0.8$ to $0.9 g$ (Figure 3) and bedrock acceleration at 1 second period $S_1 = 0.3$ to $0.4 g$. The maximum intensity of destructive earthquakes in Bali Island shown by the Seririt Earthquake (1976) and the Culik Earthquake (1979) is VIII MMI Scale (Figure 4).

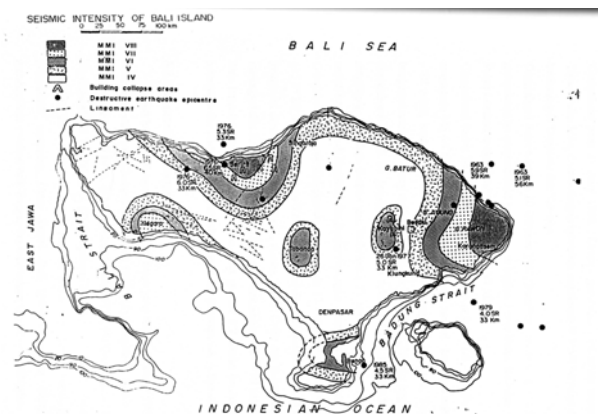


Figure 4. Composite intensity of destructive earthquake in Bali Island (Soehaimi et al, 1993).

Summary / conclusions

Earthquake events in Bali Island are controlled by three main sources: mainly low angle submarine active subduction, upper crust active faulting (offshore), and active faults onland of Bali Island.

The earthquake intensity on this island is controlled by magnitude and depth, epicentral distance and soil properties.

Dissemination of potential earthquake hazard and risk to the local people and government officials, who have responsibility for earthquake mitigation, is necessary. Settlements (building, houses) should strictly follow the building code.

Acknowledgements

Author wished to thanks to Prof. Young-Seog Kim Chairman of Preparatory Committee of the 5th International INQUA Meeting on Paleoseismology, Active Tectonic and Archeoseismology (PATA-Days) in Busan, Republic of Korea for yours invite me as a member of the Organizing Committee and participant. All of my colleagues in Quaternary Working Group of Geological Survey Institute, Geological Agency, Ministry of Energy and Mineral Resources for contributions on your seismotectonics and active fault research in Bali Island.



INQUA Focus Group on Paleoseismology and Active Tectonics



paleoseismicity.org

References

Badan Standarisasi Nasional, 2012. Tata cara perencanaan ketahanan gempa untuk struktur bangunan gedung dan non gedung, SNI 1726 : 2012

Bali Governor Office, 1976. Information of destructive earthquake of Seririt 1976. Internal report of Bali governor office.

Bali Pos July 20, 1976. The loses caused by destructive earthquake of Seririt 1976.

Geological Research and Development Centre, Department of Energy and Mineral Resources, 2004. Atlas geologi sumber daya mineral dan energi kawasan Indonesia.

NEIC, USGS., 2014. Seimicity of Bali island in years of 1973 – 2013

Purbo Hadiwidjoyo, M.M., Samodra, H and Amin, T.C., 1998. Geological Map of Bali Island, Scale : 1 : 250.000

Soehaimi, A., Kertapati, E., 1993. Seismotectonic of Bali Island, CCOP Technical Workshop, Bali 1993.



Interpretation for the propagation characteristics associated with the 1999 Chi-Chi earthquake faulting event

Kwangmin Jin(1), Young-Seog Kim (2)

(1) Mineral Resources Research Division, Korea Institute of Geoscience and Mineral Resources (KIGAM), Daejeon 305-350, Korea. Email: maxgarion@kigam.re.kr

(2) Dept. of Earth & Environmental Sciences, Pukyong National University, Busan 608-737, South Korea.

Abstract: The Chi-Chi earthquake ($M_w=7.6$) took place in central western Taiwan in 1999. The earthquake caused reactivation of the Chelungpu fault and resulted in 100 km-long surface ruptures. The fault strikes mostly N-S to NNE-SSW, however, the northern tip of the southern segment of the surface ruptures rotates clockwise to define an E-W trend, and then jumps to a shorter NNW-trending rupture. The largest vertical displacement is recorded in the Shihkang area of the Shihkang-Shangchi fault zone, where vertical slips are up to 8-10 m. The Shihkang-Shangchi fault zone displays a complex fault pattern as a linkage damage zone between two fault segments with the greatest concentration of faults and fractures. We suggest that the Shihkang-Shangchi fault zone is not a simple termination zone, but it may be an 'overstep zone' or a 'transfer zone' between two fault segments. A slip analysis along the surface ruptures indicates that the surface ruptures are composed of three fault segments and the amount of slip partly depends on the intersection angle between slip direction and fault strike. Our numerical modeling for the area surrounding the Chi-Chi earthquake ruptures indicates that Coulomb stress changes are mainly concentrated on tips and bends of the surface ruptures. It indicates that the fault propagates toward the northeast. Therefore, this study suggests that there is a high potential for future earthquake activity along the unruptured Shangchi segment. Hence, future geohazard studies in this area should be focused on the Shangchi segment so as to evaluate future potential earthquakes, to determine recurrence intervals, and to reduce future earthquake hazards.

Key words: Chi-Chi earthquake, Shihkang-Shangchi fault zone, Shangchi segment, linkage zone, fault damage zone

INTRODUCTION

The Chi-Chi earthquake (21 Sep. 1999) is the most recent major earthquake in Taiwan. This seismic event represents Taiwan's largest on-land earthquake ($M_w=7.6$) during the last century (Chung & Shin, 1999; Shin & Teng, 2001). The earthquake resulted in surface ruptures of about 100 km in length (Chung & Shin, 1999; Shin & Teng 2001). This earthquake ruptured along the pre-existing N-S to NNE-SSW trending Chelungpu reverse fault. Coseismic movement shows a northward increase in horizontal displacement along the Chelungpu fault, from 2-3 m in the south to 7-9 m in the north. In addition, vertical displacements along the N-S trending segment of the Chelungpu fault (2-6 m) are significantly greater (8-10 m) in the Shihkang area of the Shihkang-Shangchi fault zone (Lee et al., 2002). This study mainly reviews previous studies on the Chi-Chi earthquake and rupture properties, as well as heterogeneous distribution patterns of displacements along the Chelungpu fault and the Shihkang-Shangchi fault zone. In addition, the rupture patterns and the explanation for the slip distribution are reinterpreted using recently developed fault damage models (Kim et al., 2004), and a new evolution model is proposed for the Chelungpu fault and the Shihkang-Shangchi fault zone.

In addition, a Coulomb 3.1 modeling study has been applied to the earthquake slip data along the surface ruptures associated with the 1999 Chi-Chi earthquake for the purpose of demonstrating the stress changes around the ruptures.

GEOLOGICAL SETTING

Taiwan is presently located on the complex plate margin between the Eurasian and Philippine Sea plates. The convergence is occurring at a rate of 82 mm/yr on an azimuth of 299° (Blenkinsop, 2006) (Fig. 1a). According to previous studies (Lin et al., 2001), the surface ruptures associated with the 1999 Chi-Chi earthquake is generally subdivided into four or five segments based on characteristics of coseismic displacement, geometry of the surface ruptures, geological structure, and distinct change of orientation. This study mainly focuses on the northern part of the earthquake ruptures (Fig. 1), which we divide, based on distinct change in orientation and slip pattern; (1) the main N-S trending Chelungpu fault segment, (2) the E-W to NE-SW trending Shihkang-Shangchi fault segment, and (3) the NNW-SSE trending Shangchi segment (Fig. 2).

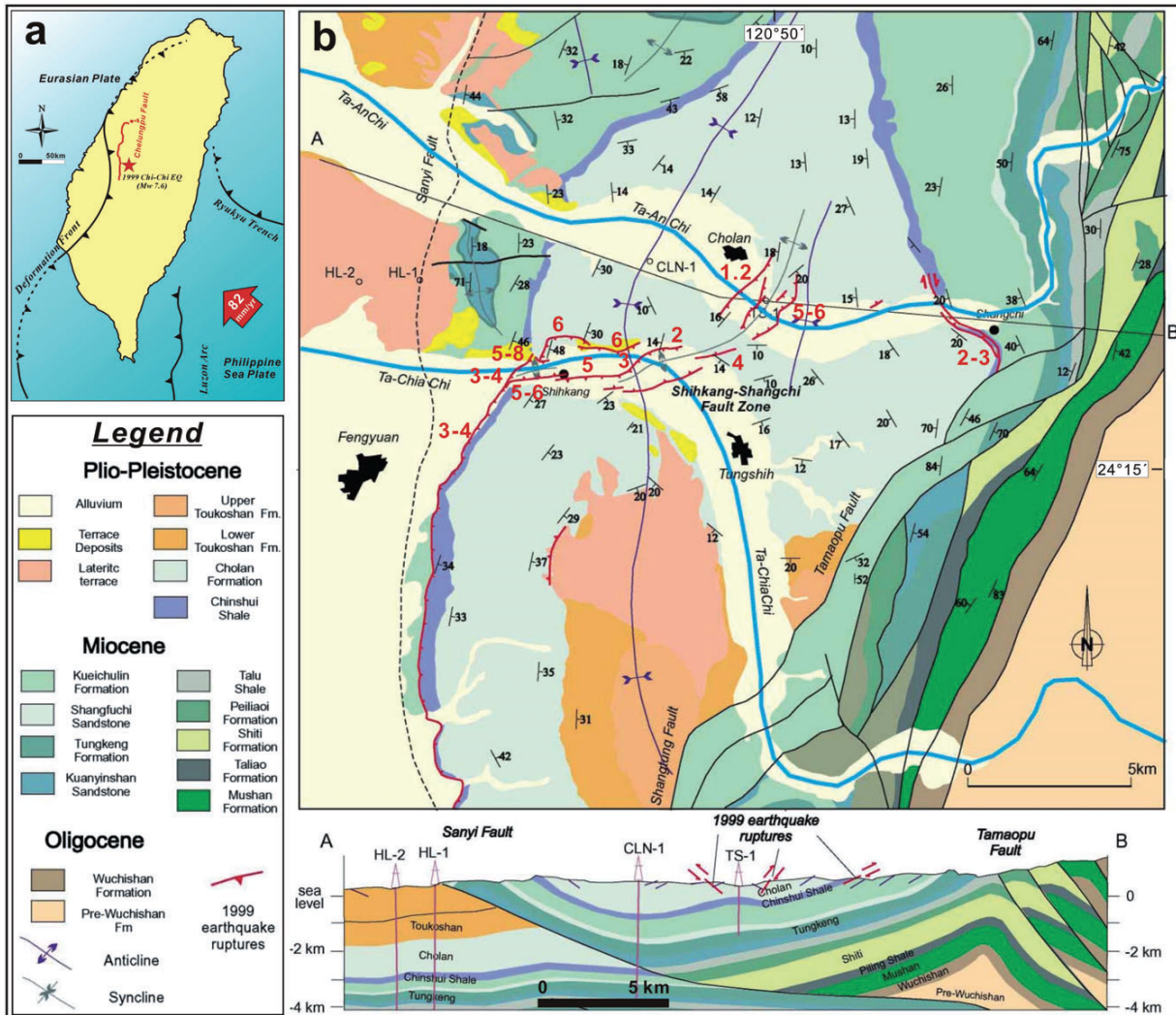


Fig. 1. (a) Tectonic setting of Taiwan. Red lines indicate the location of the Chelungpu Fault (modified from Ching et al., 2007). (b) Geological map and cross-section (modified from Lee et al., 2002).

SURFACE RUPTURE PATTERN OF SHIHKANG-SHANGCHI FAULT ZONE

The general trend of the surface ruptures associated with the earthquake is north-south to NNE-SSW. However, in the Shihkang-Shangchi Fault Zone, the trend changes abruptly clockwise 90° to an E-W trend. In addition, vertical offsets along the Shihkang-Shangchi Fault Zone are large.

Some unsolved questions with respect to the Shihkang-Shangchi fault zone stem from previous studies and include: 1) Why are displacements in the Shihkang-Shangchi fault zone greater than the main Chelungpu fault and Shangchi segment? 2) Why does the strike of the Shihkang-Shangchi fault segment change abruptly? 3) Why are strike-slip displacements dominant on both sides of the Shihkang-Shangchi fault zone? 4) Why do the Chelungpu fault and Shangchi segment show different slip senses?

This study undertook geometric and kinematic analyses on the Chi-Chi earthquake-related surface ruptures using

published data and our own field work to answer these questions. The proposed new interpretation for the Chi-Chi earthquake faulting event is mainly based on the application of recently developed fault damage models (Kim et al., 2004) and the earthquake fault migration and propagation model (e.g., Stein et al., 1997; Kim & Sanderson, 2008).

SLIP DISTRIBUTION AND APPLICATION OF THE FAULT DAMAGE MODEL

Fault damage zones refer to the volume of deformed wall rocks around a fault surface that result from the ignition, propagation, interaction and build-up of slip along the fault (Kim et al., 2004). Fault damage zones can be classified into tip-, linking-, wall-, and distributed damage zones based on their relative position with respect to a fault plane (Fig. 2).

The fault displacement gradient is relatively steep around the relay zone (Willemsse et al., 1996). These asymmetric patterns are very similar to the slip



distribution along the surface ruptures associated with the Chi-Chi earthquake.

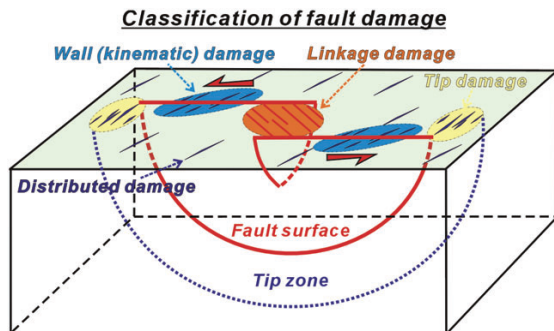


Fig. 2. Schematic diagram of the principal locations of the fault damage zones around a strike-slip fault (modified from Kim and Sanderson, 2006).

The earthquake slips along the main Chelungpu fault increase from about 3-4 m in the south to 5-8 m in the north (Fig. 1). The maximum slip is commonly reached in the Shihkang-Shangchi fault zone (8-10 m). However, the

slip distribution is variable along the ruptures, and only 2-3 m of earthquake slip is recorded along the Shangchi segment (Fig. 1). The slip components (vertical and horizontal separations; S_v & S_h) and total separations (scalar sum) are plotted from the south to the north based on the GPS data (Fig. 3). Furthermore, the separations and the ratios between the vertical separation and the horizontal separations (S_v/S_h) versus the intersection angle between slip direction and fault strike on each data points are plotted (Fig. 3c). The separation profiles with three local maxima and three local minima show an asymmetric pattern, being skewed to the north (Fig. 3b). Probably, this slip pattern depends on rupture segmentation and propagation (Kim & Sanderson, 2008), because the slips generally increase to the north and the local minima (points 6, 13, 16) are well-matched with the segment boundary or bending points (Fig. 3a). This kind of asymmetric slip distribution occurs where segments interact or displacements are transferred by relay structures (Peacock & Sanderson, 1999).

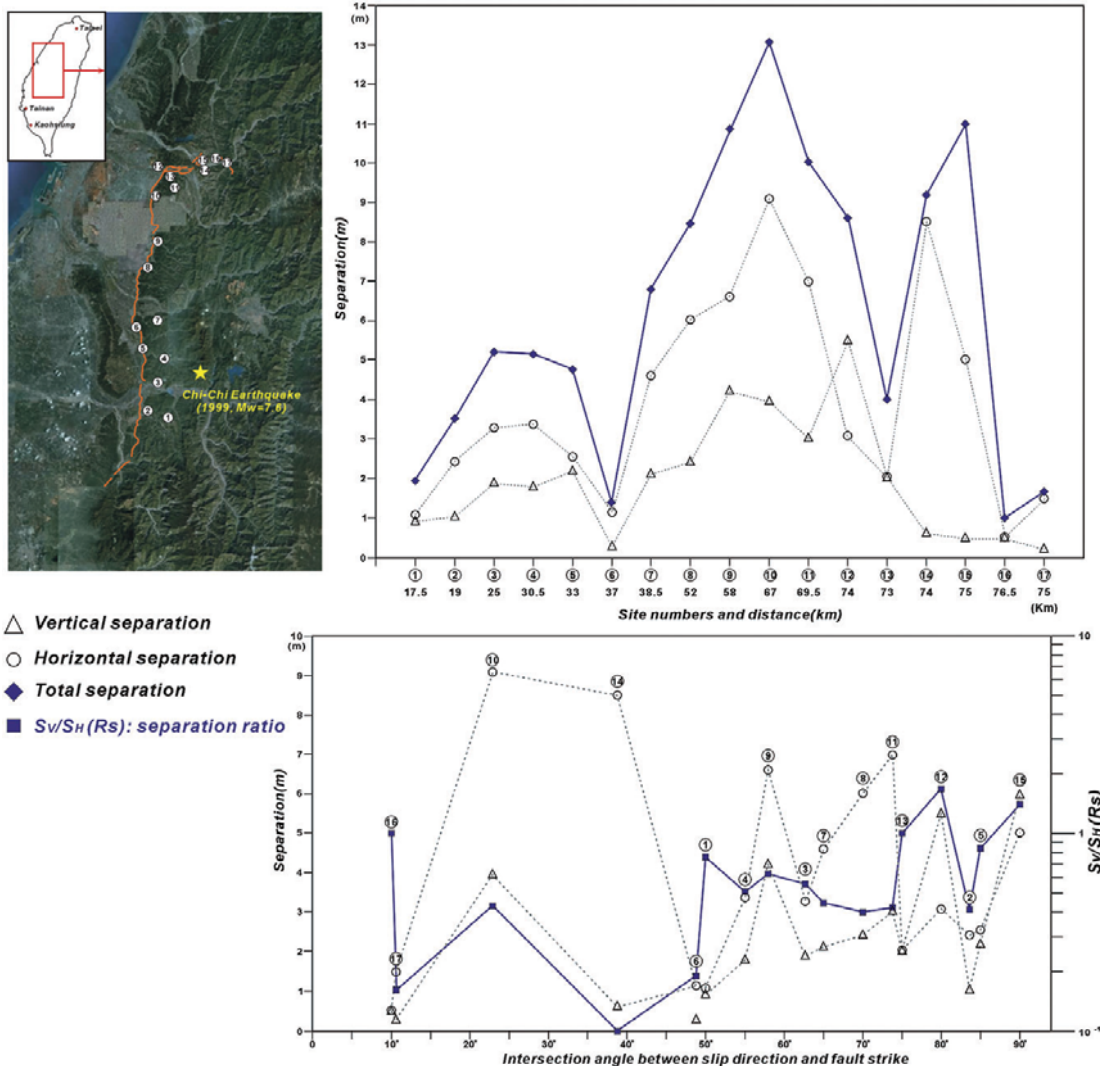


Fig. 3. Plot of vertical and horizontal separations (S_v/S_h) and separation ratio (RS) associated with the Chi-Chi earthquake.



The fault geometries and structures in the northern part of the main Chelungpu fault show oblique slip displacement, with a left-lateral strike-slip and thrust component. However, the Shangchi segment shows right-lateral strike-slip movement with a minor thrust slip component (Fig. 1). This pattern of different slip senses and fault types around the overstep zone indicates that the hangingwall of the Chelungpu fault (the Shihkang-Shangchi fault zone) extrudes like a wedge between the main Chelungpu fault and the Shangchi segment. The main Chelungpu fault (left-lateral) and Shangchi segment (right-lateral) link with thrust faults at the Shihkang-Shangchi fault zone in the form of jogs (or oversteps) between two segments (Figs. 1). This interpretation is obvious from the geometric and kinematic analyses of the fault system including in-situ measurements and coseismic GPS measurements (Yu et al., 2001). The transpressional overstep and transferring of fault patterns indicates that the Chi-Chi earthquake migrates from the main Chelungpu fault to the Shangchi segment. This unusual fault pattern (opposite slip senses with wedge-shaped push-up structure) may be due to oblique slip (strike-slip plus reverse slip) faulting. Therefore, this Chi-Chi earthquake fault is interpreted as a mode II and III mixed mode fault system.

DISCUSSION

Fault activity

When an earthquake occurs along a fault, the rock volume around the rupture breaks in response to changes in stress with distance from the rupture. These rock volumes that are brought nearer to failure are closely associated with aftershocks (Harris, 1998). Many aftershocks occurred after the Chi-Chi earthquake, and most of the aftershocks are generated around the areas of large slip. In particular, the large aftershocks ($M > 6$) of the Chi-Chi earthquake were mainly concentrated on the epicentral region of the main Chelungpu fault. However, some aftershocks are also observed around the Shihkang-Shangchi fault zone, corresponding with areas

of large slip (Ma et al., 2001), even though these areas are not located within the main fault zone.

Recently, Kim & Sanderson (2008) argued that the location of the main shock, aftershock clusters, and secondary fault distribution along a fault are closely related. Aftershock clusters are generally associated with secondary faults (or damage zones) around the main fault (Sibson, 1989). This indicates that damage zones are closely related with earthquake mechanisms and stress release around earthquake faults. This indicates that the Shihkang-Shangchi fault zone is a linking damage zone. Therefore, there is a high potential of future earthquake rupture along the northern extension of the Shangchi rupture segment.

Numerical modelling for the Chi-Chi earthquake ruptures

When an earthquake occurs, the shear stress is commonly reduced along the fault that slipped. However, new shear stress change is concentrated around fault tips (Stein, 1999). This concentration could contribute to the triggering of the next earthquake at this position. Therefore, understanding stress changes around earthquake ruptures is a very important factor in the evaluation of future earthquake hazards. We used Coulomb 3.1 to estimate the Coulomb stress change.

We modeled for two different scenarios (Fig. 4) to test our interpretation. In Figure 4c, only the associated ruptures are considered for the modeling, while the inferred fault (lineament along the Chinshui Shale) is also considered in Figure 4d. The two modeling results consistently show that the stress changes concentrated at the tips of the main Chelungpu fault, bending point of the main fault, and the Shangchi segment (Fig. 4). The main difference between the two modeling results (Fig. 4c & 4d) is the concentration of the stress change around the Shangchi segment. The Coulomb stress changes shown in Figure 4d are gradually widened toward the extended lineament (inferred fault) of the Shangchi segment. This suggests that the stress can easily be accommodated and propagated toward the north and northeast if a fault segment exists in this location.

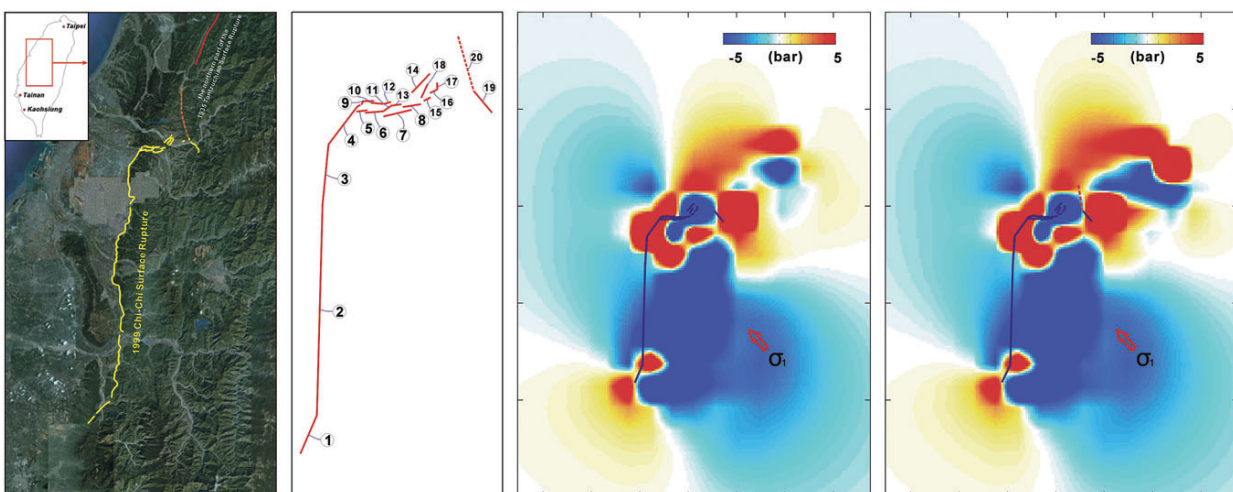


Fig. 4. Calculations of Coulomb failure stress change on surface ruptures of the 1999 Chi-Chi earthquake and along the lineament of the northern extension of the Shangchi segment. The red region indicates positive Coulomb stress changes, while the blue indicates a negative change.



CONCLUSIONS

Based on the geometric, kinematic, and geophysical analyses of the Chi-Chi earthquake fault, the northern part of the surface ruptures is a linking damage zone between fault segments. It shows a relatively high complexity and intense fault/fracture density in the zone, which may evolve from interacting tips of adjacent fault segments. An analyzed slip indicates that the ruptures are composed of three fault segments and the amount of slip is partly dependent on the intersection angle between slip direction and fault strike. Based on the Coulomb modeling, the stress change is concentrated around tips and bends along the fault system in the two cases (Fig. 4). It also demonstrates that a large stress change is concentrated around the northern end of the Shangchi segment, indicating the potential propagation toward the northern extension of the Shangchi segment (Fig. 4). These models may indicate that the high potential of future earthquake activity is centralized along the Shangchi segment (Fig. 5). Hence, we recommend that more intensive paleoseismic studies should be concentrated on the Shangchi segment and other parallel faults.

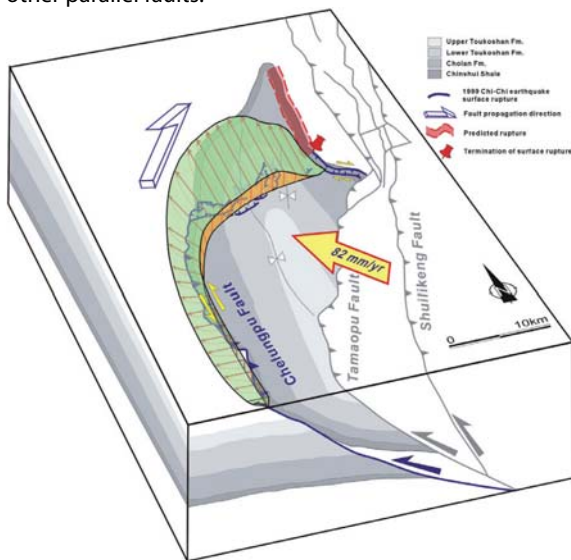


Fig. 5. Northern surface ruptures of the 1999 Chi-Chi earthquake illustrated in a 3D block diagram (modified from Lee et al. 2002). There is a high potential for future earthquake activity and related hazards along the Shangchi segment.

Acknowledgements: This research was supported by the Basic Research Project (14-1121) of the Korea Institute of Geoscience and Mineral Resources (KIGAM) funded by the Ministry of Science, ICT and Future Planning of Korea.

References

- Chung, J.K. & Shin, T.C. (1999). Implication of the rupture process from the displacement distribution of strong ground motions recorded during the 21 September 1999 Chi-Chi, Taiwan earthquake. *Terrestrial, Atmospheric and Oceanic Sciences* 10, 77-86.
- Blenkinsop, T. G. (2006). Kinematic and dynamic fault slip analyses: implications from the surface rupture of the 1999 Chi-Chi, Taiwan, earthquake. *Journal of Structural Geology* 28, 1040-1050.
- Harris, R. A. (1998). Introduction to special section: Stress triggers, stress shadows, and implications for on seismic hazard. *Journal of Geophysical Research* 103, 24347-24358.
- Kim, Y. -S., Peacock, D. C. P. & Sanderson, D. J. (2004). Fault damage zones. *Journal of Structural Geology* 26, 503-517.
- Kim, Y. -S. & Sanderson, D. J. (2006). Structural similarity and variety at the tips in a wide range of strike-slip faults: a review. *Terra Nova* 18, 330-344.
- Kim, Y. -S. & Sanderson, D. J. (2008). Earthquake and fault propagation, displacement and damage zones. *Structural Geology: New Research*, Vol. 1, pp. 99-117.
- King, G. C. P. (1986). Speculations on the geometry of the initiation and termination processes of earthquake rupture and its relation to morphology and geological structure. *Pure and Applied Geophysics* 124, 567-585.
- Lee, J. C., Chu, H. -T., Angelier, J., Chan, Y. -C., Hu, J. -C., Lu, C. -Y. & Rau, R. -J. (2002). Geometry and structure of northern surface ruptures of the 1999 Mw=7.6 Chi-Chi Taiwan earthquake: influence from inherited fold belt structures. *Journal of Structural Geology* 24, 173-192.
- Lin, A., Ouchi, T., Chen, A. & Maruyama, T. (2001). Co-seismic displacements, folding and shortening structures along the Chelungpu surface rupture zone occurred during the 1999 Chi-Chi (Taiwan) earthquake. *Tectonophysics* 330, 225-244.
- Ma, K. -F., Mori, J., Lee, S. -J. & Yu, S. B. (2001). Spatial and Temporal Distribution of Slip for the 1999 Chi-Chi, Taiwan, Earthquake. *Bulletin of the Seismological Society of America* 91, 1069-1087.
- Pachell, M.A. & Evans, J.P. (2002). Growth, linkage, and termination processes of a 10-km-long strike-slip fault in jointed granite: the Gemini fault zone, Sierra Nevada, California. *Journal of Structural Geology* 24, 1903-1924.
- Peacock, D. C. P. & Sanderson, D. J. (1991). Displacements, segment linkage and relay ramps in normal fault zones. *Journal of Structural Geology* 13, 721-733.
- Shin, T. -C. & Teng, T. -L. (2001). An overview of the 1999 Chi-Chi, Taiwan, earthquake. *Bulletin of the Seismological Society of America* 91, 895-913.
- Stein, R. S. (1999). The role of stress transfer in earthquake occurrence. *Nature* 402, 605-609.
- Stein, R. S., Barka, A. A. & Dieterich, J. H. (1997). Progressive failure on the North Anatolian fault since 1939 by earthquake stress triggering. *Geophysical Journal of International* 128, 594-604.
- Willemsse, E. J. M., Pollard, D. D. & Aydin, A. 1996. Three-dimensional analysis of slip distributions on normal fault arrays with consequences for fault scaling. *Journal of Structural Geology* 18, 295-309.
- Yu, S. B., Kuo, L. C., Hsu, Y. -J., Su, H. H., Liu, C. C., Hou, C. S., Lee, J. F., Lai, T. C., Liu, C. C., Liu, C. L., Tseng, T. F., Tsai, C. S. & Shin, T. C. (2001). Preseismic deformation and coseismic displacements associated with the 1999 Chi-Chi, Taiwan earthquake. *Bulletin of the Seismological Society of America* 91 (5), 995-1012.



The Western Australia shear zone

Whitney, Beau (1), Hengesh, James (1), and Clark, Dan (2)

(1) The Centre for Offshore Foundation Systems, The University of Western Australia, M053, 35 Stirling Highway, Perth, Western Australia 6009, Australia, Email: bbwhitney@gmail.com

(2) Geoscience Australia, GPO Box 378, Canberra, ACT, 2601, Australia, Email: dan.clark@ga.gov.au

Abstract: Tectonic geomorphology along the continental margin of Western Australia indicates the presence of an approximately 2000 km long zone of dextral-oblique neotectonic faults and folds referred to as the Western Australian shear zone (WASZ). The WASZ reoccupies older rift related structures that initially formed during periods of continental-scale fragmentation in the Paleozoic and Mesozoic Eras. Reactivation in the WASZ is coincident with late Neogene reorganization of Australia's plate boundaries and realignment of the intraplate stress field. Neotectonic deformation in the southern WASZ is dominated by transpressional inversion within the extended crustal domain between Australian oceanic crust to the west and non-extended Australian continental crust to the east. The WASZ appears to accommodate differential motion expressed as dextral transpression between oceanic and non-extended continental tectonic blocks—or micro-plates.

Key words: neotectonics, geomorphology, micro-plates, Australia, SCR

INTRODUCTION

The mechanisms by which tectonic strain is distributed within Stable Continental Region (SCR) crust are poorly understood. However, to a first order approximation, strain distribution is thought to vary predictably as a function of crustal type (age and composition) and geologic history (structure and architecture), such as described in the domain model of Clark et al. (2012). Johnston et al. (1994) and Clark et al. (2012) propose that crust extended during the Mesozoic (and in some cases the Paleozoic) tends to be more 'active' than non-extended Phanerozoic crust, which in turn is more active than non-extended Precambrian crystalline basement (cratonic interiors). Additionally, kinematic relations between reactivated crustal elements and intraplate stress fields indicate that preferentially oriented structural architecture can concentrate reactivation and thereby transmit stress generated by far-field plate boundary processes far into the plate interior (e.g., Storti et al., 2003; Hillis et al., 2008).

The central west margin of Western Australia preserves a rich record of Neogene and younger tectonic deformation (e.g. Quigley et al., 2010) that follows the extended continental margin between the Indian oceanic basin and non-extended Precambrian SCR crust. Neotectonic reactivation has been documented on preferentially oriented structures across this region (Fig. 1) (e.g., Boutakoff, 1963; Hengesh et al., 2011; Clark et al., 2012; Müller et al., 2012; Whitney & Hengesh, 2013).

Herein, we present an overview of recent tectonic geomorphological and paleoseismological studies in the Western Australia shear zone (WASZ). The WASZ is a belt of neotectonic reactivation that extends from Australia's northern plate boundary at least 2000 km into the plate interior along the former rifted margin (Whitney & Hengesh, 2013). We propose the WASZ accommodates differential motion between Australian oceanic crust on

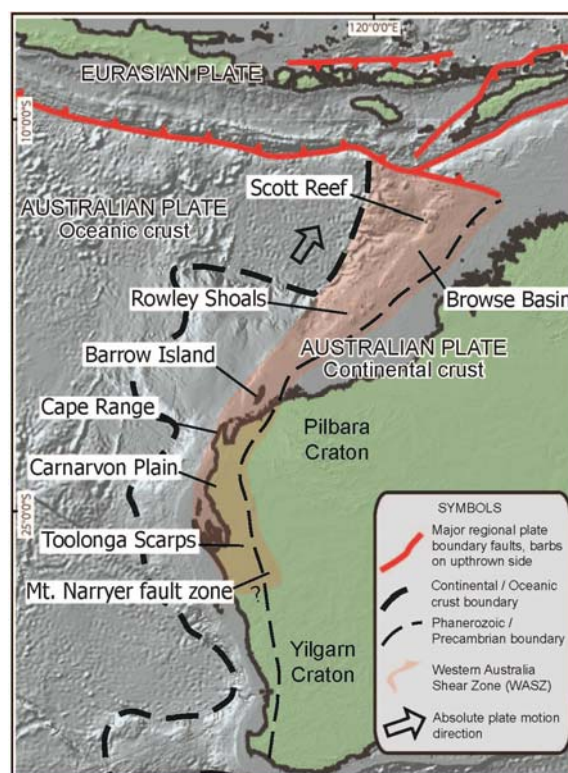


Fig. 1: Regional tectonic setting showing major tectonic elements and locations discussed in text.

the west and non-extended Australian continental crust on the east, which are effectively behaving as two micro-plates (Hengesh et al., 2011; Whitney & Hengesh, 2013). The "micro-plate" model provides a tectonic framework to explain the driving mechanism behind neotectonic deformation in this region, while the "domain" model provides a means to characterize parameters of neotectonic deformation. The domain and micro-plate models address the two most pressing questions in the field of intraplate earthquake geology. Namely, where are earthquakes prone to occur, the micro-plate model;



and, what are their likely parameters upon occurrence (e.g., recurrence, maximum magnitudes), the domain model. Patterns of seismicity, and Neogene and younger tectonic geomorphology, have the potential to provide data to further test these hypotheses within intraplate settings globally, at least for the seismogenic component of crustal strain. We discuss the micro-plate model for west-central Western Australia in this paper.

DISCUSSION

The WASZ is an approximately 2000 km long zone of actively growing faults and folds that follows the former rifted margin and continental-oceanic crust transition in Western Australia (Whitney & Hengesh, 2013). The WASZ exhibits an overall dextral-oblique sense of motion along older high-angle normal faults (e.g., McWhae, et al., 1956; Hocking, 1988). The normal faults are relicts of Mesozoic and earlier rifting associated with large-scale continental fragmentation (e.g., Lasky & Mory, 1999).

The most recent structural reactivation is widely attributed to the reorganization of the northern Australian plate boundary that initiated during the Neogene (Cathro & Karner, 2006; Audley-Charles, 2011) when the horizontal stress field in the region realigned to approximately east-west and northeast trending compression (Hillis & Reynolds, 2000; Hillis et al., 2008).

The WASZ includes both onshore and offshore structures. Tectonic geomorphology onshore includes warping and uplift of emergent marine deposits, offset marine deposits, tectonically influenced fluvial drainage patterns, and a system of faults and folds in the Mt. Narryer Region. Offshore reactivated structures include the Barrow Island anticline, Rowley Shoals Ridge, Scott Reef and faults in the Browse Basin (Fig. 1) (e.g. Boutakoff, 1963; Keep et al., 2007; Hengesh et al., 2011; Hengesh & Whitney, this volume).

The most topographically prominent structure in the WASZ is the Cape Range anticline. The structure is a doubly plunging anticline that has a flight of four emergent marine terraces on its western limb consequent of late Neogene-Quaternary tectonic uplift (van de Graaff et al., 1976; Clark et al., 2012). A late Pleistocene (Marine Oxygen Isotope Stage 5e) emergent marine sequence fringes over 400 km of coastline in the Cape Region, including the Cape Range (cf, Stirling et al., 1998). The marine sequence provides elevation and age-control to determine rates and patterns of Pleistocene tectonic deformation. High-precision leveling of shoreline features conducted to determine elevation change along the coastline demonstrates late Pleistocene tectonic uplift and subsidence consistent with late Neogene deformation on the Cape Region anticlines (Fig 2). Uplift rates for the Cape Range are estimated at between a few tens to up to 50m/Ma (0.05mm/yr) (Clark et al, 2011, 2012; Whitney & Hengesh, in review, a).

Active folds within the WASZ extend south of the Cape Region and include the Minilya folds and less

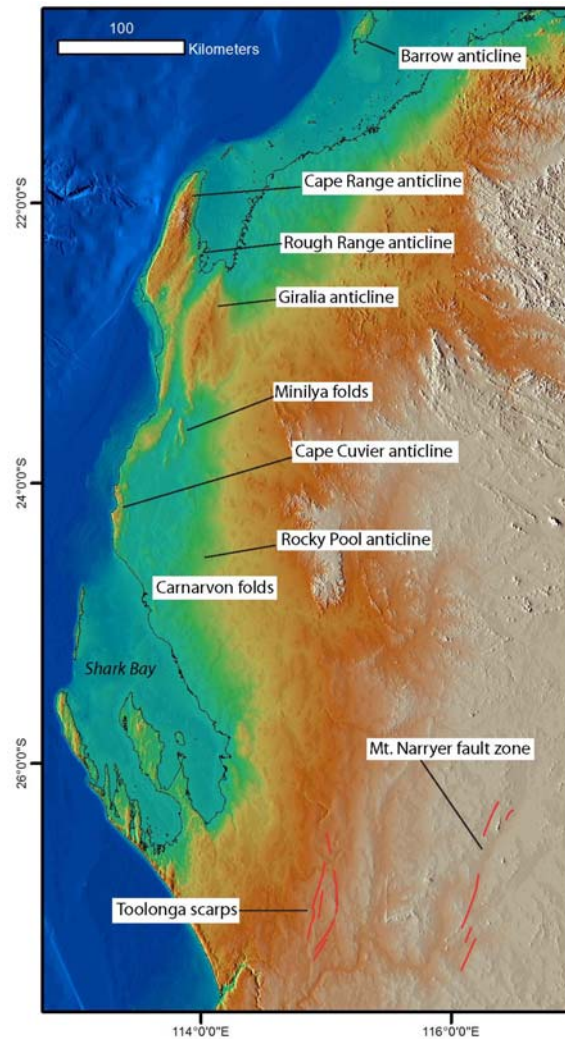


Fig. 2: DEM showing Faults and fold structures in the onshore WASZ.

topographically expressed structures across the Carnarvon alluvial plain (Fig. 2) (Denman & van de Graaff, 1977). The Rocky Pool anticline is the most topographically expressed fold east of Lake MacLeod and has documented late Pleistocene deformation (Allen, 1972). Whitney & Hengesh (in review, b) analyze channel planform characteristics and morphodynamics of ephemeral streams that cross the Carnarvon alluvial plain to determine whether tectonic deformation is evident in the fluvial geomorphological record. Their study concludes that stream response to tectonic deformation is demonstrated by channel deflections, recurrent nodal avulsions, and systematic changes in channel form and gradient within tectonically controlled reaches. Individual tectonic structures (fold hinges are evidenced by variations in channel characteristics for antecedent, supercedent, and obsequent streams within the low-gradient arid landscape. The trend and style of progressive deformation to Neogene and Quaternary deposits on the Rocky Pool anticline suggest ongoing activity (Allen, 1972).

The Toolonga group of scarps are south of the Carnarvon alluvial plain in the Southern Carnarvon and Northern



Perth basins (Fig 2). These structures trend north-south and individual scarps are greater than 60 km in length with up to 30 m of vertical displacement of the surface (Clark, 2010). Regressive marine strandlines of assumed early Pliocene age (McPherson et al., 2013) have been uplifted across these features, with total displacement across the fault complex in the order of 90 m (Clark et al., 2011). Folded Neogene sediments in the Carnarvon alluvial plain, and displacement across the Toolonga scarps in Neogene strata, indicate uplift rates less than 10m/Ma in this region of WASZ (McPherson et al., 2013).

Southeast of the Carnarvon alluvial plain and east of the Toolonga structures is a system of north-south oriented left-stepping en echelon high angle dextral-reverse faults denoted the Mt. Narryer fault zone (MNfz) (Fig. 2). The MNfz consists of at least five fault segments within a reactivated Proterozoic mobile belt at the crustal transition from the Archean Yilgarn craton to the east and the Phanerozoic Carnarvon Basin to the west. Folding in the near surface sediments is the predominant style of surface expression of reactivated basement faults, which is consistent with other neotectonic structures throughout the Western Australia shear zone. Fold expressions range in length from 11 to 68 km (total length 120 km) and deform alluvial surfaces with west-side up displacements of the Roderick, Sanford, and Murchison River alluvial deposits (cf, Whitney & Hengesh, 2013). The folds have captured and diverted active stream flow, formed sag ponds, and impounded Lake Wooleen. Shear zones within folded Pleistocene duricrust indicate a right-lateral component of motion (Whitney et al., in prep.). Age-control on folded and uplifted sediments indicate multiple late Pleistocene morphogenic events occurred within the MNfz (Hengesh et al., 2011). Fold structures within the Mt. Narryer fault zone have uplifted mid- to late Pleistocene surfaces approximately 11m, equating to uplift rates of >5 m/Ma. (Whitney et al., in prep.).

There is a paucity of neotectonic features east of the MNfz within the craton interior (Clark, 2010). East of the MNfz scarps are less frequent, spatially isolated from one another, predominantly less than 5 m high, and less than 50 km long (Clark, 2010; Clark et al., 2012).

The WASZ has elevated historic seismicity compared with the interior of the Yilgarn craton to the east and adjacent oceanic crust to the west (cf, Leonard, 2008). The WASZ is within the North West seismic zone (Hillis et al., 2008; Leonard, 2008) and has experienced multiple large magnitude historical earthquakes including an 1885 M_L 6.6 event, a 1959 M 5.9 event, and the 1941 M 7.1 Meeberrie event—Australia's largest historic earthquake (Everingham & Tilbury, 1972), as well as numerous offshore events between M5.0 and M6.6. Other than the Southwest seismic zone, the WASZ has the highest seismicity derived strain rates in Australia (Leonard, 2008). Earthquake focal mechanism data are sparse for Australia. However, a regional study collected microseismic data that yield focal mechanisms in the Carnarvon basin that

are predominantly strike-slip and consistent with regional dextral transpression (Reverts et al., 2009).

Models of intraplate stress predict an ENE principal stress direction in the onshore WASZ (Hillis and Reynolds, 2000). Modeled stress orientations and predicted trajectories are predominately based on shallow geotechnical indicators (e.g., borehole break-outs) (Hillis and Reynolds, 2000). Deeper microseismicity data (Reverts et al., 2009; Keep et al., 2012) and geomorphological data (Hengesh et al., 2011; Whitney and Hengesh, 2013) indicate an SH_{max} direction consistent with the Hillis and Reynolds (2000) stress model.

In stark contrast to the compelling geomorphological and seismological indicators, GPS data suggest that the Australian continent is not internally deforming at a detectable rate (Tregoning, 2003; Prawirodirdjo & Bock, 2004). However, these GPS data only record a 3-10 year period, stations are all located on the inboard side, or southeast, of the WASZ, and have a resolution of ~2mm/yr (Tregoning, 2003). The poor station coverage, short time-frame of observation, and the coarseness of resolution preclude the ability of geodetic measurements to detect differential intraplate motion within the WASZ.

CONCLUSIONS

Structures within the WASZ exhibit a consistent set of characteristics. Key observations include:

- faults and folds are within a discrete extended crustal domain that lies between two predominately rigid tectonic blocks;
- reactivated structures follow a dominant northeast trend;
- tectonic geomorphological indicators are concentrated within the WASZ compared with adjacent crustal domains;
- shallow surficial sediments on individual structures are gently warped into asymmetrical hanging wall anticlines above blind oblique-reverse faults;
- historical seismicity is concentrated in the WASZ;
- tectonic uplift rates range predictably from the craton margin across the WASZ from ~5-50m/Ma;
- seismicity and geomorphological data suggest a regional dextral oblique sense of motion.

We suggest the Australian plate is not behaving as a single rigid tectonic block. The data suggest the WASZ is behaving as a nascent transform boundary zone accommodating differential motion between non-extended Australian continental crust and Australian oceanic crust. Using the WASZ as an example, the micro-plate model should be examined elsewhere to test if the continent as a whole is behaving as a confederation of micro-plates that at first order are bound by former rifted continental margins and Proterozoic mobile belts. If so, the boundaries between micro-plates would be more likely to contain geomorphological indicators of tectonic deformation, have elevated post-Neogene strain rates and pose greater seismic hazard.



The efficacy of the micro-plate model has the potential to focus intraplate paleoseismological research and aid seismic hazard characterization at the continental scale. Strategically designed and longer duration GPS studies, and additional strategically located microseismicity studies are tools that could further test the Australian micro-plate model.

Acknowledgements: We gratefully acknowledge the financial support provided by the Chevron Australia Business Unit. This work forms part of the activities of the Centre for Offshore Foundation Systems (COFS), currently supported as a node of the Australian Research Council Centre of Excellence for Geotechnical Engineering. The lead author is the recipient of a SIRF scholarship from The University of Western Australia.

References

- Allen, A., 1972. Cretaceous-Holocene stratigraphy and structure, lower Gascoyne River, Carnarvon Basin. Western Australia Geological Survey Annual Report, 1972, 17-22.
- Audley-Charles, M.G., 2011. Tectonic post-collision processes in Timor. Geological Society, London, Special publications, 355, 241-266.
- Boutakoff, N., 1963. Geology of the offshore areas of north-western Australia. APEA Journal 3, 10-18.
- Cathro, D.L., Karner, G.D., 2006. Cretaceous-Tertiary inversion history of the Dampier Sub-basin, northwest Australia: Insights from quantitative basin modeling. Marine and Petroleum Geology 23, 503-526.
- Clark, D., 2010. Identification of Quaternary scarps in southwest and central west Western Australia using DEM-based hill shading: application to seismic hazard assessment and neotectonics. International Journal of Remote Sensing 31, 6297-6325.
- Clark, D., McPherson, A., Collins, C.D.N., 2011. Australia's seismogenic neotectonic record: a case for heterogeneous intraplate deformation. Geoscience Australia Record 11.
- Clark, D., McPherson, A., Van Dissen, R., 2012. Long-term behaviour of Australian stable continental region (SCR) faults. Tectonophysics 566-567, 1-30.
- Denman, P.D., van de Graaff, W.J.E., 1977. Emergent Quaternary marine deposits in the Lake MacLeod area, WA. Western Australia Geological Survey Annual Report 1976, 32-37.
- Everingham, I.B. and Tilbury, L. (1972) Information on Western Australian earthquakes 1849-1960. Royal Society of Western Australia. Journal 55, 90-96.
- Hengesh, J.V., Wyrwoll, K.H., Whitney, B.B., 2011. Neotectonic deformation of northwestern Australia and implications for oil and gas development. In: Gourvenec, S., White, D., (Eds.), Proc. 2nd International Symposium on Frontiers in Offshore Geotechnics, Perth, Western Australia, Taylor and Francis. pp. 203-208.
- Hengesh, J.V., Whitney, B.B., this volume. Quaternary Reactivation of Australia's Western Passive Margin: Inception of a New Plate Boundary?
- Hillis, R.R., Reynolds, S.D., 2000. The Australian stress map. Journal of the Geological Society of London 157, 915-921.
- Hillis, R.R., Sandiford, M., Reynolds, S.D., Quigley, M.C., 2008. Present-day stresses, seismicity and Neogene-to-Recent tectonics of Australia's 'passive' margins: intraplate deformation controlled by plate boundary forces. In: Johnson, H., Doré, A.G., Gatliff, R.W., Holdsworth, R., Lundin, E.R., Ritchie, J.D. (Eds.), The Nature and Origin of Compression in Passive Margins: Geological Society of London Special Publication, 306, pp. 71-90.
- Hocking, R.M., 1988. Regional geology of the northern Carnarvon Basin. In: Purcell, P.G., Purcell, R.R. (Eds.), Proceedings of the North West Shelf symposium, 10-12 August 1988. Perth, Petroleum Exploration Society of Australia, Perth, pp. 97-114.
- Iasky R.P., Mory, A.J., 1999. Geology and petroleum potential of the Gascoyne platform southern Carnarvon basin Western Australia. Geological Survey of Western Australia, Report 69, 51.
- Johnston, A.C., 1994. Seismotectonic interpretations and conclusions from the stable continental region seismicity database. In: Johnston, A.C., Coppersmith, K.J., Kanter, L.R., Cornell, C.A., (Eds.), The earthquakes of stable continental regions, Volume 1: Assessment of large earthquake potential, Electric Power Research Institute, p. 4-1-4-103.
- Keep, M., Harrowfield, M., Crowe, W., 2007. The Neogene tectonic history of the North West Shelf, Australia. Exploration Geophysics 38, 151-174.
- Keep, M., Hengesh, J., Whitney, B., 2012. Natural seismicity and tectonic geomorphology reveal regional transpressive strain in northwestern Australia. Australian Journal of Earth Sciences 59, 341-354.
- Leonard, M., 2008. One hundred years of earthquake recording in Australia. Bulletin of the Seismological Society of America 98, 1458-1470.
- McPherson, A., Clark, D., Whitney, B., 2013. Neotectonic evidence for a crustal strain gradient on the central-west Western Australian margin. Western Australia Basin Symposium, Perth, Australia, 16 pp.
- McWhae, J. R. H., Playford, P. E., Lindner, A. W., Glenister, B. F., Balme, B. E., 1956. The stratigraphy of Western Australia. Journal of the Geological Society of Australia 4, 1-153.
- Müller, R.D., Dyksterhuis, S., Rey, P., 2012. Australian paleo-stress fields and tectonic reactivation over the past 100 Ma. Australian Journal of Earth Sciences 59, 13-28.
- Prawirodirdjo, L., and Bock, Y., 2004. Instantaneous global plate motion model from 12 years of continuous GPS observations: J. Geophys. Res., 109, B08405, doi:10.1029/2003JB002944.
- Quigley, M., Clark, D., Sandiford, M., 2010. Late Cenozoic tectonic geomorphology of Australia. Geological Society of London Special Publication 346, 243-265.
- Revs, S. A., Keep M, Kennett, B.L.N., 2009. NW Australian intraplate seismicity and stress regime. Journal of Geophysical Research 114, doi:10.1029/2008JB006152.
- Stirling, C.H., Esat, T.M., Lambeck, K., McCulloch, M.T., 1998. Timing and duration of the Last Interglacial: evidence for a restricted interval of widespread coral reef growth. Earth and Planetary Science Letters 160, 745-762.
- Storti, F., Holdsworth, R. E., and Salvini, F., 2003, Intraplate strike-slip deformation belts, in Storti, F., Holdsworth, R. E., and Salvini, F., eds., Intraplate strike-slip deformation belts, Special Publication 210, London, Geological Society, p. 1-14.
- Tregoning, P., 2003, Is the Australian plate deforming? A space geodetic perspective, in Hillis, R.R., and Muller, R.D., eds., Evolution and dynamics of the Australian plate, Special Paper 372, Geological Society of America, p. 41-48.
- van de Graaff, W.J.E., Denman, P.D., Hocking, R.M., 1976. Emerged Pleistocene marine terraces on Cape Range, Western Australia. Western Australia Geological Survey Annual Report 1975, 62-70.
- Whitney, B.B., Hengesh, J.V., 2013. Geological constraints on Mmax values from Western Australia: implications for seismic hazard assessments. Australian Geomechanics Journal 48, 15-26.
- Whitney, B.B., Hengesh, J.V. *in review, a*. Tectonic deformation of the Cape Region, Western Australia since Marine Oxygen Isotope State 5e. Quaternary Research.
- Whitney, B.B., Hengesh, J.V. *in review, b*. Geomorphological evidence of neotectonic deformation in the Carnarvon Basin, Western Australia. Geomorphology.
- Whitney, B.B., Clark, D.J., Hengesh, J.V. *in prep*. Paleoseismology of the Mt. Narryer fault zone, west central Western Australia: a multi-segment intraplate fault system.



Slow active faults in an intracontinental setting – limits of standard morphometric analyses in tectonic geomorphology

Schürmann, Evelyn (1), Christoph Grützner (2), Jochen Hürtgen (1), Klaus Reicherter (1)

(1) Institute of Neotectonics and Natural Hazards, RWTH Aachen University, Germany

(2) Department of Earth Sciences, University of Cambridge, UK. Email: chg39@cam.ac.uk.

Abstract: We applied tectonic geomorphology techniques to intracontinental region, the Lower Rhine Graben in Germany, where known faults have very low slip rates and where erosion/sedimentation rates are high. Aim of the study is to evaluate which morphological indices can be used in such regions and what DEM resolution is required under such challenging conditions. We produced DEMs based on various data sources and with different horizontal resolutions (SRTM, ASTER and airborne LiDAR data) and calculated the stream network. Then, we applied basic procedures such as hillshade analyses, shaded relief, slope angle, slope aspect, curvature, and re-classified elevation to identify lineaments with possible tectonic origin. For these lineaments we then calculated geomorphic indices, most of them based on drainage pattern analyses. Indices used were: stream length gradient index (SL), valley floor width to valley floor height ratio (Vf), asymmetric factor (Af), basin shape index (Bs), basin hypsometry (HI), and terrain ruggedness index (TRI). Our results show that ASTER and SRTM3 data do not allow conducting detailed analyses and can only be used for general overview maps. We found that the differences between the LiDAR DEMs of 1 m and 10 m resolution are negligible for our purposes and that the 10 m DEM can be used for index calculations. We show that some of the indices still work under the challenging circumstances while others fail to reveal any tectonic imprint on the landscape.

Key words: tectonic geomorphology, slow active faults, Lower Rhine Graben

SLOW ACTIVE FAULTS AND TECTONIC GEOMORPHOLOGY

During the last decades, it has become clear that earthquakes in slowly deforming regions significantly contribute to the overall seismic risk. Faults in intercontinental settings with their usually high slip rates and short recurrence intervals are relatively well understood and their seismic hazard has been intensively studied. However, despite the fact that plate boundary mega-quakes may result in hundreds of thousands of fatalities in a single event, more people were killed by intracontinental earthquakes (England & Jackson, 2011) during the last Century. The reasons for this are manifold: underestimated recurrence intervals and maximum magnitudes, poor building standards, a general lower public awareness, specific local geological settings and site amplifications effects, and the fact that some or many faults are unknown, not known to be active, or their rupture did not reach the surface.

Tectonic geomorphology techniques can help to evaluate fault activity. The calculation of geomorphic indices from digital elevation models (DEMs) allows us to evaluate the balance between tectonic movements and erosion/sedimentation, and therefore, identify areas with tectonic activity (Burbank and Anderson, 2001). Tectonic geomorphology techniques work best where tectonic activity is high and/or sedimentation and erosion rates are low. In intracontinental regions faults often have very low slip rates and their imprint on the landscape can easily be overlooked if erosion and sedimentation outpace (vertical) movements. Limits of the technique may not only be set by the landscape itself but also by the DEM dataset and may result from

the way the indices are computed. It is therefore important to investigate which geomorphic indices can be used in such regions and what DEM resolution is required for them to work.

In this short paper we present a study from Germany. After summarizing the geological setting we discuss different types of elevation data and how they influence the calculations. We then introduce the geomorphic indices that we used and summarize the results. In the last part, we discuss our results and present possible explanations for our findings.

GEOLOGICAL SETTING

The Lower Rhine Graben (LRG) in W Germany serves as test area. It is part of the European Cenozoic Rift System. Extension here started in Late Oligocene, reactivating older structures of (pre-)Mesozoic age. During the Late Quaternary activity increased, accompanied with the rise of the Eifel mountains and associated volcanic activity in the Eifel volcanic field to the south of the working area.

The lithology varies: Paleozoic carbonates and shales (folded during the Variscan orogeny and now forming the northern Eifel mountains) are present as well as Upper Cretaceous sediments, predominantly in the south and west of the investigated area. Tertiary sands and lignite beds underlie thick Quaternary sediments including periglacial loess deposits in the rest of the study area (Fig.1). The lithology and a moderate, rather humid climate lead to high sedimentation and erosion rates. The entire study area is also intensely modified by lignite mining, farming, and amelioration for many centuries.



The LRG is an intracontinental rift with numerous normal faults in a horst and graben geometry. Variscan structures and strike NW-SE, accommodating NE-SW extension. All faults move slow and slip rates do not exceed 0.1 mm/yr, most faults slip with less than 0.06 mm/yr (Vanneste et al., 2013).

GEOMORPHIC INDICES

A number of indices are described in the literature and most of them are based on the analysis of stream networks and longitudinal stream profile analysis. In most cases one single geomorphic index alone cannot

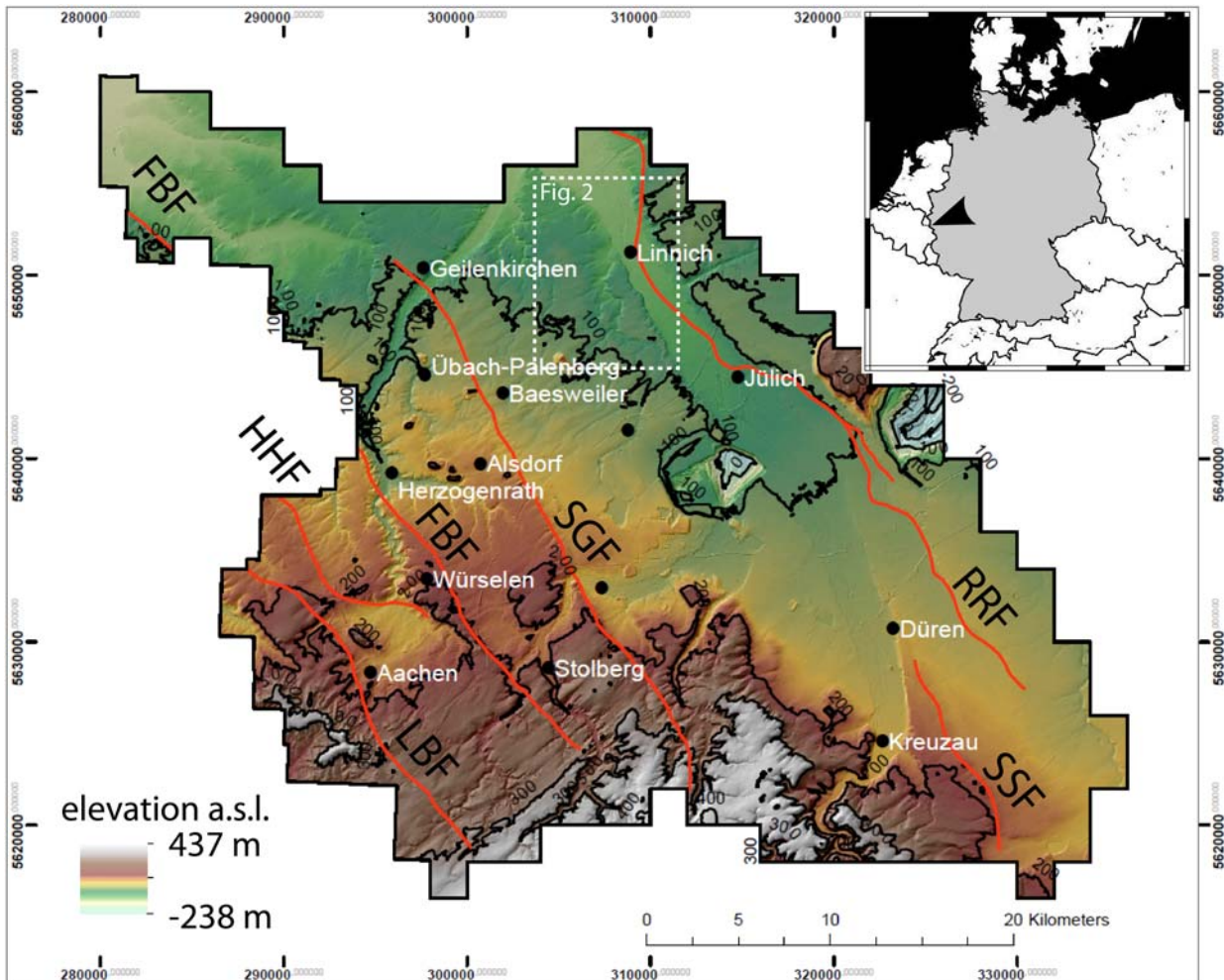


Figure 1: Topography of the study area with the main faults (red lines): FBF: Feldbiss Fault, HHF: Heerlenheide Fault, LBF: Laurensberger Fault, RRF: Rurrand Fault, SGF: Sandgewand Fault, SSF: Stockheimer Sprung Fault. Dots are cities, black lines are contour lines. Inset shows location of the study area in Germany. Note the Hambach and Inden open pit mines S of Jülich and the linear erosion features created by the River Rur between Kreuzau and Linnich. Map is in ETRS1989 UTM zone 32N, inset is in Mercator projection.

Seismicity is among the highest in Germany but still low on a global scale. Paleoseismological investigations prove a number of surface rupturing events in the late Quaternary (see Vanneste et al. (2013) and references therein). Convincing evidence for surface rupturing events in the Holocene is, however, lacking. All these factors make the LRG a perfect area for studying tectonic geomorphology under challenging conditions.

be considered significant (Hürtgen et al., 2013). Usually, a combination of different indices is used to quantify the tectonic activity of an area (El Hamdouni et al., 2008). The indices applied in this study are designed for identifying (vertical) movements in tectonically active areas, especially along mountain fronts (see Burbank and Anderson (2001) for details). Vertical tectonic movements cause changes in the course of rivers and streams, especially in their profiles. These movements lead to knick points in stream profiles, they control the shape of valleys, drainage basins and mountain fronts, and they act on erosion and sedimentation.



When rivers cross faults, often their course changes abruptly, although this may also be caused by changes in lithology. The indices work well in tectonically highly active areas, but have proved to be a useful tool in

76.69° in DEM10 to only 37.24° in the SRTM dataset. The mean slope angles are relatively constant.

The drainage patterns for the different DEMs were computed without a threshold value for the stream

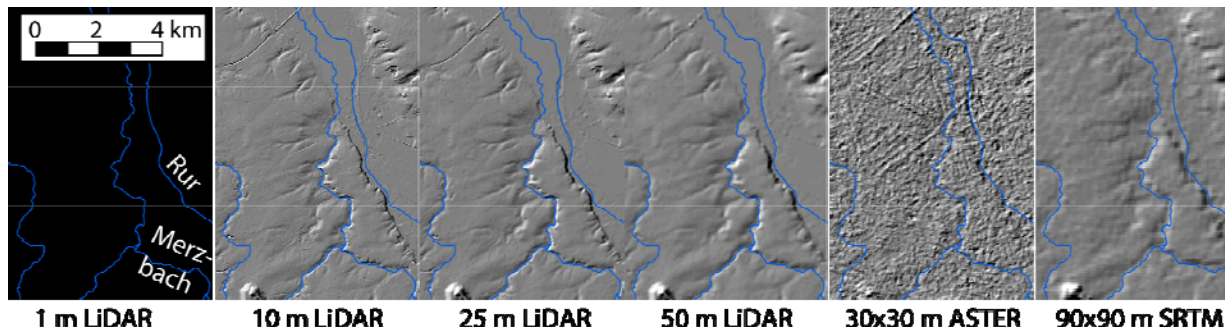


Figure 2: Comparison of the different DEMs used in this study. Note that DEM 1 produced so many shadows due to small artifacts that no geomorphological features were visible anymore.

medium activity areas, too (e.g. Spain: Silva et al., 2003; El Hamdouni et al., 2001; Hürtgen et al., 2013). Peters and van Balen (2007) addressed the tectonic geomorphology of the Upper Rhine Graben. This region can also be considered a low activity area, but its morphology is more clearly shaped by graben bounding normal faults than it is in the LRG. We used ESRI ArcGIS 10.1 and applied the following workflow in our study. Aim was to investigate the influence of DEM resolution on the results and to see which indices still work in slowly deforming regions. DEMs were calculated based on various data sources and with different horizontal resolutions: SRTM 3 (90 x 90 m tile size), ASTER (30 x 30 m tiles), airborne LiDAR (50 m, 25 m, 10 m, and 1 m point distance, respectively). We applied basic procedures such as hillshade analyses, slope angle, slope aspect, curvature, and re-classified elevation to identify lineaments with possible tectonic origin. The stream network was calculated by filling the DEMs, determining flow direction and flow accumulation, and finally delineating waterways and watersheds. For the lineaments identified we then calculated geomorphic indices, most of them based on drainage pattern analyses. Indices used were: stream length gradient index (SL), concavity index (Ac), valley floor width to valley floor height ratio (Vf), asymmetric factor (Af), basin shape index (Bs), basin hypsometry (also referred to as hypsometric integral; HI), mountain front sinuosity (S_{mf}), and terrain ruggedness index (TRI).

RESULTS

Elevation histograms reveal that both ASTER and SRTM DEMs fail to detect the small scaled variations in the terrain, especially in the area of the open pit mines. Here, the minimum elevation is underestimated by 90 and 50 m, respectively. Both datasets are characterized by spikes in the histograms, while the LiDAR data show similar results and smooth curves.

Figure 2 illustrates hillshades calculated from the different DEMs. The maximum slope values vary depending on the DEM. Generally, the coarser the DEM is the less steep are the calculated slopes, ranging from

accumulation. The output was classified using Strahler's stream classification (table 1).

The SL index was calculated for the different DEMs and for DEM10, 52 high-order streams have been analysed. The SL index highlights gradient changes in rivers is sensitive to changes in lithology and/or tectonic uplift. It is also suitable to identify knickpoints. The SL indices for the different models have been compared using the example of the river Inde (table 1). We found that the LiDAR-derived DEMs produce results which are very similar to each other, but the ASTER and SRTM datasets show noticeable deviations. Despite the fact that the mean SL values are comparable, the maximum values differ widely for single streams. All streams in the study area show relatively low SL_{mean} values, indicating gentle slopes, but may produce extreme peaks when crossing known faults or when changes in lithology occur. SL_{max} values of >900 may be produced. The density of the fault network in the study area often causes oscillating SL profiles. Generally, SL values as well as river profile shape indicate tectonic activity.

The valley floor ratio measures the ratio between valley heights to valley widths and has been measured at numerous sites for the different models. It describes if a valley is rather V-shaped (active) or U-shaped (tectonically inactive). To choose Vf sample locations, the faults were buffered by 250 m. At the intersection of this 250m line and a stream, the Vf value is measured, and also at locations where a stream crosses a fault. All streams in question are perennial. The Vf ratios suggest that the study area is tectonically inactive, even where the streams cross known active faults. This may be due to broad valleys eroded by fluvial processes. The Vf ratio results thus might be fully controlled by the strong The HI is defined as the area below the hypsometric curve of a basin and expresses the volume of a basin that has not been eroded. We calculated the HI of seven high order basins from DEM10 (table 2). High values of HI > 0.5 usually represent convex river profiles, indicating that the basins uplands have not undergone much erosion as a result of tectonic activity. Another explanation for high HI values is recent incision into a young geomorphic surface. Our calculations show that the HI results are



inconsistent and do not provide hints for the landscape's tectonic activity.

We calculated the asymmetric factor (AF) for the same seven basins. AF is used to evaluate tectonic tilting at the scale of a drainage basin. An AF value close to 50 indicates no or little tilting perpendicular to the trunk stream, AF values significantly greater or lower than 50 indicate either tectonic tilting causing river migration, or a strong lithological influence. Af values for the study area range between 26 and 68 (table 2). All basins have AF values greater or smaller than 50, AF values close to 50 do not occur. This points to tectonic activity. erosion The basin shape index BI (width of a basin divided by its length) was also calculated for the basins mentioned above (table 2). Elongated shapes are associated with relatively young basins in tectonically active areas (Ramírez-Herrera, 1998). The basins studied here are well elongated, which is a hint for a tectonically active landscape in this area.

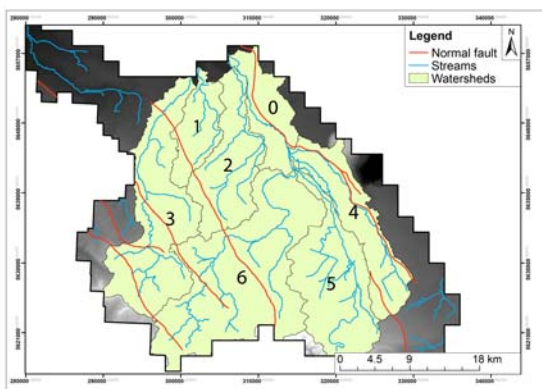


Figure 3: The basins analyzed in this study.

The mountain front sinuosity represents the ratio between the actual length of a mountain front and the length of a straight line along the mountain base. It is one of the standard indices in tectonic geomorphology but could not be applied here. Due to the slow tectonic movements no mountain front had developed.

We calculated and re-classified the terrain ruggedness index (TRI) for the study area. TRI is a measure developed to express the amount of elevation difference between adjacent cells of a digital elevation grid. High TRI values representing highly and moderately rugged terrain, occur in the Eifel region in the south. Mapped geological structures of interest, such as the Rurand Fault, the Stockheimer Sprung Fault, the Sandgewand Fault and the Feldbiss Fault can be recognized. The Laurensberger Fault and the Heerlenheide Fault can not be seen clearly, but these two faults are located in areas with a strong anthropogenic overprint. This shows that the TRI can be considered reliable for tectonic geomorphological investigations.

Table 1: Results of hypsometric integral, asymmetric factor and basin shape analysis.

Basin	Area [km ²]	HI	Af	Bs
0	70.4	0.86	64	3.5
1	60.7	0.54	26	2.9
2	115.9	0.65	33	4.1
3	193.4	0.58	66	3.8
4	114.2	0.30	38	4.8
5	156.3	0.50	33	3.4
6	296.1	0.65	68	2.5

DISCUSSION

Our results show that ASTER and SRTM3 data do not permit detailed analyses and can only be used for general overview maps. We found that the LiDAR DEMs of 25 m and 50 m point distance lack the resolution necessary for calculating geomorphic indices. Differences between the LiDAR DEMs of 1 m and 10 m resolution are negligible for our purposes, since the scale of the features we looked at exceeded several tens of meters. We used the 10 m DEM for index calculations. Especially for calculating the stream network the 1 m DEM significantly increased the computing time (more than a day on a reasonably powerful multicore PC with 8 GB of DDR3 RAM and 1GB graphics card) and the file size. The 1m data produce lots of artifacts and highlight even minor elevation changes unrelated to geomorphology, thus hampering a proper analysis.

The results of the general geomorphometric analyses of elevation, shaded relief, slope, and aspect images show that NW-SE oriented features characterize the study area. These features can be matched with known, mapped tectonic structures.

We can show that some of the indices still work under the challenging circumstances while others fail to reveal any tectonic imprint on the landscape. Indices SL, Af, TRI and Bs pointed to an active tectonic landscape even though all calculated values were typical for very low tectonic activity only. Indices HI, Vf and Smf failed to recognize the landscape as active. The reasons for this are probably complex, as the entire rift system was reactivated during the Late Quaternary and the rise of the Eifel mountain associated with volcanic activity. Another factor is provided by the varying lithology in the area from Paleozoic carbonates and shales folded during the Variscan orogeny, Upper Cretaceous sediments, Tertiary sands and lignite beds to Quaternary periglacial Loess deposits. Rock resistance and inherited tectonic structures seem to have a major influence on the activity indices in the LRG and they are often not overprinted by the young tectonics.

Acknowledgements: The LiDAR data were provided by the Geoinformationszentrum Nordrhein-Westfalen. Thomas Wiatr and Sascha Schneiderwind helped to solve GIS problems. Some figures have been produced with the Generic Mapping Tools software.



References

- El Hamdouni, R., Irigaray, C., Fernández, T., Chacón, J., & Keller, E.A. (2008). Assessment of relative active tectonics, southwest border of the Sierra Nevada (southern Spain). *Geomorphology*, 96, 150–173.
- England, P., & Jackson, J. (2011). Uncharted seismic risk. *Nature Geoscience*, 4(6), 348-349.
- Hürtgen, J., Rudersdorf, A., Grützner, C., & Reicherter, K., (2013). Morphotectonics of the Padul-Nigüelas Fault Zone, Southern Spain. *Annals of Geophysics* 56, 6, 50679.
- Peters, G., & van Balen, R. T. (2007). Tectonic geomorphology of the northern Upper Rhine Graben, Germany. *Global and Planetary Change*, 58(1), 310-334.
- Ramírez-Herrera, M.T. (1998). Geomorphic assessment of active tectonics in the Acambay Graben, Mexican volcanic belt. *Earth Surface Processes and Landforms*, 23(4), 317–332.
- Silva, P.G., Goy, J.L., Zazo, C., & Bardají, T. (2003). Fault-generated mountain fronts in southeast Spain: geomorphologic assessment of tectonic and seismic activity. *Geomorphology*, 50, 203-225.
- Vanneste, K., Camelbeeck, T., & Verbeeck, K. (2013). A Model of Composite Seismic Sources for the Lower Rhine Graben, Northwest Europe. *Bulletin of the Seismological Society of America*, 103(2A), 984-100.



Geomorphologic Indicator of Tectonic Activities in Bakauheni, Lampung, Indonesia

Akbar Cita (1), Soemantri Poedjoprajitno (1)

(1) Center for Geological Survey, Jl, Diponegoro 57 Bandung, Indonesia 40122. Email: akbarcita@gmail.com

Abstract: Morphotectonic illustrates the tectonic pattern at the surface. The research aims to inventory the distribution of landforms controlled by tectonic activities and to identify existing active faults. The study was conducted in Bakauheni with detailed investigation at Pegantungan and Jering village. Pegantungan and Jering are selected for detail investigation because the areas represent the main regional lineaments and located at site location of Sunda Strait bridge construction plan. The research applies remote sensing to identify and interpret regional lineament. Field mapping on the selected area is carried out to identify in detail morphotectonic elements, geological structures analysis and morphometric calculation. The results showed that the azimuth of lineament predominantly on the direction of N (131-140) E - N (311-320) E. Geomorphologic indicators of tectonic activities in Pegantungan indicate by some geomorphological feature such as: fault escarpment, free face, debris slopes, the deviation of rivers, and valleys fault. Geomorphologic indicators of tectonic activities in Jering indicate by Sagpond (Figure 8) and "Z" form of a river channel.

Keywords: Morphotectonic, Morphological lineament, Landsat, Morphometry, Bakauheni

INTRODUCTION

Landform is essentially controlled by endogenous and exogenous processes, known as the principle of antagonism in the evolutionary process of geomorphology (Scheidtger, 1986). Tectonic activities formed some distinctive landforms such as fault scarp, shutter ridge, sag pond and linear valley (Slemmons, 1986). The description of the tectonic activities that is reflected in the surface is known as morphotectonic.

Bakauheni is an interesting area for geomorphological indicators of tectonic activities research because it is one of the site locations of Sunda Strait Bridge. The bridge will connect two biggest islands in Indonesia, Java and Sumatra. Information about the morphotectonic condition is needed for technical consideration of the construction. The research located in Bakauheni village, South Lampung regency at the coordinate 105° 41' - 105° 47' E and 05° 48' - 05° 54' 30" S (Figure 1). Detailed investigation is carried out in Pegantungan dan Jering.

The study area is influenced by Strike Slip Sumatran Fault patterns. The fault is classified as dextral strike slip in North-South trending (Nishimura et al. (1986), Verstappen (2000). Previous researches in the area mainly only discuss about the tectonic processes (Nishimura et al. (1986), Pramumijoyo et al. (1991) or submarine morphology (Boediono et al. (2010), Noviadi (2010). Soehaimi (2011) identify that the epicentre of earthquake in the area is 30 - 100 km depth.

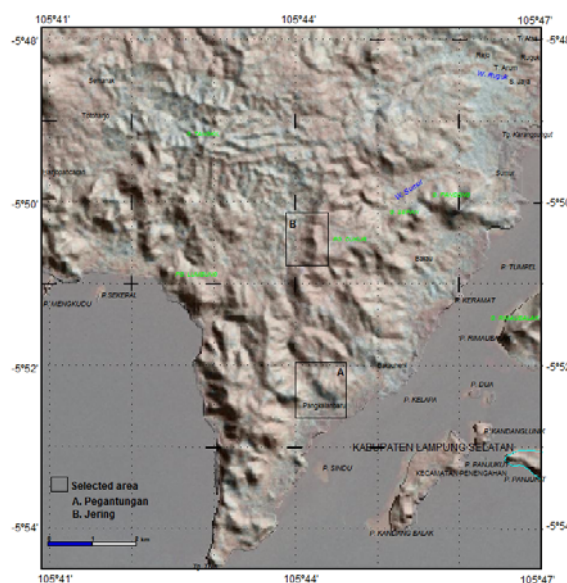


Figure 1. Research area

Geological mapping has been done by Kamawan et al. (2011) and produce 11 lithological unit such as sand, limestone, alluvium, pumice tuff, breccia tuff, Rajabasa tuff, welded tuff, columnar joint, blocky lava, sheeting lava and diorite.

Kamawan et al. (2011) also indicate some fault in the direction of North West - South East and North North East - South South West. This research aims to inventory the distribution of landforms controlled by tectonic activities and identify existing active faults.

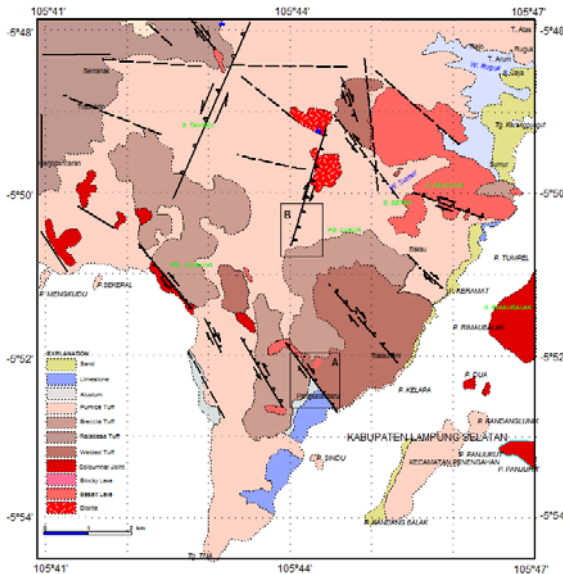


Figure 2. Geological map of Bakauheni (Kamawan et al., 2011)

METHODOLOGY

Preliminary stage of the study is to interpret Landsat images to determine the condition of landforms and to identify and interpret regional lineament. A field campaign is performed to recognise geomorphological conditions as the basis for determining the chosen area for detailed investigation. The selected area is a landform that is formed by tectonic activity.

The investigations in selected area will measure geological structure and determine the type of local fault. Morphotectonic mapping is carried out by transect method. Identification of geomorphologic indicators of tectonic activities is carried out to compare with geological structure measurement. Valley cross section parameter is calculated as morphometric indicator because the selected area located in a valley. The elevation is measured by GPS altimeter. The ratio of valley width and valley height is calculated using the formula (Bull et al., 1977):

$$Vf = \frac{2LDL}{(ETKi - EDL) + (ETKa - EDL)}$$

- Vf: Valley floor width/height ratio
- LDL: The width of the valley floor
- ETKi: The Height of left cliffs
- ETKa: The Height of right cliffs
- EDL: The valley floor elevation

RESULT AND DISCUSSION

Landform

Regional landform observations showed that the study area is composed by some processes such as: volcanic, tectonic, combination of tectonic and volcanic, tectonic and denudation, and also rivers and marine activities. Landsat interpretation of regional lineaments showed

that the highest frequency of morphology lineament is N (131-140) E - N (311-320) E (Figure 3).

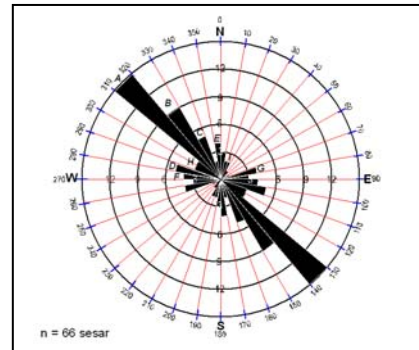


Figure 3. General direction of lineament Bakauheni

The pattern indicate that the area influenced by Sumatran fault pattern. Pegantungan and Jering are selected for detail investigation because the areas represent the two main regional lineaments and located at site location of sunda strait bridge construction plan.

A. Pegantungan

The morphotectonic map of Pegantungan allows identifying 9 geomorphologic units: Compressional hills, eroded scarp, structural valley, plateau, undulating hills, talus slope, undulating plain, alluvial plain and coral plain. Geomorphologic indicators of tectonic activities in Pegantungan indicate some geomorphological features such as: fault escarpment, free face, debris slopes, the deviation of rivers, and valleys fault.

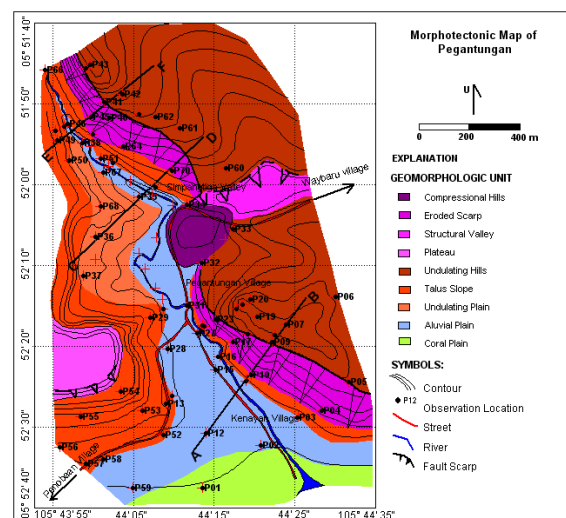


Figure 4. Morphotectonic map of Pegantungan

The analysis from Geological structure data in Pegantungan river allows concluding that Pegantungan Fault have the same direction with the regional fault pattern. The type is right thrust fault slip with the position of the fault N 325 ° E / 22 (Figure 5).

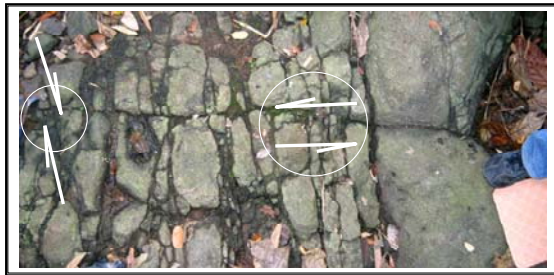


Figure 5. Joint and Fault in Pegantungan River Valley

The form of the valley in the upper stream is "V-shaped" and resembles to "U-shaped" in down stream. This indicates that the tectonic activity is reduced in the direction of the beach.

Valley cross section measurement show the value of Vf in upstream is 0,072, Vf in middle stream is 0,26 and Vf at downstream is 1,875.

The flow of Pegantungan river cut by a high waterfall (± 10 meters), then turn aside up to ± 800 meters. This deflection create landslide with orientation N 30 E. This orientation later labelled as Penobaan fault. The fault identified by escarpment that extends toward the compression hill after cutting Pegantungan River and create linier landslide (Figure 6). The presence of Penobaan Fault trending N 30 ° E adds the complexity of tectonic activities in the area. Pegantungan fault which has a field of N 325 ° E/22 ° and active, cut by a northeast - southwest trending Penobaan Fault.

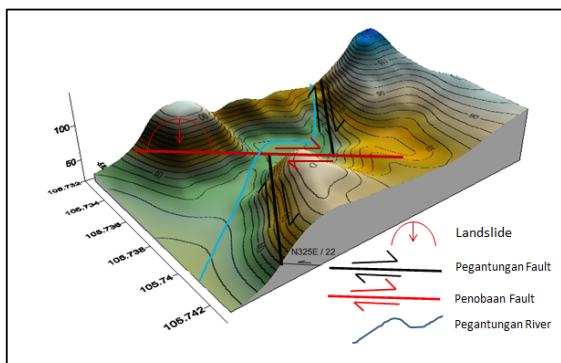


Figure 6 . Morphology Illustration of Pegantungan

B. Jering

From the morphotectonic map of Jering we identify 5 geomorphologic units: Lower old volcanic footslope, faulted old volcanic footslope, eroded scarp, talus slope and undulating hills (Figure 7).

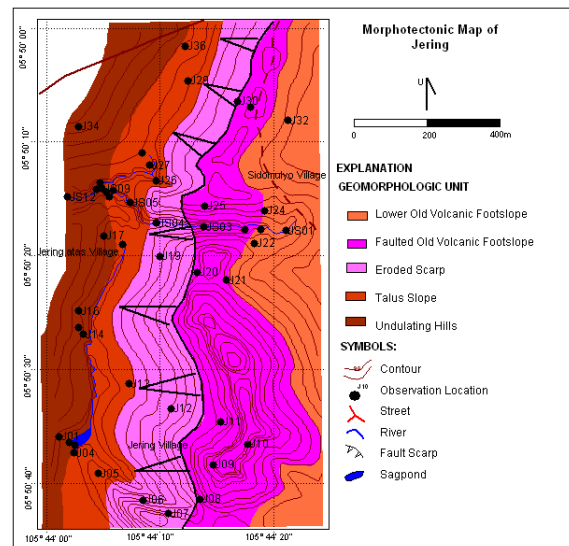


Figure 7. Morphotectonic map of Jering

Geomorphologic indicators of tectonic activities in Jering indicate by Sagpond (Figure 8) and "Z" form of a river channel at the foot of the fault escarpment is identified in Jering village.



Figure 8. Sagpond in Jering Village

Geological structure measurement resulted in Right Thrust Sip Fault and fault plane N 16 E/ 15°. The fault classify as active fault because it cut quaternary rocks. Valley cross section measurement show the value of Vf in upstream is 0,22, Vf in middle stream is 0,15 and Vf at downstream is 0,1.

Acknowledgements: The Authors express their gratitude to Ir. Asdani Soehaimi Dipl. Seis Eng. as Geodynamics of Sunda Strait working group leader and all colleagues in Center for Geological for discussion.



REFERENCES

- Andi Mangga, S., Amirudin, Suwanti, T., Gafoer, S. dan Sidarto, 1993, Peta Geologi Lembar Tanjungkarang Sumatra, Skala 1 : 250.000, Pusat Penelitian dan Pengembangan Geologi.
- Budiono, K., Susilowati, Godwin, Undang, 2010, Geologi Dasar Laut Pada Salah Satu Alternatif Rencana Poros Jembatan Jawa – Sumatera Berdasarkan Penyelidikan Geofisika, Presentasi pada Seminar Nasional Jembatan Selat Sunda, Jakarta
- Bull, W. B. and McFadden, L. D. 1977. 'Tectonic geomorphology north and south of the Garlock Fault, California', in Doehring, D. O. (Ed.), *Geomorphology in Arid Regions*, Proceedings of Eighth Annual Geomorphology Symposium, State University of New York, Binghamton, 115–138.
- Kamawan, Soemantri Poedjoprajitno, Santoso, Sukahareka Adi Saputra, Pian Sopian, 2011, Penelitian Sesar Aktif Daerah Bakauheni dan sekitarnya, Lampung, laporan Pusat Survei Geologi, tidak diterbitkan
- M. J. Rickard, 1972, Fault Classification: Discussion *Geological Society of America Bulletin*, August 1972, v. 83, no. 8, p. 2545-2546
- Nishimura, S., Nishida, J., Yokoyama, T., Hehuwat, F., 1986, Neotectonics of the Strait of Sunda, Indonesia, *Journal of Southeast Asian Earth Sciences* vol. 1 no. 2: 81 - 91, Great Britain
- Noviadi, Y., 2010, The Seafloor Morphology of Sunda Strait for Laying The Underwater Cables, *Bulletin of The Marine Geology* Volume 25 No. 2, December 2010: 103 - 113, Bandung
- Pramumijoyo, S., Sebrier, M., 1991, Neogene and Quaternary fault kinematics around the Sunda Strait Area, Indonesia, *Journal of Southeast Asian Earth Sciences* vol. 6 no. 2: 137 - 145, Great Britain
- Scheidegger, A.E., 1986, Tectonic processes and geomorphological design, *Tectonophysics* 126 (1986) 285 - 300, Elsevier Science Publisher, Amsterdam
- Slemmons, D.B., 1986, A Procedure for Analyzing Fault Controlled Lineament and Activity of Faults, International Basement Tectonics Association, Nevada USA.
- Soehaimi, Marjiyono, Soemantri.P dan Kamawan, 2011, Geodinamika dan Potensi Bahaya Gempa Bumi dalam rangka Pembangunan jembatan Selat Sunda, Prosiding Joint Convention Meeting HAGI – IAGI, Makassar
- Verstappen, H.Th., 2000, Outline of The Geomorphology of Indonesia. A Case Study on Tropical Geomorphology of A Tectonic Region, ITC – Division of Applied Geomorphological Survey (AGS), The Netherland.
- Wells, S. G., Bullard, T.F., Menges, C. M., Drake, P. G., Karas, P. A., Kelson, K. I., Ritter, J. B. and Wesling, J.R. 1988. 'Regional variations in tectonic geomorphology along a segmented convergent plate boundary, Pacific coast of Costa Rica', *Geomorphology*, 1239–265
- Zuidam. R.A., 1985, *Aerial Photo-Interpretation in Terrain Analysis and Geomorphologic Mapping*, Smiths Publishers, The Hague



Identifying an active Sumatra Fault Segment in Liwa Region using a Morphotectonic Approach

Yudhicara(1,2), Dicky Muslim(1), A. Sudradjat(1), D.H. Natawidjaja(3), and R. Siahaan(1)

- (1) Padjadjaran University, Bandung, Indonesia.
 (2) Geological Agency, Bandung, Indonesia
 (3) Indonesian Institute of Science, Bandung, Indonesia

Abstract Liwa is a region located at one of the Sumatra fault segments named Liwa fault segment. Some large earthquakes, such as Ms 7.5 on 24 June 1933 and Mw 6.4 on 18 March 1994, have been occurred on this segment and caused many casualties and damages. Those earthquakes gave permanently deformation on earth surface, reflected by geomorphic offsets observed on satellite images of DEM SRTM 30 m. Using a morphotectonic approach such as mountain front sinuosity (Smf), valley floor ratio (Vf), bifurcation ratio (Rb) and drainage density (Dd), this paper tries to explain which one is the most active fault segment between two blocks separated by the Sumatra fault whether the southwestern block or northeastern block. The Smf average values of 1,453 and 1,459 show direct uplift and related to an active tectonic movement in Liwa region. The Vf ratio shows an average of 0,36 along the main fault, values around 0,71 on the northeastern block, and values of 1,40 on the southwestern block. The smaller Vf value on the northeastern block compared with the southwestern block represents that the northeastern one is influenced by stronger tectonic movements and its lithology is more resistant compared with the southwestern block. The study area is characterized by two river drainage patterns. Those are sub-dendritic in the northeastern block and sub-parallel in the southwestern block. The northeastern block consisted of seven watersheds, while the southwestern block consisted of six watersheds. The bifurcation ratio and drainage density analysis yield that the northeastern block has larger values than the southwestern part. It shows that the northeastern block features more river branching compared with the southwestern part. This indicates that the northeastern part has been tectonically more active than the southwestern one. The morphotectonic analysis of four different indices (Smf, Vf, Rb and Dd) reflects that the northeastern block has been tectonically more active compared with the southwestern block. Eventhough, the lithology of the northeastern part is more resistant compared with the southwestern part which is proven by values of valley floor ratio (Vf), the northeastern block is more deformed than the southwestern part, due to a more strongly branched river.

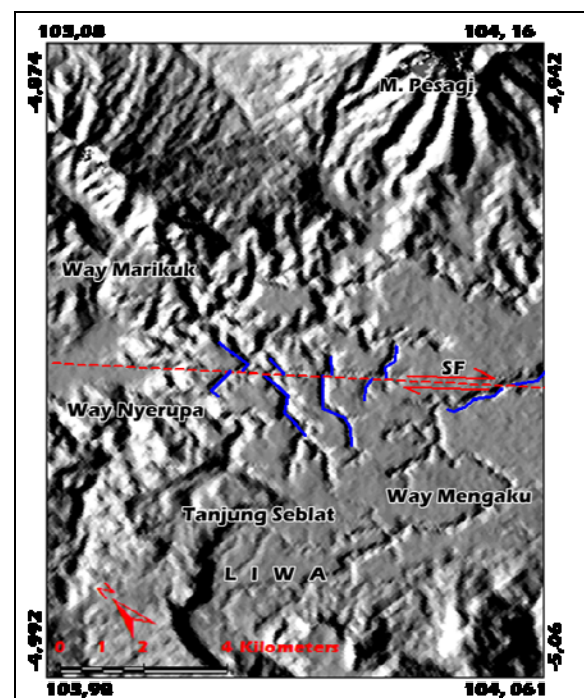
Key words: Sumatra fault, Liwa fault segment, morphotectonic, mountain front sinuosity, valley floor ratio, bifurcation ratio, drainage density.

Introduction

The Sumatra fault is a slip partition produced by the oblique subduction of the Indo-Australian plate beneath the Eurasian plate (McCaffrey, 2009). Sumatra fault has a length of around 1900 km and is divided into 19 fault segments of 60 to 200 km length for each segment. Sumatra fault is a strike slip fault which has dextral movement.

Liwa is a region located at one of the Sumatra segments named Kumering segment (Sieh and Natawidjaja, 2000; Natawidjaja and Triyoso, 2007), we call it Liwa fault segment. This segment historically produced some large earthquakes, such as Ms 7.5 on 24 June 1933 and Mw 6.4 on 18 March 1994 caused many casualties and damages. Those earthquakes gave permanently deformation on Earth's surface, reflected by geomorphic offsets, which are clearly observed on satellite images of DEM SRTM (Digital Elevation Model Shuttle Radar Topography Mission) of 30 m resolution (Figure 1). Offset distance has an average of 300 m.

There are two blocks separated by this Sumatra fault, those are the northeastern and southwestern blocks. In order to understand how tectonic influences to the region, those two blocks have been analyzed.





INQUA Focus Group on Paleoseismology and Active Tectonics



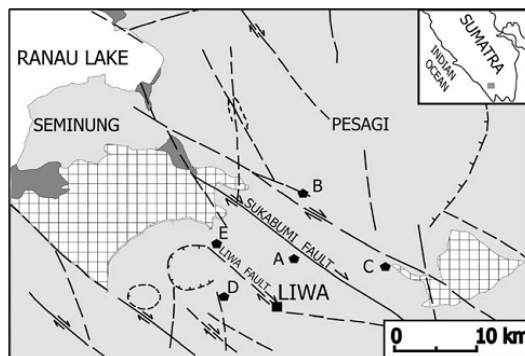
Figure 1. Offset on Liwa morphology (blue line) from SRTM 30m (SF: Sumatra fault).

For this study, we limit the Sumatra fault segments in the Liwa region which separates the two blocks, starting from the southeast of Ranau Lake, which is marked by the River of Way Marikuk and Way Nyerupa, and ends at the area of Padang Dalom.

According to Figure 1, the southwestern block seems more deformed and eroded than the northeastern block. This arises the question: Is the southwestern block more active than the northeastern block, or vice versa? This paper gives an answer to this question by using a morphotectonic approach.

Geological Setting

In general, the Liwa region is composed by three main rock units (Pardede and Gafur., 1986, Amin et al., 1994, Natawidjaya et al., 1993, Pramuwidjoyo et al., 1994). These are sedimentary rock units of Tertiary age, Quaternary volcanic rock units, and recent alluvium. The sedimentary rock units consist of laharic breccia with basaltic composition, intercalated by tufaceous sand and carbonaceous clay, which has ages of Early to Middle Miocene. This unit is covered by carbonaceous pumice intercalated by tufaceous sandstone, mud and carbonaceous clay (Amin et al., 1994), which is called Ranau tuf as product of Ranau volcano, which has a Plio-Pleistocene age. The Quaternary volcanic rock unit is identified as product of volcanoes of Seminung, Kukan, Pesagi, and Sekincau. Seminung volcanic rocks are composed by andesitic lava and laharic breccia; Pesagi volcanic composed by andesitic lava and laharic breccia; Sekincau volcanic rocks by andecites, basalts and pumices. The recent alluvium mostly consists of boulders, pebbles, gravels, sand and mud (Figure 2).



- Alluvial
- Quaternary volc. rocks
- Tertiary rocks
- Faults
- Lineaments
- Depression
- Calderas

Figure 2. Simplified geological map of Liwa (after Bellier et al., 1999)

Geological structures in Liwa have a major trending of northwest - southeast and southwest - northeast directions. Large earthquakes have occurred, such as in 1933 and 1994. The 1933 event has caused phreatic eruptions at Suoh, while the 1994 event has caused surface rupture, landslides, liquefaction, and local subsidences.

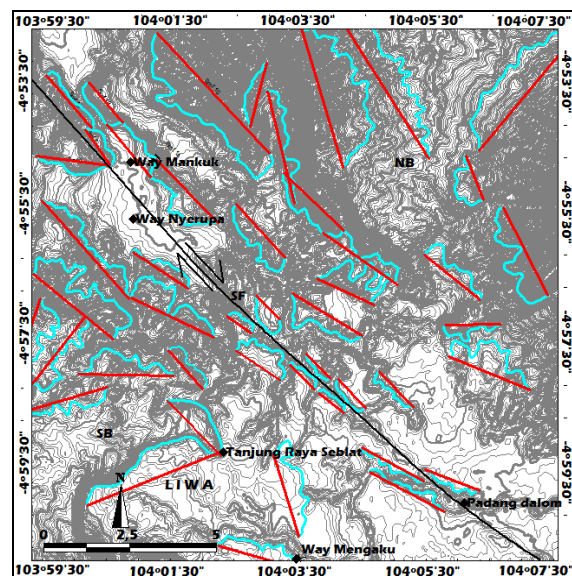
Methods

To understand the nature of tectonics in the Liwa region, a morphotectonic approach has been applied to the two blocks separated by the Sumatra fault, by using indices such as mountain front sinuosity (Smf), valley floor ratio (Vf), bifurcation ratio (Rb) and drainage density (Dd).

A statistic analysis has also been applied to elaborate the level of tectonic activity between the southwestern and northeastern block of the Sumatra fault.

Results

The mountain front sinuosity (Smf) were applied in this study, to determine whether the Sumatra fault is a pure strike slip or is there any oblique mechanism include into the system. The Smf calculation is expressed by $Smf = Lmf / Ls$. It obtains average values of 1,45 in the northeastern block and 1,46 in the southwestern block (Table 1). It indicates that there is no significant uplift observed related to an active tectonic movement in the Liwa region (Figure 3).



- Legend:
- Contour line
 - Mountain front sinuosity
 - Sumatra fault
 - Southwestern block
 - Northeastern block



Figure 3. Smf analysis

According to the statistic test, there is no difference between two blocks. So it may conclude that there is no significant vertical forces worked in the region. It means that the Sumatra fault has pure strike slip mechanism.

Table 1. Smf calculation for the two blocks.

Northeastern Block			Southwestern Block		
Ls	Lmf	Smf	Ls	Lmf	Smf
4143	5458	1,317	2429	2942	1,211
1344	2523	1,877	2017	2330	1,155
4842	7067	1,459	2440	4344	1,780
4151	6708	1,616	4051	4899	1,209
3301	4202	1,273	2257	2694	1,193
1889	2051	1,086	910,8	1154	1,267
4718	7745	1,641	948,2	1296	1,367
1998	2320	1,161	1535	2763	1,800
1228	1818	1,480	829,6	1117	1,346
1521	1979	1,301	1467	2024	1,379
1957	2560	1,308	2618	4675	1,786
2545	3756	1,476	1901	2278	1,198
2066	3459	1,674	3745	4546	1,214
2367	3115	1,316	2947	6977	2,367
2598	3514	1,352	1955	4032	2,062
2339	3301	1,411	2463	4258	1,729
939,3	1839	1,958	2766	3795	1,372
2820	4953	1,756	2677	3678	1,374
954,9	1139	1,193	2134	2360	1,106
1127	1427	1,266	2417	3090	1,278
1393	1914	1,374	Sum	29,196	
2549	4681	1,836	Average	1,459	
1585	2460	1,552			
1690	1981	1,172			
2031	2978	1,466			
Sum	36,325				
Average	1,453				

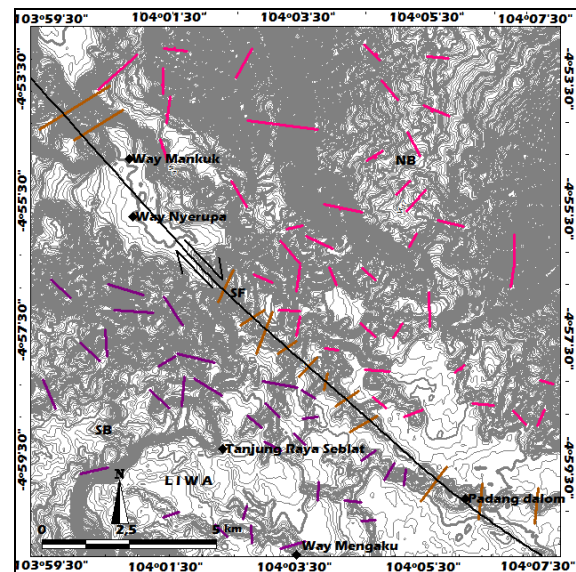
The second method is a valley floor ratio (Vf), which is the ratio of valley height and width, and expressed by $Vf = 2Vfw / [(Eld - Esc) + (Erd - Esc)]$.

The Vf is used to determine the level of tectonic activity in the region, between the two blocks. The Vf average value along the main fault is 0,39 (Table 2). This shows an active movement along the fault (according to Bull, 2007).

The calculation of Vf ratio on the northeastern block obtains the average value of 0,71, while the southwestern block results in values around 1,40. It represents that the northeastern block has experienced stronger tectonic activity, while the lithology is more resistant compared with the southwestern block (Figure 4). This is supported by statistics which show that the values of Vf in the two block shows a noticeable difference.

Table 2. Calculation of Vf ratio along the main fault.

No.	Vfw	Eld	Erd	Esc	Vf
1	18	870	770	600	0,08
2	29	800	720	595	0,18
3	24	778	775	670	0,23
4	13,2	855	860	810	0,28
5	15,5	870	825	795	0,30
6	18,3	855	825	785	0,33
7	16,1	870	850	815	0,36
8	22,4	855	860	805	0,43
9	26,5	875	865	830	0,66
10	23,3	875	870	820	0,44
11	24,3	870	860	815	0,49
12	22,4	880	850	805	0,37
13	22,8	845	845	800	0,51
Sum					4,66
Average					0,39



Legend:

- Contour line
- Vf along the fault
- Vf on the southwestern block
- Vf on the northeastern block
- Sumatra fault
- Southwestern block
- Northeastern block

Figure 4. Map of valley height and width ratio

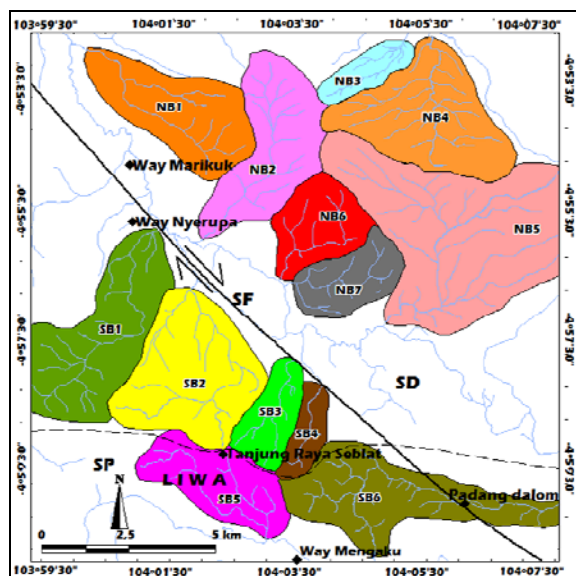


Based on the topographical map and virtually on the field compared with the river drainage pattern and the drainage pattern modification (Howard, 1967), the study area is characterized by two drainage patterns, which are sub-dendritic in the northeastern block and sub-parallel in the southwestern block. The sub-dendritic drainage pattern formed in the northeastern caused by geological and structural effects. This pattern largely passes through tuff which are dominantly covered the study area.

The sub-parallel drainage pattern formed in the southwestern part due to the formation of the ridge extending in that region, and passes the lithology of tuff. The boundary of the river drainage pattern is stretching horizontally with an East-West direction.

The larger compression resulting the more shattered rocks, in other words it will have more fractures. The more fractures, the more branches that formed the river, so it will have a higher value of bifurcation ratio (after Strahler, 1957).

The result of bifurcation ratio analysis yield that the northeastern block consists of seven watersheds, while the southwestern block consists of six watersheds (Figure 5).



Legend:

- Watershed on the northeastern block
- Watershed on the southwestern block
- Sumatra fault
- River
- Sub-dendritic drainage pattern
- Sub-dendritic drainage pattern
- Border of drainage pattern

Figure 5. Analysis of river drainage pattern, bifurcation ratio and drainage density.

The northeastern block features average bifurcation values of 4,86, while the southwestern part has average value of 4,36. The calculation of drainage density of those two blocks, yields that the northeastern block has an average value of 2,02, while the southwestern block has values around 1,80.

The larger values of watershed, bifurcation ratio and drainage density in the northeast show that the northeastern block is characterized by stronger river branching compared with the southwestern part. This indicates that the northeastern part has been tectonically more active than in the southwestern.

Based on the four used indices of morphotectonic analysis (Smf, Vf, Rb and Dd), our results obtain that the northeastern block has tectonically more active compared with the southwestern block. Eventhough the lithology of the northeastern part is more resistant compared with the southwestern part, which is proven by values of valley height and width ratio (Vf), the northeastern block is more deformed represented by a more branching river than the southwestern part.

Acknowledgements: Our deep gratitude to the Geological Agency who gave support to do the research. Many thanks to the head of Technical Implementation Unit of Mines and Geological Hazard, Indonesian Institute of Science in Liwa and his crews who have supported and given us what we needed during the fieldwork.

References

Amin, T.C., Sidarto, Santoso, Gunawan, W., 1994. The Geology of The Kotaagung Quadrangle, Sumatra, Quadrangle 1010, Scale 1: 250.000. *Geological Research and Development Center, Department of Mining and Energy of Indonesia.*

Bellier, O., Bellon, H., Sebrier, M., Sutanto, Maury, R.C., 1999. K-Ar age of the Ranau Tuffs : implication for the Ranau caldera emplacement and slip-partitioning in Sumatra (Indonesia). *Tectonophysics: 347-359.*

Bull, W.B., 2007. *Tectonic Geomorphology of Mountains: A New Approach to Paleoseismology.* ISBN: 978-1-4051-5479-6. 328 pages. November 2007, Wiley-Blackwell

Doornkamp, J. C. , 1986. Geomorphological Approaches to the Study of Neotectonics. *Journal of the Geological Society, Vol. 143, pp. 335-342, London.*

Howard, A.D., 1967. Drainage analysis in geologic interpretation: a summation, *Bulletin of the American Association of Petroleum Geologists 51: 2256-59.*

McCaffrey, R., 2009, The tectonic framework of the Sumatran subduction zone, *Annual Reviews of Earth and Planetary Sciences, 37, 345-366.*

Natawidjaja, D.H., dan Triyoso, W., 2007, The Sumatra Fault Zone: from source to hazard. *Journal of Earthquake and Tsunami, Vol. 1, No. 1, pp. 21-47.*

Natawidjaja, D.H., 2002, Neotectonics of the Sumatran Fault and Paleogeodesy of the Sumatran Subduction Zone, *Doctoral thesis, 289 pages.*

Natawidjaja, D. H., Kesumadharmas, S., 1993. Karakterisasi gerakan tanah dan sesar aktif untuk pengembangan daerah Liwa, Kabupaten Lampung Barat. *Proceeding of the 22th Annual Meeting of Indonesian Geologist Society, 6-9 Desember 1993. Bandung, Indonesia.*



INQUA Focus Group on Paleoseismology and Active Tectonics



paleoseismicity.org

Pardede, R. dan Gafur, S., 1986. The Geology of The Baturaja Qudrangle, Sumatra, Qudrangle 1011, Sekala (Scale) 1: 250.000. *Geological Research and Development Center, Department of Mining and Energy of Indonesia.*

Pramuwijoyo, S., Kumoro, Y., Sudaryanto, 1994. Neotektonik daerah Liwa dan sekitarnya, *Proceedings of Research Results of Geological Research and Development Center, Bandung, Indonesia.*

Sieh, K., and D. Natawidjaja, 2000, Neotectonics of the Sumatran fault, Indonesia: *Journal of Geophysical Research* 105, 28,295-28,326.

Strahler, A.N., 1957. Quantitative analysis of watershed geomorphology, *Transactions, American Geophysical Union*, Vol. 38, No. 6, December 1957, pp. 913-920.



A case study of the application of Airborne LiDAR technique

HyunTae Kim (1), Young-Seog Kim (1), J Ramón Arrowsmith (2), Kwang-Jae We (3)

(1) Dept. of Earth & Environmental Sciences, Pukyong National University, Busan 608-737, South Korea. Email: kimht0709@gmail.com

(2) School of Earth and Space Exploration, Arizona State University. USA

(3) Geostory Incorporated. S. KOREA.

Abstract: Earthquakes can cause serious loss of life and significant property damage. Thus, the study of active faults is important in evaluating future fault activity and hazards caused by future earthquake events. Structural mapping and the tracing of active faults are the primary steps in studies of active faults. Until now, active faults in South Korea have been mapped using aerial photography, satellite images, and low-quality DEMs. Lineament analysis as a means of identifying active faults is relatively difficult in Korea due to geological characteristics (weak tectonic activity) and dense vegetation cover. In this paper, we introduce the basic concept of the LiDAR technique (a new prospective remote sensing method) and a data analysis method that can overcome these problems. This paper will contribute to a better understanding of the airborne LiDAR technique and its application to South Korea. Some preliminary results from Korean and USA LiDAR data show the usefulness of this technique for tracing lineaments, active faults, and terraces in South Korea.

Key words: Active faults, Lineament analysis, Geomorphic analysis, Remote sensing, Airborne LiDAR

INTRODUCTION

Damage caused by earthquakes has been widely reported all over the world. Most earthquake damage above a magnitude of 6 is related to fault activity that involves surface rupturing. Most huge earthquakes of this size are known to occur because of pre-existing active fault reactivation. Therefore, active fault research is an important step for forecasting earthquakes and studying their characteristics. Active fault research is progressing in many different ways. Many researchers are studying fault activity, reactivation cycles, displacement and earthquake size. However, in order to understand the characteristics of earthquake activity, we have to define active fault existence first. Previously we analyse fault related lineaments using aerial photography or satellite image. This method brings

about a great improvement in active fault recognition. Thus, recent active faults are shown as clear lineaments. This is the most basic, yet crucial information for active fault mapping. Airborne LiDAR removes vegetation and buildings on the ground by filtering. This method is very useful in South Korea as most areas are covered in thick difficult to penetrate vegetation and are in non-tectonic areas.

LiDAR data from Hanjin information Systems & Telecommunication Company is used in this study, from the Samchuck, Mt. Bomun in Daejeon city, Weolsung area and Pochun arboretum in South Korea (Fig. 1a). Also, from the Cape Blanco state park and Kern area in USA (Fig. 1b) the focus of this study is using new processing and interpretation tools to re-process old data to make it more useful and accurate.

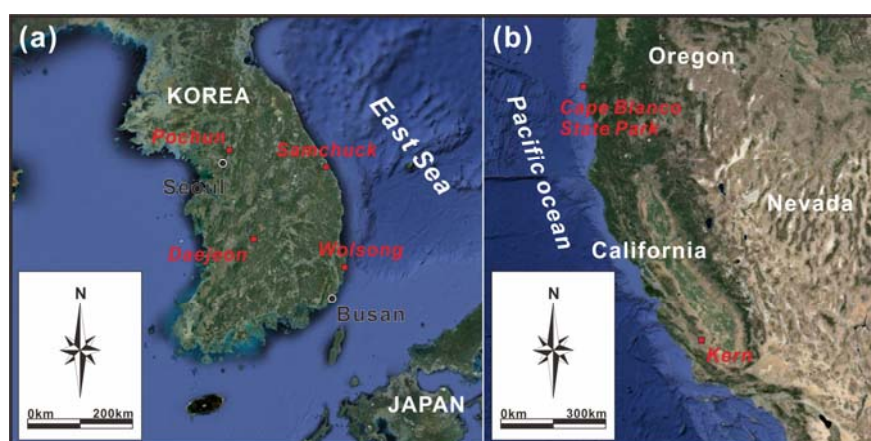


Fig. 1: Location maps of the study areas. (a) Locations of the four sites selected in Korea. (b) Locations of two sites selected in the USA (image is from Google Maps).



BACKGROUND OF AIRBORNE LIDAR TECHNIQUE

Aircraft equipped with a laser scanner are also equipped with GPS (Global Positioning System) and INS (Inertial Navigation System) to give a true location. When the data is processed, a topographic map can be produced using 3-Dimensional coordinates (Lee, 2006). Many researchers are carrying out studies in filtering techniques from LiDAR binary data (Kraus and Pfeifer, 1998; Haugerud and Harding, 2001; Zhang et al., 2003). In South Korea many researchers are also studying new filtering methods (Lee, 2006; Chung et al., 2005; Yoon et al., 2006). These kinds of technique give us basic information for detailed field-trip planning (e.g. Arrowsmith et al., 2009).

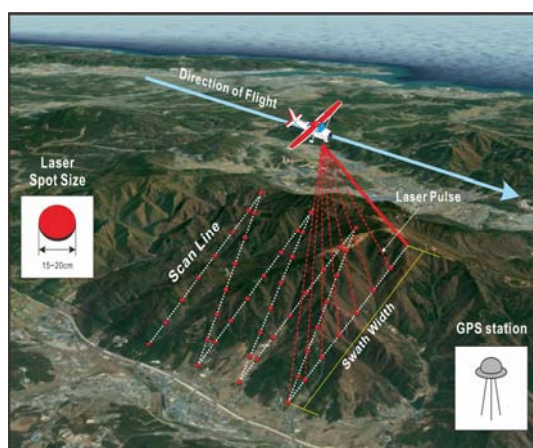


Fig. 2: Schematic diagram for collecting airborne LiDAR data (image is from Google Map).

APPLICATIONS OF LIDAR TECHNIQUE TO SOUTH KOREA

Recently, many countries have collected LiDAR data from various areas and they have conducted many research projects using this data (Blair et al., 1999; Haugerud et al., 2003). South Korea has started to collect LiDAR data from several years ago. However, these studies have generally been used in city planning projects (Lee and Yu, 2003), natural hazards (Han et al., 2009), etc. So far, LiDAR hasn't been used in geological studies to the degree that it has in other countries. This method removes vegetation or buildings using filtering techniques to give us better geological data from Airborne LiDAR. After filtering, we are able to classify two kinds of point, obstructions (vegetation, building) and ground. In this study, the sample data is taken from the Samchuck area and the Bomun Mountain area in Daejeon, South Korea. These areas are mostly covered by vegetation. We used Optech ALTM 30/70 laser scanner, the aircraft altitude was between 1,200 and 1,400m and the point spacing was 3.5 point per m².

Vegetation

First, we processed the Samchuck area in the eastern part of Korean Peninsula. We removed the vegetation image (Bare earth) showing topography and lineaments in a non-tectonic area clearer than all other images. We can clearly recognize previously unclear streams (Fig. 3d).

Lineament

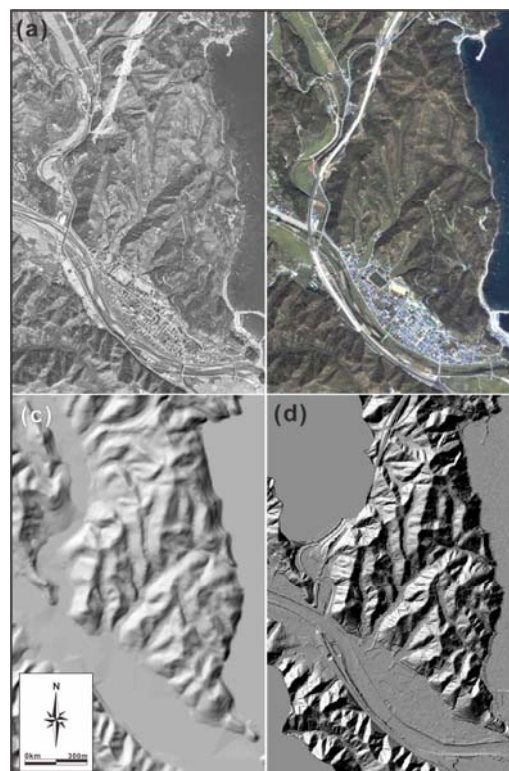


Fig. 3: Comparison of remote sensing images from the Samchuck area. (a) Aerial photograph (sourced from the National Geographic Information Institute), (b) satellite photograph (image is from Google Map), (c) hillshade image from a topographic map, and (d) hillshade image from airborne LiDAR.

Mt. Bomun in Daejeon city has much more vegetation than the Samchuck area (Fig 4a). This area's vegetation is similar to typical mountain vegetative cover that is seen throughout South Korea, after filtering the LiDAR images using the new software applications we are able to view much more information than we were previously (Fig 4b). Fig.4c shows an image that has been filtered using the software and it is quite clear that weak lineaments have become stronger, rivers are easily visible and weak lineaments now become clear. It is also quite easy to see clear displacement of rivers along strong lineaments. Weulsung area has vegetation like Mt. Bomun in Daejeon city (Fig 5^a). This area is very important area because of nuclear power plant.

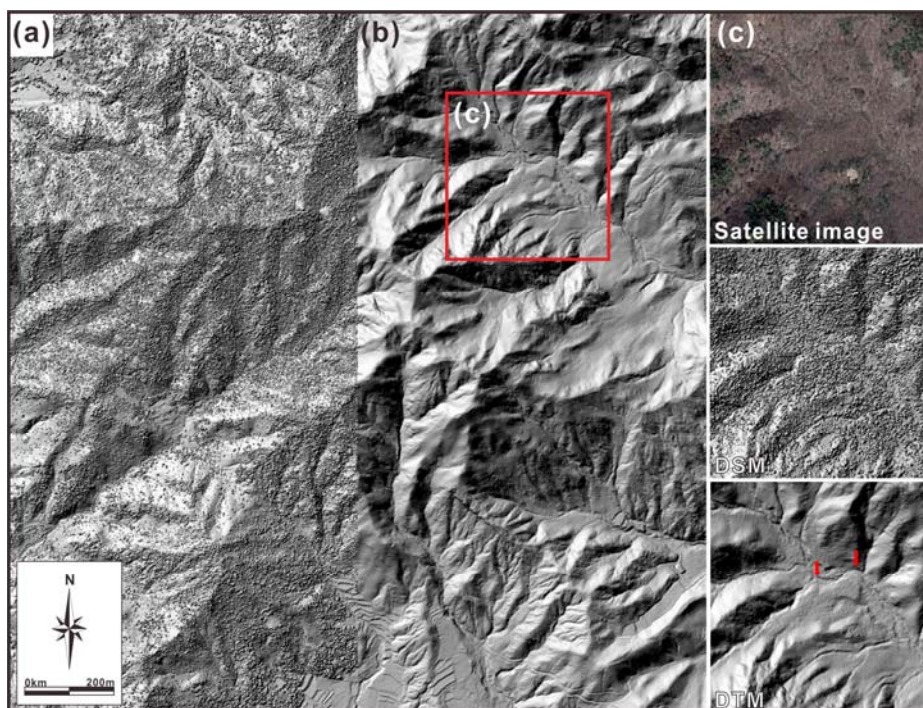


Fig. 4: Satellite image and airborne LiDAR mosaic image of Mt. Bomun in Daejeon. (a) Before removing vegetation (DSM), (b) after removing vegetation (DTM), and (c) image comparison among satellite, DSM, and DTM images for the same area. Arrows in the DTM image indicate a stream that is offset across the lineament.

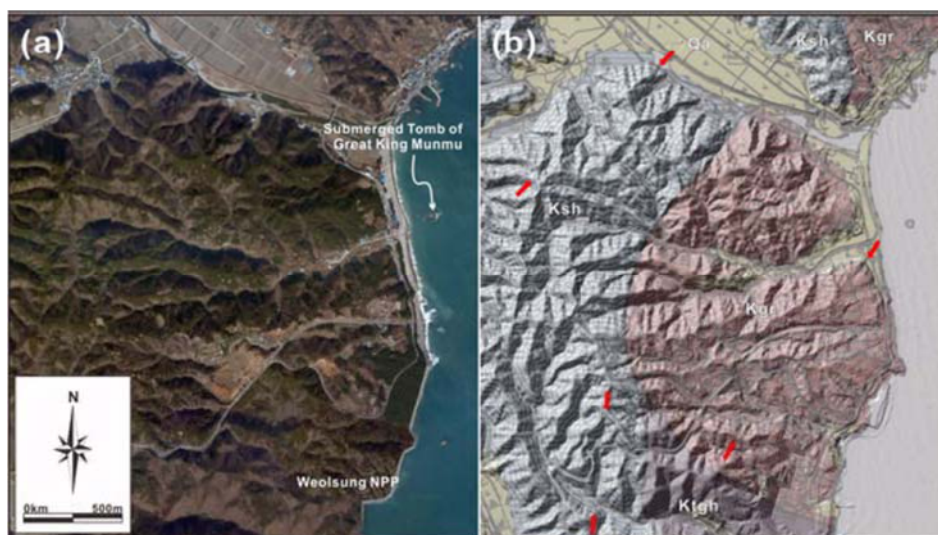


Fig. 5: Analysis of airborne LiDAR data from the Weolsung area, SE Korea. (a) Satellite image of the study area (image is from the Daum map), and (b) bare earth image with geological map (modified from Korea Institute of Geoscience and Mineral). Red arrows indicate lineaments. Ksh: black shale, Kgr: Bulguksa Group biotite granite, Ktgh: Bulguksa Group hornblende granite, Qa: Quaternary deposit.

CONCLUSION

In this study, we analysed already collected data and we were able to remove a high percentage of vegetative cover and, as software applications improve we will be able to create higher quality images. Moving to the

future, we must also look at creating new higher quality images.

The characteristics of vegetation in Korea are of great importance. One of the most difficult data accumulation issues is the high vegetation cover in South Korea. The transmission of Airborne LiDAR can change depends on season, with 20-40% transmissivity in the summer which results in poor imagery and a huge increase to around 70% in the winter (Yoon and Lee, 2006). It is quite obvious



that if we collect data at a suitable time of year, when the level of transmissivity is highest, we would be able to get far superior images to work with.

Acknowledgements: We thank to reviewers of this paper.

References

- Arrowsmith, J. R. and Zielke, O., 2009, Tectonic geomorphology of the San Andreas Fault zone from high resolution topography: An example from the Cholame segment. *Geomorphology*, 113, 70-81.
- Blair, J. B., Rabine, D. L., and Hofton, M. A., 1999, The laser vegetation imaging sensor: a medium-altitude, digitisation-only, airborne laser altimeter for mapping vegetation and topography. *Journal of Photogrammetry and Remote sensing*, 54, 115-122.
- Chung, D. K., Goo, S. H., Eo, J. H., and Yoo, H. H., 2005, DTM Extraction from LiDAR data by filtering method. *GIS/RS Joint Spring Symposium, Construction Engineeris Hall*, 19 May 2005, 355-361.
- Han, J. -G., Kim, S. -P., Chang, D. -H., and Chang, T. -S., 2009, Estimation of inundation damages of urban area around Haeundae beach induced by super storm surge using airborne LiDAR data. *The Journal of GIS Association of Korea*, 17(3), 341-350.
- Haugerud, R. A. and Harding, D. J., 2001, Some algorithms for virtual deforestation (vdf) of lidar topographic survey data. *International Archives of Photogrammetry and Remote Sensing*, 34-3(W4), 211-217.
- Haugerud, R. A., Harding, D. J., Johnson, S. Y., Harless, J. L., Weaver, C. S., and Sherrod, B. L., 2003, Highresolution LiDAR topography of the Puget Lowland, Washington-a bonanza for earth science. *GSA Today, Geological Society of America* 13(6), 4-10.
- Kim, Y. -S., Kihm, J. -H., and Jin, K., 2011, Interpretation of the rupture history of a low slip-rate active fault by analysis of progressive displacement accumulation: an example from the Quaternary Eupcheon Fault, SE Korea. *Journal of the Geological Society*, 168, 273-288.
- Kraus, K. and Pfeifer, N., 1998, Determination of terrain models in wooded areas with airborne laser scanner data. *Journal of Photogrammetry and Remote Sensing*, 53, 193-203.
- Kyung, J. -B., 1997, Paleoseismological study on the Mid-northern part of Ulsan Fault by trench method. *The Journal of Engineering Geology*, 7(1), 81-90.
- Lee, I., 2006, A feature based approach to extracting ground points from LiDAR data, *Korean Journal of Remote Sensing*, 22(4), 265-274.
- Yoon, J. -S. and Lee, K. -S., 2006a, Prospects for understanding forest structure using LiDAR. Proceedings of the KSRS spring conference, *Korean Journal of Remote Sensing*, 149-152.
- Yoon, J. -S., Lee, K. -S., Shin, J. -I., and Woo, C. -S, 2006b, Characteristics of airborne LiDAR data and ground points separation in forested Area. *Korean Journal of Remote Sensing*, 22(6), 533-542.
- Zhang, K., Chen, S. -C., Whitman, D., Shyu, M. -L., Yan, J., and Zhang, C., 2003, A progressive morphological filter for removing nonground measurements form airborne LiDAR data. *IEEE Transactions on Geoscience and Remote Sensing*, 41(4), 872-882.



Damaged speleothems and their implications for paleo-earthquakes: A case study from Seongryu Cave in Uljin, Korea

Jin-Hyuck Choi, Young-Seog Kim

Dept. of Earth & Environmental Sciences, Pukyong National University, Busan 608-737, South Korea. Email: cjh9521@pknu.ac.kr

Abstract: This study investigates the damage and/or regrowth characteristics of speleothems: stalactites, stalagmites, columns, and curtains, in limestone Seongryu Cave in Uljin, Korea, and examines their relationships with paleo-earthquakes. Some stalactites were broken along a sub-horizontal cutting plane and have fallen to the floor of the cave. Stalagmites were tilted 20°~30° to the east or truncated. Columns, joined speleothems of stalactites and stalagmites, were broken by low dipping thrust faults. The strike of all fault planes is within the range of N20°~40°E and dips are between 10°~20°N. Most of the offset is relatively constant (around 0.1 m). On the cave wall, convex-shaped re-growths of speleothems can be observed along minor fractures, and these fractures can be classified into two dominant fracture sets (N60°E~E-W/20°~40°NW and N30°~50°W/20°NE or 20°SW). The damage and regrowth patterns are various, and depend on the type of speleothems. Each type shows, however, a relatively consistent kinematic deformation pattern. These results indicate that the destruction and re-growth of speleothems in Seongryu Cave may be due to ground shaking or surface rupturing resulting from an earthquake rather than other causes such as human activity.

Key words: Seongryu Cave, speleothems, damaged characteristics, re-growth, paleo-earthquake.

INTRODUCTION

The term 'speleoseismite' can be defined as speleothems in caves damaged by an earthquake (e.g. Cadorn et al., 2001; Lacave et al., 2004; Kagan et al., 2005). Recently, paleoseismological studies based on speleoseismites are actively being carried out due to the very high accuracy in age dating analysis, in particular for the past 500,000 years (Kagan et al., 2005; Braun et al., 2010). This method can be very useful in regions characterized by long recurrence intervals of earthquakes, because it is difficult to approach paleo-earthquakes which have occurred before instrumental and historical times.

One of the most notable studies using speleoseismites has been performed by Kagan et al. (2005). They interpret the recent history of paleo-earthquakes along the Dead Sea Transform based on damaged

speleothems and their age information in the limestone caves near the fault. This is well represented in Figure 1. They focus mainly on damaged or fractured stalagmites and their regrowth (Fig. 1a), collapsed ceilings with pre-seismic stalactites and post-seismic stalagmites (Fig. 1b), and fallen ceiling pieces on the core sample from a flowstone deposit (Fig. 1c). Furthermore, the age data for a wide range of well-preserved damaged speleothems were used to interpret a temporal history of multiple earthquakes (Fig. 1d-e).

This study focuses on the damage patterns of speleothems in the Seongryu Cave in Uljin, Korea. For this purpose, a structural analysis of damaged or regrown speleothems was carried out. Then, several other factors associated with paleo-earthquakes, such as large-scale or Quaternary faults near the cave and historical earthquake distributions are discussed in detail.

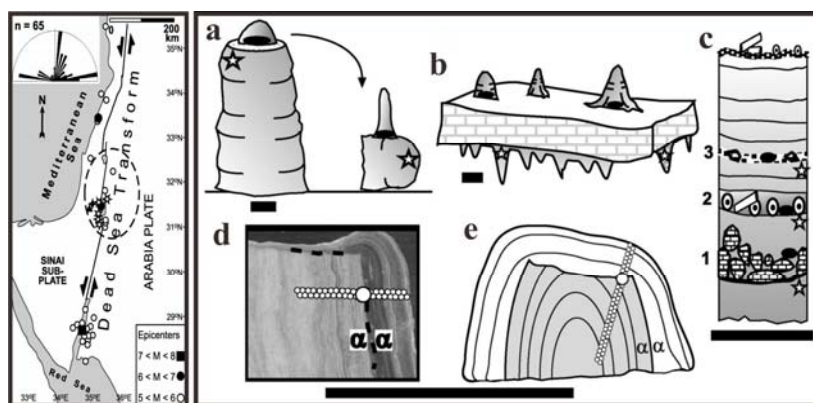


Fig. 1: An example of a paleoseismology study using speleothems in caves along the Dead Sea Transform (from Kagan et al., 2005). Open stars and solid ellipses mark pre- and post-earthquake deposits, respectively, and scale bars = 10 cm.

STUDY AREA & SEONGRYU CAVE

Seongryu Cave is located at the eastern part of the Korean Peninsular, and developed in the Ordovician Geunnam Formation of the Joseon Supergroup. Predominant deformational features around the cave group in two sets: N-S to NNE-SSW and NE-SW trending compressive structures like folds and thrust faults. Maehwa Fault, a N-S trending and vertically dipping fault, is developed next to the cave, and the NE-SW trending Quaternary Gusan Fault is located 2.5 km southwest of the cave.

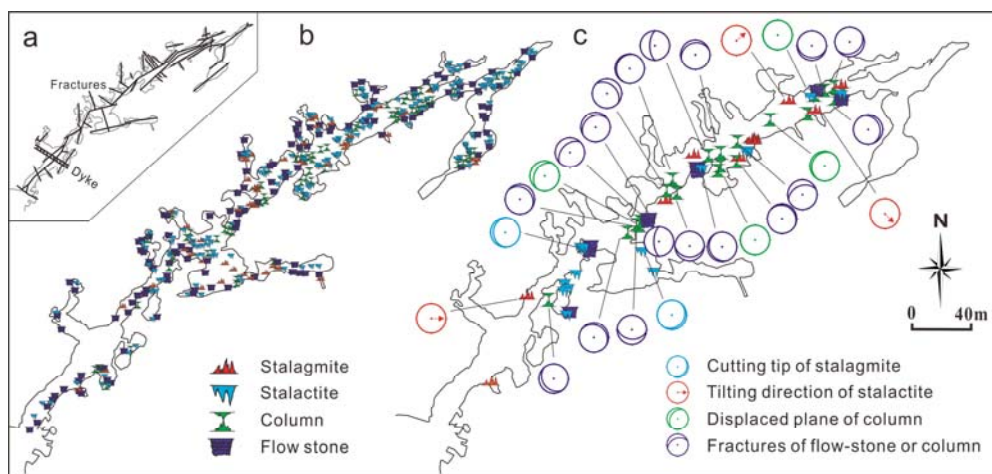


Fig. 2: Distributional maps of the fractures (a); modified from the Cave Research Institute of Korea, 2007), dominant speleothems (b), and damaged speleothems (c) in the Seongryu Cave.

For the Seongryu Cave, the main passage and branches are about 330 m and 540 m, respectively, making the total length of the cave about 870 m (Cave Research Institute of Korea, 2007). The bedding is approximately NE-SW trending, and is characterized by subvertical or slightly southeastern dip. Figure 2a shows a map of the cave as well as a distribution of geologic structures which were mapped in the cave. This cave is one of the most common corrosion caves around the study site (Cave Research Institute of Korea, 2007), and seems to be mainly developed along the structural discontinuities such as bedding and fractures.

STRUCTURAL ANALYSIS

Stalactites

Stalactites, one of the most common speleothems in limestone caves, are generally formed by deposition of calcium carbonate and other minerals, which are precipitated from mineralized water solutions. Stalactites in the Seongryu Cave are frequently observed and characterized by various dimensions and vertical lengths of 1-5 m. Numerous stalactites are broken, but only their lower part appears to be damaged by subhorizontal cutting planes. The fallen fragments are often well preserved on the cave floor. In some cases, new stalactites have developed on the cutting plane, resulting from the continuous flow of fluids after the damages occurred.

Stalagmites

A stalagmite is defined as a type of rock formation that rises from the floor of a cave due to the accumulation of material deposited on the floor from ceiling drippings, and commonly developed in limestone caves. They form through deposition of calcium carbonate and other minerals, which is precipitated from mineralized water solutions.

Although the extent and density of the damage on stalagmites in the Seongryu Cave is relatively lower than

that of other speleothems, some of them are obviously tilted or fallen down. Note that they are characterized by a similar direction and angle of the tilting: they dip to the east with angles of about 20°. One of the most interesting points is the re-growth of tilted stalagmites, which can be inferred by different colours and a vertical boundary between them.

Columns

A column in limestone caves can be formed by the connection between stalactites (ceiling formation) and stalagmites on the floor. The columns are generally characterized of hourglass shape. Columns are frequently observed all over the Seongryu Cave, and some of them have separated by either subhorizontal extension fractures or low angle faults (Fig. 3). Note that numerous broken stalactites and their fragments are observed around the deformed columns. As the deformed columns themselves act as an offset marker on each five columns, the strike/dip of the fault planes, shear senses, and amounts of displacement were measured. The results indicate that the strike of all fault planes is within the range of N20~40°E and dips are around 10~20°NW. Additionally, the amount of offset is relatively constant (around 0.1 m), with only one exception.

Flowstone

Flowstones are composed of sheet-like deposits of calcite formed where water flows down the walls or along the floors of a cave, and they are typically found in limestone caves. As flowstones cover basement rocks, they can be one of the most obvious evidences of rock deformation associated with paleo-earthquakes. Numerous flowstones in the Seongryu Cave are fractured and some of them are filled with newly deposited calcite (Fig. 4). In the latter case, they commonly show a projecting pattern and different colours with their surrounding undamaged flowstones. This may result from a local regrowth of speleothems by

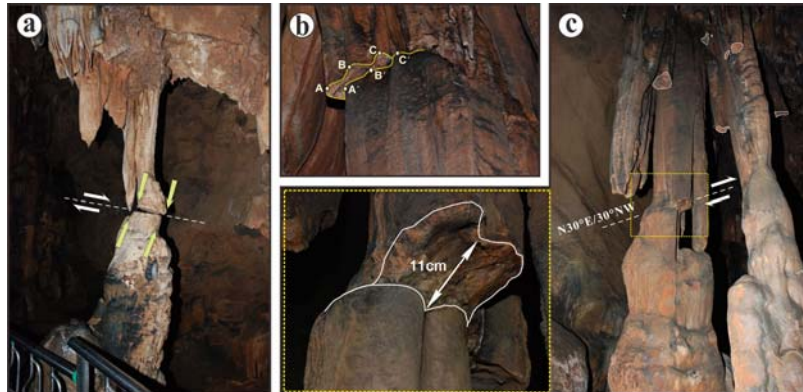


Fig. 3: Most of the damaged columns are displaced by sub-horizontal fault planes (a, b). Some of them show typical characteristics of thrust faulting (c).

concentration of fluid flow along the fractures. On the cave wall, a convex-shaped regrowth of speleothems and their related fractures can be classified into two dominant sets: set-1 of N60°E~E-W/20~40°NW and set-2 of N30~50°W/20°NE or 20°SW (Fig. 4e)

IMPLICATIONS FOR PALEO-EARTHQUAKE

Deformed speleothems show various patterns of deformation, such as cutting, tilting, fracturing, and faulting, depending on the kind of speleothems. On the other hand, the result of field-based structural analysis indicates that deformational characteristics for each speleothem are relatively consistent in mainly orientation and dip of fractures (including cutting planes) and faults. In the latter case, the sense and amount of slips are also almost same. Furthermore, the low angle of dip of fractures and faults is a common feature even if the kinds of speleothems are different. Note that these consistent patterns of deformed speleothems may indicate that deformations occurred due to tectonic process rather than other origins.

Concerning the possible origins of the deformation, firstly the stalactites can be cut or broken either by human activities, such as tourism development and vandalism, or by natural effects, such as cave floods and earthquakes. As some deformed stalactites are observed at a high level and out of reach of humans, we argue that the natural origins are more likely to have caused the deformation. The sharpness of the cutting planes may support that falling stalactites have been caused by pre-existing fractures and/or external impacts. Secondly, the stalagmites can only be tilted from natural causes, and we argue that there are two possibilities: One is the erosion of cave deposits on the

floor and associated chambers, and this is supported by local false floors under the flowstones. Another origin can be ground motion due to earthquakes. The similarity in the direction and angle of tilting may indirectly support this argument. Next, the consistent displacement of slip surfaces on the columns is one of the most remarkable evidences of earthquake-derived deformation. In particular, this argument can be supported by numerous fractures that are intensely developed around faulted columns as well as by several faulted columns showing a giant

size that cannot be broken by human activities. Lastly, the consistency of fractures on flowstones, which can be inferred as the extension of the fractures on the basement rock, is also one of the structural characteristics of the tectonic deformation.

The results of the field-based structural analysis imply that the damaged speleothems in Seongryu Cave have been deformed probably by natural or external forces such as ground shaking and fault movement associated with paleo-earthquakes (Fig. 5). This interpretation is the first identification of speleoseismites in Korea.

In order to more clearly identify the speleoseismite, it is necessary to examine active tectonics around the cave. Maehwa Fault is the nearest large-scale fault around the Seongryu Cave, and characterized by its surficial expression as a N-S trending and at least 27 km long lineament. The fault zone elements indicate that the fault underwent dominantly strike-slip movement, and left-lateral slip sense can be inferred based on the offset of basement rocks. Gusan Fault, one of the Quaternary faults around the study site, shows N30°E/55°SE and is

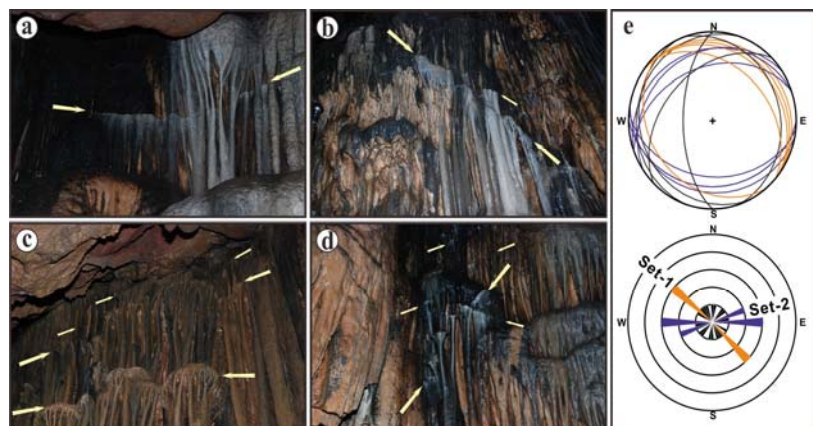


Fig. 4: Damage patterns on curtains show minor fractures and regrowth of speleothems along them (a-d). These fractures can be classified into two dominant fracture sets (e).

characterized by a dominant left-lateral fault movement. Quaternary slip was inferred as about 94.63 cm based on

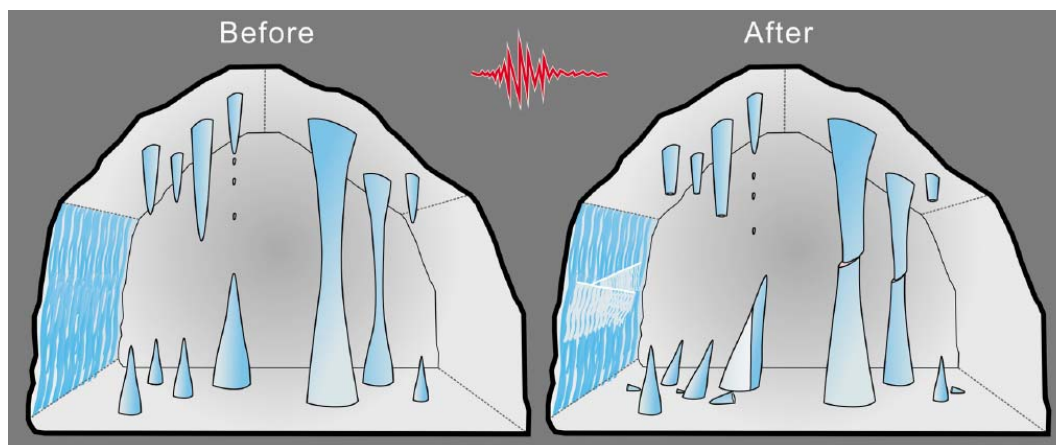


Fig. 4: A schematic diagram showing possible damage to speleothems during paleo-earthquakes.

the slickenline (24° → 220°) and apparent displacement of Quaternary fluvial deposits (0.4 m). The inferred moment magnitude (M_w) is in a range of 6.4-6.9 based on the inferred slip amount, and if it is supposed as one event (Jin et al., 2013). The OSL and Be^{10} ages of the Quaternary sediments are 41-50 ka and 80-88.4 ka, and the ESR age of the fault gouge is 369 ka (Jin et al., 2013).

Two above mentioned faults have some geometric and kinematic similarities with those of the cave. The results of structural analysis for two fault zones indicate that a strike-slip movement was dominant along these faults. Note that the main trends of two faults (nearly N-S and NE-SW directions, respectively) match well with the results of lineament analysis. Especially the NE-SW direction is also parallel to the main trend of the cave and its fractures. Although it is not easy to correlate fault activity and speleoseismites in Seoungryu Cave, we argue that in future studies these faults should be carefully considered as one possible source of paleo-earthquakes that lead to the formation of speleoseismites.

FURTHER STUDY

One of the advantages of speleoseismology is that it allows precise dating using a high-resolution stable or radioactive isotope record on the speleothems. Note that age information can be used to infer the timing of each earthquake and the recurrence interval. These are key data in paleoseismological studies (e.g. Kagan et al., 2005). One of the main characteristics of speleoseismites in Seoungryu Cave is the regrowth or new deposition on damaged parts of speleothems, such as small stalactites on the cutting planes, vertical regrowth of stalagmites on tilted or broken speleothems, and convex-shape

regrowth along fractures. Thus, in further study, it is needed to examine the age dating of damaged and newly deposited speleothems to understand the relationship between speleoseismites and paleo-earthquakes.

Acknowledgements: We would like to thank Dr. Kim, Ryeon for his help for cave exploration. We greatly value the careful review undertaken by Dr. Elisa Kagan

References

- Braun, Y., Kagan, E., Bar-Matthews, M., Ayalon, A. and Agnon, A., 2010. Dating speleoseismites near the Dead Sea Transform and the Carmel Fault: Clues to coupling of a plate boundary and its branch. *Isr. J. Earth Sci.*; 58: 257-273.
- Cadorin, J.F., Jongmans, D., Plumier, A., Camelbeeck, T., Delaby, S. and Quinif, Y., 2001. Modelling of speleothems failure in the Hotton cave (Belgium): Is the failure earthquake induced?. *Netherlands Journal of Geosciences/Geologie en Mijnbouw*, 80, 315-321.
- Cave Research Institute of Korea, 2007, Scientific investigation of the Seoungryu Cave, Uljington, Gyeongsangbukdo, Korea. 28-163 pp (in Korean with English abstract).
- Jin, K., Kim, Y.-S., Kang, H.C. and Shin, H.C., 2013, Study on developing characteristics of the Quaternary Gusan Fault in Uljin, Gyeongbuk, Korea. *Journal of the Geological Society of Korea*, 49(2), 197-207 (in Korean with English abstract).
- Jun, M.-S. and Jeon, J.S., 2010, Focal Mechanism in and around the Korean Peninsula. *Jigu-Mulli-wa-Mulli-Tamsa*, 13, 198-202 (in Korean with English abstract).
- Kagan, E.J., Agnon, A., Bar-Matthews, M. and Ayalon, A., 2005, Dating large infrequent earthquakes by damaged cave deposits. *Geology*, 33, 261-264.
- Lacave, C., Koller, M.G. and Egozcue, J.J., 2004, What can be concluded about seismic history from broken and unbroken speleothems?. *Journal of Earthquake Engineering*, 8, 431-455.



Preliminary study on developing characteristics of the Quaternary Gusan Fault

Kwangmin Jin (1), Young-Seog Kim (2), Hee Cheol Kang (2), Hyeon Cho Shin (3)

- (1) Mineral Resources Research Division, Korea Institute of Geoscience and Mineral Resources (KIGAM), Daejeon, Korea.
 Email: maxgarion@kigam.re.kr
 (2) Dept. of Earth & Environmental Sciences, Pukyong National University, Busan 608-737, South Korea.
 (3) Civil & Architecture Engineering Department, KEPCO Engineering & Construction Company, Inc., Sungnam, Korea.

Abstract: The Gusan Fault is a Quaternary fault discovered in the middle east part of the Korean peninsula, which affects Quaternary fluvial deposits as well as Precambrian leucocratic granite gneiss. Slickenlines on the surface of the Gusan Fault indicate strike-slip dominant movement sense. Age dating results on the Quaternary fluvial deposits and fault gouges of the Gusan Fault demonstrate that the NE-SW trending Gusan Fault might be activated at least two times within 500 ka B.P. Based on the trench survey across the fault in the Quaternary fluvial deposits covering the basement, aligned long axes of pebbles within the Quaternary fluvial deposits indicate that the Gusan Fault was activated after the development of the Quaternary fluvial deposits. The inferred slip associated with the Quaternary fault movement, based on a suggested relationship between true displacement and apparent displacement, is about 1 m. It is a good indication of neotectonics in this area and to be studied in detail, although this fault is a small scale fault.

Key words: Quaternary Gusan Fault, strike-slip fault, fluvial deposits, trench survey

INTRODUCTION

The studied area lies between the northeastern part of the Yeongnam Massif and the northern part of the Gyeongsang Basin. The basement around the study area consists of Precambrian gneiss and Paleozoic sedimentary rocks. These rocks have been intruded by Mesozoic and Cenozoic igneous rocks (Fig. 1).

The area around the Gusan Fault is comprised by Precambrian leucocratic granite gneiss, which is partially covered by the Quaternary fluvial deposits (Yun & Shin, 1963), some of which are related with river meandering. The major geologic structure in this area is the N-S trending Maehwa Fault. The Gusan fault located about 2 km from the Maehwa Fault to the west. Based on the aerial photograph and lineament analysis, N-S, NNE-SSW and ENE-WSW trending lineaments are well developed around the Gusan Fault (Fig. 2).

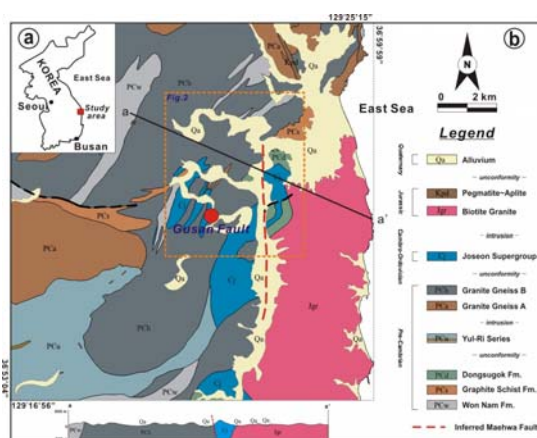


Fig. 1. Location and geological maps around the study area (modified from the Yun & Shin, 1963).

GENERAL GEOLOGY

The studied area lies between the northeastern part of the Yeongnam Massif and the northern part of the Gyeongsang Basin. The basement around the study area consists of Precambrian gneiss and Paleozoic sedimentary rocks. These rocks have been intruded by Mesozoic and Cenozoic igneous rocks (Fig. 1).

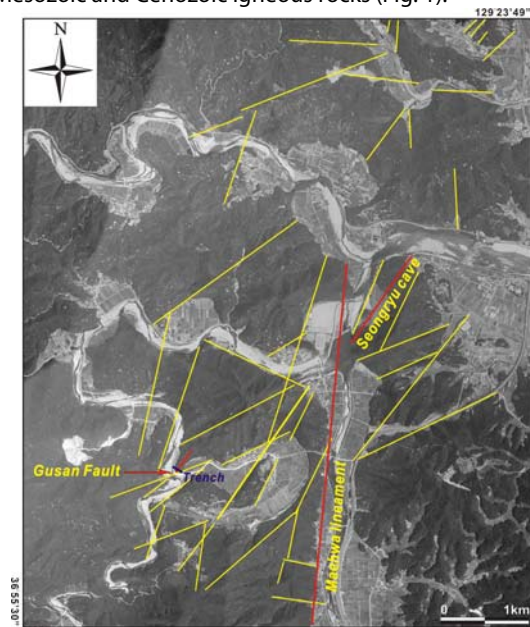


Fig. 2. Aerial photograph and lineament analysis around the Gusan Fault. It shows the N-S, NNE-SSW and ENE-WSW trending lineaments. Red lines show the Seongryu Cave, Gusan and Maehwa faults. Yellow lines indicate dominant lineaments around the study area. The small blue line shows the location and direction of the trench across the Gusan Fault.



The area around the Gusan Fault is comprised by Precambrian leucocratic granite gneiss, which is partially covered by the Quaternary fluvial deposits (Yun & Shin, 1963), some of which are related with river meandering. The major geologic structure in this area is the N-S trending Maehwa Fault. The Gusan fault located about 2 km from the Maehwa Fault to the west. Based on the aerial photograph and lineament analysis, N-S, NNE-SSW and ENE-WSW trending lineaments are well developed around the Gusan Fault (Fig. 2).

GENERAL DESCRIPTION OF THE GUSAN FAULT

The Gusan Fault is discovered at the road-cut section in the western part of the Maehwa Fault, which is located about 2 km away from the Maehwa Fault (Fig. 2). The Gusan Fault cuts the Precambrian granite gneiss and Quaternary fluvial deposits (Fig. 3). The Quaternary fluvial deposits are relatively poorly sorted, showing grain size variation of pebbles. Slickenlines on the Precambrian granite gneiss show strike-slip movement with 25 cm vertical separation in the road-cut section (Fig. 3). The general attitude of the Gusan Fault in the Precambrian leucocratic granite gneiss is N30°E/55°SE and the lineation of the slickenlines is 24°→220° on the fault, and the thickness of the fault gouge zone is approximately 1 cm (Fig. 3). This fault gouge zone is also observed in the fluvial deposits indicating faulting event after the deposition. However, the dip-angle of the fault plane is 42° in the fluvial deposits indicating dip-angle decrease toward the surface.

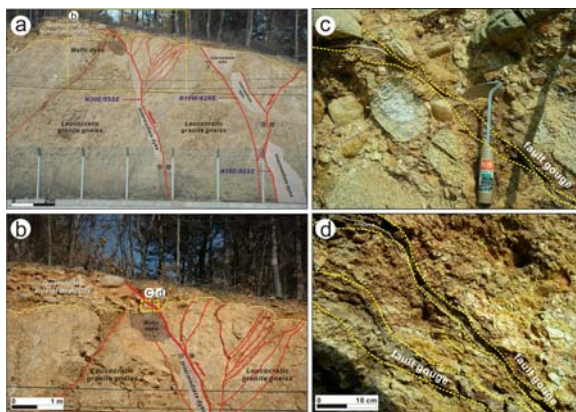


Fig. 3. Photographs of the Gusan Fault. (a) Overview and sketch of the Gusan Fault. (b) Detailed photograph and sketch of the upper part of the fault. The fault cuts the Precambrian leucocratic granite gneiss and Quaternary fluvial deposits. Red color lines show the fault and fractures associated with the Gusan Fault. (c) & (d) Detailed photographs and sketch of the fault gouge in the Quaternary fluvial deposits. The brown color gouge cuts the Quaternary fluvial deposits.

TRENCH SURVEY ON THE GUSAN FAULT

To understand the characteristics of the Gusan Fault, we dig a new trench in the upper part of the exposed Gusan Fault (Fig. 4). The orientation of the trench is N46°W, almost perpendicular to the fault. We excavated the trench as a single slot (California-style) type (McCalpin, 1996). The width of the trench is 1 m, the maximum depth is 2.3 m, and the length is about 3.5 m (Fig. 4). Log of the trench section was made using 0.5×0.5 m grids. Figure 4b & 4c shows a photo mosaic and simplified sketch of the section. The poorly sorted fluvial deposits consist of mixture of well-rounded boulders and pebbles, and sand (Fig. 4). Boulders and pebbles mainly composed of leucocratic granite gneiss and volcanic rocks (Fig. 4). The long axis of the dominant boulders is about 40-50 cm (Fig. 4).

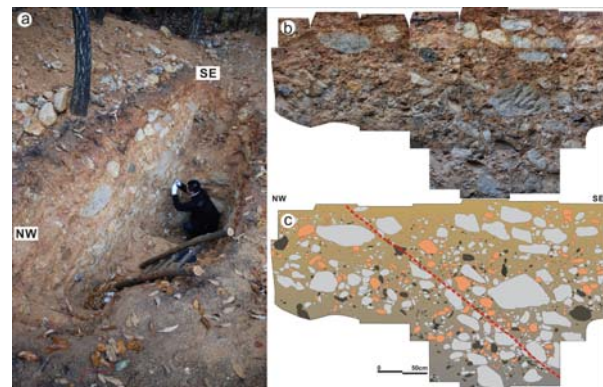


Fig. 4. Photographs of the trench of the Gusan Fault. (a) Overview of the trench across the Gusan Fault developed in the Quaternary fluvial deposits. (b) & (c) Photomosaic and sketch of the northern trench wall of the upper part of the Gusan Fault. The dotted line indicates the inferred fault trace showing clast fabrics. It indicates that the Gusan Fault obviously passes the Quaternary fluvial deposits.

In general, fault zones in clast-rich unconsolidated deposits are identified by consistent clast fabric different from adjacent strata (McCalpin, 1996). The shear along fault plane may rotate clasts resulting in the long axes of the pebbles parallel to the fault plane called. Strike-slip fault movement would rotate clasts into near-vertical orientations (long axes aligned with dip direction) (Yount et al., 1987). In the trench of the Gusan Fault, this kind of preferred orientation is observed along the inferred fault plane (Fig. 4). The dip-angle of the aligned boulders and pebbles is about 39°SE (Fig. 4). This angle is very similar to the dip of fault gouge in the fluvial deposits on the road-cut section. Similar cases have already been reported in the surface rupture associated with 1999 Chi-Chi earthquake in Taiwan and the East Bear Lake fault in Utah (Fig. 5).

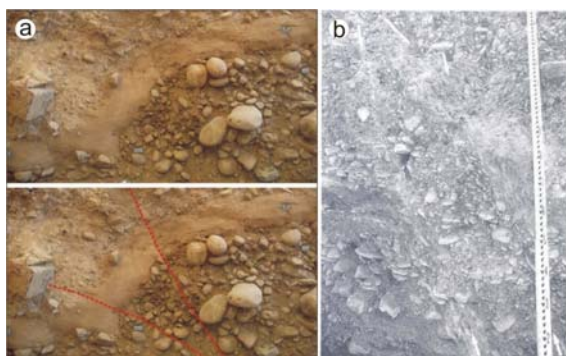


Fig. 5. Examples of the clast fabric. (a) Clast fabric associated with the 1999 Chi-Chi earthquake. (b) Clast fabric along the East Bear Lake Fault, Utah. Note that anomalous parallel clast fabric and slight discoloration of gravel along the fault planes.

DISCUSSION

Inferred slip associated with the Quaternary fault movement

A method to get true displacement based on the relationship between apparent displacement and true displacement is suggested by Xu et al., (2009). It is useful for the following three cases. First, observed section of outcrops may not be occasionally vertical. Second, the bedding plane is not horizontal or the strike of the bedding plane is not parallel to the fault plane. Third, faults are not complete dip- or strike-slip faults (Xu et al., 2009).

Although the Gusan Fault shows sub-horizontal slickenside lineation on the fault plane (24° → 220°), we could not detect the true displacement on the horizontal plane because the fault is covered by the Quaternary fluvial deposits. Hence, we adopted the approach to obtain the true displacement using an apparent displacement measured from an arbitrary line on a fault plane, which is introduced by Xu et al. (2009).

The equation is as follow:

$$S_t = S_m \sin(\varphi + \beta) / \sin(\gamma + \beta) = S_m / \sin(\gamma) \quad (1)$$

Here, S_t is the true displacement, S_m is the apparent displacement, φ is the pitch of the observation line on the fault plane, γ is the pitch of slip lineation, β is the pitch of a cutoff (Xu et al., 2009). On the Gusan Fault, the considered parameters of the fault are as follows: S_m is 40 cm, φ is 90° , γ is 24° → 220° , β is 0° . The calculated true displacement of the Gusan Fault, based on Eqs. (1), is 94.63 cm.

Age of the Gusan Fault

The age of a fault is one of important factors in the analysis of earthquake hazard. KOPEC (2008) have attempted to date the Quaternary fluvial deposits and fault gouges using optical stimulated luminescence (OSL), electron spin resonance (ESR), and ^{10}Be . Although these studies yielded inconsistent age data, based on OSL analysis the ages of the fluvial deposits may lie in the range of 41-50 ka. ESR analysis for the Gusan Fault

results in 369 ka. However, ^{10}Be age analysis indicates in the range of 80-88.4 ka. More data and logical interpretation are necessary to determine the exact faulting events because the data were obtained from different methods.

Although the number of faulting events is another concern in active fault study, there is no distinct evidence to interpret deformation events such as deformed colluvial wedges or stratigraphic offsets (e.g. Burbank & Anderson, 2001; Keller & Pinter, 2002). Therefore, further work is necessary to determine the number of deformation events along the Gusan Fault.

CONCLUSION

The Gusan Fault cuts the Precambrian basement as well as the Quaternary fluvial deposits indicating an active fault. Slickenlines on the fault plane indicate dominantly strike-slip movement. Based on the trench survey in the Quaternary fluvial deposits, aligned long axes of pebbles in the Quaternary fluvial deposits demonstrate that the Gusan Fault was activated after the deposition of the fluvial deposits. The inferred true slip associated with the Quaternary fault movement is about 94 cm. Although the age data related with the Quaternary fluvial deposits and fault gouges, they demonstrate that the Gusan Fault probably activated two times within 500 ka B.P.

Acknowledgements: This research was supported by the Basic Research Project (14-1121) of the Korea Institute of Geoscience and Mineral Resources (KIGAM) funded by the Ministry of Science, ICT and Future Planning of Korea.

References

- Burbank, D.W. & Anderson, R.S. (2001). Tectonic Geomorphology. *Blackwell Science*, Oxford.
- Keller, E.A. & Pinter, N. (2002). Active Tectonics: Earthquake, Uplift, and Landscape, 2nd edn. Prentice Hall, Englewood Cliffs, NJ.
- Kim, Y.-S., Park, J.Y., Kim, J.H., Shin, H.C. & Sanderson, D.J. (2004b). Thrust geometries in unconsolidated Quaternary sediments and evolution of the Eupcheon Fault, southeast Korea. *The Island Arc* 13, 403-415.
- Kim, Y.-S., Peacock, D.C.P. & Sanderson, D.J. (2004a). The fault damage zones. *Journal of Structural Geology* 26, 503-517.
- Korea Institute of Geology, Mining & Materials (KIGAM). (1998). An Investigation and Evaluation of Capable Fault: Southeastern Part of the Korean Peninsula. 301p. (in Korean with English abstract).
- Korea Power Engineering Company (KOPEC) (2002). The Preliminary Site Assessment Report (PSAR) for the new Weolsung Reactors 1 and 2, Unpublished Report. KOPEC, Yongin.
- Korea Power Engineering Company (KOPEC) (2008). The Preliminary Site Assessment Report (PSAR) for the new Uljin Reactors 1 and 2, Unpublished Report. KOPEC, Yongin.
- Kyung, J.B. & Chang, T.W. (2001). The Latest Fault Movement on the Northern Yangsan Fault Zone around the Yugye-Ri Area,



INQUA Focus Group on Paleoseismology and Active Tectonics



paleoseismicity.org

Southeast Korea. *Journal of the Geological Society of Korea* 37, 563-577 (in Korean with English abstract).

McCalpin, J.P. (2009). *Paleoseismology*, Second Edition. Academic Press, San Diego, 588p.

Ree, J.-H., Lee, Y.-J., Rhodes, Ed J., Park, Y., Kwon, S.-T. Chwae, U., Jeon, J.-S. & Lee, B. (2003). Quaternary reactivation of Tertiary faults in the southeastern Korean Peninsula: Age constraint by optically stimulated luminescence dating. *The Island Arc* 12, 1-12.

Xu, S., Nieto-Samaniego, A.F. & Alaniz-Álvarez, S.A. (2009). Quantification of true displacement using apparent displacement along an arbitrary line on a fault plane. *Tectonophysics* 467, 107-118.

Yount, J.C., Shroba, R.R., McMasters, C.R., Huckins, H.E. & Rodriguez, E.A. (1987). Trench logs from a stand of the Rock Valley fault system, Nevada Test Site, Nye County, Nevada. U. S. *Geol. Surv. Misc. Field Stud. Map MF-1824*, Scale 1:20.

Yun, S.K. & Shin, B.W. (1963). Geological report of the Uljin sheet (1:50,000). Geological Survey of Korea, 1-23 pp (in Korean with English abstract).



Operation and Management of Eupcheon Fault Monitoring System in South Korea

Jong Sun Hwang, Sung-Il Cho, Weon-Hack Choi, Jae-woong Ryu

Korea Hydro & Nuclear Power Co., Ltd. 1312-70 Yuseong-daero, Yuseong-gu, Daejeon, Korea (estwing@khnp.co.kr)

Abstract: The Eupcheon Fault Monitoring System (EFMS) has been operated by Korea Hydro & Nuclear Power Co., Ltd from Jan, 2012. Fault movements and seismic events were monitored by seismometers, strainmeters, creepmeter, GNSS, and other gauges, etc. The trend of compression signal, atmosphere and earth tide effect were removed. 4-directional raw data values from the strainmeters were converted to 3-directional (areal, gamma1, gamma2) nanostrain data. Seasonal variations of the creepmeter were also removed by extracting the common components from temperature. GNSS data showed mainly atmospheric effects. Several earthquake occurred in vicinities of EFMS but did not show any reactivation or movement of fault. The enhanced monitoring system will contribute significantly in geo-tectonic safety assessment of nuclear plants and other critical facilities related to the national security.

Key words: Eupcheon Fault, Strainmeter, Creepmeter, GNSS

Introduction

Eupcheon Fault Monitoring System (EFMS) was constructed to identify seismic safety around Shin-wolsung Nuclear Power Plant site and Build up the foundation for study on fault movement and predicting earthquakes (Cho et al., 2012; KHNP, 2011). Central Research Institute (CRI) of Korea Hydro & Nuclear Power Co., Ltd (KHNP) are operating and monitoring the fault from Jan. 2012. CRI launched the research project related to fault monitoring system in Apr, 2013 and presented several research results via papers. Fig. 1 is the locations of fault monitoring system that shows lots of installed instruments including three seismometers, two strainmeters, two Trimble GNSS, one creepmeter, two groundwater level meters, and other gauges, etc. Observations acquired from those instruments are transmitted to CRI in real time, and data processing for improving data accuracy are implemented

Table 1 shows the details of instruments install near Eupchoen Fault. The GTSM Strainmeter is a high-precision equipment that can measures nano-scale strain in borehole (around 150m depth) and widely used to monitor the changes of strain of active fault. Borehole seismometer was also installed in borehole (around 150 m depth) and measures the stress changes. A Creepmeter is also installed across the fault line and directly measures the movement of fault using 0.025 mm accuracy sensor. Trimble GNSS calculate the relative displacement between EF01 and EF02 site and post-processed with 10-min interval.

Data Processing

GTSM strainmeter data were converted to strain according to GTSM manual (GTSM, 2008). Second, the trends of compression signals were removed by 2nd order polynomial(UNAVCO, 2008). Third, tide and atmospheric pressure effect were corrected using Baytap08 program (Tamura and Agnew, 2008). Finally, 4-directional strains from strainmeter were converted to 3-directional (areal, gamma1, gamma2) nanostrain data. Areal component strain shows the summation of strain from all directions.

Creepmeter is significantly affected by ambient temperatures because the sensor is installed between two Invar rods. In EFMS, without any ground displacement, creepmeter annually changes 0.15mm due to seasonal temperature variations. To remove this effect, displacement and temperature data from 2011 were analysed and pull-out the common components and one-year mean displacement data were extracted.



Fig. 1 Locations of fault monitoring instruments (red dots) and Eupcheon Fault (solid red line)



Table 1. Characteristics of measuring Instruments

		Accuracy	Sensor Depth	Measuring Items
Strainmeter		$> 5 \times 10^{-10}$	EF01 : G.L. -153.3m EF02 : G.L. -175.4m	Strain Value
Water Level Meter	Water Level	$\pm 0.05\text{cm}$	EF01 : G.L. -25m EF02 : G.L. -20m	Groundwater Level, Temperature
	Temperature	$\pm 0.05^\circ\text{C}$		
Borehole Seismometer		62.2 V/m/s (Sensitivity)	EF01 : G.L. -145m EF02 : G.L. -155m	Seismic Wave
GPS		Horizontal : $\pm 5\text{mm}$ Vertical : $\pm 5\text{mm}$	Surface	Displacement
Surface Seismometer		$2 \times 750 \text{ V/m/s}$ (Sensitivity)	Surface	Seismic Wave
Creepmeter	Displacement	$\pm 0.025\text{mm}$	Surface	Displacement, Temperature
	Temperature	$\pm 1^\circ\text{C}$		

Earthquake near Eupcheon Fault

In 2013, four earthquakes that magnitude over 2.0 were observed near Eupcheon Fault. All earthquakes have small magnitude around 2.0 to 3.0, and did not affect fault itself (no strain trend changes were not shown). Fig. 2 shows the strainmeter and seismometer data acquired in 12th, Aug, 2013. The magnitude of earthquake is 3.1 and the distance from the epicentre is around 26km. Both observations showed only dynamic stress effect that did not affect the fault itself. Creepmeter also showed only the effect of temperature variation and GNSS post-processed data affected by the delay from ionosphere.

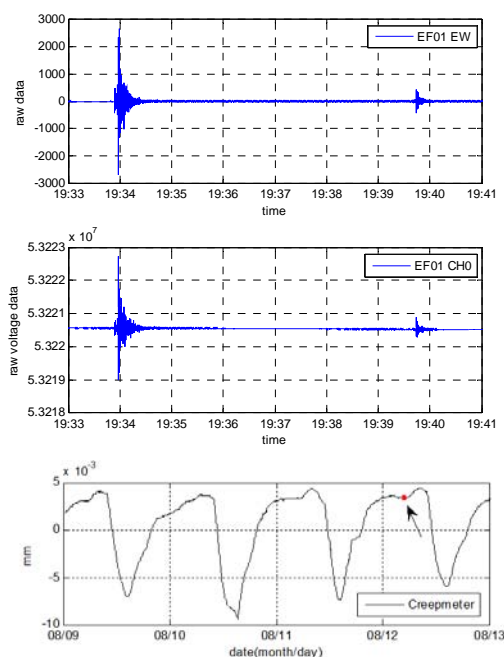


Fig. 2 Earthquake observed by seismometer(upper) and strainmeter(middle). Both data showed the effect of dynamic stress and similar patterns. Creepmeter indicated only temporal undulations (lower).

Conclusion and Discussion

EFMS is installed and operated by CRI, KHNP and cutting-edge instruments are well managed and processed to monitor any activities related to Eupcheon Fault. Each instrument is corrected from environmental errors like tide, temperature, atmospheric pressure, and etc. In 2013, several earthquakes were observed, but any displacement of fault (by creepmeter and GNSS) or changes of strain were not detected yet. It can suggest that Eupcheon Fault is very stable status, and not affected or triggered by earthquake in 2013. However, the small size of earthquake does not allow proving the stability of the fault, which has to be permanently monitored. EFMS can help monitoring the safety of nuclear plants and nuclear waste disposal site near Wolsung Power Plant. Korea radioactive waste Agency (KORAD) also start to operating fault monitoring system in 2014, therefore reliable and detail data can be acquired if both KHNP and KORAD data are combined.

Acknowledgements: This work was partly supported by the Radioactive Waste Management of the Korea Institute of Energy Technology Evaluation and Planning (KETEP) grant funded by the Korea Government Ministry of Trace Industry & Energy (2012171020001).

References

Cho, S.-I., W. -H. Choi, J. S. Hwang, (2012), Analysis of displacement data changes observed by Fault Monitoring System. Annual Conference of the Geological Society of Korea (Abstracts), Jeongseon, October 24-27,20 (in Korean).
 GTSM, (2008), <http://www.gtsmtechnologies.com/strain/unavco/GeneratingStrainData.pdf>.
 KHNP, (2011), The installation report on Eupcheon Fault Monitoring System. 315-316.
 UNAVCO, (2008), Plate Boundary Observatory (PBO) strain meter data, http://cws.unavco.org:8080/cws/learn/uscs/2008/2008strainmeter/handouts/strainmeter_data.pdf
 Tamura, Y.,D. C., Agnew D. C., (2008),
 Tamura, Y, D. C, Agnew, (2008), Baytap08 User's Manual, Scripps Institution of Oceanography Technical Report



Last Glacial Neotectonic Records in Prehistory Archeological Sites of Inland, Korea

Kim, Ju-Yong

Dept. of Quaternary Geology Research, Korea Institute of Geoscience and Mineral Resources (KIGAM), Daejeon 305-350, South Korea.
Email: kjy@kigam.re.kr

Abstract: This study aims to reveal Quaternary displacements found in some archeological excavation sites of inland part of Korean peninsula. In particular the Last Glacial soil-sedimentary deposits (since ~ 65 Ka) show displacements recorded in middle or late Paleolithic sites in Korea. It is well-known that important displacements were recorded in the alluvial fan deposits and mass movements along the Ulsan faults, but it also true that similar displacements are found at fluvial terrace deposits near Daejeon(Sintanjin), paleosoils and slope sediments near Jeonju city and Kimpo, and regoliths above the basement. Displacements like 'Thrust-Up Toward West (TUTW)' in regoliths developed on the granites can be found also near Pyeontaek area; TUTW displacements of the paleosoils developed on the slope sediments, ca 30~50ka dated by ¹⁴C and OSL, are found at the Mansuri site near Cheongju city, and also in Kimpo and Jeonju city; Significant vertical vein-rupture was observed in the fluvial terrace deposits, dated as old as about ~ 45 Ka by ¹⁴C and OSL, at Nosanri site near Daecheong Reservoir in the Keum river, where sands were filled into vertical cracks of about 2 cm in diameter. These displacement evidences may imply that Korean Peninsula has been influenced by the neotectonic compressional movement that might have been sustained even since the latest Last Glacial Period (ca 25~ Ka).

Key words: Displacement records, Prehistorical excavation sites, Neotectonic movement, Compressional regime, Last Glacial

INTRODUCTION

In Korea neotectonically important Quaternary deposits have been known to be distributed mainly at the southeastern part of Korean peninsula, where neotectonic movement might have been strongly influenced and sustainably remained up to now due to relative proximity to the compressional tectonic regime triggered by subduction of both the Amurain Plate and the Phillipine Plate. The information on the late Quaternary displacements induced by 'Thrusting-Up Towards West (TUTW)' movement has been accumulated so far in many trench profiles near the Nuclear Power Plant (NPP) sites and the surrounding Quaternary outcrops in the SE part of Korea (Choi, et al, 2003; Lee, 1987). Except for marine terrace system, some other surface environments can be categorized and may be inventorized for inland illustrations of Quaternary displacements. For instance, TUTW displacements along the Ulsan faults in the SE part of Korea have been pretty well documented and traced by the Korean paleoseismologists (Inoue, ety al, 2006; KHNP, 2006). It is well-known that along the Ulsan Fault quite a lot of important TUTW displacements have been recorded in the alluvial fan deposits and mass movements in particular. But TUTW displacements in the fluvial deposits, slope and Paleosoils of inland side are relatively little known so far. This study therefore aims to provide some Quaternary displacement information other than marine terrace in the East Coast and outside of Ulsan Fault. For this purpose fluvial deposits near Daejeon(Sintanjin), paleosoils and slope sediments near Jeonju city and Kimpo, and regoliths above the basement near Pyeontaek are included in this research.

STUDY AREAS AND DESCRIPTION OF DISPLACEMENT

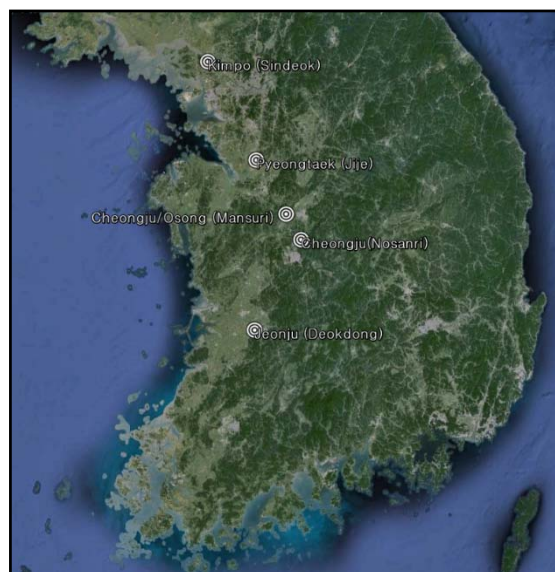


Fig. 1: Distributional maps of five sites of prehistorical excavation, including Kimpo (Sindeok), Pyeongtaek (Jije), Cheongju/Osong (Mansuri), Cheongju (Nosanri) and Jeonju (Deokdong) from north to south direction.

Paleosoils on basement (regoliths)

TUTW displacements of the paleosoils developed on basement were observed at Kimpo county. Prehistorical excavation trenches in Sindeok site (37°42' 50" N, 126°37' 29" E) of Kimpo Count (Fig.2) and Jijae site (37° 1' 0" N, 127°3' 50" E) of Pyeongtaek city (Fig.3), both showing hanging-wall thrusting up toward west along the sharp fault boundary and resulted Jurassic granite overring late Quaternary Paleosoils in the right side.

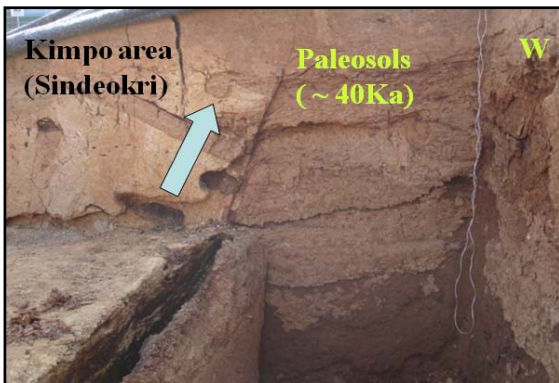


Fig. 2. Prehistorical excavation trench of Sindeok site of Kimpo count. The hanging wall thrust up toward west along the sharp fault boundary, resulting Jurassic granite thrusting up Paleosols in the right.

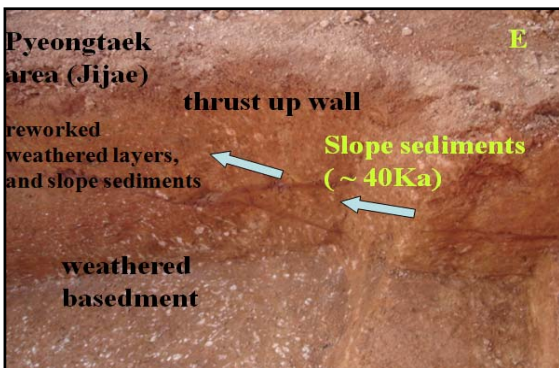


Fig.3. Prehistorical excavation pit in Jijae site of Pyeongtaek city. The hanging wall thrust up toward west along the sharp fault boundary, and multiple fault-branchings remain in the regoliths of Jurassic granite.

Paleosols on slope sediments

TUTW displacements in the Paleosols and slope sediments are observed at Mansuri Paleolithic site (36°37' 58" N, 127°19' 50" E) at both Mansuri site of Cheongju city (Fig. 4) and Deokdong site (35°49' 45" N, 127°3' 53" E) of Jeonju city (Fig 5). At the prehistorical excavation pit in Mansuri site of Cheongju city, the hanging wall thrust up toward west along the sharp fault boundary in the reddish brown paleosols. The displaced fault remained in relatively low angle, subjacent soliflucted slope sediments and Jurassic granite (Fig.4).

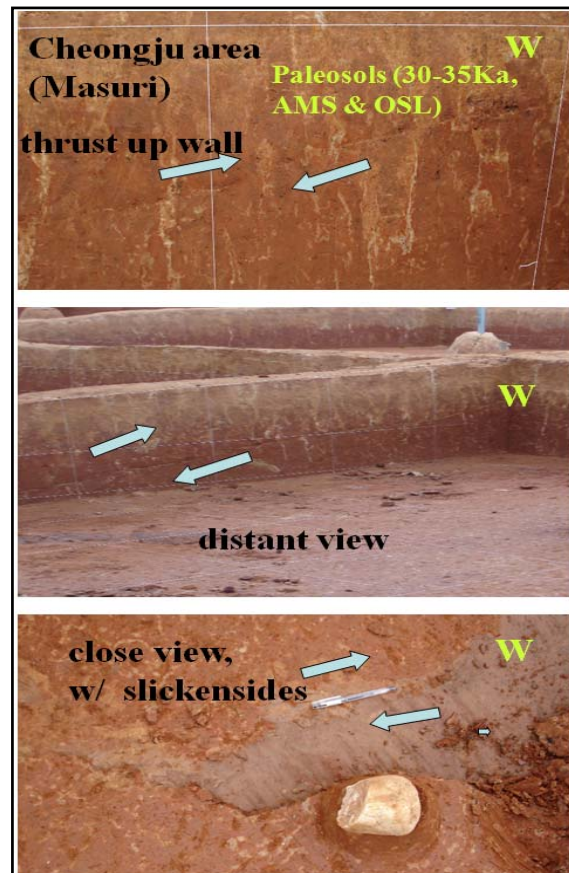


Fig. 4: Prehistorical excavation trench in Mansuri site of Cheongju city. The hanging wall thrust up in low angle toward west along the sharp fault boundary. superjacent on the slope sediments composed of mud and gravels.

At Deokdong site of Jeonju city, TUTW displacements are observed also in the both paleosols and slope sediments (Fig. 5). At this prehistorical excavation pit the hanging wall thrust up toward west about 40 cm in vertical distance along the fault boundary in the dark brown and/or reddish brown Paleosols. The displaced fault was branched in soliflucted slope sediments and Paleosols (Fig.5).

Fluvial sand and gravels

Significant vertical vein-rupture was observed in the Last Glacial fluvial deposits at Nosanri site (36°27' 21" N, 127°26' 30" E) near Daechong Reservoir in the Keum river. Here vertical cracks of about 2 cm in diameter, extending towards to the basement, caused by seismic rupture were filled by sands derived from eolian (?) cover sands on the fluvial deposits.

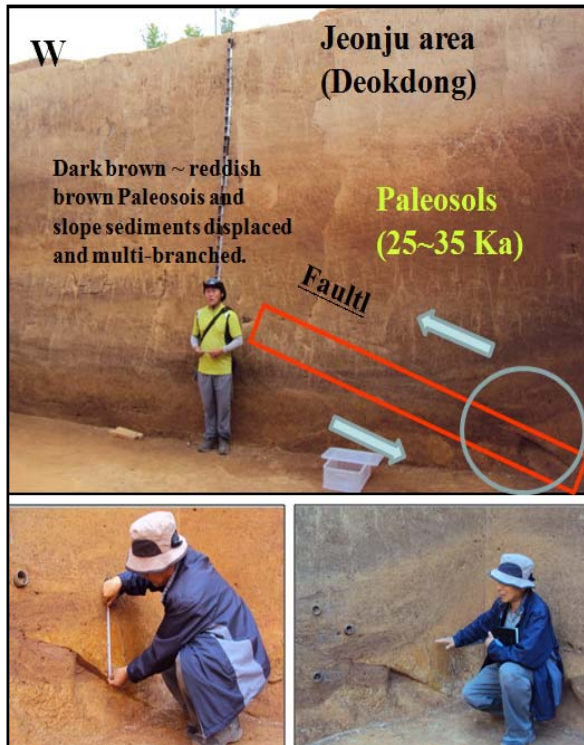


Fig. 5: Prehistorical excavation pit in Deokdong site of Jeonju city. The hanging wall thrust up about 30 cm along the sharp fault boundary, which displaced both soliflucted /slope sediments and Jurassic granite.

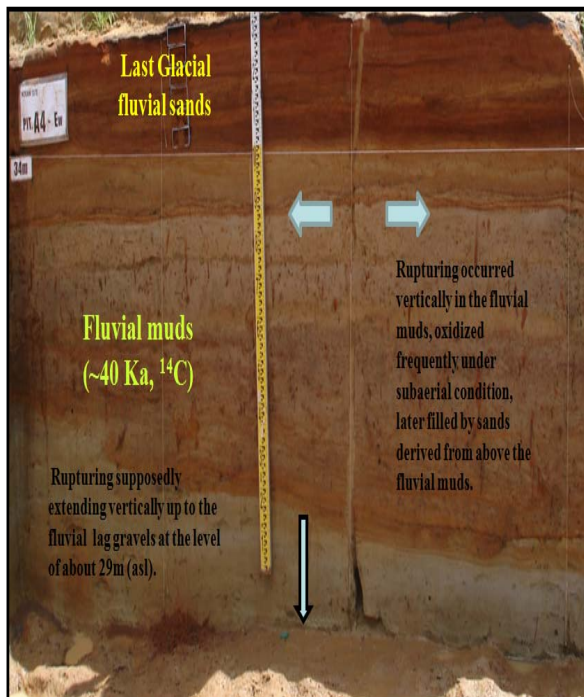


Fig. 6: Prehistorical excavation pit in Nosanri site of Cheongju city, rupturing vertically the Last Glacial fluvial muds and infilling with sands derived from sands mantled above the muds.

CHRONOLOGY OF DISPLACEMENT

From the five illustrations mentioned-above, Paleosoils of Mansuri site near Cheongju city show prevalence of reddish brown Paleosoils, superjacent either by slope sediments or on fluvial terrace sands and gravels (> 70Ka) (Fig. 7), which are distributed at the level of about 12m above the present river bottom. The Paleosoils were formed since the middle of the Last Glacial Period (ca ~ 45 Ka). Therefore the chronology of TUTW displacements can be presumed as younger than 45 Ka in Mansuri site of Cheongju city (Fig. 7), and ca 30 Ka at Deoldong in Jeonju city (Fig. 8), respectively. In Nosanri site near Daecheong Reservoir in the Keum River, a significant vertical vein-rupturing observed in the fluvial deposits and it can be interpreted as younger than ca ~ 30,000 yrBP by ¹⁴C for fluvial muds. These displacement evidences of inland Korean Peninsula can support the neotectonic compressional movement that might have been sustained even since the later Glacial Period (ca ~ 25 Ka). In Sindeokri site of Kimpo County and Jije site of Pyeongtaek city, Jurassic basement was subjacent by soliflucted regoliths and/ or relic sediments. The datings are not available now, but it is generally covered by reddish brown or dark brown MIS 3 Paleosoils prevailed in Korea so that the displaced age may be younger than 25~45 ka maximally.

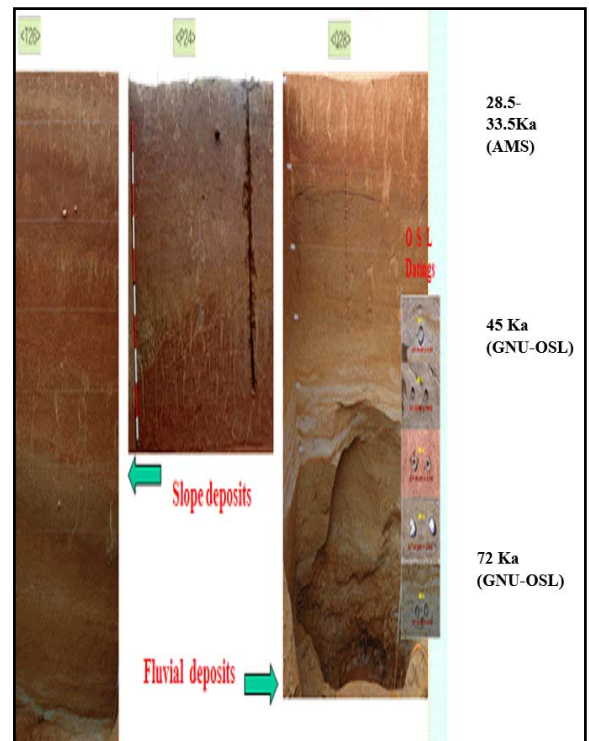


Fig. 7. OSL and Radiocarbon carbon ages of the reddish brown Paleosoils show 28.5~33.5 Ka, so that the latest TUTW displacement may be younger than ca 30 Ka in Mansuri site of Cheongju city.

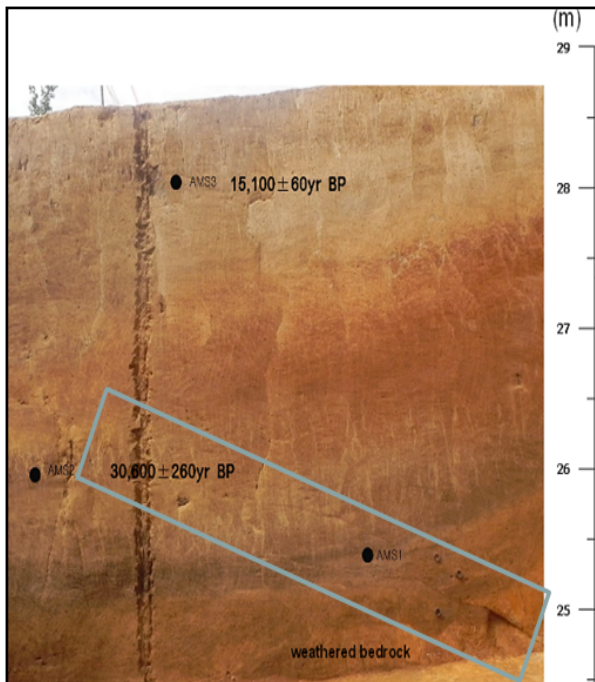


Fig. 8. Radiocarbon carbon ages of the reddish brown and dark brown Paleosoils indicate the latest TUTW displacement is younger than ca 30 ka in Deokdong site of Jeonju city.

IMPLICATION OF THRUSTING MOVEMENT

All the displacements mentioned-above in the terrestrial environment of inland side of Korean Peninsula have been triggered by the neotectonic compressional movement which in turn thrust up the landmass of Korean Peninsula during the Quaternary (Choi, 2003; Choi et al, 2008). Compressional neotectonism also can explain the uplift history of Korean Peninsula which can be computed with the help of various chronological methods (radiocarbon, OSL datings, paleomagnetic polarity, tephra, etc.), which may in turn be applicable to map paleoshoreline angles of marine terraces along the coastal area (Choi, et al, 2003, 2009; Kim, et al, 2008; Choi, et al, 2008). For the elaboration of spatial and temporal variability of displacement features of Quaternary faults it is essential to accumulate further the neotectonic information on various time scale in Korea. In near future displacement evidences of the last a few tens of thousand years may be obtained and it might have been sustained even since the latest Glacial Period (ca ~ 25 Ka) in Korea.

FURTHER STUDY

Further chronological data and prehistory excavation evidences will be needed, which will support for the neotectonic movements, i.e, frequency and intensity; It may be presumed that the Quaternary displacement will become much younger than ca 20ka (Last Glacial Maximum, LGM). In addition it will be highly prospected that much more recent neotectonic evidences will be obtained from the prevailing prehistorical excavation sites in Korea.

Acknowledgements: This study has been performed with financial support from the KIGAM R/D project (14-4805), and greatly indebted from Dr McCalpin and anonymous reviewer for their valuable and constructive comments and suggestions.

References

- Choi J.H. A.S. Murray A.S., Cheong C.S., Hong D.K., Chang H.W., 2003. The resolution of stratigraphic inconsistency in the luminescence ages of marine terrace sediments from Korea. *Quaternary Science Reviews* 22, 10–13.
- Choi J.H., Kim J.W., Murray A.S., Hong D.K., Chang H.W., Cheong C.-S., 2009. OSL dating of marine terrace sediments on the southeastern coast of Korea with implications for Quaternary tectonics. *Quaternary International* 199 (1–2), 3–14.
- Choi, S.-J., 2003. Marine terrace of Jinha-Ilgwang area, Southeast, Korea. *Economic and Environmental Geology* 36, 233–242.
- Choi, S.-J., Merritts D.J., Ota Y., 2008. Elevations and ages of marine terraces and late Quaternary rock uplift in southeastern Korea. *Journal of Geophysical Research* 113 (B10403), 1–15.
- Inoue, D., Choi, W.H., 2006. The activity of Ulsan Fault System based on marine terrace age study at the southeastern part of Korean Peninsula. Central Research Institute of Electric Power Industry Japan (CRIEPI); Report N05012, pp. 6–15.
- KHNP, 2006. Geomorphic and Geochronologic Survey of Coastal Terraces on the East Coast of the Korean Peninsula. Korea Hydro and Nuclear Power Co. Ltd., Final Report-E03NJ07, 309–386.
- Kim Ju-Yong, Keun-Chang Oh, Dong Yoon Yang, Weon Hack Choi, Sei Sun Hong, Jin Young Lee, 2008. Stratigraphy, chronology and implied uplift rate of coastal terraces in the southeastern part of Korea. *Quaternary International* 183, 76–82.
- Lee, D. Y., 1987, Stratigraphical research of the Quaternary deposits in the Korean Peninsula, *Korean J. Quat. Res.*, 1, 3–20



Surface deformation characteristics at two locations in Peninsular India and its implications on seismic hazard

Biju John (1), C.P Rajendran (2), Yogendra Singh (1)

- (1) National Institute of Rock Mechanics, Kolar Gold Fields, Karnataka- 563117 India b_johnp@yahoo.co.in
 (2) Jawaharlal Nehru Centre for Advanced Scientific Research, Bangalore 560064 India

Abstract: Moderate earthquakes in the intra-plate regions can cause significant damage. Such regions, in general, experience earthquakes at unexpected locations. The 1993 Killari (M=6.3) earthquake of central Peninsular India occurred in a terrain where there was no historic evidence of damaging earthquakes. The rupture zone produced by this earthquake was studied in detail. The exploration, on 500 m long main rupture zone, identified modification of surface deformation induced by the red bole and clay occurring in the intra-trap zone. In another study, a similar rupture zone was identified in the southern part of Peninsular India where the deformation pattern observed are similar to the one reported at Killari. The clay zone observed at interface between the laterite cap and the crystalline parent rock controls the rupture pattern at this zone. Even though there are no historic earthquakes observed in this region the nature of deformation suggest that these might have produced by moderate event/s. Both these rupture zones have similar deformation pattern and characteristic clay injections. These observations will be a yardstick for future studies in similar seismotectonic setup.

Key words: SCR earthquakes, surface rupture, clay injection.

INTRODUCTION

Continental interiors (Stable Continental Regions or SCR) generally exhibit geologic evidence of neotectonic stability; nevertheless they are not devoid of earthquakes. Even though earthquakes are occurring in such SCRs, the rate of seismicity is low in comparison to plate boundaries (Johnston and Kanter 1990). However, historic data in SCRs indicate that many earthquakes in these regions caused substantial destruction. Studies also suggests that intraplate continental regions contain many potential seismogenic faults, but rarely produce earthquakes (Coppersmith and Young, 1989; Seeber and Armbruster, 1993). Paleoseismic studies of many surface rupturing continental interior earthquake show that the return period is very large (Crone et al 1992; Machatte et al., 1993).

Historically Peninsular India was also experiencing earthquakes (Fig. 1). Review of stress field associated with seismicity in Peninsular India suggests that damaging earthquakes usually occur at favorably oriented preexisting faults (Gowd et al., 1996). The 1993 Killari earthquake induced huge damage to life and property. This event produced surface rupture in the epicentral area. A similar surface rupture was observed in the southern part of Peninsular India within one of the major faults identified in the region. This paper describes the deformational style of these surface ruptures and their similarities.

OBSERVATIONS FORM CENTRAL PENINSULAR INDIA

The 1993 Killari epicentral area is situated within the Deccan traps which lie uncomfortably over Precambrian rocks. Several studies mapped the ground deformation

induced by this event (Pande et al., 1995; Seeber et al., 1996; Rajendran et al., 1996). This surface rupture, coseismically produced during the 1993 earthquake, was a rare phenomenon. Only ten stable continental region earthquakes were known to have ruptured the surface prior to Killari earthquake (Johnston and Kanter 1990; Adams, et al., 1992). The surface deformation zone, located near Talni village (Fig. 2), extends over a strike length of about 3 km in NW-SE direction with a width of about 300 m (e.g. Seeber et al., 1996). Even though the regional alignment of ground cracks was observed in a NW-SE direction in the trend of the tributary of Tirna river, prominent deformation zone trends have WNW-ESE direction.

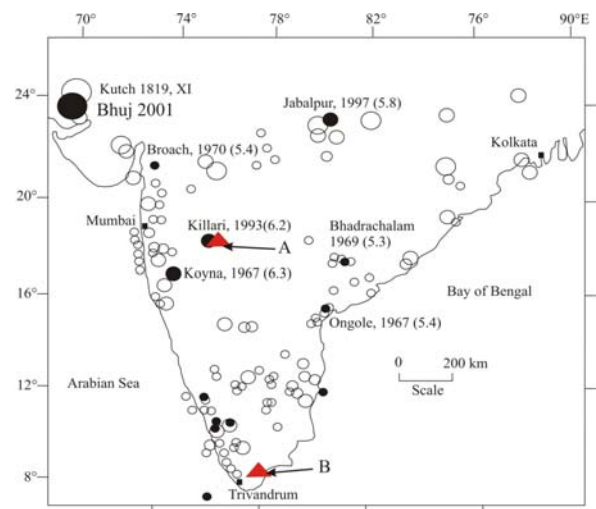


Fig. 1 Peninsular India and epicenters of earthquakes; Triangles show the study areas described in this paper.



Paleoseismic studies in this rupture zone identified older deformational structures (Rajendran et al 1996; Rajendran and Rajendran, 1999; John 2003). These studies conclude that the trap rocks in the Killari area have indeed been affected by previous seismic event/s, and are characterized by a unique pattern of deformation.

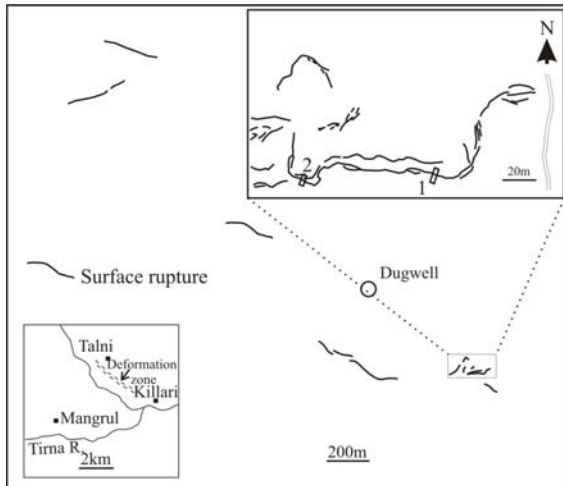


Fig. 2 Rupture zone in Killari; inset: the regional map showing E-W flowing Tirna river and NW-SE trending tributary.

The shallow trench excavated by Seeber et al. (1996) in the E-W segment of the rupture exposed a reverse sense of throw and a south dipping fault. According to Seeber et al. (1996), the mode of faulting observed in these trenches was influenced by the geometry of the preexisting exfoliation fractures of basaltic rocks.



Fig. 3 Photograph of western wall of trench 1 (courtesy: Pande. P) shows a distinct highly weathered southern block and a much more compact northern block. Note the yellow coloured clay injection at the bottom.

During the trench investigations it was found that red bole and clay observed in the intra-trap squeezed up along the rupture. Trench -1 oriented in N15°E- S15°W direction was located in the southern scarp of the E-W segment where the soil cover varies from 10 to 45 cm (Fig. 2; Pande et al., 1995). Although no fault plane is visible in the eastern wall of the Trench-1 (Fig. 3), a yellow clayey material was found at the bottom of the

trench wall. This yellow material was later identified as clay, rich in montmorillonite.

Trench -2 measuring 5 m long, 2 m wide and 2 m deep was dug (N20°E) close to the western end of the rupture zone (Fig. 2). At 1.9 m, the trench exposed the red bole layer. Several structures, including a low angle (~ 15°) northeast dipping thrust fault were exposed on the eastern wall (John 2003). In the western wall of the trench a wide impact zone, at the interface of a block of fragmented basalt on the south and more compact basalt on the north, was observed. The impact zone comprised minute fragments of basalt embedded in yellowish and whitish clay (Fig. 4). The XRD studies indicate that these yellow materials are composed of montmorillonite-rich clay. This clay at the impact zone had a 'dome shape' and its continuity could be traced to the underlying red bole layer. This shows that this material was emplaced to a higher level, during the faulting episodes.

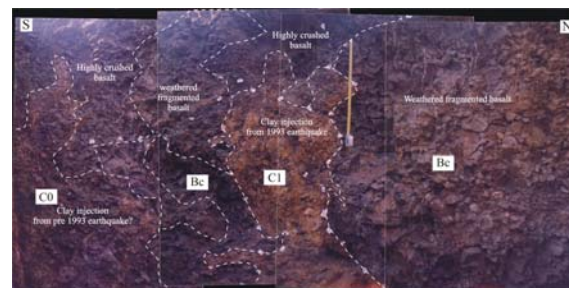


Fig. 4 Photograph of western wall of trench TR. Bc: relatively compact rock; C1: clay injection due to the present event. Note that the clay C1 has split the Bc during the injection; C0 shows clay enrichment possibly during an earlier event. A distinct compact northern block can be easily distinguished from a crushed and/or shattered southern block. The clay injection (C1) associated with 1993 event shows an intense yellow colour, which seems to break through the interface of crushed basalt and the northern massive basalt (Bc) (John 2003).

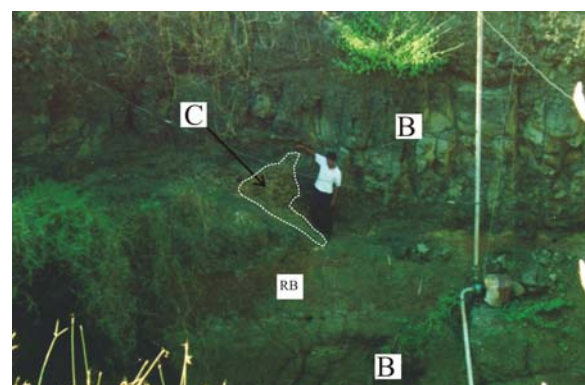


Fig. 5 Fault identified in the dug well marked in figure 2; B: the hard basalt rock; RB: the red bole; C: the clay perturbation/injection. The man standing has 170 cm height.

Further evidence for the pattern of near-surface deformation was obtained from a dug well (Fig. 5), located ~500 m northwest of main surface rupture (see



Fig. 2 for location). The well section essentially shows what appeared to be older thrust sheets, interlayered with red bole material (Rajendran et al 1996; Rajendran and Rajendran, 1999; John 2003). Apparently the thrust sheets formed in basalt layers had propagated along the slipping surface provided by incompetent beds (red bole layers), capped with a thin layer of clay enriched in montmorillonite (Rajendran et al 1996; John 2003). Just like in the rupture zone, a clay perturbation is also observed at the bottom of the top flow (Fig. 5).

OBSERVATIONS FROM SOUTHERN PENINSULAR INDIA

The second study area is located in the eastern side of the Western Ghats (Fig. 6). The Achankovil shear system is one of the major crustal scale structures in this part of Peninsular India. A number of NW-SE trending parallel lineaments demarcate this 15-20 km wide shear zone (Rajesh and Chetty, 2006). Many studies were carried out to understand the origin and depiction of this structure. Low level seismicity reported in this region, however, does not suggest any relation with this shear zone and thus no significant study was carried out to understand its neotectonic behaviour.

The NW-SE trending Thenmala fault is located in the southwestern end of this shear zone (Fig. 6 shows its southeast continuity). Even though this fault is very clear in the hills, its signature in plain area was not identified in earlier studies. Later studies, delineated the signatures of these faults further in the southeast from satellite images. The trace of the fault is visible with distinct geomorphic features on either side (Fig. 6). A major drainage seems to be abandoned in the southwestern block of the fault whereas a big natural pond developed in the northeastern block in the study area (Fig. 6). The traces of these faults are observed as multiple slip planes with varying deformation pattern (Praseeda et al., 2014).



Fig. 6 Satellite image of location B of figure no 1. Dotted line shows continuity of Thenmala fault identified in the area; A: abandoned drainage; P: pond developed; R: the active canal; H: the hill that separate the fault; K: the knick point in coastline; S: the location of surface rupture (courtesy: Google earth.com).

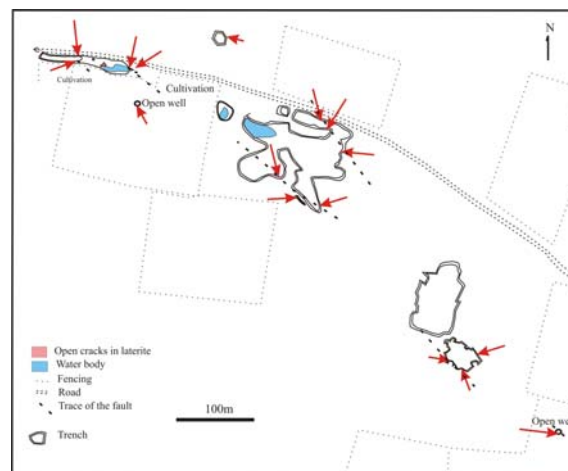


Fig. 7 Rupture zone identified at location B marked in Figure 1. The arrows indicate the locations where faults are studied.

Field studies identified a zone of fractured laterite extending beyond 500 m (Fig. 7). The laterite developed on crystalline rocks shows hard vermicular nature (Fig. 8). A thin layer of aeolian deposit, also was observed over the laterite, which were deposited in Middle to Late Holocene (Alappat, et al., 2013). A detail study carried out in this rupture zone identified reverse movement faults in the laterite. These faults show no evidence of leaching after the faulting/fracturing event. This may indicate that the faulting might have occurred after ending of the laterization process.



Fig. 8 Rupture zone observed in the area at location 2 marked in figure 7.

The deformation pattern observed in this area was similar to the surface rupture mapped by Gordon and Lewis, (1980) on laterite terrain during 1968 M= 6.9 Meckering earthquake. Reverse faulting at places trapped aeolian deposits under the hanging wall (Fig. 9).

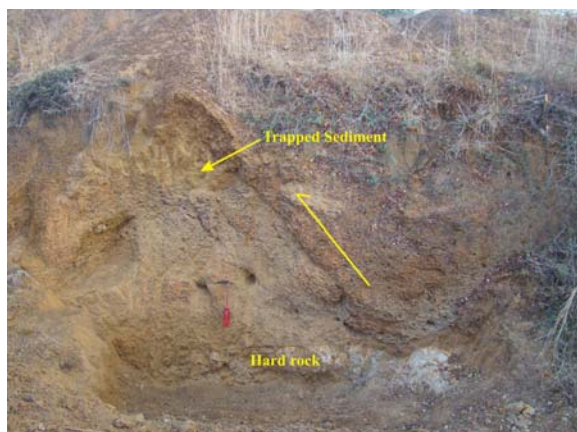


Fig. 9 Trapped aeolian sediment in one of the fault (location 3 of figure 7).

The presence of aeolian deposits within the fault zone may indicate that the faulting is geologically young (younger than Middle to Late Holocene?). Faulting was also observed in gneissic rocks at two dug wells on either end of this zone (see Fig. 6 for location). A detailed trench investigation identified a dome shaped clay zone at the places wherever the basement fault terminate against the laterite (Fig. 10).



Fig. 10 Clay injections identified in one of the faults identified in rupture zone (location 13 of figure 6).

Discussion

Detailed evaluation of the nature of deformations at Killari indicates that the near surface faulting/rupturing was controlled by red bole and clay that are found within the inter-trap zone. Fault propagation was also modified by this slipping interface. Trench studies in the rupture zone identified clay injections into the overlying rocks along the slip planes (Fig. 10). Similar features were also found in the older deformation pattern identified in the area.

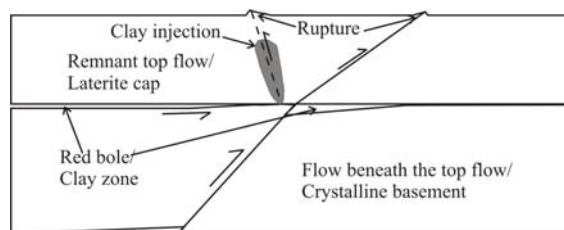


Fig. 11 Synoptic model showing deformation pattern at top level of the rupture zones observed at both locations studied.

The rupture zone identified in the southern Peninsular India has similar deformation pattern. It was observed that the clay zone in the interface between the laterite and gneissic rock controlled the deformation style. Clay injections into the overlying laterite were observed at locations where the faults terminated against laterite (Fig. 11).

The NW-SE systems are identified as one of the favorable fault orientations for reactivation in Peninsular India (Gowd et al 1996). The two rupture zones studied are also associated with NW-SE trending faults and have similar deformational pattern. These observations will provide a clue for future active fault and paleoseismic studies in Peninsular India.

Acknowledgements: The work is a part of DST and NPCIL funded projects. The BJ and YS thanks Director, NIRM for permission to publish this work.

References

Adams, J., J.A. Percival, R.J. Wetmiller, J.A., Drysdale & P.B. Robertson, (1992). Geological controls on the 1989 Ungava surface rupture: a preliminary interpretation. *Geol. Surv. Can.* 92-1c, 147-155.

Alappat, L., P. Morthekai, A.Vidyasagar, S. Srinivasalu, D. V. Reddy & A.K. Singhvi (2013). Chronology of deposition of coastal Red dunes (Teri sands) in South India and its palaeoenvironmental implications. - *Chronology 2nd Young Scientists Meeting PAGES Abstract volume 46*.

Coppersmith, K.J & R.R. Young, (1989). Issues Regarding Earthquake Source Characterization and Seismic Hazard Analysis within Passive Margins and Stable Continental Interiors *In Earthquakes at North-Atlantic Passive Margins: Edited by S. Gregersen, & P Basham, W Peter.* 601-631.

Crone, A.J., Machette, M.N & Bowman, J.R., (1992). Geologic investigations of the 1988 Tennant Creek, Australia, Earthquakes—implications for paleoseismicity III stable continental regions. *U.S. Geol. Surv. Bull.* 2032-A, 51.

Gordon, F.R & Lewis, J.D., (1980). The Meckering and Calingiri earthquakes October 1968 and March 1970. *Geological Survey of Western Australia, Bulletin 126*.

Gowd, N., S.V., Srirama Rao & K.B., Chary, (1996). Stress field and seismicity in the Indian shield: effects of the collision between India and Eurasia. *PAGEOPH* 146, 503-531.

John, B., (2003). Characteristics of near surface crustal deformation associated with shield seismicity: two examples from peninsular India. Unpublished PhD thesis.

Johnston, A.C. & L.R. Kanter, (1990). Earthquakes in stable continental crust. *Scientific American* 262, 68-75.

Machette, M.N., A.J. Crone & J.R. Bowman, (1993). Geologic investigations of the 1986 Marryat Creek, Australia



INQUA Focus Group on Paleoseismology and Active Tectonics



paleoseismicity.org

- earthquake — implications for paleoseismicity in stable continental regions. U.S. Geol. Surv. Bull. 2032-B, 29p.
- Pande, P., S.K., Gupta, N.V. Venkataraman & B. Venkataraman, (1995) Terrain changes consequent to the Killari earthquake of 30th September, 1993, *GSI, Spl. Pub.*, No.27, 215-220.
- Praseeda, E., B. John, C. Srinivasan, Y Singh & P Samui, (2014). Thenmala fault system, southern India: implication to Neotectonics (JGSI in press).
- Rajendran, C.P & K. Rajendran, (1999). Geological investigations at Killari and Ter, Central India and implications for paleoseismicity in the shield region. *Tectonophysics* 308, 67-81.
- Rajendran, C.P., K., Rajendran & B., John, (1996). The 1993 Killari (Latur), Central India earthquake: an example of fault reactivation in the Precambrian crust. *Geology* 24, 651–654.
- Rajesh, G, K & T.R.K. Chetty, (2006). Structure and tectonics of the Achankovil shear zone, Southern India. *Gondwana Research*, v. 10, pp. 86-98.
- Seeber L & J.G. Armbruster. (1993). Natural and Induced Seismicity in the Lake Erie-Lake Ontario Region: Reactivation of Ancient Faults with Little Neotectonic Displacement *Geogr. Phys. Quat.* 47, 363-378
- Seeber, L., G. Ekstrom, S.K. Jain, C.V.R. Murty, N. Chandak & J.G. Armbruster, (1996). The 1993 Killari earthquake in central India: A new fault in Mesozoic basalt flow? *J. Geophys. Res.*, 101, 8543-8560.



Active tectonics in southern South America: a general review about its development and mechanisms

Andrés Folguera (1), Guido Gianni (1), Lucía Sagripanti (1), Emilio Rojas Vera (1), Bruno Colavitto (1), Darío Orts (1), Víctor A. Ramos (1)

(1) Instituto de Estudios Andinos. Laboratorio de Tectónica Andina. Conicet. Facultad de Ciencias Exactas y Naturales. Universidad de Buenos Aires. Email: andresfolguera2@yahoo.com.ar

Abstract: A range of processes acted during the Quaternary producing topography from the Chilean coast, where the Pacific ocean floor is being subducted, to the Brazilian-Argentinean Atlantic platform area: On one hand, active mountains in the passive margin whose origin is discussed; and on the other hand, processes associated with the activity of the eastern Andes, highly active at the Subandean region bordering the Altiplano plateau and at the Pampean flat subduction zone. We focus our analysis in the southern Central and Patagonian Andes, where orogenic processes are linked to particular mechanisms: i) impact of mantle plumes and local weakening of the lithosphere that yield under horizontal stresses producing active deformational zones, ii) dynamic topography associated with the opening of asthenospheric windows during the subduction of the Chile ridge and slab tearing processes, with the development of active extensional troughs, and iii) subduction of oceanic plateaus determining out-of-sequence active thrust fronts.

Key words: Neotectonics, exhumation Andes, subduction zone.

INTRODUCTION

Active uplift in the Andes has been generally associated with contraction imposed by the convergence between the Pacific subducted plates and the South American plate (Schellart et al., 2011). However, in the last years multiple mechanisms have been recognized along the Andes that produce, together with orogenic forces, regional to local exhumation of the upper crust. Additionally, segments where exhumation seems to be governed by thrusting are not clearly delimited and their associated mechanisms are not totally understood. In general terms a narrow band of active thrusts has been described bordering the eastern Altiplano and Pampean regions from southern Perú and Bolivia to central Argentina between 10° and 33°S (Figure 1). This segment coincides with a broad and high plateau associated with important amounts of intracrustal earthquakes that denote active mountain building processes. South of 33°S, crustal seismicity on the eastern Andes diminishes sensibly, becoming mountain morphology narrower and lower. Even though orogenic mechanisms are described for these southern Andes, at least discontinuously, in the last years other factors have been proposed as linked to active uplift, in particular for the Patagonian region.

The Andes are formed over a subduction system of three oceanic plates beneath the South American plate. This configuration shows a noticeable symmetry with an Altiplano at its mid sector flanked by two flat subduction settings, the Peruvian in the north and the Pampean-Chilean in the south (Figure 1). Topography is higher at the mid sector and diminishes steadily towards both edges of the subductive system, where narrow mountain systems are connected to transform limits between the

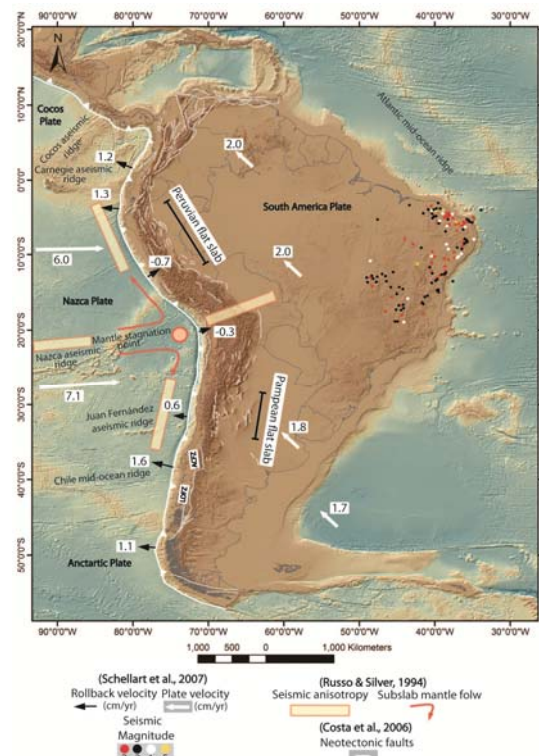


Fig. 1: Exhumation mechanisms associated with the Central Andes and Atlantic passive margin.

South America, Caribbean and Scotia plates respectively (Figure 1).

Even though this system has a striking symmetry, from north to south the Cocos, Nazca and Antarctic plates sink beneath the western border of South America at different rates. While Nazca penetrates beneath the continent with varying-relatively high rates between 6 and 7 cm/yr, the Antarctic plate sinks at just 2 cm/yr. This



change has been attributed to the migration of the triple junction between Nazca, Antarctica and South American plates, from south to north in the last 14 My that provoked the opening of an asthenospheric window beneath Patagonia and mechanical disconnection of Antarctica and Nazca plates at depth, consequently producing a drastic drop in slab pull forces (Cande & Leslie, 1986).

ACTIVE TECTONICS IN THE CENTRAL ANDES AND ATLANTIC PASSIVE MARGIN

Anomalous high topography is visualized north and south of the Arica bend region where the Altiplano is developed (Figure 1). The Altiplano region is affected by delamination of the lower lithosphere producing a high topography partially linked to isostatic readjustments (Sobolev and Babeyko, 2005). This feature is eastwardly flanked by the Eastern Cordillera and Subandean system that accommodated contraction since the last 10 Ma up to the present (Brooks et al., 2011). At the Atlantic Brazilian margin another topographic anomaly is recognized in a passive margin (Figure 1). This has been associated with active mountain uplifts restricted to the Atlantic coastal area associated with crustal seismicity and neotectonics (Riccomini & Assumsao, 2009). These uplifts are coincident with the area where the Chilean forearc is relatively static respect to the Brazilian Atlantic spreading center (Schellart et al., 2011).

Neotectonic deformation between 27 and 36°S along the Andes is associated with orogenic mechanisms determined by the Pampean-Chilean flat subduction zone (27-33°S) and a segment to the south where the Nazca plate changes its angle of subduction smoothly from flat to 30°E (Pesicek et al., 2012). Here the foreland area is fragmented in a series of active basement blocks such as the Sierras Pampeanas and the San Rafael Block (Costa & Vita-Finzi, 2006).

ACTIVE TECTONICS IN NORTHERN PATAGONIA

The area interposed between 36 and 38°S shows transitional characteristics between the Southern Central and the Patagonian Andes. Active structures that accommodate shortening and strike-slip displacements are present at the Payenia volcanic field in the retroarc zone. Evidences of young deformation are found in volcanic products of < 2 Ma age, while morphometric analyses through the fluvial network allow the recognition of a non- equilibrium state for most of the fluvial channels (Galland et al., 2007).

Part of the retroarc zone is affected by regional uplift linked to the development of extensional troughs such as the Las Loicas extensional system (Folguera et al., 2007). These systems are spatially linked to a complex pattern of mantle plumes that are impacting the lower crust at the retroarc zone (Burd et al., 2014). A main asthenospheric anomaly is branched into a series of

minor anomalies that impact the lower crust at the sites of neotectonic activity suggesting a mechanical connection between thermally-weakened crust and horizontal crustal yielding (Galland et al., 2007; Messenger et al., 2010).

South 38-39°S, a slab tear has been described from seismic tomographies after the 27/2/10 Maule earthquake (Pesicek et al., 2012). This slab tear determines a slab window south of 38°S through a W-NW direction that coincides with the development of the Loncopué trough and an attenuation of the Moho that reduces the Andean roots at these latitudes up to 33 km (Folguera et al., 2007), uplifting and stretching the Agrío fold and thrust belt.

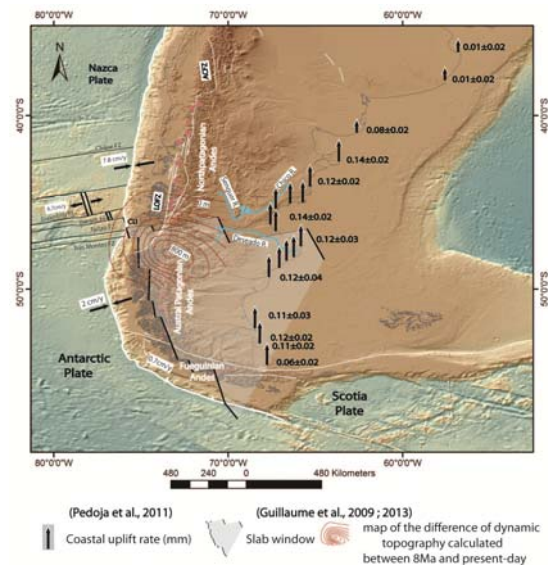


Fig. 2: Active uplift mechanisms in Patagonia: i) extension and isostatic rebound during the opening of an asthenospheric window (Lagabrielle et al., 2007), ii) forearc detachment along the Liqueñe-Ofqui fault zone (Lavenu & Cembrano, 1999), iii) a transform plate boundary between Scotia and South American plates. Uplift rates of the Atlantic Ocean taken from Pedoja et al. (2011) and deflected river patterns from Gillaume et al. (2009).

Collision of transform zones segmenting the Chile ridge has explained diachronous deformation and exhumation as out-of-sequence thrust fronts from the coastal sectors in the latest Pliocene-early Quaternary, to the arc and retroarc zones up to the Pleistocene an even locally Holocene times (Folguera and Ramos, 2009).

In the last years, geodetic and satellite-gravity (GRACE) measurements associated with the Mw 8.8 Maule earthquake (27/2/2010) have shown the role of large rupture zones along the Pacific subduction zone in the active uplift that affects the area interposed between the coast and the high Andes. On one hand, co-seismic displacements after 170 years of interseismic strain accumulation have shown that the coastal areas emerged creating a topography that explains at least in part morphology along the western coastal zone (Fariás et al., 2011). On the other hand, crustal-scale extension



affects the upper plate during co- and post-seismic displacements due to a strong gradient in horizontal displacements from 7-8 cm/y in the western retroarc zone to more than 3 m along the coastal zone. This extension has been proposed as responsible for regional uplift of the upper plate during co- and post-seismic stages (Aaron et al., 2013).

ACTIVE TECTONICS IN SOUTHERN PATAGONIA

The Southern Patagonian region shows particular mechanisms for young to active uplift (Figure 2). Young and buoyant oceanic crust subducts at the Pacific margin decoupling a forearc sliver through the Liquiñe-Ofqui fault zone (LOFZ) (Lavenu & Cembrano, 1999; Folguera et al., 2004). This fault zone runs through more than 1,000 km through the arc front accommodating strike-slip to reverse displacements creating topography along the North Patagonian Andes (Figure 2).

Its southern edge occurs at the point of collision of the Chile ridge against the trench from which a slab window opens beneath southern Patagonia (Figure 2) (Lagabrielle et al., 2007). The latitudinal extent of this slab window coincides with abnormally high exhumation rates through the Atlantic coast and the scarp morphology of the Patagonian cliffs (Pedoja et al., 2011) (Figure 2). In relation to this, Darwin (1846) had already observed the occurrence of shells on terraces at various elevations, which he explained by large-scale uplift over a 2,000 km of coastline. The eastern Patagonia uplift is constant through time and twice the uplift of the rest of the South American Atlantic margin, implying a linkage with the subduction of the Chile ridge and the associated dynamic uplift (Pedoja et al., 2011). Additionally, fluvial fluctuations have been linked to the development of an asthenospheric upwelling coming through the opened window that would be related to surface regional uplift (Guillaume et al., 2009; Lagabrielle et al., 2007).

Finally, localized uplift in the southern extreme of Patagonia is almost entirely linked to the activity of a transform boundary zone between Scotia and South American.

DISCUSSION

Mechanisms associated with uplift along the Andes in the last 2 Ma show to be highly contrasting. While in the Central Andes predominates contraction mainly associated with thrust activity concentrated in the eastern Andean slope, and isostatic rebound in areas of over-thickened crust suffering delamination of lower crust, in the Southern Central and Patagonian Andes to the south asthenosphere dynamics, co-seismic deformation and collision of ocean bathymetric highs become predominant factors.

In particular, exhumation across the South American plate at the Arica region, located at the central sector of

the Andean subduction configuration, is associated with the neotectonic activity of the Eastern Cordillera and Subandean System bordering the Altiplano region. A nearly static trench, where the slab roll back is inhibited by a perpendicular-to-the-trench mantle flow, would favor the westward subduction of the Brazilian craton beneath the Subandean region, inducing high shortening rates and consequently exhumation. Crustal thickening beneath the Altiplano region has led to delamination of lower crust and lithospheric mantle that still operates today producing isostatic readjustments at the highest Andes. This stationary trench also explains why the Atlantic passive margin is associated at these latitudes with a neotectonic topography in central Brazil that would be partially accommodating horizontal displacements imposed by the ridge push forces originated in the Atlantic. To the south, between 27 and 33°S, flat subduction of the Nazca plate induces neotectonic activity on most of the mountain systems that are forming part of the eastern Andean slope, such as the Precordillera and Sierras Pampeanas systems, while more limitedly over fault systems developed over the western Andean slope.

South of the Pampean-Chilean flat subduction zone, between 34 and 38°S, exhumation seems to be linked to activity of reverse faults affecting the foreland area in the eastern Malargüe fold and thrust belt and San Rafael Block, following the same trend of young tectonic activity existent to the north, although mantle dynamics appear as a second order mechanism controlling sectors where the crust yields in association with higher thermal fluxes imposed by a complex system of mantle plumes.

South of 38°S, a strong tearing in the subducted Nazca plate is associated with neotectonic extensional systems, where the lower crust is attenuated and consequently experience isostatic readjustments. Growth of the Pacific coastal zone is influenced by co-seismic vertical displacements and by extension achieved during this and post-seismic stages imposed by the slower elastic recovering of the asthenosphere after large earthquakes in the subduction zone. From 38 to 46°S, a forearc crustal sliver is detached from South America along the Liquiñe-Ofqui fault system in relation to the oblique subduction of young-highly buoyant oceanic lithosphere attached to the Chile ridge. South of 46°S, a slow subduction regime imposed by the collision of the Chile ridge in the last 14-12 Ma coincide with the opening of a slab window. An associated asthenospheric upwelling induces an uplifting foreland topography that is provoking the lateral migration of main rivers of Patagonia and exhuming anomalously high cliffs along the Atlantic coast. South of 50°S a transform-fault boundary between the South America and Scotia plates controls younger deformations and uplifting sectors through the southern edge of South America.

CONCLUDING REMARKS

Active exhumation at the Central Andes is mainly governed by thrusting that accommodates horizontal displacement of the South American craton beneath the



orogenic front. To the south, other processes appear as second-order factors that control active exhumation such as distribution of mantle plumes, co- and post-seismic uplifts associated with large earthquakes, subduction of young oceanic lithosphere and detachment of microplates along the fore and arc zones and finally mantle upwellings induced by asthenospheric windows linked to ridge subduction and tearings in the subducted slab. This revision exemplifies the high complexity in the patterns of distribution and mechanisms associated with exhumation in a subduction setting. In particular, constitutes a general framework for the Southern Andes to link different kind of processes to an evolving landscape during the Quaternary.

References

- Aaron, F., R. W. Allmendinger, J. Cembrano, G. González & G. Yáñez, (2013). Permanent fore-arc extension and seismic segmentation: Insights from the 2010 Maule earthquake, Chile. *Journal of Geophysical Research: Solid Earth* 118, 724–739.
- Brooks, B., M. Bevis, K. Whipple, R. Arrowsmith, J. Foster, T. Zapata, E. Kendrick, E. Minaya, A. Echalar, M. Blanco, P. Euillades, M. Sandoval & R. Smalley, (2011). Orogenic-wedge deformation and potential for great earthquakes in the central Andean backarc. *Nature Geoscience*, doi: 10.1038/NGEO1143
- Burd, A.I., J.R. Booker, R. Mackie, A. Favetto & M.C. Pomposiello, (2014). Three-dimensional electrical conductivity in the mantle beneath the Matru Volcanic Field in the Andean back-arc of Argentina Pay un near 36.5 S: Decapitation of a mantle plume by resurgent upper mantle shear during slab steepening? *Geophys. J. Int.* 1, 1–12.
- Cande, S. & R. Leslie, (1986). Late Cenozoic tectonics of the Southern Chile trench. *Journal of Geophysical Research* 91, 47–496.
- Costa, C. & C. Vita-Finzi, (1996). Late Holocene faulting in the southeast Sierras Pampeanas of Argentina. *Geology* 24 (12), 1127–1130.
- Darwin, C.R., (1846). Geological observations on South America. Being the third part of the geology of the voyage of the Beagle, under the command of Capt. Fitzroy, R.N. during the years 1832 to 1836. Smith Elder and Co., London, 279 pp.
- Fariás, M., D. Comte, S. Roecker, D. Carrizo, & M. Pardo, (2011). Crustal extensional faulting triggered by the 2010 Chilean earthquake: The Pichilemu Seismic Sequence. *Tectonics* 30, DOI: 10.1029/2011TC002888
- Folguera, A., V. Ramos, R. Hermanns, & J. Naranjo, (2004). Neotectonics in the foothills of the Southernmost Central Andes (37°–38°S). Evidence of the strike-slip displacement along the Antifiñir-Copahue fault zone. *Tectonics* 23 (TC 5008), 23 pp.
- Folguera, A., A. Introcaso, M. Giménez, F. Ruiz, P. Martínez, C. Tunstall, E. García Morabito, & V.A. Ramos, (2007). Crustal attenuation in the Southern Andean retroarc determined from gravimetric studies (38°–39°30'S): The Lonco-Luán asthenospheric anomaly. *Tectonophysics* 439, 129–147.
- Folguera, A. & V. Ramos, (2009). Collision of the Mocha fracture zone and a less than 4 Ma old wave of orogenic uplift in the Andes (36°–38°S). *Lithosphere* 1 (6), 1–6.
- Galland, O., E. Hallot, P.R. Cobbold, G. Ruffet, & J. De Bremond d'Ars, (2007). Volcanism in a compressional Andean setting: A structural and geochronological study of Tromen volcano (Neuquén province, Argentina). *Tectonics* 26, DOI: 10.1029/2006TC002011
- Guillaume, B., J. Martinod, L. Husson, M. Roddaz, & R. Riquelme, (2009). Neogene uplift of central eastern Patagonia: Dynamic response to active spreading ridge subduction? *Tectonics* 28, DOI:10.1029/2008TC002324
- Lagabrielle, Y., M. Suárez, J. Malavieille, D. Morata, F. Espinoza, R.C. Maury, B. Scalabrino, L. Barbero, R.D. Cruz, E. Rossello, & H. Bellon, (2007). Pliocene extensional tectonics in the Eastern Central Patagonian Cordillera: geochronological constraints and new field evidence. *Terra Nov.* 19, 413–424.
- Lavenu, A. & J. Cembrano, (1999). Compressional- and transpressional-stress pattern for Pliocene and Quaternary brittle deformation in fore-arc and intra-arc zones (Andes of Central and Southern Chile). *J. Struct. Geol.* 21, 1669–1691.
- Messenger, G., B. Nivière, J. Martinod, P. Lacan, & J.-P. Xavier, (2010). Geomorphic evidence for Plio-Quaternary compression in the Andean foothills of the southern Neuquén Basin, Argentina. *Tectonics* 29, 12.
- Pesicek, J.D., E.R. Engdahl, C.H. Thurber, H.R. DeShon, & D. Lange, (2012). Mantle subducting slab structure in the region of the 2010 M8.8 Maule earthquake (30–40°S), Chile. *Geophys. J. Int.* 191, 317–324.
- Pedoja, K., V. Regard, L. Husson, J. Martinod, B. Guillaume, E. Fucks, M. Iglesias & P. Weill, (2011). Uplift of Quaternary shorelines in eastern Patagonia: Darwin revisited. *Geomorphology* 127, 121–142.
- Riccomini, C. & Assumpcao, M., (2009). Quaternary tectonics in Brazil. *Episodes* 22 (3), 221–225.
- Schellart, W., D. Stegman, R. Farrington & L. Moresi, (2011). Influence of lateral slab edge distance on plate velocity, trench velocity and subduction partitioning. *Journal of Geophysical Research* 116 (B10408),
- Sobolev, S.V. & A.Y. Babeyko, (2005). What drives orogeny in the Andes? *Geology* 33 (8), 617–620.



Quaternary Reactivation of Australia's Western Passive Margin: Inception of a New Plate Boundary?

Hengesh, James (1, 2) and Beau Whitney(1)

- (1) The Centre for Offshore Foundation Systems, The University of Western Australia, M053, 35 Stirling Highway, Perth, Western Australia 6009, Australia, Email: james.hengesh@uwa.edu.au
 (2) Interface Geohazard Consulting, LLC, 20 Plumeria Pl, Lahaina, Hawaii 96761

Abstract:

Alignment of northwestern Australia's passive margin with the terminations of the eastern Java trench and western Banda arc has triggered a new phase of reactivation along the Phanerozoic North West Shelf rift system. Dextral faulting in Browse basin cross-cuts Middle to Late Miocene inversion structures and offsets the seafloor. Similarities in displacements between Quaternary and Tertiary horizons demonstrate an absence of progressive deformation and recent onset of faulting consistent with the timing of the collision of the passive margin with the Savu-Rote ridge 0.2 to 1.8 Ma. The reactivated faults may be interpreted as forming a new plate boundary and the third arm of a nascent triple junction. The geological expression of youthful faulting and rates of seismic activity indicate that faults in Browse basin are capable of producing M_{max} earthquakes of moment magnitude (M_w) 7.0 to M_w 7.75 with recurrence intervals of $\sim 1,000$ years as opposed to the 10^4 to 10^5 years common in stable continental regions.

Key words: Active faulting, fault reactivation, neotectonics, geomorphology, seismic hazards, North West Shelf, Australia,

INTRODUCTION

Australia's North West Shelf (NWS) is known as a passive continental margin that formed during rifting of Antarctica and India away from Australia during fragmentation of Gondwanaland (Larson, 1977). The NWS preserves a long history of tectonic deformation including formation of a Devonian intracontinental rift system (Yeates, 1987), development of the Triassic to Late Cretaceous rifted continental margin (AGSO North West Shelf Study Group, 1994; O'Brien et al., 1999) and oceanic basins, and reactivation of these former rift systems during the Late Miocene to recent (O'Brien et al., 1999; Cathro & Karner, 2006; Keep et al., 2007). The former rift basins are major depocentres that accumulated up to ~ 20 km of Paleozoic and Mesozoic syn- and post-tectonic sediments (AGSO, 1994; O'Brien et al., 1999). Neogene fault reactivation has deformed basin sequences and developed inversion structures of significant economic value (Longley et al., 2002). Reactivation of the former rift systems has continued through the late Quaternary to present with regional lithospheric scale warping, folding of Last Interglacial (LIG) shoreline deposits (Whitney & Hengesh, in review; Hengesh et al., 2011), and faults that offset the seabed. Earthquake activity yields deformation rates consistent with several millimeters per year (mm/yr) of motion across the former rifted margin; a rate inconsistent with the concept of a "stable continental region".

This paper presents information on the characteristics of faulting and seismicity along the NWS, discusses the kinematic forces that may be the driving mechanisms for reactivation of this system of faults, and briefly addresses related hazards.

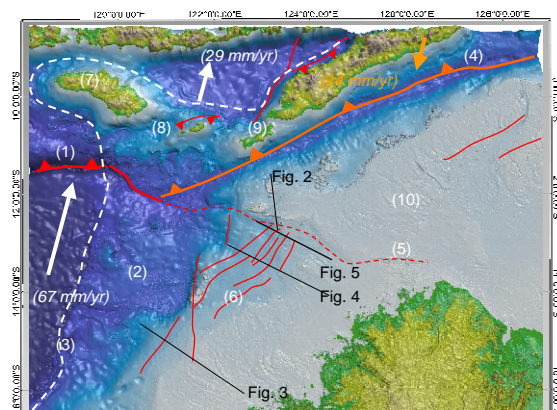


Fig. 1: Regional tectonic setting showing major tectonic elements and locations discussed in text. (1) Java Trench; (2) Scott Plateau; (3) Continent-Ocean boundary; (4) Timor trough (orange); (5) Browse-Bonaparte transition (red-dashed); (6) Browse Basin fault zone (red active traces); (7) Sumba; (8) Savu; (9) Rote; and (10) ~Bonaparte Basin. White arrows indicate plate motion directions relative to Sunda Shelf. Orange arrow relative to Australia.

TECTONIC SETTING

The Australian plate is migrating northward along an azimuth of 011° to 015° at a rate of 56 to 72 mm/yr relative to a fixed Sunda Shelf reference frame (Bock et al., 2003; Nugroho et al., 2009) and is converging with the Sunda Arc subduction zone (red line) and the Banda Tectonic Collision Zone (orange line) (Fig. 1). The NWS part of the western Australian passive margin trends in a north-northeast direction until it is truncated by the Banda arc (Fig. 1). The transition from oceanic to continental lithosphere within the Australian plate profoundly changes the style of deformation along the



northern plate boundary (Silver et al., 1983; McAffrey, 1988, Harris et al., 2009).

There is northward directed Type B (Benioff) subduction (Bally, 1983) of Indian oceanic crust west of the Scott Plateau (120°E). However, east of this location the oceanic crust has been fully consumed and subduction along the Banda trench has ceased (Hall, 2011; Audley-Charles, 2011). The former subduction zone has become blocked by the Australian continental lithosphere and evolved into a Type A (Ampferer) subduction zone (Bally, 1983) or tectonic collision zone (TCZ) where the former accretionary prism has emerged along large scale nappe structures to form Timor and Sumba islands and the Suva-Rote ridge.

The islands of Sumba, Savu and Flores are aligned with the westernmost margin of the Australian continental plate (Fig. 1) and are being internally deformed as a result of the collision (Harris et al., 2009; Roosmawati & Harris, 2009; Rigg & Hall, 2011). They also are moving toward 011° to 015°, but at 23 to 32 mm/yr, about one third the velocity of the Australian plate (Harris et al., 2009; Nugruho et al., 2009). This implies that two thirds of the motion is accommodated by deformation of the back-arc Flores thrust system, the island arc, and accretionary prism. The collision also is causing regional warping of the northern ~500 km of the Australian plate recognizable by the sinuous shoreline morphology, drowned Last Interglacial (LIG) reef deposits (Collins, 2002), and subsided Stage 8 low stand coastal deposits (Hengesh et al., 2011). Table 1 illustrates subsidence rates in the Browse basin.

Table 1. Submergent estuarine features and shoreline angles yield subsidence rates of 0.2 to 0.29 mm/yr. *Depth and age of MIS 5e from Scott Reef provide baseline subsidence curve (Collins, 2002).

Marine Isotope Stage	Formation (m)	Current Elev. (m)	Elev. Difference (m)	Age (Ka)	Subs. Rate mm/yr
2	-120	-125	-5	18	-0.28
5e*	+5.5	-30	-35.5	125	-0.28
6	-128	-155	-27	137	-0.20
8	-108	-180	-72	250	-0.29

Type B subduction along the Sunda and Banda trenches began about 12 Ma in the Timor region and ceased about 4 million years ago (Audley-Charles, 2011). The initiation of subduction about 12 Ma coincides with the timing of fault reactivation and basin inversion along the passive margin (AGSO, 1994, Keep et al., 1998), but the onset of continent-arc collision in the past 0.2 to 1.8 Ma at Scott Plateau, directly on the rifted margin, coincides with a more recent pulse in activity along the passive margin. Removing the oceanic crustal buffer along the northern continental margin allowed initiation of dextral shear along the margin of western Australia. The former rift systems are now accommodating a portion of the strain as the Indian Ocean crust is efficiently subducted from Scott Plateau (120°E) to the west, whereas the TCZ

and subduction roll-back are deforming the continental margin (Hall, 2009; Audley-Charley, 2011) and reducing relative plate motion rates east of 120°E.

ACTIVE TECTONIC STRUCTURES ALONG THE WESTERN PASSIVE MARGIN

Harris et al. (2009), and Roosmawati and Harris (2009) have demonstrated that the collision of the westernmost Australian continental margin with the Banda trench at the continental transition initiated near Sumba (2-3 Ma), then migrated southeast to Savu (0.5-1.0 Ma), and then Rote about 0.2 Ma. The ongoing collision on Savu has formed both north and south vergent thrusts, has caused uplift of pelagic chalk from depths of >2,500m to the surface in less than 1.0 Ma, and has caused emergence of the accretionary prism. This collision also triggered reactivation of the former rift structures on the western continental margin.

2D and 3D seismic data from Browse basin have been interpreted to assess the characteristics of recent faulting along this portion of the "passive margin". Browse basin is separated from Bonaparte basin to the north by a major west-northwest trending bathymetric scarp (Fig. 1). The scarp extends across the continental shelf along the trend of Ashmore Reef and aligns with the tear fault that separates the Timor trough from the Java trench (Fig. 1). The bathymetric lineament lies above a major structure that subdivides Browse and Bonaparte basins (Keep and Harrowfield; 2008) (Fig. 2) and has generated approximately 100m of up-on-the-north relief across a drowned Pleistocene erosion surface and the faults appear to offset the seafloor.

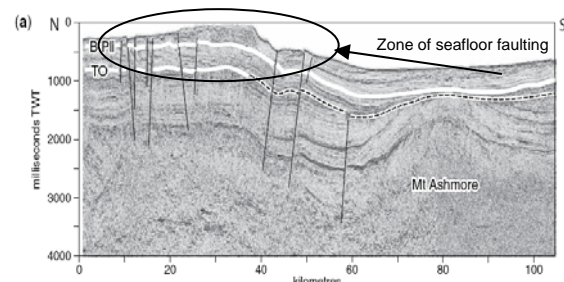


Fig 2. N-S trending 2D seismic line across Ashmore reef trend (Browse Bonaparte transition). Modified from Keep and Harrowfield (2008). The faults cut Pliocene deposits and appear to have seafloor expression.

Faulting north of this structure in Bonaparte basin is characterized by sinistral transtensional deformation related to flexure of the Australian continental lithosphere at the Banda TCZ (Bourget et al., 2012) and the highly oblique sense of motion between Australian continental margin and the TCZ. Nugruho et al. (2009) measured 15 to 24 mm/yr of oblique convergence between Timor and Darwin, which can be partitioned into slip that is normal to, and parallel to, the plate boundary.

Deformation south of the Browse-Bonaparte transition is characterized by folding and inversion of basin deposits



as well as dextral strike slip faulting. Figs. 3 and 4 show examples of 2D lines from the 1996 AGSO Browse basin high resolution seismic (BBHR) survey. There are two prominent styles of deformation. Fig. 3 illustrates a simple inversion structure or anticline that formed during Middle Miocene time (AGSO, 1997). This is a fault cored fold that deforms Latest Cretaceous through Late Miocene marine carbonates and clastic shelf deposits. The concordant horizons demonstrate a lack of progressive deformation until Late Miocene time. The fold is truncated by a Late Miocene/Pliocene erosion surface that provides evidence for no Pliocene or younger deformation.

The second style of deformation in Browse basin involves active faulting with shallow subsurface or seafloor expression. Fig. 4 is a 2D seismic line from the BBHR survey across Caswell sub-basin on the outer shelf (Simpson & Cooper, 2008). The faulting on this survey extends from the base of the survey at approximately 3 seconds TWT to the shallow sub-bottom sediments. The fault throw at the base Tertiary, Middle Miocene, and sub-bottom is all in the range of 0.04 to 0.06sec TWT (Fig. 4), or approximately 50m. The similarity in throw from the surface to the base of the section shows a lack of progressive deformation and suggests the onset of faulting was very recent.

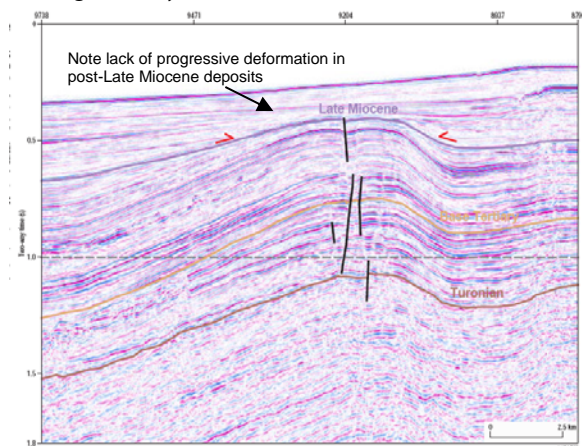


Fig 3. Portion of 2D high resolution seismic line 175-03 (modified from AGSO, 1997) showing Middle to Late Miocene inversion.

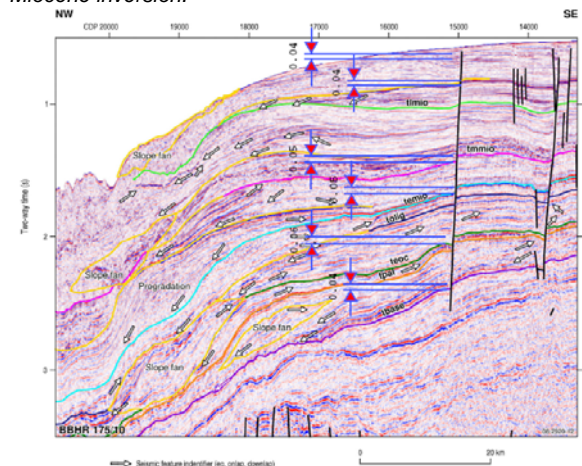


Fig 4. Example seismic line BBHR 175-10 showing similarity in fault throw from early Tertiary to Recent on the outer shelf of Caswell Sub-basin. (Modified from Simpson & Cooper, 1998).

A significant zone of transtensional faults offset the seafloor within the north-central Caswell sub-basin (Fig. 5). These appear to be the most recently active faults in the Browse basin.

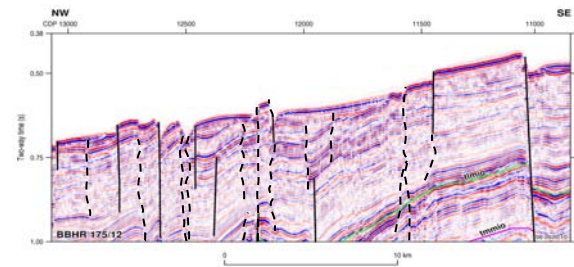


Fig 5. Faulting of the present-day seafloor in the northern Caswell sub-basin. Portion of seismic line BBHR-175/12 on middle shelf location (modified from Simpson and Cooper, 2008).

The Caswell fault initiate near the Ashmore structure and trends in a southwest direction. The fault does not align with the deeper Jurassic/Triassic basin margin and so may be soft-linked to these deeper basement faults as suggested by Keep and Moss (2000).

DISCUSSION

The recently active faults in Browse basin (e.g. Caswell, Bassett, and Scott Reef faults) appear to be forming in a step-over between the eastern basin margin and the Scott Reef trend. As the Scott Plateau is migrating northward at 64.3+/-0.2 mm/yr (relative to stable Sunda Shelf), the role back of Timor at the Timor trough (~24 mm/yr relative to Australia) is impeding the western continental margin (Browse and Bonaparte basins) and creating a dextral transtensional pull-apart along the southern margin of the Ashmore structure. North of Ashmore Reef the kinematics of the plate boundary change and the dominant style of deformation is sinistral normal oblique. Across the Sunda trench and Timor trough the dominant style is contractional folding and thrusting with secondary normal faulting.

The Middle to Late Miocene style of deformation in the area involved structural inversion of the basin fill related to subduction along the Banda trench between 4 to 12 Ma. This pattern of deformation changed in the last 0.2 to 1.8 Ma as Savu and Rote have become involved in the collision (Harris et al., 2009). Seismicity across the Browse basin yields recurrence parameters of $a=4.6906$ and $b=1.11$. Combining these recurrence parameters with empirically derived relations between magnitude and displacement, for each 0.1 magnitude bin between M_w 5 and M_w 7.75, yields deformation rates of approximately 8 mm/yr across Browse basin. The magnitude-frequency relations for Browse basin indicate that earthquakes in the M_w 7.0 to M_w 7.5 range have a recurrence of approximately 1,000 to 1,500 years. Given



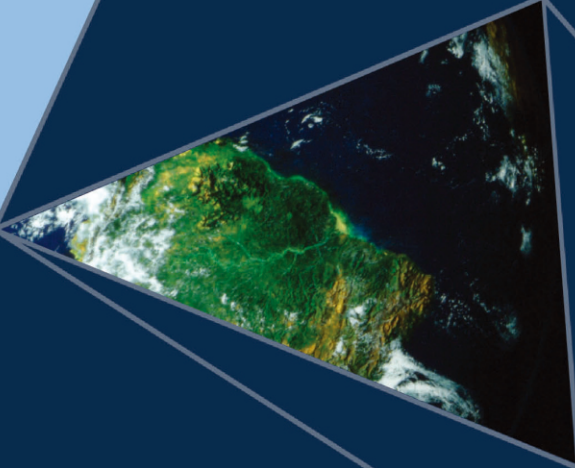
that there are multiple Quaternary active faults in the basin, and slip would be partitioned across several of these faults, these relations seem reasonable.

Due to the youthful age of the collision at the continental transition the evidence of recent tectonic deformation is only beginning to be expressed. Evidence for two pulses of reactivation of the plate margin (Middle–Late Miocene and Pleistocene) are observable along a 1600 km part of the western passive margin referred to as the Western Australia Shear Zone (WASZ) (Whitney & Hengesh, this volume). The onset of this new pulse of deformation may represent initiation of a new plate boundary system and possibly the third arm of a nascent triple junction.

Acknowledgements: We gratefully acknowledge the financial support provided by the Chevron Australia Business Unit (Project PDEP AES 12-P1ABU-82). This work forms part of the activities of the Centre for Offshore Foundation Systems (COFS), currently supported as a node of the Australian Research Council Centre of Excellence for Geotechnical Engineering.

References

- AGSO North West Shelf Study Group, (1994). Deep reflections on the North West Shelf: Changing perceptions of basin formation. In: Purcell, P.G and R.R. (Eds), *The Sedimentary Basins of Western Australia: Proceedings of the Petroleum Exploration Society of Australia Symposium*, Perth, WA, 1994, 63–76.
- AGSO Browse Basin Project Team, (1997). Browse Basin high resolution study, North West Shelf, Australia, Interpretation Report. AGSO record 1997/38.
- Audley-Charles, M. G. (2011). Tectonic post-collision processes in Timor. In: Hall, R., Cottam, M. A. & Wilson, M. E. J. (eds), *The SE Asian Gateway: History and Tectonics of the Australia–Asia Collision*. Geological Society, London, Special Publications, 355, 235–260.
- Bally, A. W. (ed.) (1983). *Seismic Expression of Structural Styles. Studies in Geology*, American Association of Petroleum Geologists, 15 (3 volumes).
- Bock, Y., L. Prawirodirdjo, J.F. Genrich, C.W. Stevens, R. McCaffrey, C. Subarya, S.S.O. Puntodewo & E. Calais, (2003). Crustal motion in Indonesia from Global Positioning System measurements: *Journal of Geophysical Research*, v. 108, no. B8, p. 2367, ETG-3.
- Bourget, J., R.B. Ainsworth, G., Backe, & M. Keep, (2012). Tectonic Evolution of the "Giant" Bonaparte Continental Shelf: Impact on Sediment Distribution during the Pleistocene. *Australian Journal of Earth Sciences*, 59, 877–897.
- Cathro, D.L., & G.D. Karner, (2006). Cretaceous-Tertiary inversion history of the Dampier Sub-basin, northwest Australia: Insights from quantitative basin modeling. *Marine and Petroleum Geology* 23, 503–526.
- Collins, L.B., (2002). Tertiary Foundations and Quaternary Evolution of Coral Reef Systems of Australia's North West Shelf, in Keep, M. & Moss, S. J. (Eds) 2002, *The Sedimentary Basins of Western Australia 3*, Proceedings of the Petroleum Exploration Society of Australia, Perth, p. 129–152.
- Harris, R., M. W., Vorkink, C. Prasetyadi, E. Zobell, N. Roosmawati, & M. Apthorpe (2009). Transition from subduction to arc-continent collision: Geologic and neotectonic evolution of Savu Island, Indonesia. *Geosphere*, 5(3), 152–171.
- Hengesh, J.V., B.B. Whitney, and A., Rovere, (2011). A tectonic influence on seafloor stability along Australia's North West Shelf, Proceedings of the Twenty-first (2011) International Offshore and Polar Engineering Conference, Maui, Hawaii, USA, June 19–24, 2011, Copyright © 2011 by the International Society of Offshore and Polar Engineers (ISOPE), ISBN 978-1-880653-96-8 (Set); ISSN 1098-6189 (Set); 596–604.
- Hall, R., (2011). Australia–SE Asia collision: plate tectonics and crustal flow. In: Hall, R., Cottam, M. A. & Wilson, M. E. J. (eds) *The SE Asian Gateway: History and Tectonics of the Australia–Asia Collision*. Geological Society, London, Special Publications, 355, 73–104.
- Keep, M., C.M. Powell & P.W., Baillie, (1998). Neogene deformation of the North West Shelf, Australia: in Purcell, P.G. and Purcell, R. R. (eds.), *The Sedimentary Basins of Western Australia 2*. Proceedings of the Petroleum Exploration Society of Australia, Perth, 1998, 81–91.
- Keep, M. & S.J. Moss (2000). Basement reactivation and control of Neogene structures in the Outer Browse Basin, Northwest Shelf, *Exploration Geophysics*, 31, 424–432.
- Keep, M., M. Harrowfield, & W. Crowe, (2007). The Neogene tectonic history of the North West Shelf, Australia. *Exploration Geophysics* 38, 151–174.
- Keep M. & M. Harrowfield, (2008). Elastic flexure and distributed deformation along Australia's North West Shelf: Neogene tectonics of the Bonaparte and Browse basins. In H. Johnson, A.G. Dore, R.W. Gatliff, R. Holdsworth, E. Lundin & J.D. Ritchie (eds), *The Nature and Origin of Compressive Margins*. Geological Society, London, Special Publications, 306, 185–200.
- Larson, R. L. (1977). Early Cretaceous breakup of Gondwanaland off western Australia. *Geology*, 5(1), 57–60.
- Longley, I.M., C. Buessenschuett, L. Clydsdale, C.J. Cubitt, R.C. Davis, M.K. Johnson, N.M. Marshall, A.P. Murray, R. Somerville, & T.B., Spry, (2002). The North West Shelf of Australia – a Woodside Perspective, in KEEP, M. & MOSS, S.J. (Eds), *The Sedimentary Basins of Western Australia 3: Proceedings of the Petroleum Exploration Society of Australia Symposium*, Perth, WA, 2002, 28–88.
- McCaffrey, R., (1988). Active tectonics of the eastern Sunda and Banda Arcs: *Journal of Geophysical Research*, v. 93, p. 15,163–15,182.
- Nugroho, H., R., Harris, A.W., Lestariya, & B. Maruf, (2009). Plate boundary reorganization in the active Banda Arc-continent collision: Insights from new GPS measurements: *Tectonophysics*, v. 479, Issues 1–2, Arc-continent Collision, p. 52–65.
- O'Brien, G. W. M. Morse, D. Wilson, P. Qalfe, J. Colwell, R., Higgins & C. B., Foster, (1999). NW Shelf-Margin-scale, basement-involved compartmentalisation of Australia's North West Shelf: A primary control in basin-scale rift, depositional and reactivation histories. *APPEA Journal*, 39(1), 40–63.
- Rigg, J. W. & R. Hall, (2011). *Structural and stratigraphic evolution of the Savu Basin, Indonesia*. Geological Society, London, Special Publications, 355(1), 225–240.
- Roosmawati, N., & R. Harris, (2009). Surface uplift history of the incipient Banda arc-continent collision: Geology and synorogenic foraminifera of Rote and Savu Islands, Indonesia. *Tectonophysics*, 479(1), 95–110.
- Silver, E.A., R., Reed, R., McCaffrey, & Y., Joyodiwiryo, (1983). Back arc thrusting in the eastern Sunda arc, Indonesia: A consequence of arc-continent collision: *Journal of Geophysical Research*, v. 88, p. 7429–7448, doi: 10.1029/JB088iB09p07429.
- Simpson, A. and M. Cooper, (2008). Description, Distribution and Potential CO₂ Storage/Seal Capacity of the Cenozoic Sandstones and Carbonates, Browse Basin, Western Australia, *Geoscience Australia Record 2008/13*.
- Yeates, A. N., M. T., Bradshaw, J. M., Dickens, A. T., Brakel, N. F., Exon, R. P., Lanford, S. M., Mulholland, J. M., Totterdell & M. Yeung, (1987). The Westralian Superbasin, an Australian link with Tethys: in McKenzie, K.G. (ed.), *Shallow Tethys 2: 2nd International symposium on Shallow Tethys*, Wagga Wagga, p. 199–213.



The 5th International INQUA Meeting on
**Paleoseismology,
Active Tectonics and
Archeoseismology**



paleoseismicity.org

KIGAM 한국지질자원연구원
Korea Institute of Geoscience and Mineral Resources

